Deconstructing Accelerated Testing Environments for Exfoliation Corrosion of Al-Cu-Li Alloy 2060

A Dissertation

Presented to

the faculty of the School of Engineering and Applied Science

University of Virginia

---

in partial fulfillment

of the requirements for the degree

Doctor of Philosophy

by

Mary Elizabeth Parker

May

2018

APPROVAL SHEET

The dissertation
is submitted in partial fulfillment of the requirements
for the degree of
Doctor of Philosophy

Mary E. Parker
AUTHOR

The dissertation has been read and approved by the examining committee:

Robert G. Kelly
Advisor

James Burns, Chair

John R. Scully

Osman Ozbulut

James Moran

Accepted for the School of Engineering and Applied Science:

Craig H. Benson, Dean, School of Engineering and Applied Science

May
2018

Abstract

Third-generation aluminum-copper-lithium (Al-Cu-Li) alloys are attractive for aerospace applications because of their improved strength-to-weight and stiffness-to-weight ratios, fracture toughness, and corrosion resistance compared to legacy alloys such as AA2024. Al-Cu-Li alloys can suffer from localized corrosion during service, and accelerated laboratory testing is an important tool for quickly assessing corrosion properties. Many standardized tests for high-strength aluminum-alloys exist, but these tests do not all correlate well with service results. Furthermore, different tests that are aimed at assessing the same corrosion behavior can produce drastically different results for the same alloy temper.

Exfoliation is a specific form of localized corrosion that occurs in rolled alloys that have an elongated grain structure, and it can be service life-limiting for many high-strength Al alloys. Three accelerated tests for exfoliation corrosion were considered in this study, including ASTM G34 (a constant immersion test), ANCIT (a modified G34 test), and ASTM G85-A2 (a cyclic acidified salt spray test). These tests were chosen because they produce different results for Al-Cu-Li alloy 2060. Each test incorporates various strategies for accelerating corrosion, such as high chloride concentration, low solution pH, elevated testing temperature, increased oxidizing power, and/or relative humidity cycling, but the impact of these parameters on exfoliation corrosion is not well understood. Both the under-aged AA2060-T3 temper (exfoliation-susceptible) and the near peak-aged AA2060-T86 temper (exfoliation-resistant) were considered in this study.

The roles of individual test parameters were isolated by measuring the impact of altered testing conditions on electrochemical kinetics and corrosion morphology. It was found that the low solution pH of ASTM G34 caused an increase in the cathodic reaction kinetics compared to ANCIT testing, due to fast proton reduction kinetics in highly acidic solutions (pH <1). The elevated testing temperature of ANCIT caused a significant increase in anodic kinetics, which made ANCIT more aggressive overall. This increase in anodic kinetics resulted in faster exfoliation formation in AA2060-T3, which was the expected corrosion morphology based on seacoast exposures. Although exfoliation formed on the susceptible -T3 temper during exposure to ANCIT, the resistant -T86 temper experienced an unrealistic severity of attack in ANCIT.

A common method of increasing corrosion rate during accelerated corrosion testing is to add an oxidizing agent with reduction kinetics faster than oxygen reduction (ORR) and proton reduction. The impact of two oxidizing agents, hydrogen peroxide (H_2O_2) and potassium persulfate (K_2S_2O) on corrosion kinetics during accelerated testing of AA2060-T3 and -T86 was investigated as a part of this work. H_2O_2 produced faster cathodic kinetics than $K_2S_2O_8$ did, but the cathodic kinetics of $K_2S_2O_8$ could be manipulated by adjusting solution pH and adding aluminum chloride ($AlCl_3$). Faster kinetics does not always result in the desired corrosion morphology, however, and AA2060-T3 and T86 samples exposed to solutions containing both $K_2S_2O_8$ and $AlCl_3$ could not be distinguished by temper.

Relative humidity (RH) was found to be a critical parameter for cyclic salt spray testing. Dry bottom (DB) and wet bottom (WB) ASTM G85-A2 was performed in two different chamber brands, and exposure results were different for the different brands. Seemingly small differences in chamber operation caused RH to be significantly different during the dry air purge and dwell periods in the two chambers. In chamber Brand 2, the low RH during the dwell period (17% - 20.5%) caused corrosion kinetics to slow, and only mild exfoliation formed after 4 weeks of exposure. It was shown that a more moderated RH (77% - 61%) during the dwell period was more appropriate for accelerating exfoliation. Two modified cyclic salt spray tests were designed to have higher RH during the dwell period, and both tests produced higher corrosion kinetics and faster exfoliation formation compared to the standard test. Additional high-strength aluminum alloys (AA7075, AA2024) were exposed to the modified tests, and both tests could correctly distinguish between exfoliation-resistant and susceptible tempers.

Acknowledgements

Thank you to my wonderful advisor Dr. Robert Kelly. I have grown as a scientist and as a person because of your mentorship. Thank you for all the time and energy you have spent helping me work through this process.

I would like to thank my committee members, Drs. John Scully, Jimmy Burns, Jim Moran, and Osman Ozbulut for participating in this process. Thank you for your time and your thoughtful review.

Thank you to past and present CESE members. Being a part of CESE has provided me with support, mentorship, and friendship. A special thank you to my group members, especially Piyush Khullar, Lindsey Blohm, and Gilbert Liu for your friendship and support. Another special thank you to the undergraduate students Srishti Shrivastava and Russell Repasky who did excellent laboratory work to support this research.

Thank you to all the faculty and staff members of the Materials Science Engineering department who keep this department running. A big thanks to Kim Fitzhugh-Higgins for her continuous support and encouragement.

Finally, I would like to thank my boyfriend Ehsan Monazami who has been with me every step of the way throughout this process. His support and encouragement have played a huge role in my success at UVA.

Table of Contents

List of Figures

List of Tables

1. Introduction

1.1 Background

High-strength aluminum alloys (Al alloys) are valued in the aerospace industry for their high strength-to-weight ratios, but these alloys can suffer from localized corrosion during service, especially when exposed to corrosive atmospheric environments where salt aerosols deposit on the metal surface. Maintenance schedules and lifetime predictions rely on the ability to understand and predict the corrosion behavior of aluminum alloys under atmospheric conditions. Accelerated laboratory testing is an important tool for quickly assessing corrosion properties, and outdoor exposure at seacoast or industrial sites provide insight into the likely behavior of aluminum alloys in service. Many standardized laboratory tests for high-strength aluminum-alloys exist, but these tests do not all correlate well with service results. Furthermore, different tests that are aimed at assessing the same corrosion behavior can produce drastically different results for the same alloy temper. No fundamental explanation for the discrepancies in these accelerated corrosion test results has been previously presented.

1.2 Al-Li alloys

The primary alloy of interest in this study was a third-generation aluminum-copper-lithium (Al-Cu-Li) alloy, AA2060. Al-Cu-Li alloys are attractive for aerospace applications because they provide an opportunity for improved strength-to-weight and stiffness-to-weight ratios, fracture toughness, and corrosion resistance compared to legacy alloys such as AA2024.[1,2] It has been estimated that for every 1% Li added to the alloy composition, a 3% decrease in density and 6% increase in Young's elastic modulus are achieved.[1,2]

1.2.1 History of Al-Li Alloy Development

Aluminum-lithium (Al-Li) alloys were used in aerospace applications as early as the 1950's. However, it was not until the 1980's that 2nd generation Al-Li alloys were developed with the intention of replacing legacy alloys such as AA7075 and AA2024. The 2nd generation alloys, including AA2090, AA2091, and AA8090, had significant density reduction compared to other high-strength Al alloys, but also suffered from property anisotropy and low fracture toughness.[1,3]

The anisotropy and toughness issues were resolved with 3rd generation Al-Li alloys through adjustments in alloy composition and thermomechanical processing. With these improvements, 3rd generation Al-Li alloys have proven promising for aerospace applications.[1-3] More specifically, Al-Cu-Li alloy 2060 has been proposed for use as fuselage and wing construction.[2]

1.2.2 Al-Cu-Li Alloy Microstructure

Al-Li alloys achieve their strength through age-hardening. The primary strengthening precipitates present depend on the composition of that material but may include: T_1 (Al_2CuLi), δ' (Al_3Li), and θ' (~Al_2Cu).[1] The T_1 phase is an effective hardening precipitate, but δ' can decrease toughness. The δ' precipitate forms in alloys with high Li content (>1.4 -1.5%), but the T_1 phase is usually the primary strengthening precipitate in Al-Li alloys with moderate Li content (0.6% - 1.5%)[7].

The primary strengthening phase in near peak-aged AA2060-T8 has been reported to be the T_1 precipitate (Al_2CuLi).[4,5] Cai et al. examined the microstructure of AA2060-T8 sheet material (2 mm thick) and found thin platelets of the T_1 phase on {111} planes within the Al-matrix. The S' (Al_2CuMg) phase and a small amount of the θ' (Al_2Cu) phase were also observed.[5] According to Connally and Buchheit, the T_1 precipitate tends to form on both matrix dislocations and subgrain boundaries.[6,7] Some alloy tempers utilize a pre-stretch to increase the number of matrix dislocations and encourage precipitation of strengthening phases within grains. [8]

The aging condition of an alloy can have a significant impact on the type and extent of corrosion susceptibility. Some Al-Cu-Li alloys undergo a transition in intergranular corrosion (IGC) susceptibility during aging where under-aged tempers are more vulnerable to IGC than peak-aged and near peak-aged tempers. The improvement in IGC resistance at near peak-aged tempers correlates with an improvement in stress corrosion cracking and exfoliation resistance.[9,10] The transition in corrosion morphology with aging suggests that changes in microstructure reduce the susceptibility of grain boundaries to attack during aging. No studies on the changes of AA2060 microstructure with aging were found in the literature, but Ott et al.[11] presented an investigation of grain boundary evolution during aging for AA2050 (Al-3.30% Cu-0.77% Li-0.39% Mn-0.32% Mg-0.17% Ag-0.10% Si-0.08% Zr-0.06% Fe-0.03%Ti-0.02% Zn), which has similar Cu and Li content to that of AA2060 (Al-3.95% Cu-0.85% Mg-0.75% Li-0.4% Zn-0.3% Mn-0.25% Ag-0.11%Zr). It was found that for under-aged AA2050, fine T_1 precipitates and very small (1 to 2 nm) precipitates resembling the S' phase were present on grain boundaries. With additional aging, T_1 precipitates grew longer (up to 100 nm in the over-aged condition), but the thickness did not change significantly. The small (1 to 2 nm) S' precipitates also grew with increased aging time, reaching 10 to 20 nm in the peak-aged condition and further coarsening in the over-aged condition.[11] Ott et al. also used Auger electron spectroscopy (AES) to show that in under-aged AA2050, grain boundary chemistry was enriched in Li compared to the matrix.[10] The standard reduction potential of Li is very low (-3.04 V_{SHE}) compared to Al (-1.662 V_{SHE}),[12] and lithium enrichment on grain boundaries in under-aged Al-Cu-Li alloys may be the cause for IGC susceptibility in these materials.

For rolled alloys with an elongated grain structure, IGC can develop into exfoliation corrosion. Due to the occluded nature of IGC fissures, Al^{3+} produced by the anodic dissolution of Al can accumulate. When the Al^{3+} concentration exceeds the solubility limit of the electrolyte within the fissure, voluminous corrosion products will form within the IGC fissure. This precipitation may occur faster or slower in various parts of the fissure depending on solution pH of the electrolyte within the fissure. The corrosion products that form within the IGC fissure have a larger volume than the dissolved Al along a grain boundary, and the corrosion products put pressure on the un-corroded grains around the affected grain boundary. With a large enough pressure, un-corroded grains will be wedged upward creating an exfoliation blister.[13]

It is the interaction between alloy microstructure and exposure environment that determine corrosion rate and morphology. While progress has been made in understanding the microstructural features for Al-Li alloys at various aging conditions, there is still more to be learned. The focus of the current work, however, lies in deconstructing the exposure environment rather than the alloy microstructure. Standard accelerated corrosion tests can generate dramatically different results for the same alloy and temper. Deconstructing the environments Al-Li alloys are exposed to during accelerated testing is necessary to explain discrepancies in testing results and to develop effective accelerated laboratory tests for new generation alloys.

1.3 Exfoliation Corrosion Mechanism

Like many other high-strength Al alloys, Al-Cu-Li alloys are susceptible to a form of localized corrosion called exfoliation. Exfoliation corrosion (EC) occurs in rolled or extruded alloys that have an elongated grain structure as shown in Figure 1.1. Localized attack along grain boundaries or other microstructural features produces voluminous corrosion products that put pressure on surface grains. At some point the blister may burst open, exposing more area to aggressive solution and allowing the intact grains to be lifted upward.[13] An example of EC from the ASTM G34 standard is shown in Figure 1.1. ASTM G34 (EXCO) is a standard full immersion test for exfoliation susceptibility.[14]

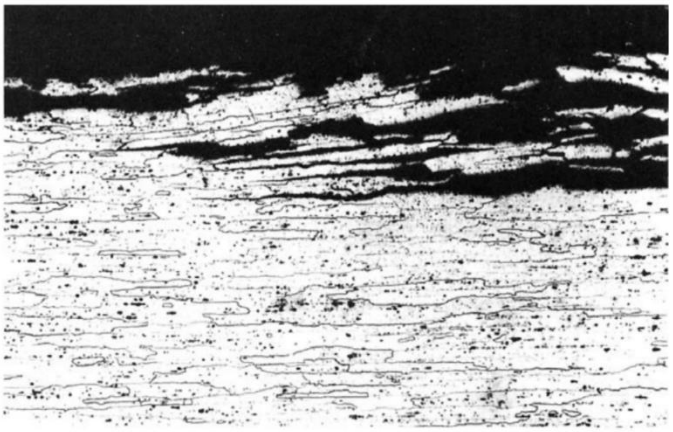

Figure 1.1: Example of an exfoliation (EC) blister from the ASTM G34 standard. From reference 14.

The nature of the exfoliation process has not yet been fully explained. Some claim that propagation is driven primarily by dissolution of grain boundaries and that the grain lifting is simply a byproduct of intergranular corrosion (IGC) in a material with elongated grains. Others say that the wedging effect is actually critical to exfoliation formation via a stress corrosion mechanism.[8,9] McNaughtan et al. measured the corrosion product wedging forces generated when several 7XXX series alloys were exposed to ASTM G34 solution (Figure 1.2[a]) as well as the threshold stress intensity for stress corrosion cracking (K_{ISCC}) for each alloy.[15] The authors showed that there was an inverse linear relationship between K_{ISCC} and the corrosion product wedging force for each alloy considered, which they took as evidence that exfoliation proceeds by a stress corrosion cracking (SCC) mechanism. The relationship between K_{ICC} and corrosion product wedging force is shown in Figure 1.2(b). While a correlation between EC and SCC susceptibility exists in many high-strength Al alloys,[9] conclusive data identifying the mechanism of exfoliation formation is not available.

The possible role of hydrogen embrittlement during exfoliation corrosion has also been explored. Several researchers have shown that hydrogen adsorption in AA2024-T3 occurs during exposure to ASTM G34 solution.[16-18] Kamoutsi et al. showed that hydrogen embrittlement can occur in AA2024-T351 during exposure to ASTM G34 solution, and the amount of adsorbed hydrogen increased with increasing exposure time to ASTM G34.[18] As with proposed connection between EC and SCC, conclusive data supporting the role of hydrogen embrittlement in EC is not available.

In the current work, focus was given to the environmental conditions that produce EC rather than the EC mechanism itself. There are still many unanswered questions regarding the EC mechanism, but the morphology of EC is well defined in ASTM G34 and other sources.[13,14,] Due to the difficulty in measuring specific localized corrosion mechanisms during accelerated testing, assessment of attack morphology is used by alloy producers and the aerospace industry to differentiate between types of attack such as pitting, IGC, and EC after accelerated testing exposure.

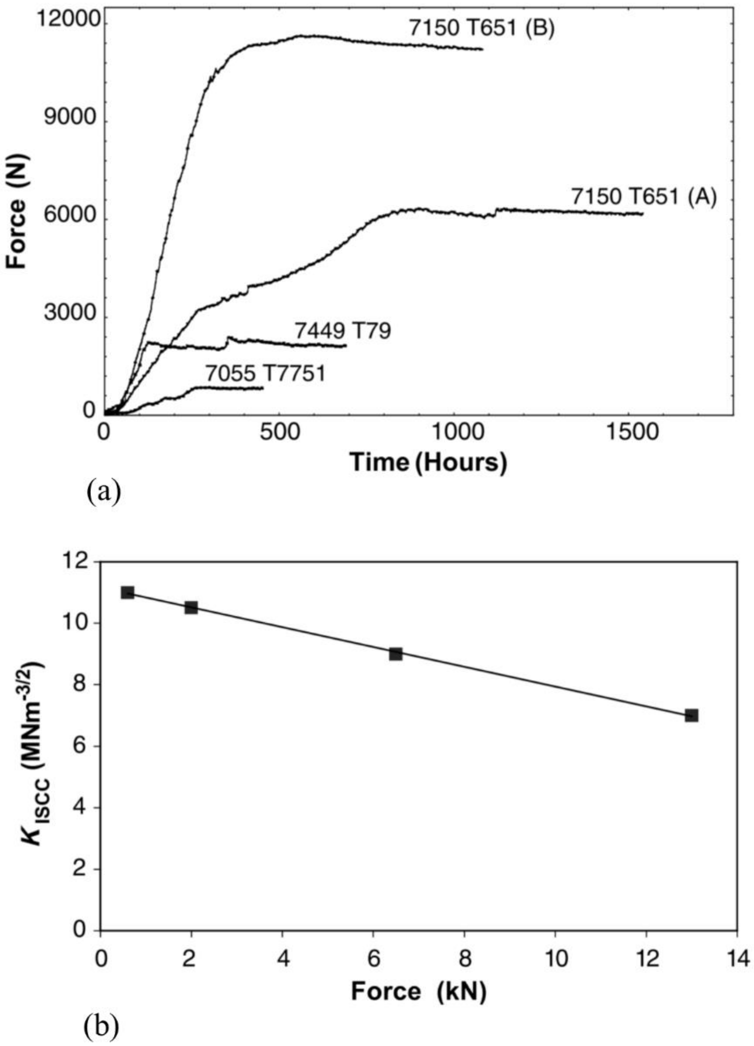

Figure 1.2: (a) Corrosion product wedging forces during exposure of several 7XXX series alloys to ASTM G34 solution. (b) Relationship between corrosion product wedging forces measured in ASTM G34 and K_{ISCC} for each alloy. From reference 15.

1.4 Accelerated Testing of High-Strength Aluminum-Alloys

Accelerated corrosion testing is an important tool for alloy producers and the aerospace industry that aids in alloy and temper design, material selection, and lot acceptance. As new generation high-strength aluminum alloys are being produced, many standardized tests designed for legacy alloys are failing to reproduce service results for the new alloys. Improved corrosion testing protocol is needed, but data to guide changes is lacking.

1.4.1 Variation among Exposure Sites

While outdoor exposure is sometimes considered the "gold standard" of accelerated corrosion testing, it should be noted that exposure sites differ in their severity. Figure 1.3 presents exfoliation ratings (according to ASTM G34 visual rating system) for an exfoliation-susceptible temper of AA2124 at several seacoast and industrial exposure sites. The exfoliation rating varied significantly, from pitting only (P) at St. Louis, MO to very severe (ED) at Pt. Judith, RI.[19] Outdoor exposure remains one of the most reliable predictors of performance in the field, but the relative severity of exposure sites must be considered when evaluating alloy performance.

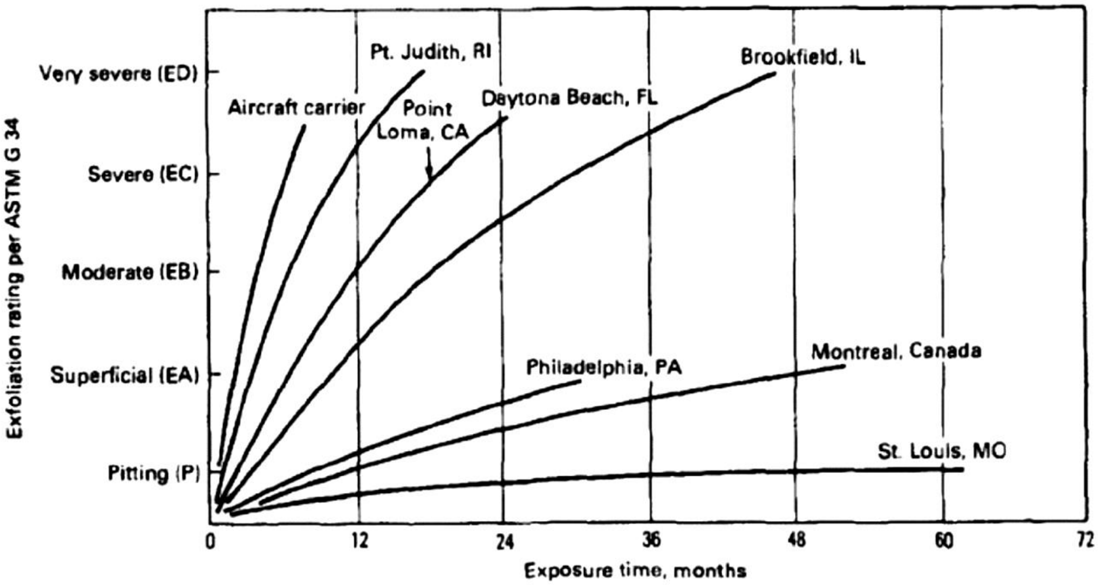

Figure 1.3: Exfoliation ratings for an exfoliation-susceptible temper of AA2124 at various seacoast and industrial environments. From reference 19.

Just as severity of outdoor exposure sites varies, the corrosiveness during service depends on the structure (aircraft, ship, etc.) and the location(s) of that structure. According to a joint program by the NAVY, ASTM, and Aluminum Association, the environment aircraft carriers encounter can be up to twice as aggressive as Point Judith, RI,[20] which is the standard testing site for one of the major aluminum alloy producers.

1.4.2 Standard Immersion Tests

Exfoliation susceptibility is traditionally evaluated according to the ASTM G34 (EXCO) rating system. Samples are compared to images in the standard (Figure 1.4) and assigned a rating: N = No appreciable attack, P = Pitting, IG = Intergranular attack, EA through ED = mild to severe Exfoliation[14,21]. Although this system originated with ASTM G34, it has been used for evaluating exfoliation in several accelerated tests.

ASTM G34 was developed to distinguish between the exfoliation corrosion behavior of various AA7075 and AA7178 (Al-Zn-Mg) tempers. This test was widely accepted because the results correlated well with long-term seacoast exposures.[22] However, when the test was applied to other AA7050, AA7150, Al-Cu alloys, and early Al-Li alloys, it failed to predict the corrosion behavior observed after seacoast exposures. In the case of AA7050 and 7150, researchers found that excessive general corrosion of samples made it difficult to distinguish between the exfoliation-resistant and susceptible tempers. For Al-Cu and Al-Li alloys, ASTM G34 did not always correctly rank tempers in terms of their exfoliation susceptibility.[23]

ASTM G34 testing results are misleading for Al-Li-Cu alloys such as AA2060 because in this test, the exfoliation-resistant over-aged temper developed more severe exfoliation than the susceptible under-aged temper.[9] Figure 1.5 shows the exfoliation ratings for various AA2060 tempers after seacoast exposure at Point Judith RI and after ASTM G34 testing. Mild exfoliation (EA) is indicated for under-aged tempers after ASTM G34 exposure while the peak-aged and over-aged conditions experienced more severe exfoliation (EB). This behavior was opposite to the trend observed after seacoast exposures where the peak-aged and over-aged tempers experienced only pitting (P).

In response to these inconsistencies, researchers developed a modified ASTM G34 test called ANCIT. This test had a higher starting pH to reduce general corrosion, and a small amount of $AlCl_3$ (0.0224 M) was added. ANCIT testing results correlated well with seacoast exposures for AA7050, AA7150, AA2024, and 2nd generation Al-Li alloys.[23]

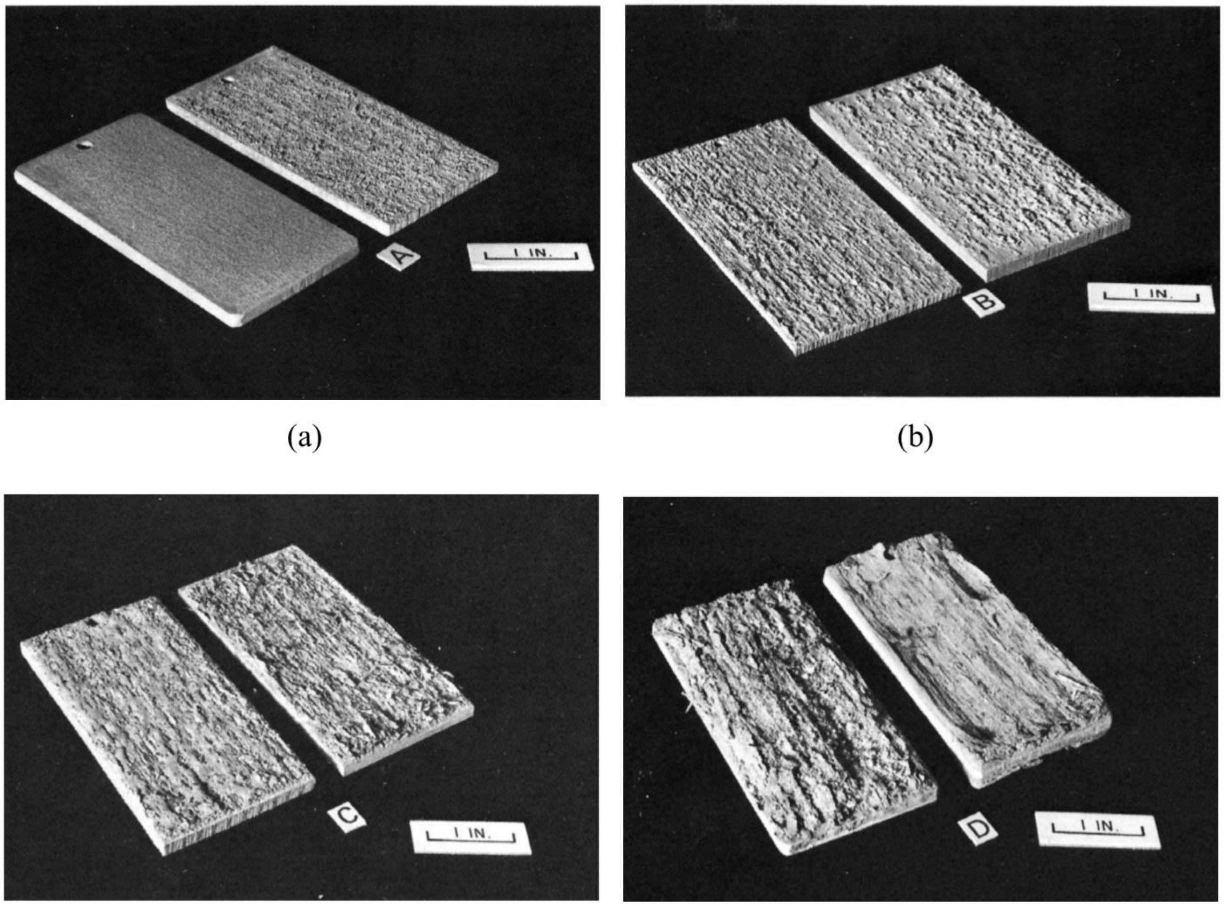

(a) (b)

(c) (d)

Figure 1.4: Summary of standard exfoliation rating images from ASTM G34. Examples are shown of (a) EA exfoliation rating, (b) EB exfoliation rating, (c) EC exfoliation rating, and (d) ED exfoliation rating. From reference 14.

1.4.3 Laboratory Atmospheric Corrosion Testing

ASTM G85-A2, also known as MASTMAASIS (Modified ASTM Acetic Acid Salt Intermittent Spray) can be performed in two ways. Under wet bottom (WB) conditions, the cabinet drain is closed and several inches of water are added to the cabinet bottom. This water reservoir in the chamber bottom is supposed to cause relative humidity (RH) to rise during dwell or soak periods of the test. In contrast, the cabinet drain is open during dry bottom (DB) exposures, allowing the chamber floor to dry during dry air purge and dwell periods. Both variations of the test include a repeating sequence of wet and dry cycles, and use an acidified salt solution (pH 2.8

– 3.0). DB ASTM G85-A2 has been shown to work well for 3rd generation Al-Li alloys. In Figure 1.5, the AA2060 exfoliation ratings for ASTM G85-A2 testing follow the same trend as the seacoast exposure.[9]

Although ASTM G85-A2 is considered one of the best accelerated exfoliation tests for Al alloys, inconsistencies in results among different laboratories have been reported.[9,24] Unlike immersion tests, which tend to produce consistent results if the standard is carefully followed, the exposure conditions during cyclic salt spray testing can change significantly when different equipment brands run the same wet-dry cycle. Another issue was the lack of guidance for parameters that impact severity of testing. For example, a wide range of RH during each stage of testing is allowed by the standard.[25]

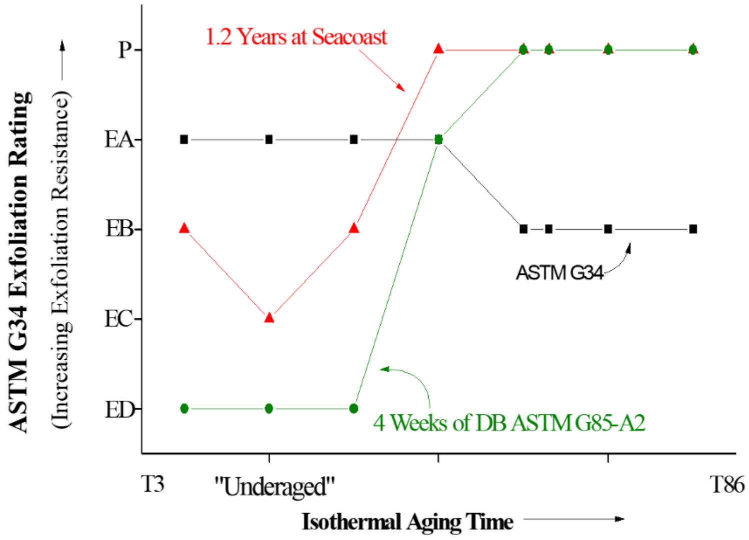

Figure 1.5: Exfoliation ratings for various AA2060 tempers after seacoast exposure at Point Judith RI, DB ASTM G85-A2, and ASTM G34. From reference 9.

Each of the standard tests described above is successful for one or more type of high-strength Al alloy, but there is not a strong scientific understanding of what makes a particular test effective for a particular alloy. Consequently, accelerated testing alone cannot be relied upon for new alloy development, and long-term seacoast exposures must be used to confirm the performance of new alloys.

1.5 Hypothesis

Although several accelerated corrosion tests exist for EC, different tests can produce drastically different results for the same alloy temper. Accelerated test design in the past has followed an Edisonian approach without a fundamental understanding of the role of each environmental parameter. Consequently, test design for new generation alloys such as AA2060 is labor intensive and time consuming. With a stronger understanding of the impact of key testing variables on exfoliation formation, future development of laboratory tests for new generation alloys can be based on the relationship between environmental parameters and electrochemical kinetics rather than trial and error.

In the current work, three accelerated tests for exfoliation were deconstructed (ASTM G34, ANCIT, and ASTM G85-A2) in terms of their key testing parameters. Factors studied under full-immersion conditions included exposure temperature, impact of added oxidizing agents, impact of solution pH, and impact of aluminum chloride ($AlCl_3$). For atmospheric corrosion testing, the role of RH and time of wetness (TOW) were investigated. A detailed description of relevant literature for each factor is included in the introduction sections of the chapters in this dissertation. After considering the current state of the field, the following hypothesis was chosen to provide the basis of this work.

- A moderate level of cathodic kinetics should be utilized during accelerated corrosion testing of Al-Cu-Li alloys such that excessive attack does not occur in the exfoliation resistant temper.

1.6 Objectives

The purpose of this work was to develop a fundamental understanding of the impact of the environmental parameters of three accelerate corrosion tests (ASTM G34, ANCIT, and ASTM G85-A2) on the exfoliation corrosion behavior of AA2060. Additionally, the impact of using alternative oxidizing agents in corrosion testing is investigated.

1.7 Organization of Dissertation

Different aspects of immersion and atmospheric corrosion testing were investigated in each chapter of this dissertation. Figure 1.6 presents a visual representation of the dissertation organization.

Chapter 1 is the introduction section, and this section presents concepts that are relevant to the project. The history of Al-Li alloy development is given, and the concept of exfoliation corrosion explained. The benefits and problems of several standard accelerated tests are also discussed in this section.

In Chapter 2, the behavior of AA2060-T3 and AA2060-T86 in ASTM G34 and ANCIT exposure tests was characterized. Neither test produced exfoliation in the susceptible -T3 temper within the standard exposure time, but exfoliation did form in AA2060-T3 after 7 days of exposure to ANCIT. An unrealistic degree of attack formed in the exfoliation-resistant -T86 temper during that time period. An initial screening of testing variables was performed using a half-fraction factorial design of experiments. It was found that the presence of nitrate (NO_3^-) had a statistically significant impact on both corrosion potential (E_{corr}) and polarization resistance (R_p). Solution pH also had a statistically significant impact on R_p. This work has been published in M.E. Parker, R.G. Kelly, "Investigation of the Impact of Accelerated Testing Variables on the Exfoliation Corrosion of AA2060." *Corrosion* 72, 11 (2016): p. 1342-1350.

Chapter 3 presents a more in depth look at the electrochemical role of each environmental parameter in ASTM G34 and ANCIT. A specific topic of interest was the behavior of AA2060-T3 in ANCIT, which formed exfoliation blisters much faster (7 days) than AA2060-T3 in ASTM G34 (4 weeks). It was found that in fresh testing solution, cathodic kinetics in ASTM G34 were faster than cathodic kinetics in ANCIT for both tempers. The low solution pH in fresh ASTM G34 solution (<1) provided fast cathodic kinetics through proton reduction. However, solution pH increased during testing, and after 24-h of immersion, cathodic kinetics were faster in the ANCIT solution than in the ASTM G34 solution. Anodic kinetics were impacted by exposure temperature and the presence of KNO_3. Anodic kinetics increased with increasing temperature, making exfoliation form faster during ANCIT exposures than during ASTM G34 exposures. The presence of KNO_3 actually decreased anodic kinetics by competing with Cl^- for sites within the protective oxide film on Al. Although these measurements were made under full immersion conditions, the results of this chapter provided a foundation for understanding the cyclic salt spray test (ASTM G85-A2). For example, it was shown in this chapter that the elevated temperature in ANCIT (52^{o}C) promoted exfoliation formation. The exposure temperature during ASTM G85-A2 was also elevated (49^o), and this elevated temperature most likely resulted in increased anodic kinetics and contributed to the acceleration of exfoliation.

In Chapter 4, the role of two oxidizing agents, hydrogen peroxide (H_2O_2) and potassium persulfate ($K_2S_2O_8$), in accelerated corrosion testing was investigated. Oxidizing agents are commonly used to accelerate corrosion kinetics during immersion testing, but different oxidizing agents can have different impacts on Al alloys. For example, KNO_3 acted as an oxidizing agent during ANCIT testing and generated faster cathodic kinetics than the oxygen reduction reaction, but KNO_3 also caused the anodic kinetics of AA2060 to slow. Investigating the impact of other oxidizing agents on the corrosion behavior of AA2060 provided a deeper understanding of the behavior of Al-Li alloys during immersion testing. H_2O_2 was found to be a powerful oxidizing agent, but it decomposed after being added to a test solution and could not be stored for more than a few hours before the concentration measurably decreased. $K_2S_2O_8$ was stable for days after mixing, but cathodic kinetics were not as fast for this species as they were for H_2O_2. The cathodic kinetics of $K_2S_2O_8$ were manipulated by decreasing solution pH and adding aluminum chloride ($AlCl_3$). Both of these changes increased cathodic kinetics, but the under-aged and near peak-aged tempers could not be distinguished after exposure to the solution containing $AlCl_3$ as they both formed pitting. In other solutions, intergranular corrosion (IGC) developed in the under-aged temper rather than pitting. Neither H_2O_2 nor $K_2S_2O_8$ were found to be appropriate for exfoliation testing of Al-Li alloys, but these oxidizers could be used to quickly distinguish between intergranular corrosion (IGC) and pitting susceptibility.

In Chapter 5, the behavior of AA2060-T3 and -T86 in dry bottom (DB) ASTM G85-A2 was characterized. Several techniques for measuring properties in-situ were presented, and the impact of relative humidity (RH) on time of wetness (TOW) and potential was investigated. It was found that the RH during DB ASTM G85-A2 dropped very low (17% - 20.5%) during the dry air purge and dwell periods of the repeating 6 hour cycle. The TOW sensor showed that drying did not occur instantaneously, and moisture was detected on the sensor until 1.5 - 4 hours after the start of the dry air purge. It should be noted, however, that salt accumulation on the sensor was much greater than on the AA2060 samples. It was difficult to determine the TOW specifically for the AA2060 samples, but visually these samples appeared to be dry 5 - 10 minutes after the start of the dry air purge. Open circuit potential (OCP) measurements showed that a transition in OCP profile occurred from day 2 to day 8 of the test. After 2 days, the OCP was stable during the salt spray cycle and decreased during the dry cycle. After 8 days of exposure, however, a potential peak was measured about 10 minutes into the dry air purge. It was hypothesized that this potential peak was a sign of increasing oxygen reduction kinetics as the electrolyte film on the sample decreased. The measurement techniques presented in this chapter were used to further deconstruct the ASTM G85-A2 test in Chapter 6. The work in presented in Chapter 5 has been published at M.E. Parker, R.G. Kelly. "Deconstructing DB ASTM G85-A2 Testing Environment with In-Situ Measurements" Corrosion 2017, (NACE International, 2017).

Chapter 6 presents a detailed comparison of the testing conditions and corrosion morphology after exposure to dry bottom (DB) and wet bottom (WB) ASTM G85-A2 using two different types of salt spray chambers. RH was found to play a critical role the formation of exfoliation. AA2060-T3 exfoliation under DB conditions was more severe in chamber Brand 1, which generated a moderate RH (72.9% to 79.9%) during the dry air and dwell periods when running DB ASTM G85-A2. In chamber Brand 2, RH during the dry air purge and dwell period was low (17% - 20.5%), and this caused corrosion kinetics to slow significantly. Under WB conditions in chamber Brand 1, RH was very high (86.5% - 87.8%) even during the dry air purge and dwell periods. Under these conditions, the no exfoliation blisters formed on the susceptible -T3 temper. At the very high RH, rinsing prevented corrosion products from accumulating on the sample and along grain boundaries, which was needed for exfoliation formation in AA2060-T3. After learning the importance of RH control during ASTM G85-A2 testing, two modified cyclic salt spray tests were designed. Both RH profiles utilized a 1 minute dry air purge and operated under WB conditions, but performing this program in two different chambers (both Brand 2) produced slightly different RH profiles. Mod WB 1 had an average RH of 61.5% during the dwell period, and Mod WB 2 had an average RH of 74% during the dwell period. Both modified tests produced exfoliation in the susceptible temper after just 12 days of exposure. This was much faster than the 4 weeks required by the standard test. AA7075 and AA2024 samples were also exposed to the modified tests, and both tests could distinguish between exfoliation-resistant and susceptible tempers.

Conclusions for the project are presented in Chapter 7, as well as the technological impact of the work. Chapter 8 presents recommended future work. Several interesting topics that could not be fully investigated in the current work are discussed in this section.

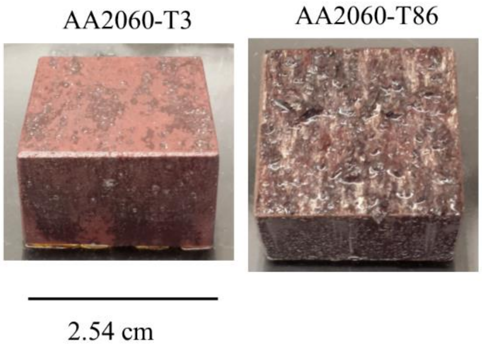

Chapter 2:
Investigating the Impact of Accelerated Testing Variables on the Exfoliation Corrosion of AA2060

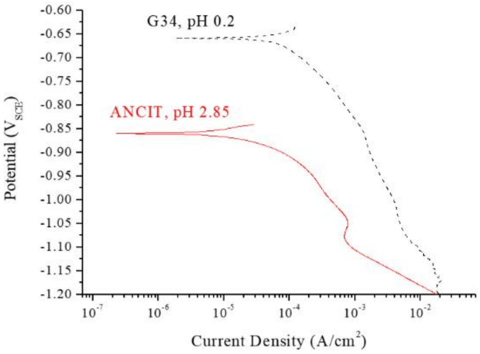

Chapter 3:
Deconstructing the Electrochemical Basis of ASTM G34 and ANCIT Immersion Tests

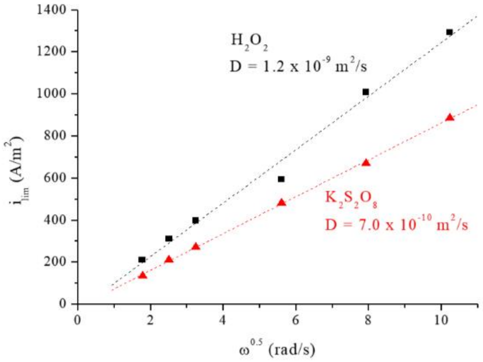

Chapter 4:
The Role of H_2O_2 and $K_2S_2O_8$ in Accelerated Corrosion Testing

Chapter 5:
Deconstructing DB ASTM G85-A2 Testing Environment with In-Situ Measurements

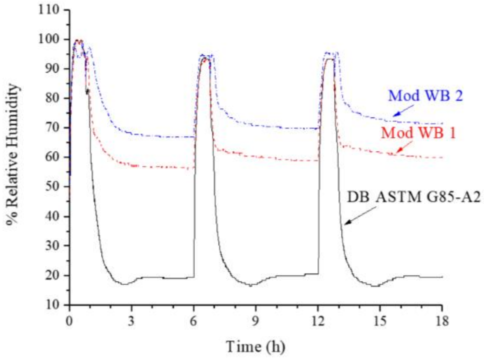

Chapter 6:
Improved Atmospheric Corrosion Testing for High-Strength Aluminum Alloys

Figure 1.6: Visualization of dissertation organization.

1.8 References

1. R.J. Rioja, J. Liu, *Metal. Mater. Trans. A* 43 (2012): p. 3325-3337.
2. T. Dursun, C. Soutis, *Mater. Design* 56 (2014): p. 862-871.
3. C. Giummarra, B. Thomas, R.J. Rioja, "New Aluminum Lithium Alloys for Aerospace Applications," Proceedings of the Light Metals Technology Conference (2007).
4. X. Zhang, W. Yang, R. Xiao, *Mater. Design* 88 (2015): p. 446-450.
5. B. Cai, Z.Q. Zheng, D.Q. He, S.C. Li, H.P. Li. "Friction Stir Weld of 2060 Al-Cu-Li Alloy: Microstructure and Mechanical Properties." *J. Alloys and Compounds.* 649 (2015): p. 19-27.
6. B.J. Connolly, "The Transition from Localized Corrosion to SCC of Al-Li-Cu Alloy AA2096 as a Function of Isothermal Aging Heat Treatment at 160°C" (Ph.D. diss., University of Virginia, 2002), p. 12-16.
7. R.G. Buchheit, J.P. Moran, G.E. Stoner, *Corrosion* 50, 2 (1994): p. 120-130.
8. D. Tsivoulas, *Met. Mat. Trans A* 46A (2015): p. 2342-2346.
9. J.P. Moran, F.S. Bovard, J.D. Chrzan, P. Vandenburgh, "Corrosion Performance of New Generation Aluminum-Lithium Alloys for Aerospace Applications," 13th Int. Conf. on Aluminum Alloys, held June 3-7, 2012 (Hoboken, NJ: John Wiley & Sons, Inc., 2012).
10. N. Ott, Y. Yan, S. Ramamurthy, S. Kairy, N. Birbilis, *Scrip. Mater.* 119 (2016): p. 17-20.
11. N. Ott, S.K. Kairy, Y. Yan, N. Birbilis. *Metallurgical Materials Tran. A.* 48A (2017): p. 51-56.
12. McCafferty, E. *Introduction to Corrosion Science*. Springer 2010, p. 188.
13. M.J. Robinson, *Corrosion Sci.* 23, 8 (1983): p. 887-899.
14. ASTM G34-1, "Standard Test Method for Exfoliation Corrosion Susceptibility in 2XXX and 7XXX Series Aluminum Alloys" (West Conshohocken, PA: ASTM International, 2001), p. 1-7.
15. D. McNaughtan, M. Worsfold, M.J. Robinson, Corrosion Sci. 45 (2003): p. 2377-2389.
16. G.N. Haidemenopoulos, N. Hassiotis, G. Papapolymerou, V. Bontozoglou, *Corrosion* 54, 1 (1998): p. 73-78.
17. P.V. Petroyiannis, E. Kamoutsi, AL. TH. Kermanidis, S.G. Pantelakis, V. Bontozoglou, GN. Haidemenopoulos, *Fatigue Fract. Engng. Mater. Struct.* 28 (2005): p. 565-574.

18. H. Kamoutsi, G.N. Haidemenopoulos, V. Bontozoglou, S. Pantelakis, *Corrosion Sci.* 48 (2006): p. 1209-1224.
19. J.R. Davis (Ed.), "Intergranular and Exfoliation Corrosion" In Corrosion of Aluminum and Aluminum Alloys (ASTM International, 1999) p. 69.
20. V.S. Agarwala, "Corrosion Monitoring of Shipboard Environments," in Degradation of Metals in the Atmosphere, eds. S.W. Dean and T.S. Lee, STP 965 (Philadelphia, PA: ASTM, 1988), p. 354-365.
21. ASTM G112-92, "Standard Guide for Conducting Exfoliation Corrosion Tests in Aluminum Alloys" (West Conshohocken, PA: ASTM International, 2015), p. 1-7.
22. D.O. Sprowls, J.D. Walsh, M.B. Shumaker, "Simplified Exfoliation Testing of Aluminum Alloys," in Localized Corrosion – Cause of Metal Failure, STP 516 (Philadelphia, PA: ASTM, 1971), p. 38-65.
23. S. Lee, B.W. Lifka, "Modification of the EXCO Test Method for Exfoliation Corrosion Susceptibility in 7XXX, 2XXX, and Aluminum-Lithium Alloys," in *New Methods for Corrosion Testing of Aluminum Alloys*, eds. V.S. Agarwala, G.M Ugiansky, STP 1134 (West Conshohocken, PA: ASTM International, 1992), p. 1-19.
24. F. Bovard, J. Tardiff, T. Jafolla, D. McCune, G. Courval, K.A. Smith, F. Lee, J. Repp, S. Ramamurthy, R.J. Shaffer, F.M. Vartolas. "Development of an Improved Cosmetic Corrosion Test for Finished Aluminum Autobody Panels" (Warrendale, PA: SAE, 2007). SAE Paper 2017-01-0417.
25. ASTM G85-02, "Standard Practice for Modified Salt Spray (Fog) Testing" (West Conshohocken, PA: ASTM International, 2002), p. 1-14.

2. Investigating the Impact of Accelerated Testing Variables on the Exfoliation Corrosion of AA2060

Summary:

In this chapter, the behavior of AA2060-T3 and AA2060-T86 in ASTM G34 and ANCIT exposure tests was characterized. Neither test produced exfoliation in the susceptible -T3 temper within the standard exposure time, but exfoliation did form in AA2060-T3 after 7 days of exposure to ANCIT. An unrealistic degree of attack formed in the exfoliation-resistant -T86 temper during that time period. An initial screening of testing variables was performed using a half-fraction factorial design of experiments. It was found that the presence of nitrate (NO_3^-) had a statistically significant impact on both corrosion potential (E_{corr}) and polarization resistance (R_p). Solution pH also had a statistically significant impact on R_p.

The work presented in this chapter has been reported in the following publication:

- M.E. Parker, R.G. Kelly. "Investigation the Impact of Accelerated Testing Variables on the Exfoliation Corrosion of AA2060." *Corrosion*. 72, 11 (2016): p. 1342-1350.

2.1 Abstract

Aluminum-lithium alloys are attractive for aerospace applications because of their improved strength-to-weight and stiffness-to-weight ratios, fracture toughness, and corrosion resistance compared to legacy alloys such as AA2024 and AA7075. Many standardized accelerated tests are used to evaluate the corrosion resistance of high-strength aluminum alloys, but these tests can produce drastically different results for the same alloy. The purpose of this study is to provide a quantitative, technical understanding of the roles of key testing variables in two accelerated tests for exfoliation corrosion, EXCO and ANCIT. Accelerated testing was performed on under-aged and near peak-aged tempers of aluminum-lithium alloy AA2060, and a five-factor design of experiments was used to determine the impact of key testing variables on the corrosion potential and polarization resistance of AA2060. It was found that ANCIT testing produced exfoliation in the susceptible temper (T3) in a much shorter time than EXCO testing did. ANCIT was also more aggressive toward the -T86 temper compared to EXCO. The design of experiments showed that the addition of an oxidizing agent (NO_3^-) to the testing solution had a statistically

significant impact on both corrosion potential and polarization resistance. The solution pH, as well as the interaction between solution pH and added oxidizing agent, had statistically significant effects on polarization resistance.

2.2 Introduction

Heat treatable high-strength aluminum alloys (Al alloys) have long been considered essential components of aircraft design.[1] The need to create more efficient and more cost-effective air transport has driven the development of new high-performance Al alloys with lower density and higher strength, stiffness, and fracture toughness. Corrosion resistance is also a critical property because aerospace structures are exposed to corrosive atmospheric conditions during service.

2.2.1 Accelerated Testing of Aluminum Alloys

Al alloys have good resistance to general corrosion as a result of a protective oxide film, but most Al alloys can experience localized corrosion damage such as pitting, intergranular corrosion (IGC), or exfoliation. Accelerated corrosion tests are used to evaluate the susceptibility of alloys to localized corrosion. It is crucial that accelerated tests accurately reproduce the corrosion behavior observed in service because they are used for material lot acceptance and new alloy and temper development.[2] Many standardized accelerated tests are currently used for evaluating localized corrosion susceptibility of high-strength Al alloys (ASTM Standards G34, G85, G110, and B117),[3-6] but these tests can produce drastically different results for the same alloy.[7]

The focus of the current work is to develop a framework for understanding the discrepancies between accelerated testing methods and for designing improved tests. Accelerated testing for exfoliation corrosion susceptibility of AA2060 (aluminum-lithium alloy)[8] will be used to illustrate this framework. This alloy has been studied by Moran, et al., who demonstrated that the -T3 temper is susceptible to exfoliation during seacoast exposures, while the -T86 (near peak-aged) temper is resistant.[7] Considering both a highly susceptible and a highly resistant temper will provide a basis for understanding the mechanisms at work in accelerated tests for exfoliation corrosion of this alloy.

2.2.2 Laboratory Tests for Exfoliation

Exfoliation is thought to occur in alloys with an elongated grain structure when voluminous corrosion products form along grain boundaries during IGC. The corrosion products provide a wedging stress that lifts the intact grains above to form exfoliation blisters.[9]

The accelerated tests for exfoliation of interest to this work include ASTM G34 (a constant immersion test called EXCO) and ANCIT (aluminum-nitrate-chloride-immersion test, a modified version EXCO).[3,10] Figure 2.1 shows the behavior of several AA2060 tempers after 1.2 y of seacoast exposure and after EXCO testing.[7] EXCO results did not correlate well with the seacoast results and even produced an opposite trend in terms of exfoliation resistance of AA2060 tempers. According to EXCO, the under-aged tempers appeared to have superior exfoliation resistance compared to the -T86 temper, but in the seacoast exposure, the -T86 temper was more resistant, as shown in Figure 2.2.

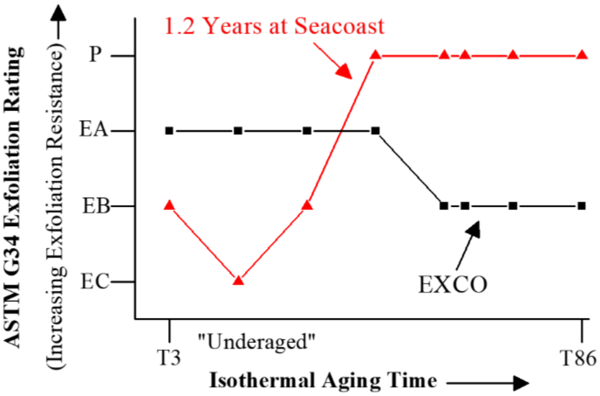

Figure 2.1: Exfoliation ratings for various tempers of AA2060 after seacoast exposure and EXCO testing. Adapted from reference 7.

EXCO fails to reproduce seacoast results for other aluminum-alloys as well. This was the motivation for the development of the ANCIT test. Lee, et al., observed that EXCO failed to produce expected results for 7X50, 2024 (UNS A92024(1)), or 2090 (UNS A92090) Al alloys.[10]

---

(1) UNS numbers are listed in *Metals and Alloys in the Unified Numbering System*, published by the Society of Automotive Engineers (SAE International) and cosponsored by ASTM International.

They thought this may be a result of the extremely low pH of the EXCO solution, and noted that after 24 h of immersion, the solution pH increased to about 3. The group also noticed that after 24 h, there were traces of aluminum ion (Al^+) resulting from dissolution of the metal. The testing environment for ANCIT was guided by these observations, but there is still not a fundamental understanding of what makes EXCO successful for some Al alloys and ANCIT successful for others.

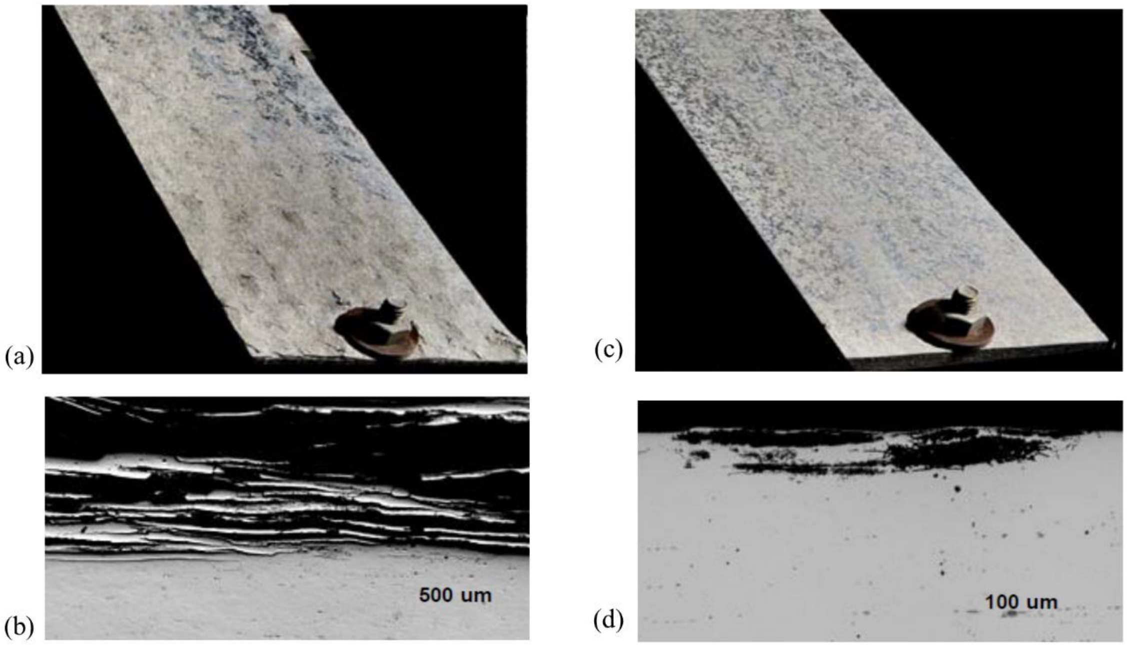

Figure 2.2: (a) Macro-photo and (b) micrograph of under-aged AA2060 after 1.2 years exposure at seacoast. (c) Macro-photo and (d) micrograph of commercial T8e86 AA2060 after 1.2 years exposure at seacoast. Images from reference 7.

2.2.3 Key Testing Variables in EXCO and ANCIT

In order to understand discrepancies in these accelerated exfoliation tests, ANCIT and EXCO were deconstructed in terms of their key testing variables. Four key variables were identified: the addition of oxidizing agents, the testing temperature, and the chloride content and pH of the testing solution. Both EXCO and ANCIT incorporate these variables at some level, but the tests have different values for some variables (e.g., pH of 0.4 vs. pH of 3.2).

2.2.4 Localized Corrosion Mechanisms in Al-Cu-Li Alloys

It is important to consider the various localized corrosion mechanisms for Al-Cu-Li alloys because exfoliation initiates from other forms of corrosion such as IGC. Intergranular attack in these alloys is generally attributed to the effects of hardening phases that form on grain boundaries. For alloys like AA2060, the primary hardening precipitate is the hexagonal T_1 phase (Al_2CuLi).[11-13] Both Connolly and Buchheit have reported that the T_1 phase tends to form on subgrain boundaries and matrix dislocations.[11,14] The precipitation of T_1 results in the creation of a Cu depleted zone; however, Buchheit, et al., showed that the T_1 phase is anodic with respect to both the matrix and the Cu depleted zone. They suggested that the corrosion mechanism was selective dissolution of the T_1 phase rather than of the Cu depleted zone.[14] However, commercially pure (99.99%) Al was used to simulate the Cu depleted zone in this study, and the role of Li in the matrix was not considered.

Many Al-Cu-Li alloys have a transition in IGC susceptibility during aging where under-aged tempers are more vulnerable to IGC than peak-aged and near peak-aged tempers. However, IGC susceptibility increases again upon over-aging. The improvement in IGC resistance at near peak-aged tempers correlates with an improvement in stress corrosion cracking and exfoliation resistance.[7,13] Recent work by Ott, et al., revealed some of the changes that occur in Al-Cu-Li alloy grain boundary chemistries upon aging. They found that in naturally aged AA2050, grain boundaries were depleted in Cu and highly enriched in Li compared to the matrix, which would lead to preferential dissolution of grain boundaries. The grain boundaries of the over-aged sample were enriched in Cu, which would create a Cu depleted area around the grain boundaries that is susceptible to attack.[13]

2.3 Experimental Procedures

2.3.1 Materials and Sample Preparation

The AA2060 used in this work was provided by Alcoa Inc. in the form of a 3.5 cm thick plate. This material was received in the -T3 (under-aged) and -T86 (near peak-aged) tempers, and the composition is shown in Table 2.1.[8] All samples were polished to a 1200 grit finish, cleaned ultrasonically in deionized water, and rinsed in ethanol before testing. Keller's etch was used to reveal grain boundaries before optical microscopy and scanning electron microscopy (SEM).

Table 2.1: AA2060 Composition (wt. %)

Li	**Cu**	**Mg**	**Ag**	**Zr**	**Mn**	**Zn**	**Al**
0.75	3.95	0.85	0.25	0.11	0.30	0.40	Bal.

2.3.2 EXCO (ASTM G34) Testing

EXCO, a constant immersion test, was performed according to ASTM G34[3] for the standard 4-d period, as well as modified testing times. AA2060-T3 samples were exposed for 4-d, 7-d, and 28-d, while AA2060-T86 was tested for 6-h, 4-d, and 7-d.

The EXCO testing environment included a solution of 4 M sodium chloride (NaCl), 0.5 M potassium nitrate (KNO_3), and 0.1 M nitric acid (HNO_3). This provided 0.6 M nitrate ion (NO_3^-), which is an oxidizing agent. The pH of this solution was 0.4, and the testing temperature was 25°C. Figure 2.3 shows the sample dimensions used for this test. Post-testing analysis included visual examination of exposed surfaces, as well as cross sectioning for optical microscopy. SEM was also used for select samples.

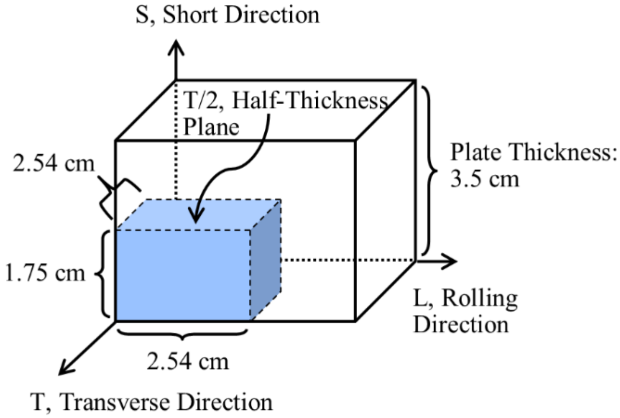

Figure 2.3: Schematic diagram showing the size and orientation of samples with respect to the original plate material.

2.3.3 ANCIT (Modified EXCO) Testing

ANCIT is a modified EXCO test that does not currently have an ASTM specification. This accelerated exfoliation test was developed to replace EXCO for some aluminum alloys.[10] The

ANCIT test solution was 4 M NaCl, 0.6 M KNO_3, and 0.0224 M $AlCl_3$, resulting in a solution pH of 3.2. This test operated at a temperature of 52°C. Both AA2060-T3 and AA2060-T86 were tested in ANCIT for the standard 2-d period and also for an extended time of 7-d. After testing, samples were examined visually and cross sectioned for optical microscopy.

2.3.4 Design of Experiments

A half-fractional factorial design of experiments (DOE) was used to investigate the impact of key testing variables on corrosion potential (E_{corr}) and polarization resistance (R_p). Five factors were considered in this DOE, requiring a total of 16 experiments. Replicates were not used in this study as the intention was to screen several factors in an efficient manner. A more in-depth study of the parameters found to be significant will be a topic of future work.

A summary of the five factors in this DOE are shown with their low and high values in Table 2.2. These were chosen after considering the testing environments of EXCO and ANCIT and include chloride concentration [Cl^-], solution pH, an added oxidizing agent [NO_3^-], testing temperature, and alloy temper. Minitab[†], a commercially available statistical software package by Minitab Inc., was used to generate a testing matrix from the high and low values of the five factors. A half-fractional factorial design was used to reduce the number of experiments necessary while maintaining good resolution.

Table 2.2: Summary of the Five Factors Used in Design of Experiments

Factor	High Level	Low Level
[Cl-]	4 M	1 M
Solution pH	5.6	0.4
Oxidizer (NO_3^-)	0.6 M	0 M
Temperature	52°C	30°C
Alloy Temper	T86	T3

[†] Trade name.

Electrochemical measurements were performed in a standard three-electrode cell using a saturated calomel reference electrode (SCE) and a platinum counter electrode. Corrosion potential (E_{corr}) and polarization resistance (R_p) were measured using a linear polarization scan starting at 0.05 V vs. open-circuit potential (OCP) and scanning down to –0.4 V_{OCP} at a rate of 0.5 mV/s. The scan was preceded by a 24-h OCP delay to allow the system to approach steady state. The solution for each of the 16 tests was outlined by the DOE, which specified a value for [Cl^-], [NO_3^-], solution pH, testing temperature, and alloy temper.

After E_{corr} and R_p were measured, these data were entered into the commercial software for analysis. The average effect of single factors and two-factor interactions on E_{corr} and R_p were calculated. The threshold for statistical significance was determined using Lenth's pseudo-standard error (PSE), which is a standard method for studies without replicates. To calculate the threshold, Lenth's PSE was multiplied by the t-value at $\alpha = 0.05$ and degrees of freedom, df = 5. This method is described in detail elsewhere.[15]

2.4 Results

2.4.1 EXCO (ASTM G34) Results

EXCO results after 4-d and 7-d of testing (Figure 2.4) did not correlate well with observations at seacoast (Figure 2.2). The -T3 temper, which has been shown to exfoliate during seacoast exposures,[7] formed no exfoliation blisters visible to the naked eye. In contrast, the -T86 temper, which is resistant to exfoliation at seacoast, had a flaky appearance. Cross sections after 7-d of testing revealed grain lifting on the T/2 plane of both tempers (Figure 2.5 [a] and [b]), which is an indication of exfoliation. In addition, cross sections shown in Figure 2.5(c) and (d) show that attack from the ST plane was hairline IGC for the -T3 temper and selective grain attack (SGA) for the -T86 temper. SGA was identified by locating partially dissolved grains where dissolution did not cross over grain boundaries. An example of SGA is circled in Figure 2.5(d).

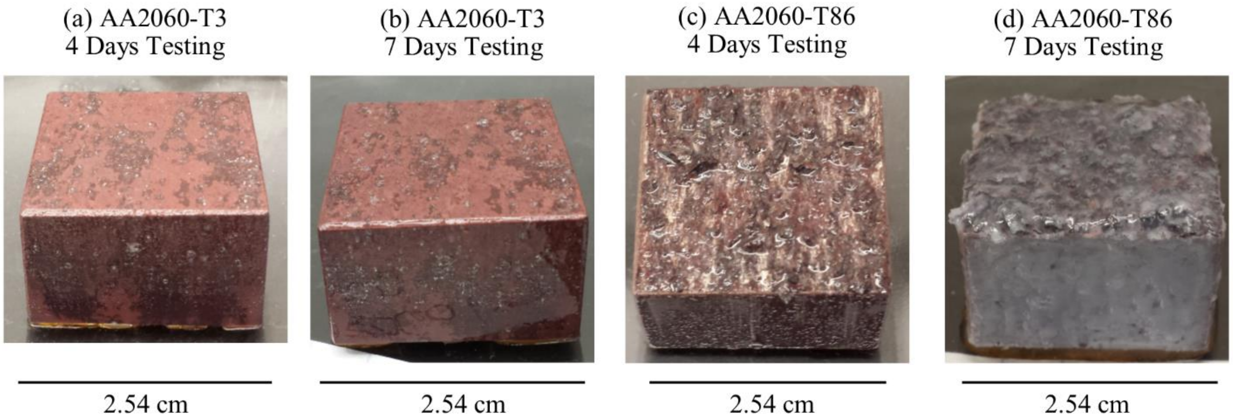
(a) AA2060-T3
4 Days Testing

(b) AA2060-T3
7 Days Testing

(c) AA2060-T86
4 Days Testing

(d) AA2060-T86
7 Days Testing

Figure 2.4: The T/2 surface after EXCO testing of (a) AA2060-T3 for 4 days, (b) AA2060-T3 after 7 days, (c) AA2060-T86 for 4 days, and (d) AA2060-T86 for 7 days. Exfoliation blisters visible to the naked eye did not form on the susceptible -T3 temper even after 7 days of testing. After 4 days of EXCO testing, the resistant -T86 temper had a flaky appearance.

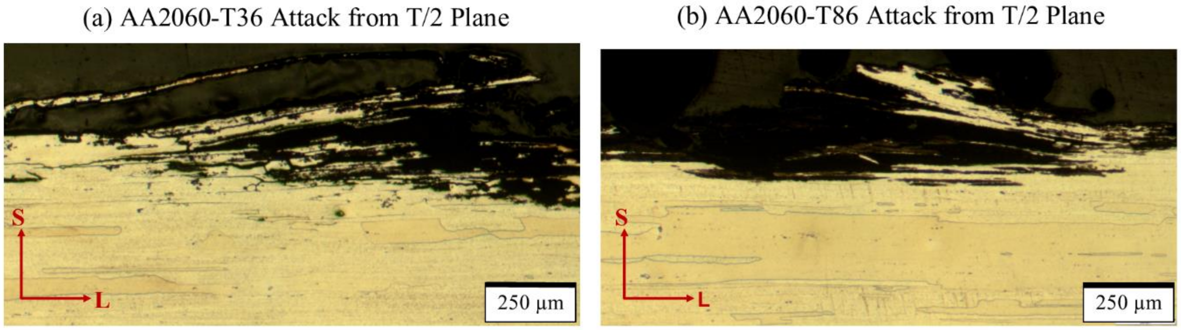
(a) AA2060-T36 Attack from T/2 Plane

(b) AA2060-T86 Attack from T/2 Plane

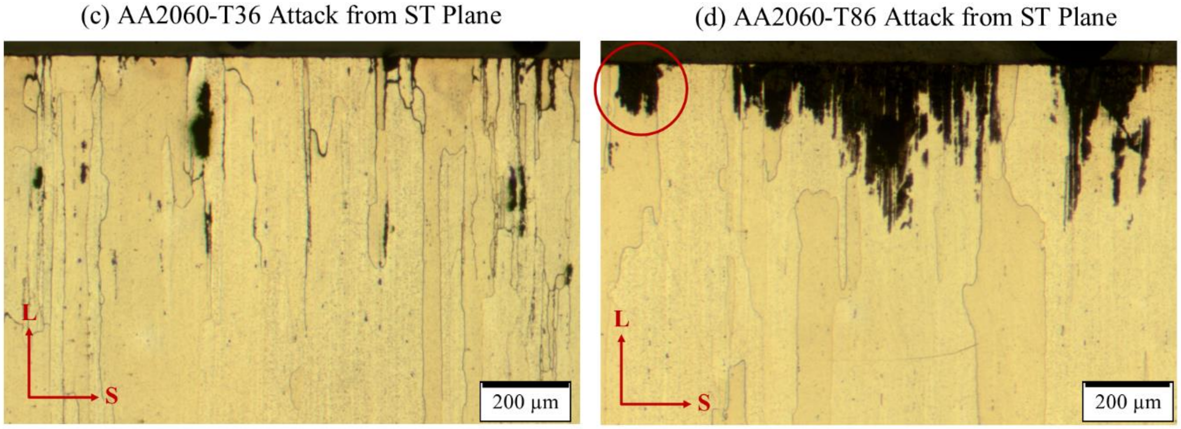
(c) AA2060-T36 Attack from ST Plane

(d) AA2060-T86 Attack from ST Plane

Figure 2.5: Micrographs showing attack from the T/2 plane on (a) AA2060-T3 and (b) AA2060-T86, and from the ST plane on (c) AA2060-T3 and (d) AA2060-T86 after 7 days of EXCO testing. An example of SGA is circled in red.

Although there were no exfoliation blisters visible to the naked eye on the AA2060-T3 sample after 7-d of testing, the cross section shown in Figure 2.5(a) indicated that exfoliation had initiated. Testing time was extended to 4 weeks for this sample in order to determine if more significant exfoliation attack would form with longer exposure time. Figure 2.6(a) shows that large exfoliation blisters formed on the T/2 surface of AA2060-T3 after 4 weeks of EXCO testing. The cross section in Figure 2.6(b) confirms the presence of significant grain lifting.

Additional testing was performed on the -T86 temper to better understand the early stages of attack in this material. Testing time was only 6 h, and Figure 2.7(a) shows the attack on the T/2 surface after this period. Blisters on this sample were small and difficult to see without magnification, but SEM imaging confirmed the presence of blisters on the T/2 surface (Figure 2.7[b]). The optical microscopy showed grain lifting associated with a blister (Figure 2.7[c]).

Figure 2.6: (a) Photo and (b) micrograph of AA2060-T3 after 4 weeks of EXCO testing. Grain lifting and exfoliation blisters are visible on the T/2 surface.

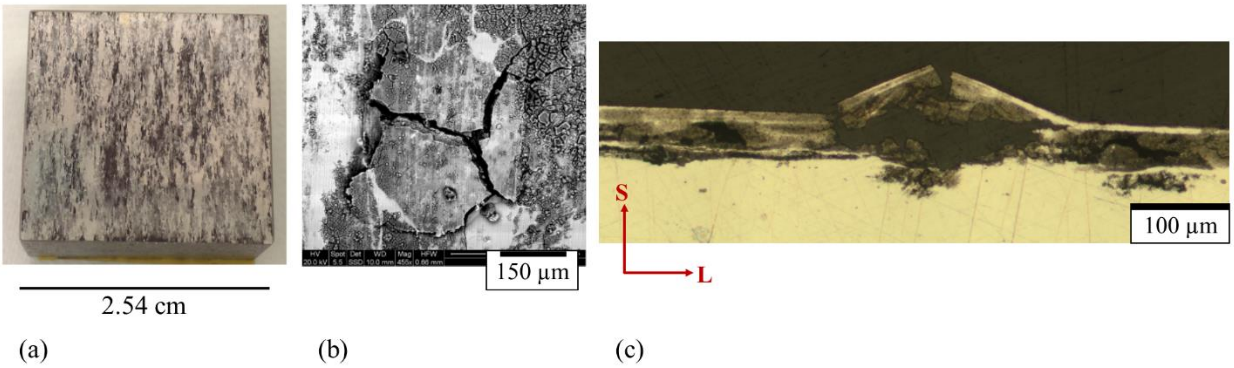

Figure 2.7: (a) Photo, (b) SEM micrograph, and (c) optical micrograph showing attack on the T/2 surface of AA2060-T86 after 6 hours of EXCO testing. (b) Shows an exfoliation blister from the top and (c) shows grain lifting in cross-section.

2.4.2 ANCIT Results

Neither AA2060-T3 nor -T86 showed signs of exfoliation blisters after 2-d of testing, but they both were covered in powdery corrosion product (Figure 2.8[a] and [c]). However, the tempers were easily distinguishable after 7-d of testing. The -T3 temper formed severe exfoliation attack on the T/2 surface, and cross sections confirmed the presence of significant grain lifting (Figure 2.8[b] and Figure 2.9[a]). The -T86 temper also experienced severe corrosion attack, but no exfoliation blisters were visible. The cross section for the -T86 temper showed deep pitting (Figure 2.9[c]), and selective grain attack was revealed at higher magnification (Figure 2.9[d]).

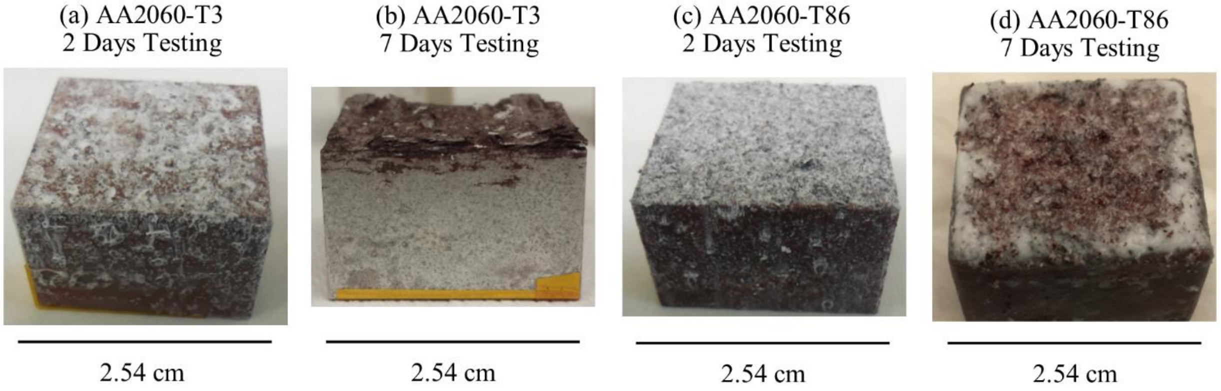

Figure 2.8: Photos of the T/2 surface after ANCIT testing of (a) AA2060-T3 for 2 days, (b) AA2060-T3 for 7 days, (c) AA2060-T86 for 2 days, and (d) AA2060-T86 for 7 days. Samples were indistinguishable after the standard testing time of 2 days, but severe exfoliation is visible on the AA2060-T3 sample after 7 days.

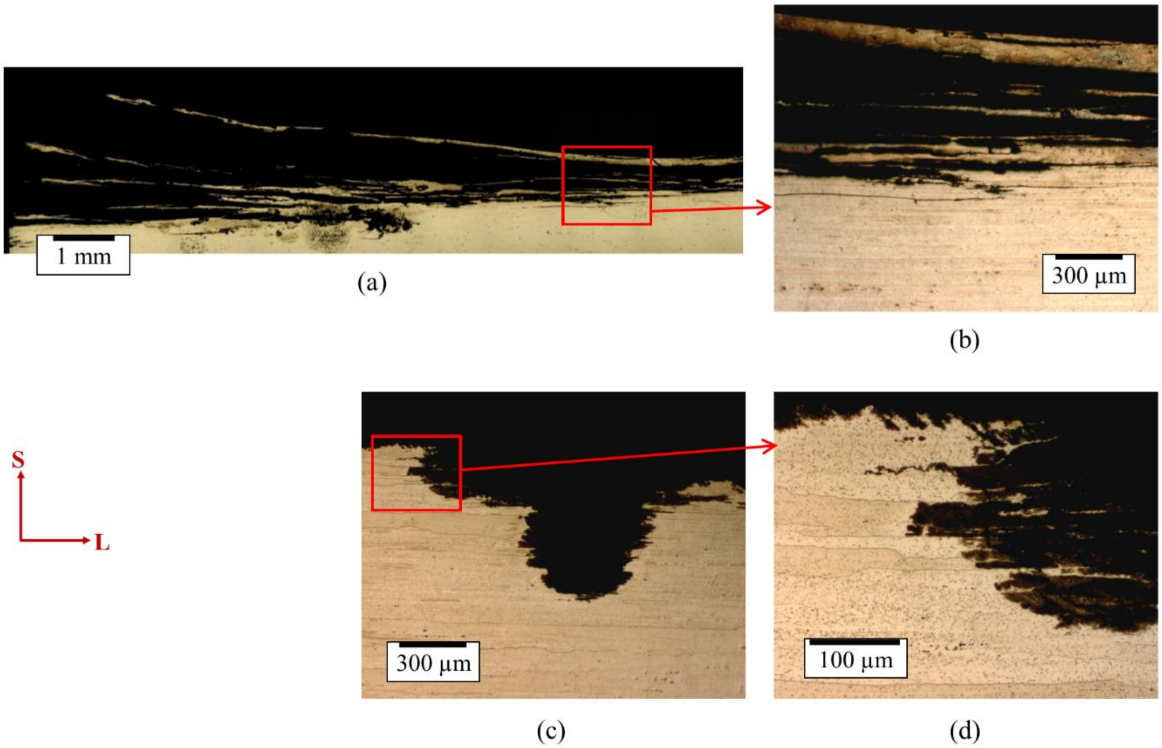

Figure 2.9: (a) Micrograph showing attack on the T/2 surface of AA2060-T3 after 7 days of ANCIT testing, higher magnification shown in (b). (c) Micrograph showing attack on the T/2 surface of AA2060-T86 after 7 days of ANCIT testing, higher magnification shown in (d).

2.4.3 Design of Experiments Results

A half-fractional factorial design of experiments was used to find the average effect of the four key testing variables on electrochemical parameters. Figure 2.10(a) and (b) show the Pareto chart of effects for the corrosion potential (E_{corr}) and polarization resistance (R_p), respectively. It was found that factor C, the addition of an oxidizing agent (0.6 M NO_3^-) to the testing solution, was the only variable to have a statistically significant impact on E_{corr}. Factor A (solution pH), factor C (the addition of an oxidizing agent), and the AC interaction all had a statistically significant effect on R_p. Table 2.3 shows a summary of the average effects for all single factors and two-factor interactions. A positive effect indicated that an increase in that factor led to an increase in the corresponding measured outcome (E_{corr} or R_p). A negative effect meant that an increase in that factor resulted in a decrease in the measured outcome.

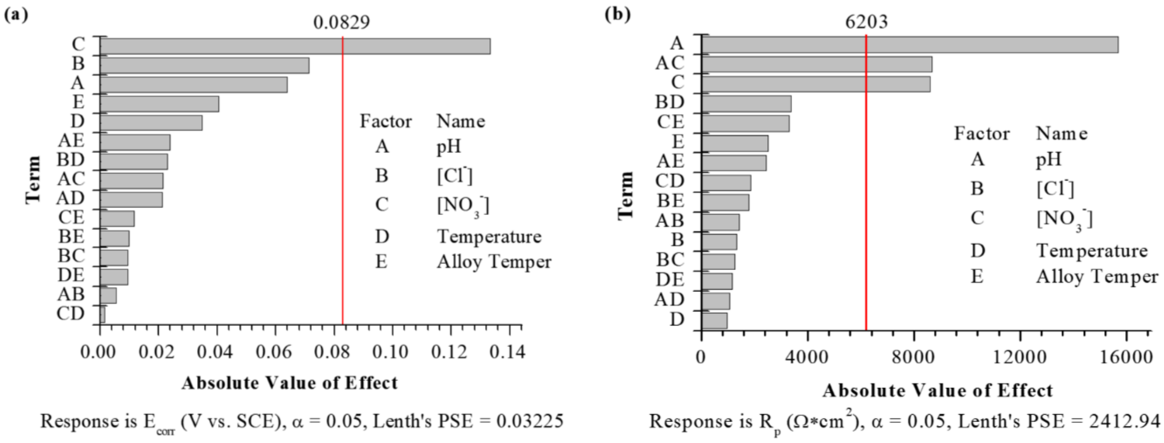

Figure 2.10: Pareto chart of the effects for (a) Ecorr and (b) Rp. Factor C (addition of 0.6 M NO3-) was found to have the most significant impact on Ecorr, while factors A (pH), C (addition of 0.6 M NO3-), and AC interaction had the most effect on Rp.

Table 2.3: Summary of the Average Effect of Factors on Ecorr and Rp

Effect on E_{corr} (V vs. SCE)			**Effect on R_p (Ω-cm^2)**		
Factor	**Label**	**Average Effect**	**Factor**	**Label**	**Average Effect**
$[NO_3^-]$	C	0.1334	pH	A	15693
$[Cl^-]$	B	-0.0714	pH*$[NO_3^-]$	AC	-8679
pH	A	-0.0639	$[NO_3^-]$	C	-8609
Temper	E	-0.0404	$[Cl^-]$*Temperature	BD	3375
Temperature	D	-0.0349	$[NO_3^-]$*Temper	CE	3298
pH*Temper	AE	0.0239	Temper	E	-2524
$[Cl^-]$*Temperature	BD	-0.0231	pH*Temper	AE	-2442
pH*$[NO_3^-]$	AC	0.0216	$[NO_3^-]$*Temperature	CD	-1876
pH*Temperature	AD	0.0214	$[Cl^-]$*Temper	BE	-1791
$[NO_3^-]$*Temper	CE	0.0116	pH*$[Cl^-]$	AB	1426
$[Cl^-]$*Temper	BE	0.0099	$[Cl^-]$	B	1341
Temperature*Temper	DE	0.0094	$[Cl^-]$*$[NO_3^-]$	BC	-1255
$[Cl^-]$*$[NO_3^-]$	BC	-0.0094	Temperature*Temper	DE	-1176
pH*$[Cl^-]$	AB	0.0054	pH*Temperature	AD	1059
$[NO_3^-]$*Temperature	CD	0.0016	Temperature	D	975
Threshold for Statistical Significance		0.0829	**Threshold for Statistical Significance**		6203

2.5 Discussion

2.5.1 Comparison of Accelerated Tests

Exfoliation behavior for AA2060-T3 and -T86 in EXCO did not agree with the seacoast results for this alloy reported by Moran, et al.[7] The -T3 temper, which has been shown to form exfoliation within 1.2 y of exposure at seacoast, did not form blisters that were visible to the naked eye after 7-d of EXCO testing. In contrast, the -T86 temper experienced more severe attack than the -T3 temper and had a flakey appearance.

A better understanding of the attack morphology was gained using optical microscopy. Both samples exhibited the grain lifting associated with exfoliation,[10] indicating that exfoliation had initiated in both tempers. This was confirmed for the -T3 temper as large exfoliation blisters formed on this sample with extended testing time (4 weeks). However, exfoliation blisters were not expected in the -T86 temper as there was no evidence of intergranular attack in this material after EXCO testing, and exfoliation is usually thought to begin with IGC.[10] Figure 2.5(d) showed that corrosion did not proceed along grain boundaries in the -T86 temper, and the observed attack was better explained by selective dissolution of susceptible grains or possibly selective dissolution of subgrains. Because this material was rolled as a part of its thermomechanical processing, subgrains could be quite narrow in the S direction. It is possible that attack along narrow subgrains could produce wedging forces similar to that generated by IGC. EXCO testing of the -T86 temper for 6 h demonstrated that small blisters formed quickly in this material, providing additional evidence that the attack morphology could be considered exfoliation.

Like EXCO, ANCIT failed to predict the exfoliation behavior of AA2060 within the standard testing time (2-d). However, after 7-d of testing, severe exfoliation was observed on the -T3 temper. The attack on the -T86 temper was very severe after ANCIT testing, but the morphology was pitting rather than exfoliation. It is not yet well understood why exfoliation on AA2060-T3 forms must faster in ANCIT than in EXCO, but there are only a few differences between the two tests that could be responsible. The chloride and nitrate concentrations are the same in both tests, but the solution pH is higher in ANCIT (3.2 vs. 0.4), the temperature is higher (52°C vs. 25°C), and there is a small addition of aluminum chloride to the ANCIT testing solution (0.0224 M). Investigating the impact of temperature, pH, and $AlCl_3$ on the attack rate and morphology of AA2060 will be an area of future work.

The hairline IGC observed in the -T3 temper was most likely caused by segregation of Li to the grain boundaries, which was reported by Ott et al. to occur in under-aged AA2050.[13] Hairline IGC can occur in aluminum alloys even when the anodic pathway along the grain boundaries is non-continuous. For example, Lim et al.[19] reported that IGC could propagate in AA5XXX alloys even on grain boundaries with low β-phase coverage (β-phase is anodic to the matrix and causes IGC susceptibility). It has been proposed that IGC propagates in AA5XXX alloys even in the absence of a continuous anodic path because an aggressive fissure solution chemistry develops when β-phase dissolves.[19]

2.5.2 Design of Experiments

The design of experiments showed that the addition of an oxidizing agent to the testing solution (0.6 M NO_3^-) had a statistically significant impact on both corrosion potential and polarization resistance. In general, the presence of NO_3^- resulted in an increase in E_{corr} and a decrease in R_p. The decrease R_p corresponds to an increase in corrosion current, i_{corr}, as these two parameters are inversely proportional. Using mixed potential theory, the simultaneous increases in E_{corr} and i_{corr} indicate an increase in cathodic kinetics. The cathodic kinetics of this system are usually limited by the diffusion of oxygen to the corroding surface, but the addition of 0.6 M NO_3^- provided a cathodic reaction faster than oxygen reduction, leading to an increase in both E_{corr} and i_{corr}.

It was also shown that the solution pH had a statistically significant effect on polarization resistance. Making the pH more acidic resulted in lower R_p, which corresponds to a higher i_{corr}. This may have been a result of thinning of the oxide layer on aluminum at low pH, which would increase the diffusion limiting current of oxygen reduction on aluminum and increase i_{corr}.

The interaction of solution pH and the added oxidizer also had a statistically significant impact on polarization resistance, where a simultaneous increase in solution pH and addition of the oxidizer resulted in a decrease in R_p. When pH was considered alone, an increase in pH (more alkaline solution) actually led to an increase in R_p. However, the interaction of factors sometimes leads to a different result than those factors individually.

These results demonstrate the potential for tuning an accelerated test to provide particular electrochemical kinetics by increasing or decreasing the levels of added oxidizer and solution pH. Other authors have reported that some aluminum alloys have IGC susceptibility only within a particular range of potentials.[16-18] Exfoliation of AA2060-T3 initiates with IGC, and it is possible that exfoliation will form within a specific potential range as well. In that case, the ability to adjust electrochemical kinetics by changing the levels of oxidizing agent and solution pH would be helpful in accelerated test design. Areas of future work will be identifying the potential range for exfoliation susceptibility of AA2060 and designing modified accelerated tests with better correlation to seacoast exposure results.

2.6 Conclusions

The findings of this study can be summarized as follows:

- Neither EXCO nor ANCIT predicted the exfoliation behavior of AA2060 tempers at seacoast during the standard testing time.
- Exfoliation formed in AA2060-T3 after 4 weeks of EXCO exposure.
- AA2060-T86 experienced some grain lifting after 4-d of EXCO exposure, most likely as a result of corrosion product buildup along susceptible subgrains. Small blisters were observed on this sample even after just 6 h of EXCO testing.
- Exfoliation of AA2060-T3 occurred more quickly during ANCIT testing (7-d) than in EXCO testing (4 weeks).
- Out of the five factors used in the design of experiments, adding nitrate, an oxidizing agent, to the testing solution had the most significant impact on corrosion potential. The polarization resistance was most affected by the solution pH, the addition of an oxidizing agent, and the interaction of these two factors.

2.7 Acknowledgments

This work was supported by Rolls-Royce and the Office of the Undersecretary of Defense Corrosion University Pilot Program, Contract #: W911NF-14-2-0005. The authors would also like to recognize Srishti Shrivastava for her assistance with microscopy.

2.8 References

1. E.A. Starke Jr., J.T. Staley, *Prog. Aerospace Sci.* 32 (1996): p. 131-172.

2. K.R. Baldwin, C.J.E. Smith, *Aircraft Eng. Aerospace Tech.* 71, 3 (1999): p. 239-244.

3. ASTM G34-1, “Standard Test Method for Exfoliation Corrosion Susceptibility in 2XXX and 7XXX Series Aluminum Alloys” (West Conshohocken, PA: ASTM International, 2001), p. 1-7.

4. ASTM G85-02, “Standard Practice for Modified Salt Spray (Fog) Testing” (West Conshohocken, PA: ASTM International, 2002), p. 1-14.

5. ASTM G110-92, “Standard Practice for Evaluating Intergranular Corrosion Resistance of Heat Treatable Aluminum Alloys by Immersion in Sodium Chloride + Hydrogen Peroxide Solution” (West Conshohocken, PA: ASTM International, 2003), p. 1-3.

6. ASTM B117-03, “Standard Practice for Operating Salt Spray (Fog) Apparatus” (West Conshohocken, PA: ASTM International, 2011), p. 1.

7. J.P. Moran, F.S. Bovard, J.D. Chrzan, P. Vandenburgh, “Corrosion Performance of New Generation Aluminum-Lithium Alloys for Aerospace Applications,” 13th Int. Conf. on Aluminum Alloys, held June 3-7, 2012 (Hoboken, NJ: John Wiley & Sons, Inc., 2012).

8. R.J. Rioja, J. Liu, *Metal. Mater. Trans. A* 43 (2012): p. 3325-3337.

9. M.J. Robinson, *Corros. Sci.* 22, 8 (1982): p. 775-790.

10. S. Lee, B.W. Lifka, “Modification of the EXCO Test Method for Exfoliation Corrosion Susceptibility in 7XXX, 2XXX, and Aluminum-Lithium Alloys,” in *New Methods for Corrosion Testing of Aluminum Alloys*, eds. V.S. Agarwala, G.M Ugiansky, STP 1134 (West Conshohocken, PA: ASTM International, 1992), p. 1-19.

11. B.J. Connolly, “The Transition from Localized Corrosion to SCC of Al-Li-Cu Alloy AA2096 as a Function of Isothermal Aging Heat Treatment at 160°C” (Ph.D. diss., University of Virginia, 2002), p. 12-16.

12. Ph. Lequeu, K.P. Smith, A. Daniélou, *J. Mater. Eng. Perform.* 19, 6 (2010): p. 841-847.

13. N. Ott, Y. Yan, S. Ramamurthy, S. Kairy, N. Birbilis, *Scrip. Mater.* 119 (2016): p. 17-20.

14. R.G. Buchheit, J.P. Moran, G.E. Stoner, *Corrosion* 50, 2 (1994): p. 120-130.

15. D.G. Montgomery, *Design and Analysis of Experiments,* 5th ed. (New York, NY: Wiley, 2001), p. 228-231, 254-255.

16. J.R. Galvele, S.M. de De Micheli, *Corros. Sci.* 10 (1970): p. 795-807.

17. I.L. Muller, J.R. Galvele, *Corros. Sci.* 17 (1977): p. 179-193.

18. W. Zhang, G.S. Frankel, *Electrochim. Acta* 48 (2003): p. 1193-1210.

19. M.L.C. Lim, R.G. Kelly, J.R. Scully, *Corrosion* 72, 2 (2016): p. 198-220.

3. Deconstructing the Electrochemical Basis of ASTM G34 and ANCIT Immersion Tests

Summary:

This chapter presents a more in depth look at the electrochemical role of each environmental parameter in ASTM G34 and ANCIT. A specific topic of interest was the behavior of AA2060-T3 in ANCIT, which was shown in Chapter 2 to form exfoliation blisters much faster than AA2060-T3 in ASTM G34. It was found that in fresh testing solution, cathodic kinetics in ASTM G34 were faster than cathodic kinetics in ANCIT for both tempers. The low solution pH in fresh ASTM G34 solution (<1) provided fast cathodic kinetics through proton reduction. However, solution pH increased during testing, and after 24-h of immersion, cathodic kinetics were faster in the ANCIT solution than in the ASTM G34 solution. Anodic kinetics were impacted by exposure temperature and the presence of KNO_3. Anodic kinetics increased with increasing temperature, making exfoliation form faster during ANCIT exposures than during ASTM G34 exposures. The presence of KNO_3 actually decreased anodic kinetics by competing with Cl^- for sites within the protective oxide film on Al. Although these measurements were made under full immersion conditions, the results of this chapter provided a foundation for understanding the cyclic salt spray test (ASTM G85-A2). For example, it was shown in this chapter that the elevated temperature in ANCIT (52^{o}C) promoted exfoliation formation. The exposure temperature during ASTM G85-A2 was also elevated (49^o), and this elevated temperature most likely resulted in increased anodic kinetics and contributed to the acceleration of exfoliation.

3.1 Abstract

ASTM G34 and ANCIT are both full immersion tests intended for measuring exfoliation susceptibility of aluminum alloys (Al alloys). ASTM G34 works well for certain 7XXX series alloys such as 7178 and 7075, but this test fails to reproduce the attack observed in natural environments for many other Al alloys. ANCIT was designed to replace ASTM G34 for alloys such as 7050, 7150, 2024, and 2090, but even this improved test does not correlate well with seacoast for the newest generation aluminum-copper-lithium (Al-Cu-Li) alloys. The purpose of the current work is to deconstruct ASTM G34 and ANCIT and explain the electrochemical impact of each testing variable. Understanding the role of each component of the testing environment will

allow more intelligent design of future immersion tests, reducing the need for time consuming trial and error. It was found that cathodic kinetics in fresh ASTM G34 solution were driven primarily by H^+ reduction due to the low solution pH (0.2 - 0.4), but cathodic kinetics were dominated by NO_3^- reduction in ANCIT solution. The small amount of $AlCl_3$ present in ANCIT solution seemed to impact the mechanism by which NO_3^- was reduced, but the origin of this effect was not well understood. The presence of NO_3^- slowed anodic kinetics, but this effect was more significant for AA2060-T3 than for AA2060-T86. The elevated temperature during ANCIT exposure increased anodic kinetics, and this was identified as the key difference between the two tests that caused exfoliation to form faster in ANCIT than in ASTM G34. Although the solution pH started out much lower in ASTM G34 (0.2 - 0.4) than in ANCIT (2.8 - 3.2), the pH increased during the first 24-h of ASTM G34 resulting in a similar solution chemistry for the remainder of testing time in both tests. The evolution of solution chemistry had implications for cathodic kinetics as the fast H^+ reduction kinetics in ASTM G34 was a result of the low solution pH in fresh solution.

3.2 Introduction

Exfoliation corrosion (EC) is a form of localized corrosion that can be life limiting for high-strength aluminum alloys. Several accelerated corrosion tests for EC exist (ASTM G34, ANCIT, ASTM G85-A2), but these tests produce different results for the same alloy temper. The current study deconstructs the electrochemical basis of two constant immersion tests (ASTM G34 and ANCIT) to provide an understanding of the discrepancies in testing results.

3.2.1 History of ASTM G34 and ANCIT

ASTM G34, also known as the EXCO exfoliation test, was first used in the early 1970s as a full immersion test for measuring exfoliation susceptibility of aluminum alloys.[1] Exfoliation corrosion (EC) occurs in rolled or extruded alloys that have an elongated grain structure. Localized attack along grain boundaries or other microstructural features produces voluminous corrosion products that put pressure on the elongated grains. This early stage of attack is referred to as an exfoliation blister. As attack progresses, the wedging force from corrosion products may lift grains upward and expose more area to aggressive solution.[2-4]

Several possible solution chemistries were considered during the development of ASTM G34, but after a round robin test program, the solution 4.0 M NaCl, 0.5 M KNO_3, and 0.1 M HNO_3

was found to produce consistent results. Another test developed in this same study was the ASSET test (1.0 M NH_4Cl, 0.25 M NH_4NO_3, 0.01 M $C_4H_{12}N_2O_6$, and 10 ml hydrogen peroxide per liter of solution). The ASSET test was recommended for 5086 and 5456 aluminum alloys, while EXCO was developed for Al-Zn-Mg-Cu alloys such as 7178 and 7075. Both of these tests incorporated the combination of a chloride compound and a nitrate compound, and Sprowls et al. emphasized the importance of using the correct ratio of Cl^- to NO_3^-.[1] This use of Cl^- and NO_3^- was derived from a stress corrosion cracking test for "Duralumin," which is an early trade name for aluminum-copper alloys.[5] The purpose of this test was to drive intergranular corrosion and minimize general corrosion while the sample was under stress so that the tendency for stress corrosion cracking could be quickly evaluated. Zaretskii et et al.[5] explored several solution chemistries with different Cl^-:NO_3^- ratios and settled on a solution of 4 M NaCl, 0.1 M HNO_3, and 0.5 M KNO_3 (later used as the basis for the EXCO test). The authors proposed that the importance of NO_3^- was in its role as a "depolarizer." This outdated term refers to a substance which oxidizes H_2 to form water. Most species once thought of as depolarizers are now called oxidizing agents, which facilitate the oxidation of another species by accepting one or more electrons from that species.

Once EXCO became an ASTM standard (G34)[6], it was approved for 7XXX and 2XXX series alloys, and this test is still used today to evaluate exfoliation susceptibility of 7XXX and 2XXX series alloys. However, it was soon found that ASTM G34 could not be extended to all 2XXX and 7XXX series alloys. Lee and Lifka demonstrated that ASTM G34 results could not differentiate between exfoliation-resistant and susceptible tempers of 7050, 7150, 2024, and 2090.[7] The authors claimed that G34 caused too much general corrosion in both tempers, making it difficult to distinguish the presence of exfoliation by visual inspection of the surface after testing. In some cases, the G34 test would cause more attack in the exfoliation-resistant temper than the exfoliation susceptible temper. The fast rate of general corrosion was attributed to the very low starting pH (reported as 0.4) of the G34 solution, so Lee and Lifka set out to design an improved immersion test at a more moderate pH.

This improved test, which later became known as ANCIT, was based on the solution chemistry measured after AA7150 was immersed in G34 solution for a 24-h period, as that was the time needed for the solution pH to stabilize at around 3.2. In addition to the NaCl, KNO_3, and HNO_3 in the original solution, four predominate species were detected in the solution including

Al^{3+}, Mg^{2+}, Zn^{2+}, and Cu^{2+}. All of these were present in the 7150 alloy composition and entered the test solution as corrosion processes occurred. Out of all the cations observed, Al^{3+} was present in the largest amount (604 mg/L). Lee and Lifka investigated the impact of each of the cations on the exposure results and found that the addition of 604 mg/L of Al^{3+} (added as $AlCl_3{\bullet}6H_2O$) to a solution of 4 M NaCl and 0.6 M KNO_3 provided a good distinction between exfoliation-resistant and exfoliation-susceptible tempers of 7150. However this test was not aggressive enough for the 2024 or 2090 and the testing temperature was increased from room temperature to 52°C. No mechanism for the role of Al^{3+} in this system was proposed. The final "best modified" testing procedure was to use a solution of 4 M NaCl, 0.6 M KNO_3, and 0.0224 M $AlCl_3{\bullet}6H_2O$ with a solution pH between 2.8 and 3.2. For 7XXX series alloys room temperature was recommended, while for 2XXX series alloys elevated temperature (52°C) was recommended. This "best modified" test was later named ANCIT.

Recent work has shown that even the "best modified" ANCIT test can fail when used for new generation Al-Cu-Li alloys. Parker et al. showed that while ANCIT did produce severe exfoliation in the susceptible under-aged T3 temper of AA2060 after 7-days of exposure, the attack on the resistant T86 temper was much more severe than that displayed after seacoast exposures.[8] This result demonstrates the continual need that has existed to update constant immersion tests as new generation alloys are developed. Although constant immersion tests have many advantages (easy to control, fast, reproducible), they tend to be over designed and only work for a small number of aluminum alloys. Each new immersion test for exfoliation claims to be the universal test for aluminum alloys, but as soon as a new generation alloys is developed a new test is needed. Consequently the purpose of this work is not to develop yet another improved test, but to deconstruct ASTM G34 and ANCIT to explain why they behave the way they do. Understanding the electrochemical role of each component of the testing environment will allow more intelligent design of future immersion tests, reducing the need for time consuming trial and error.

3.2.2 Key Testing Variables in ASTM G34 and ANCIT

The ANCIT testing environment has many similarities to ASTM G34, but there are a few key differences. The parameters of each test are outlined in Table 3.1. Both tests contained 4 M NaCl and 0.6 M NO_3^-. In G34, that nitrate level was achieved using a combination of HNO_3 and KNO_3, while only KNO_3 was used in ANCIT. The addition of nitric acid to the G34 solution led to a very low pH. In practice, this pH was between 0.2 and 0.4. ANCIT solution also included a small addition of $AlCl_3$. Al^{3+} is a lewis acid and the pH after this addition ranged between 2.8 and 3.2. The final difference between G34 and ANCIT was testing temperature. G34 was performed at room temperature, but 52°C was recommended for 2XXX series alloys when exposed to ANCIT.

Table 3.1: Testing Parameters for ASTM G34 and ANCIT.

Parameter	**ASTM G34**	**ANCIT**
NaCl	4 M	4 M
HNO_3	0.1 M	N/A
KNO_3	0.5 M	0.6 M
$AlCl_3$	N/A	0.0224 M
Solution pH	0.4 – 0.2	2.8 – 3.2
Temperature	25°C	52°C

3.2.3 Role of Key Testing Variables in Chloride Solutions

3.2.3.1 Nitrate

Previous work in this study showed that in general, the presence of NO_3^- resulted in an increase in corrosion potential (E_{corr}) and a decrease in polarization resistance (R_p), which was attributed to the fast cathodic kinetics provided by NO_3^- reduction.[8]

In the early work on ASTM G34, the specific role of NO_3^- was never explained. However, Keddam et al. proposed that the addition of nitrate provided a fast cathodic reaction to support the dissolution of Al.[9] Three alloys were studied, AA2024-T87, AA2219-T87, and AA6013-T6, and in each case an acceleration of the cathodic reaction at the start of immersion in G34 solution was observed. The proposed reduction reaction for NO_3^- consumed protons (H^+), so cathodic kinetics were expected to slow with the depletion of H^+ in solution (rising pH). While this mechanism was supported by the data presented, the authors did not provide any method to distinguish the NO_3^- reduction reaction from other possible reduction reactions. For example H^+ reduction would be expected to be very fast initially when the pH was low (0.4), and this reaction would also slow with increasing pH.

Nitrate compounds have also been used as anodic inhibitors for aluminum, and this property was reported as early as 1969.[10,11] Böhni and Uhlig showed that increasing $NaNO_3$ concentration (ranging from 0.2 M to 0.5 M) when NaCl was fixed at 0.1 M caused an increase in the critical potential of pure aluminum (99.99%).[12] The proposed mechanism for this increase was the competition of NO_3^- with Cl^- for sites on the metal surface.

More recently, Pyun et al. reported that the addition of 0.1 M $NaNO_3$ to a 0.1 M NaCl solution caused an increase in the pitting potential of pure aluminum (99.999%) from -0.71 V_{SCE} (measured in 0.1 M NaCl alone) to -0.35 V_{SCE}.[13] In contrast to the competitive adsorption theory, the authors claimed that NO_3^- ions actually became incorporated into the protective oxide film on aluminum, thereby blocking Cl^- ions from becoming incorporated. This hypothesis was supported by the detection of nitrogen in the oxide film (after immersion in a nitrate containing solution) using Auger electron spectroscopy. In addition, a marked reduction in pitting during an anodic potentiostatic hold was observed even in nitrate-free environments if the sample had previously been exposed to a nitrate containing solution, which would not be expected to occur if adsorption was controlling.

3.2.3.2 Solution pH

Another important testing parameter was solution pH. Unlike Cl^- and NO_3^-, which were present in the same amount in both ASTM G34 and ANCIT, solution pH differed for the two tests. Previous work in this study showed that solution pH had a statistically significant impact on polarization resistance (R_p). At the lower solution pH (0.4), R_p was significantly lower (i.e., higher i_{corr}) than at neutral pH.[8]

The protective oxide film on aluminum, which prevents general corrosion but leaves the alloy susceptible to localized attack, is stable at neutral pH. However, this film degrades when exposed to very acidic or very basic environments. Figure 3.1 shows measured corrosion rates for several alloys including early generation Al-Li alloys as well as commercially pure Al. In each case, the corrosion rate was low within a pH range of 3 – 11.[14] Below pH 3, a small increase in corrosion rate was observed, and a dramatic increase in corrosion rate occurred below pH 2.

In addition to the impact on the protective oxide film, a low solution pH can provide fast cathodic kinetics as the concentration of H^+ increases. At near-neutral pH, oxygen (O_2) reduction is the fastest naturally occurring oxidant available because the diffusion limiting current of H^+ reduction is low. As the H^+ concentration increases in more acidic solutions, the diffusion limited current will increase and eventually surpass that of O_2 reduction.

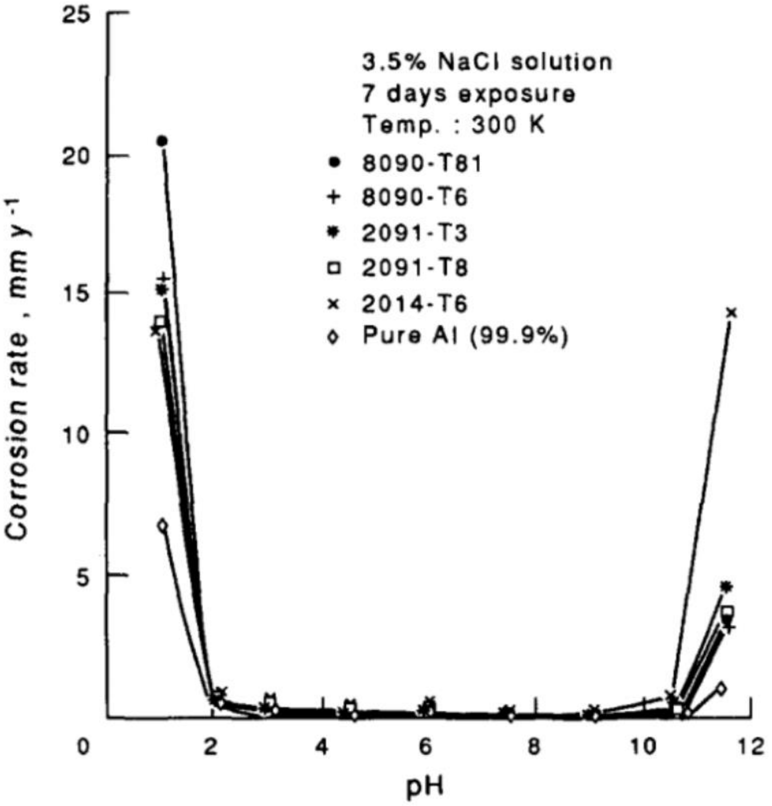

Figure 3.1: The impact of solution pH on corrosion rate for AA8090-T81, 8090-T6, 2091-T3, 2091-T8, 2014-T6, and pure Al (99.9%) in 3.5% NaCl. From reference 14.

Using an acidic solution pH is a common tool for accelerated corrosion processes, but the full impact of low solution pH must be considered so that corrosion mechanisms are not changed significantly from those observed during service.

3.2.3.3 $AlCl_3$

The mechanisms surrounding Al^{3+} are of great interest to those studying the localized corrosion of Al alloys because Al^{3+} tends to accumulate in crevices, fissures or other occluded sites. For example, Cooper et al. measured high levels of Al^{3+} (1.5 M) near the crack tip in an Al-

Zn-Mg-Cu alloy exposed to 0.5 M Na_2CrO_4, 0.05 M NaCl.[15] As Al^{3+} accumulates in a fissure, the hydrolysis of the metal cations will form an aggressive acidic environment. It has also been postulated that the accumulation of positive charge from Al^{3+} will draw Cl^- into cracks and fissures. Consequently, $AlCl_3$ is commonly included in simulated crack/crevice solutions.[18]

$AlCl_3$ and other aluminum salts have been shown to increase mass loss in Al alloys. Aqueous solutions of aluminum salts tend to be acidic due to the hydrolysis of Al^{3+}, but Foley et al. reported that mass loss of AA1199 and AA7075 depended more on the type of aluminum salt rather than the solution pH. Solutions of $AlCl_3$ and $Al(NO_3)_3$ caused significant mass loss, while $Al_2(SO_4)_3$ did not (solution pH was similar in each case). The underlying mechanism for the impact of $AlCl_3$ on corrosion rate has not yet been established.[17]

3.2.3.4 Temperature

Temperature was another point of difference between ASTM G34 and ANCIT. Temperature can affect cathodic kinetics by increasing the diffusion rate of oxidizing species that are diffusion limited. However, if O_2 reduction is the primary source of cathodic kinetics, increasing temperature will eventually cause cathodic kinetics to slow because of the reduced O_2 concentration.[18]

Temperature can also have an impact on anodic kinetics. For example, the pitting potential of 304 and 316 type stainless steel both decrease with increasing temperature.[18] Bohni and Uhlig found that for 99.99% Al in 0.1 M NaCl the critical pitting potential did not change significantly from 0^oC to 40^oC.[12] Later work by Foroulis and Thubrikar agreed with Bohni and Uhlig's results, but Foroulis et al. also showed that a significant decrease in steady-state critical pitting potential occurred for pre-anodized aluminum in 0.1 M KCl at temperatures higher than 40^oC. The authors could not provide a definitive explanation for this behavior, but they suggested that the structure and degree of hydration of the electric double layer on the oxide-electrolyte interface may be impacted by temperature.[19] In addition, El-Etre reported an increase in weight loss for pure Al in 2.0 M HCl with increasing temperature over the range 30^oC – 70^oC.[20]

3.2.4 Localized Corrosion Mechanisms in Al-Cu-Li Alloys

The alloy of interest in this study was Al-Cu-Li alloy 2060. The aging condition of an alloy can have a significant impact on the type and extent of corrosion susceptibility. AA2060, like many Al-Cu-Li alloys, undergoes a transition in intergranular corrosion (IGC) susceptibility during aging where under-aged tempers are more vulnerable to IGC than peak-aged and near peak-aged tempers. Exfoliation in Al-Cu-Li alloys usually initiates from grain boundary attack, and the improvement in IGC resistance at near peak-aged tempers correlates with an improvement in EC resistance.[21,22] The transition in corrosion morphology with aging suggests that changes in microstructure reduce the susceptibility of grain boundaries to attack during aging.

No studies on the changes of AA2060 microstructure with aging were found in the literature, but Ott et al. presented an investigation of grain boundary evolution during aging for AA2050 (Al-3.30% Cu-0.77% Li-0.39% Mn-0.32% Mg-0.17% Ag-0.10% Si-0.08% Zr-0.06% Fe-0.03%Ti-0.02% Zn), which has similar Cu and Li content to that of AA2060 (Al-3.95% Cu-0.85% Mg-0.75% Li-0.4% Zn-0.3% Mn-0.25% Ag-0.11%Zr). It was found that for under-aged AA2050, fine T_1 precipitates and very small (1 to 2 nm) precipitates resembling the S' phase were present on grain boundaries. With additional aging, T_1 precipitates grew longer (up to 100 nm in the over-aged condition), but the thickness did not change significantly. The small (1 to 2 nm) S' precipitates also grew with increased aging time, reaching 10 to 20 nm in the peak-aged condition and further coarsening in the over-aged condition.[23] Ott et al. also used Auger electron spectroscopy (AES) to show that in under-aged AA2050, grain boundary chemistry was enriched in Li compared to the matrix.[22] The standard reduction potential of Li is very low (-3.04 V_{SHE}),[18] and lithium enrichment on grain boundaries in under-aged Al-Cu-Li alloys may be the cause for IGC susceptibility in these materials.

For rolled alloys with an elongated grain structure, IGC can develop into exfoliation corrosion. Due to the occluded nature of IGC fissures, Al^{3+} produced by the anodic dissolution of Al can accumulate. When the Al^{3+} concentration exceeds the solubility limit of the electrolyte within the fissure, voluminous corrosion products will form within the IGC fissure. The corrosion products that form within the IGC fissure have a larger volume than the displaced Al along a grain boundary, and the corrosion products put pressure on the un-corroded grains around the affected grain boundary. With a large enough pressure, un-corroded grains will be wedged upward creating an exfoliation blister.[3] This process can occur in under-aged Al-Cu-Li alloys which are susceptible to IGC, presumably due to Li enrichment on grain boundaries.[22] Peak-aged and near peak-aged tempers have lower IGC susceptibility and tend to be resistant to exfoliation.[21]

It is the interaction between alloy microstructure and exposure environment that determine corrosion rate and morphology. While progress has been made in understanding the microstructural features for Al-Li alloys at various aging conditions, there is still more to be learned. The focus of the current work, however, lies in deconstructing the exposure environment rather than the alloy microstructure. Understanding the electrochemical role of the testing parameters in ASTM G34 and ANCIT will provide the tools necessary to develop more effective accelerated laboratory tests.

3.3 Experimental Procedures

3.3.1 Materials and Sample Preparation

Under-aged AA2060-T3 and near peak-aged AA2060-T86 were considered in this study. The nominal AA2060 composition is presented in Table 3.2.[24]

Table 3.2: Composition of AA2060.

Li	Cu	Mg	Ag	Zr	Mn	Zn	Al
0.75	3.95	0.85	0.25	0.11	0.30	0.40	Bal.

All exposed sample surfaces were polished to a 1200 grit surface, cleaned ultrasonically with deionized water, and rinsed with ethanol before exposure. In all cases, the T/2 plane (half thickness plane of the plate material) was the surface of primary interest.

3.3.2 Electrochemical Measurements

Electrochemical measurements were performed using a standard three-electrode cell with a saturated calomel reference electrode (SCE), a platinum mesh counter electrode, and a 1 cm^3 exposure window for the working electrode. Approximately 250 ml of solution was used for each test so that corrosion processes would not affect the bulk solution chemistry. A scan rate of 0.5 mV/s was used for all electrochemical measurements.

The impact of various testing parameters on AA2060 cathodic and anodic kinetics was measured using linear polarization scans. Open circuit potential (OCP) was measured for 10 minutes before starting the anodic or cathodic scans. Cathodic scans were performed by linearly polarizing samples from +0.025 V above the OCP to -1.2 V_{SCE}, and anodic scans ran upward in potential from -0.025 V below the OCP until a current of 0.1 A/cm^2 was reached. When solution pH adjustments were required, HCl and NaOH were used. If a large amount of HCl was required to achieve the desired pH, the NaCl concertation was reduced to maintain a fixed Cl$^-$ concentration.

A limited number of cathodic measurements were performed using a platinum (Pt) wire working electrode. The wire was 1 mm in diameter, and approximately 16 mm of the wire was immersed in solution for each test.

In the ASTM G34 and ANCIT testing solutions, several oxidizing agents were available to drive cathodic kinetics (O_2, H^+, and NO_3^-). The dominant cathodic reaction was determined for both testing environments by measuring cathodic kinetics in solutions with modified chemistry. For example, if cathodic kinetics in the G34 solution did not decrease when the NO_3^- was omitted from the test solution, it would be reasonable to assume that NO_3^- kinetics were slow and were not contributing significantly to cathodic kinetics. The impact of H^+ reduction could be investigated by adjusting solution pH. The testing environments used to determine the dominant cathodic reaction in ASTM G34 and ANCIT are presented in Table 3.3. For solutions resembling G34, room temperature was used. For solutions resembling ANCIT, a temperature of 52^{o}C was used. Solution pH adjustments were performed using HCl. If more than a few drops of HCl were required to reach the desired pH, the NaCl concentration was reduced to maintain a total Cl$^-$ concentration of 4.0 M.

Table 3.3: Environments used for determining dominant cathodic reaction in ASTM G34 and ANCIT

	Cl$^-$ (M)	**HNO_3 (M)**	**KNO_3 (M)**	**HCl (M)**	**$AlCl_3$ (M)**	**pH**	**T (^{o}C)**
Soln 1. (G34)	4.0	0.1	0.5	N/A	N/A	0.2	24
Soln. 2	3.9	N/A	N/A	0.1	N/A	0.27	24
Soln. 3 (ANCIT)	4.0	N/A	0.6	N/A	0.0224	2.85	52
Soln. 4	4.0	N/A	N/A	N/A	N/A	~6	52
Soln. 5	4.0	N/A	0.6	N/A	N/A	~6	52
Soln. 6	4.0	N/A	0.6	N/A	N/A	2.85	52
Soln. 7	4.0	N/A	N/A	N/A	0.0224	2.94	52

3.3.3 Evolution of Testing Environment over Time

Solution pH was monitored over several days during AA2060-T3 and -T86 exposure in ASTM G34 and ANCIT using a commercially available electrode with a saturated KCl fill solution. Sample size was 2.54 x 2.54 x 1.75 cm for both tests. ASTM G34 was carried out according to the standard. ANCIT does not have an ASTM designation, but the same procedure as ASTM G34 was followed except for the differences in solution chemistry and temperature outlined in Table 3.1. The recommended exposure time for 2XXX series alloys in ASTM G34 is 4 days,[6] but according to Lee and Lifka, the appropriate exposure time is 2 days in ANCIT.[7] Consequently, photographs of exposure samples were taken on day 4 of ASTM G34 and day 2 of ANCIT.

The impact of exposure time on cathodic kinetics was investigated by measuring kinetics on fresh AA2060-T3 and -T86 samples in solution that had been recovered after a 24-h ASTM G34 or ANCIT immersion test. Cathodic polarization was performed in a standard three-electrode cell with a 1 cm^2 exposure window for the working electrode.

An attempt to capture the influence of surface condition on kinetics was made by monitoring polarization resistance (R_p) and OCP for a full sized (2.54 x 2.54 x 1.75 cm) AA2060-T3 sample over a 24-h period in ASTM G34 and ANCIT. The large sample area was needed for the natural evolution of solution chemistry to occur. A volume-to-metal surface area ratio of 10 to 30 mL/cm^2 is required by the standard.[6] In this work, the volume-to-metal surface area ratio was 16 mL/cm^2. A wire was attached to the back of the AA2060-T3 working electrode, and the full back surface of the sample was masked with Kapton tape. The four sides and top surface of the cuboid sample were exposed to test solution. R_p was measured with a short linear polarization scan (-0.025 V_{OCP} to +0.025 V_{OCP}). Due to possible issues with current distribution over the cuboid sample, the data collected in this test was used to find qualitative trends rather than quantitative corrosion rates.

3.3.4 Impact of Temperature on Exfoliation Formation in AA2060-T3

An additional immersion test was completed to investigate the impact of exposure temperature on exfoliation formation in the susceptible AA2060-T3 material. ANCIT usually is performed at an elevated temperature (52^{o}C), but in this case an AA2060-T3 sample was exposed to ANCIT solution at a lower temperature of 30^{o}C. All other factors in the test were kept the same.

The exposure lasted for 7-days because this was the time required for exfoliation to form in ANCIT at 52°C.[8]

3.4 Results

3.4.1 ASTM G34 and ANCIT Exposures

Previous work in this study demonstrated that ASTM G34 and ANCIT, two full immersion tests designed to reveal exfoliation susceptibility, could not correctly distinguish between the exfoliation-susceptible and exfoliation-resistant tempers of Al-Cu-Li alloy 2060 within the standard exposure time.[8] Figure 3.2 shows AA2060-T3 and AA2060-T86 after 4 days of exposure to ASTM G34 and 2 days exposure to ANCIT (4 days and 2 days are the standard exposure time for each test). In both cases, the exfoliation-susceptible -T3 temper shows no evidence of blistering, while both the exfoliation-resistant -T86 samples appeared flakey. It was shown previously that with extended testing time (7 days for ANCIT and 4 weeks for ASTM G34), exfoliation blisters would form in the susceptible temper indicating that the problem was one of rate of attack rather than type of attack.[8]

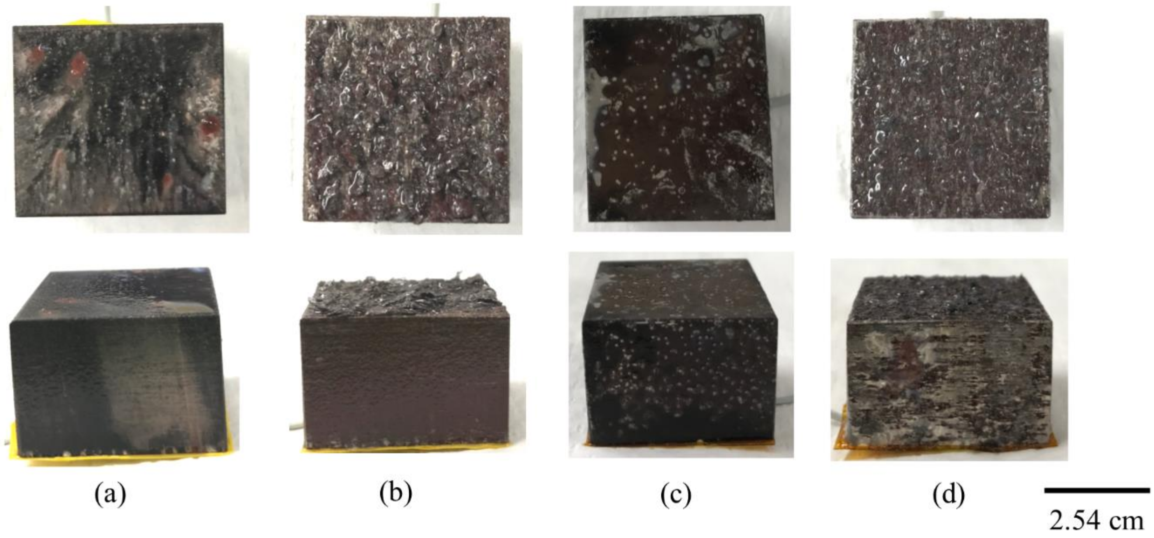

Figure 3.2: (a) AA2060-T3 and (b) AA2060-T86 after 4 days exposure to ASTM G34. (c) AA2060-T3 and (d) AA2060-T86 after 2 days exposure to ANCIT.

3.4.2 Deconstructing the Role of Nitrate

3.4.2.1 Impact on Cathodic Kinetics

Figure 3.3 shows the cathodic reactions in both ASTM G34 and ANCIT solutions for (a) AA2060-T3 and (b) AA2060-T86. In both cases cathodic kinetics were faster in the G34 solution. However from this data alone, it was impossible to identify the dominant reduction reaction for each test. Corrosion potential (E_{corr}), polarization resistance (R_p) and the inverse of R_p (directly proportional to corrosion current) are presented in Table 3.4.

NO_3^- was one possible oxidizing agent in ASTM G34 solution, but H^+ reduction was also considered because of the solution low pH (0.2-0.4). Kinetics for AA2060-T86 in a nitrate-free solution of 3.9 M NaCl and 0.1 M HCl (pH 0.27) are compared to kinetics for this alloy in G34 solution in Figure 3.4. Kinetics were only slightly higher for the NO_3^- containing solution.

At the moderate solution pH in ANCIT (2.8 – 3.2), H^+ kinetics were expected be slower than other available oxidizers such as O_2 and NO_3^-. O_2 reduction kinetics were investigated by cathodically polarizing samples in a neutral 4 M NaCl solution. At this pH, H^+ concentration was low and O_2 reduction was the dominant cathodic reaction. O_2 cathodic kinetics were similar for both tempers. When 0.6 M KNO_3 was included in the test solution, a marked increase in cathodic kinetics was observed. Although E_{corr} did decrease for the -T3 temper when the pH of the KNO_3 solution was lowered to 2.85, the overall cathodic kinetics were very similar for NO_3^- containing solutions at neutral pH and 2.85 pH. This result indicated that H^+ reduction was slower than NO_3^- reduction even at pH 2.85.

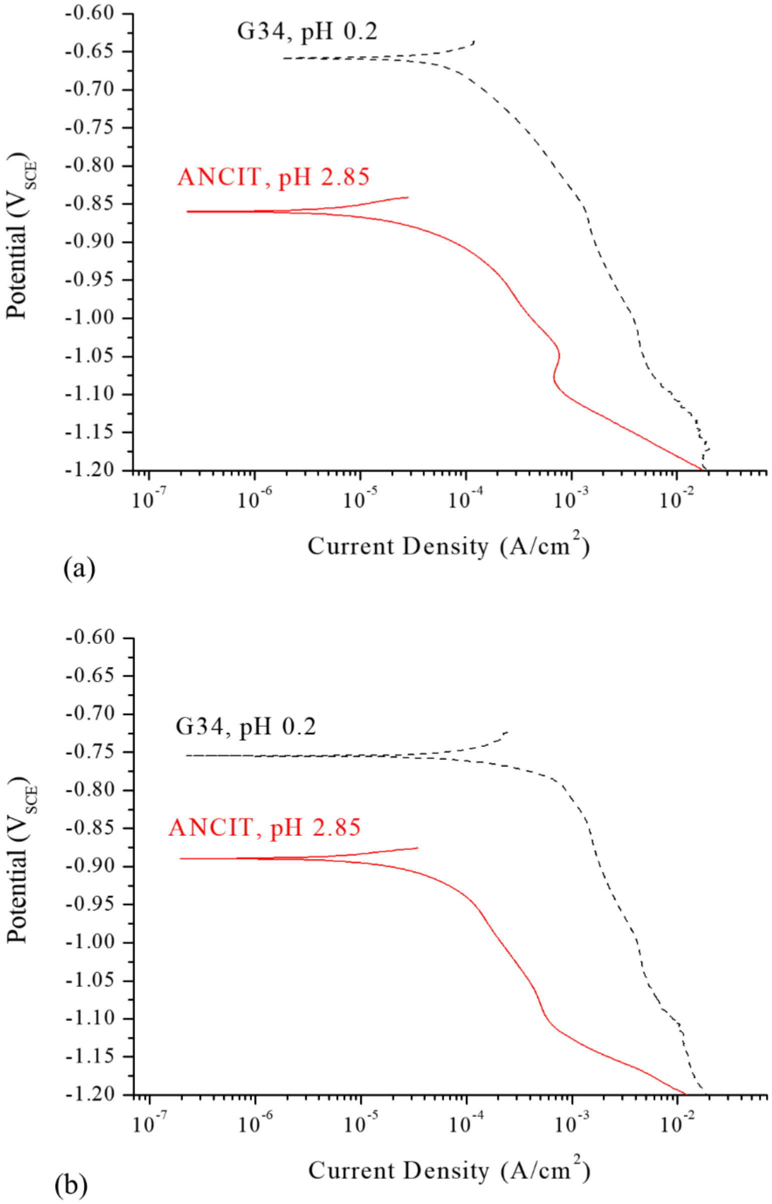

Figure 3.3: Cathodic kinetics for (a) AA2060-T3 and (b) AA2060-T86 in ASTM G34 and ANCIT after a 10 minute wait period for OCP to stabilize.

Table 3.4: Summary of E_{corr}, R_p, and $1/R_p$ for AA2060-T3 and -T86 in fresh ASTM G34 and ANCIT solutions.

	Solution	**E_{corr} (V_{SCE})**	**R_p (Ω-cm^2)**	**$1/R_p$ (Ω^{-1}-cm^{-2})**
AA2060-T3	G34	-0.659	145	6.90×10^{-3}
	ANCIT	-0.859	806	1.24×10^{-3}
AA2060-T86	G34	-0.755	70.3	1.42×10^{-2}
	ANCIT	-0.890	571	1.75×10^{-3}

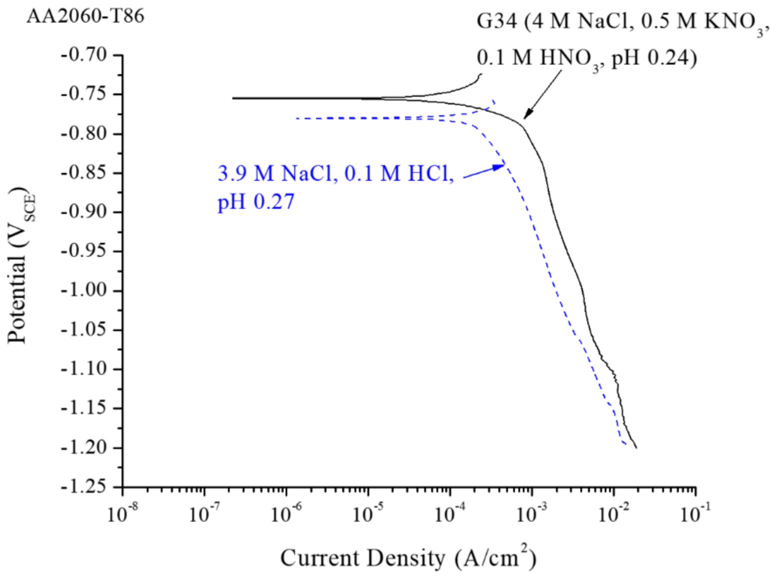

Figure 3.4: Cathodic polarization scan for AA2060-T86 in G34 solution (4 M NaCl, 0.5 M KNO_3, 0.1 M HNO_3, pH 0.24) as well as a nitrate-free solution of 3.9 M NaCl, 0.1 M HCl, pH 0.27. Test were performed at room temperature, which was the standard exposure temperature for ASTM G34.

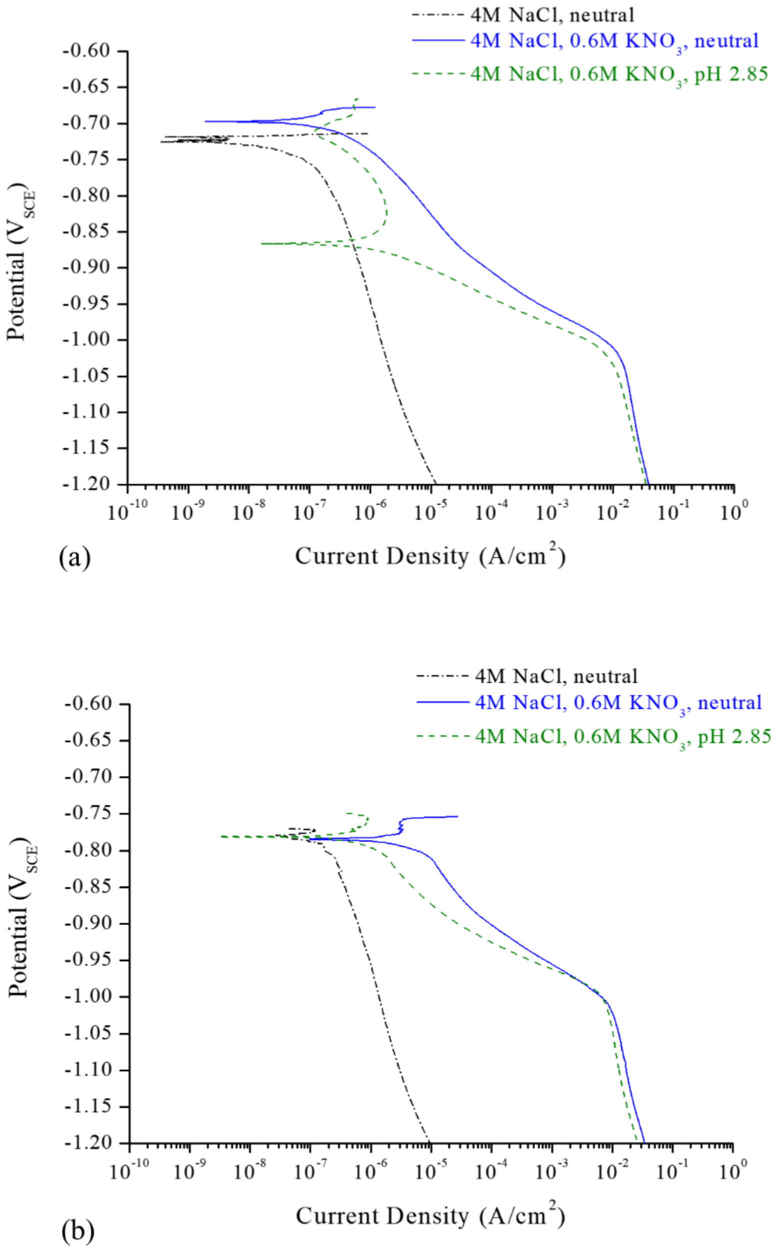

Figure 3.5: Cathodic polarization scans for (a) AA2060-T3 and (b) AA2060-T86 in various nitrate containing and nitrate-free solutions. All tests were performed at 52°C, which was the standard exposure temperature for the ANCIT test.

3.4.2.2 Impact on Anodic Kinetics

Figure 3.6 compares anodic kinetics for (a) AA2060-T3 and (b) AA2060-T86 in ASTM G34 and ANCIT solutions. Anodic kinetics were faster in ANCIT than in ASTM G34 for both tempers. A passive region and breakdown potential were visible for samples exposed to ANCIT, but cathodic kinetics were too fast to observe these features in the ASTM G34 solution.

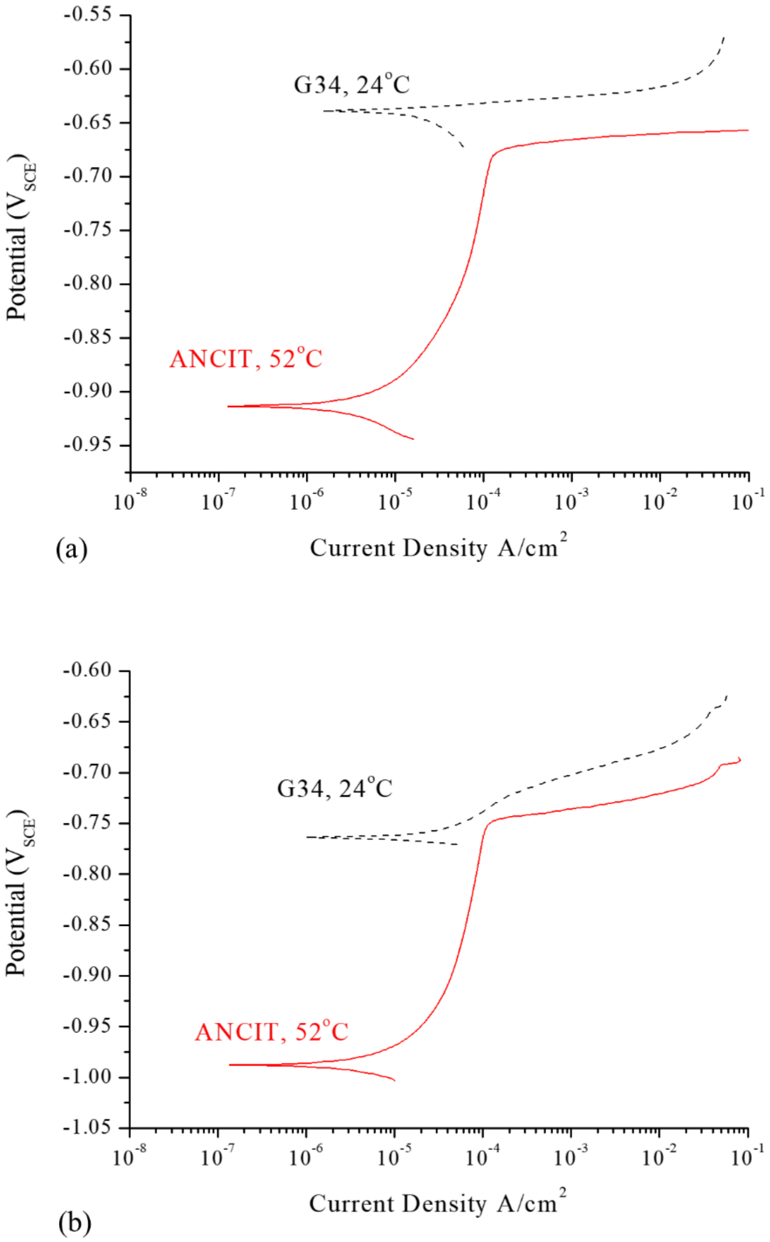

Figure 3.6: Anodic kinetics for (a) AA2060-T3 and (b) AA2060-T86 in ASTM G34 and ANCIT solution.

Figure 3.7 shows that by altering the Cl^-:NO_3^- ratio, the corrosion potential (E_{corr}) was shifted. Increasing NO_3^- concentration from 0.1 M to 0.6 M (constant Cl^-) caused an increase in E_{corr} for AA2060-T8, while increasing Cl^- from 1 M to 4 M (constant NO_3^-) caused a decrease in E_{corr}. NO_3^- has been reported to increase the pitting potential for Al by competitively adsorbing into the protective oxide film, thereby blocking Cl^- adsorption.[13] The increase in E_{corr} with decreasing Cl^-:NO_3^- may have been a result of increasing pitting potential.

Anodic polarization scans were measured for AA2060-T3 and -T86 in a 4 M NaCl solution with and without 0.6 M KNO_3. Figure 3.8(a) and (b) show anodic polarization scans for AA2060-T3 and AA2060-T86 respectively. Although passive current and breakdown potential were not observed in these scans, a reduction in anodic kinetics with the addition of KNO_3 was observed. The effect was more significant for the -T3 temper than for -T86 temper.

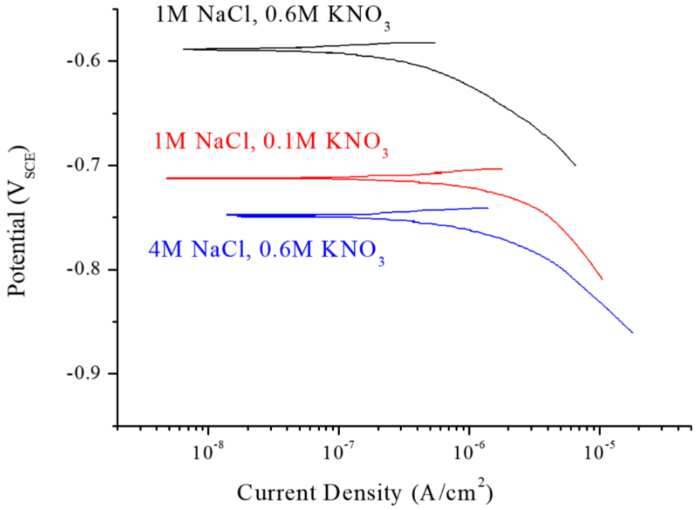

Figure 3.7: Linear polarization scans for AA2060-T86 showing changes in E_{corr} with various Cl^-:NO_3^- ratios. Measurements were performed at room temperature.

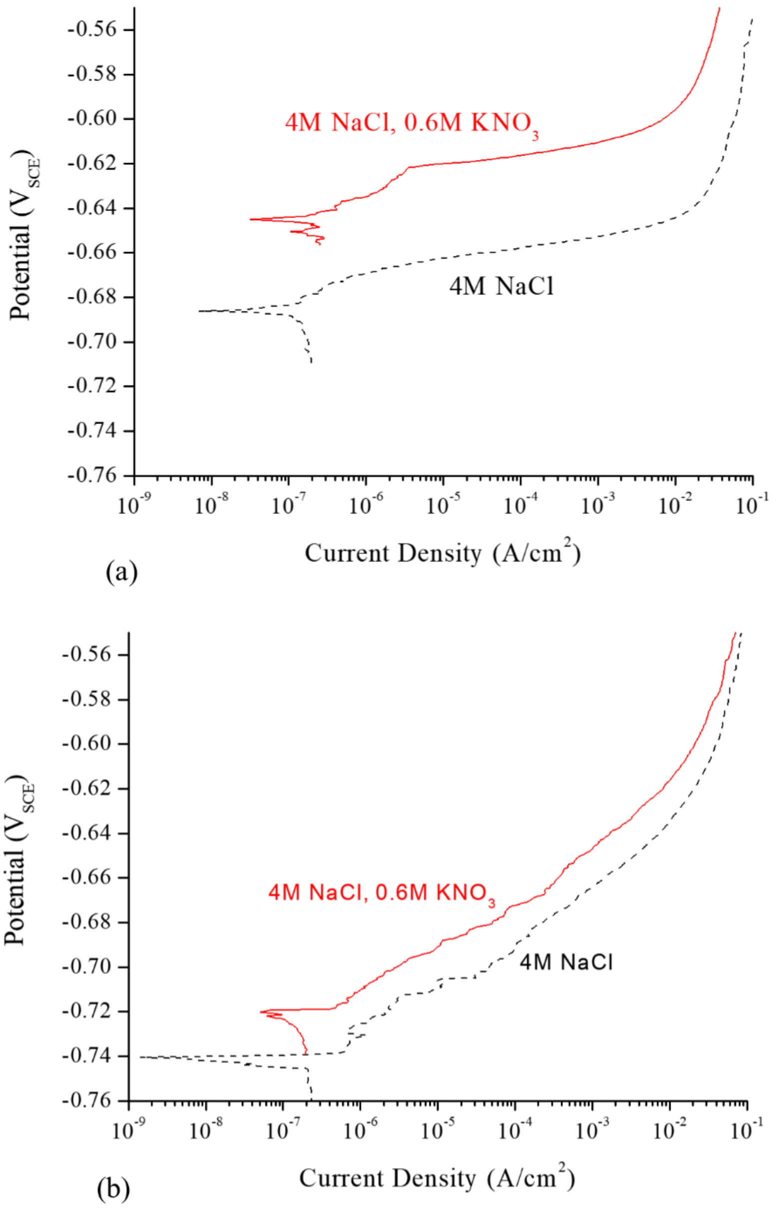

Figure 3.8: Anodic polarization scans for (a) AA2060-T3 and (b) AA2060-T86 in neutral 4 M NaCl with and without 0.6 M KNO_3. Scans were measured at room temperature.

3.4.3 Role of $AlCl_3$

The small amount of $AlCl_3$ (0.0224 M) included in ANCIT may seem insignificant, but this addition had an impact on cathodic kinetics. Cathodic kinetics in ANCIT solution (4 M NaCl, 0.6 M KNO_3, 0.0224 M $AlCl_3$, pH 2.85) are compared to kinetics in 4 M NaCl, 0.6 M KNO_3, pH

2.85) in Figure 3.9. Although both solutions contained the same amount of NO_3^-, the slope of the cathodic line was different in the two tests indicating a possible change in mechanism. The cathodic kinetics for the solution containing $AlCl_3$ but free of NO_3^- was slower than both NO_3^- containing solutions.

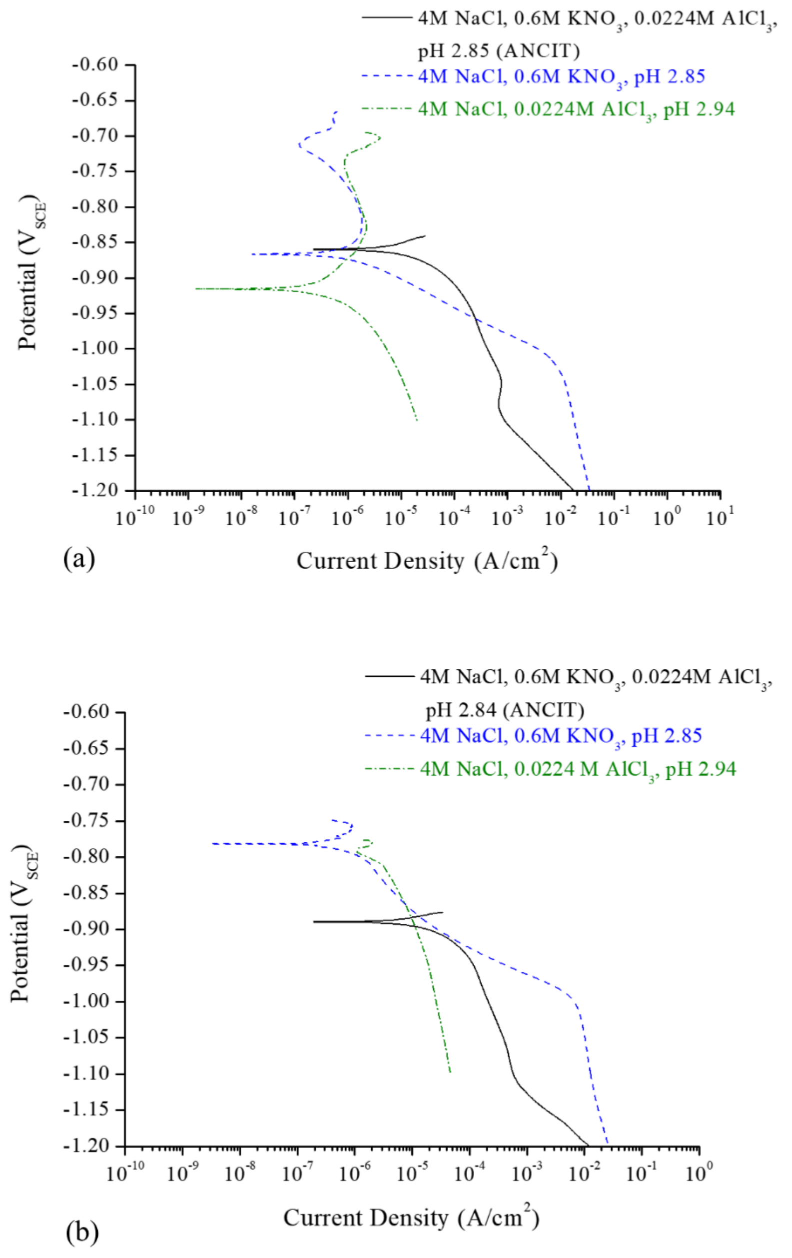

Figure 3.9: Cathodic polarization scans for (a) AA2060-T3 and (b) AA2060-T86 in ANCIT solution, in 4 M NaCl, 0.6 M KNO_3, pH 2.85, and in 4 M NaCl, 0.0224 M $AlCl_3$, pH 2.94. All tests were performed at 52°C, which was the standard exposure temperature for the ANCIT test.

Although kinetics were not faster in ANCIT solution (4 M NaCl, 0.6 M KNO_3, 0.0224 M $AlCl_3$, pH 2.85) than in the 4 M NaCl, 0.6 M KNO_3, pH 2.85 solution at all potentials, $1/R_p$ (directly proportional to i_{corr}) was higher in ANCIT solution for both tempers. E_{corr}, R_p, and $1/R_p$ for both solutions are summarized in Table 3.5.

Table 3.5: Summary of E_{corr}, R_p, and $1/R_p$ for AA2060-T3 and -T86 in solutions with and without $AlCl_3$.

	Solution	**E_{corr} (V_{SCE})**	**R_p (Ω-cm^2)**	**$1/R_p$ (Ω^{-1}-cm^{-2})**
AA2060-T3	4M NaCl, 0.6M KNO_3, 0.0224M $AlCl_3$, pH 2.84	-0.859	794	1.3 x10^{-3}
	4M NaCl, 0.6M KNO_3, pH 2.85	-0.866	8,256	1.2 x 10^{-4}
AA2060-T86	4M NaCl, 0.6M KNO_3, 0.0224M $AlCl_3$, pH 2.84	-0.889	569	1.8 x 10^{-3}
	4M NaCl, 0.6M KNO_3, pH 2.85	-0.782	14,752	6.8 x 10^{-5}

The impact of $AlCl_3$ on cathodic kinetics was also measured with a Pt wire working electrode. In a solution of 4 M NaCl (pH adjusted to 2.85 with HCl), only O_2 reduction and H_2O reduction lines were observed (Figure 3.7). However, in a solution of 4 M NaCl and 0.0224 M $AlCl_3$ (pH 2.85 naturally), H^+ reduction became faster than O_2 reduction below -0.4 V_{SCE}.

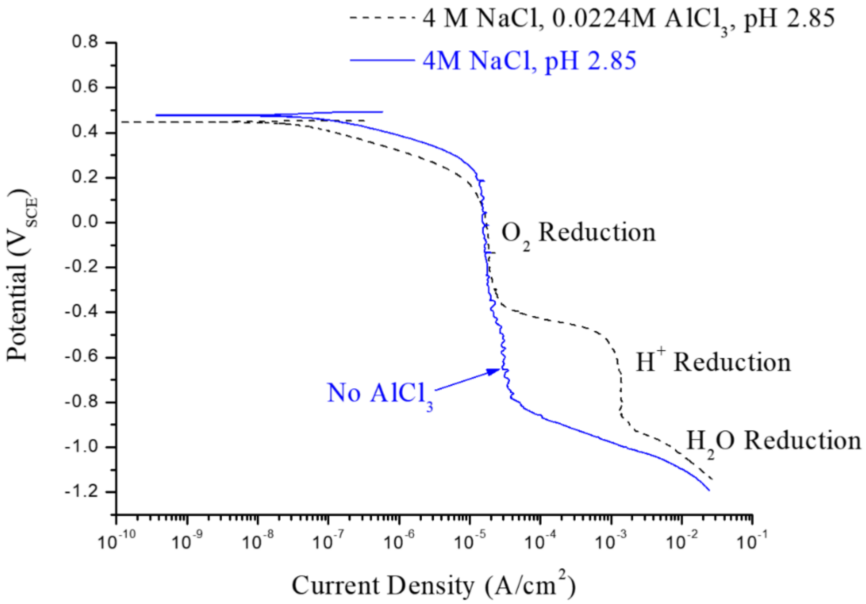

Figure 3.10: Cathodic kinetics measured on a Pt wire in 4 M NaCl, pH 2.85, with and without $AlCl_3$. Tests were performed at 52°C.

3.4.4 Impact of pH on Anodic Kinetics

In general, solution pH had little impact on anodic kinetics in solutions of constant [Cl^-] and [NO_3^-]. Figure 3.11(a) shows anodic kinetics for AA2060-T3 in several solutions. For solutions ranging from neutral to pH 2.89 (ANCIT solution), anodic kinetics were very similar. For a solution of pH of 0.24 (ASTM G34 solution), however, i_{corr} appeared to be faster than for the other solutions. This was due to the faster cathodic kinetics in the ASTM G34 solution. For the -T86 temper (Figure 3.11[b], solutions with neutral pH, 2.90, and 2.89 pH anodic kinetic were very similar. However, at pH 0.24 (ASTM G34 solution), anodic kinetics were noticeably faster. It should also be noted that the presence of 0.0224 M $AlCl_3$ in the ANCIT solution did not impact anodic kinetics.

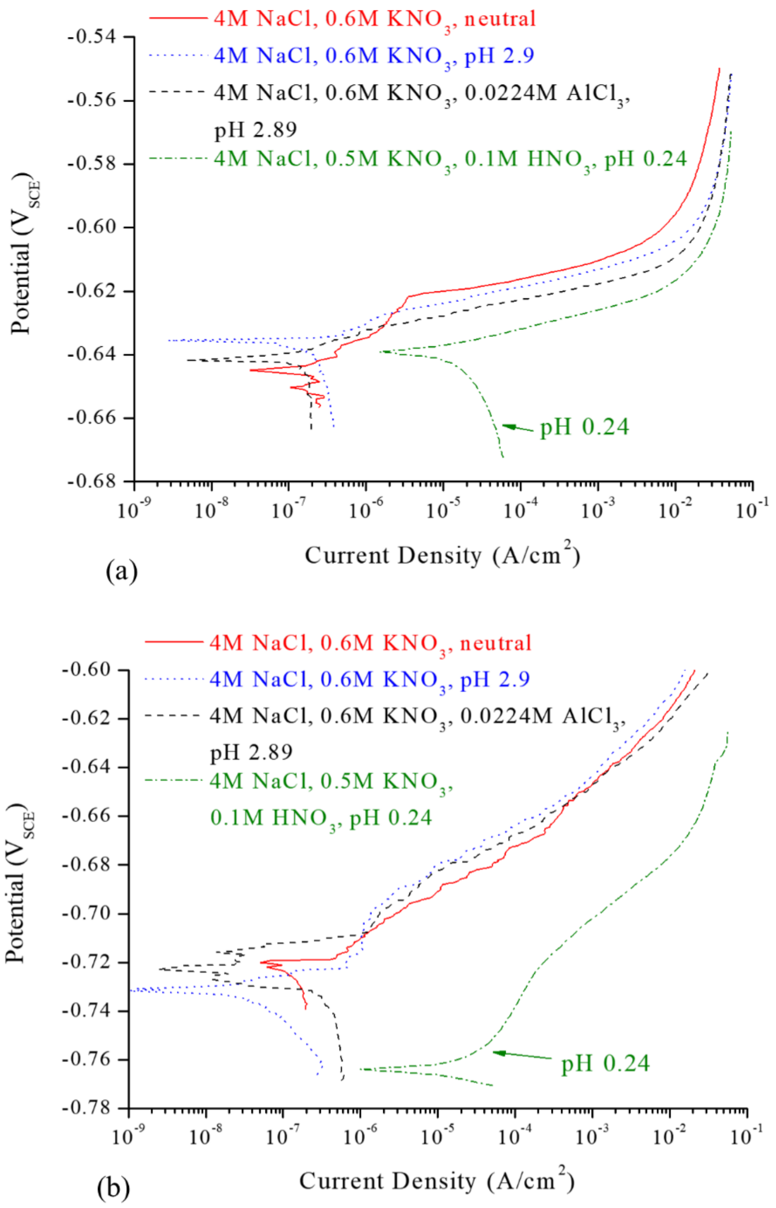

Figure 3.11: Impact of solution pH on anodic kinetics of (a) AA2060-T3 and (b) AA2060-T86. All solutions contained 4 M NaCl, and all measurements were made at room temperature.

3.4.5 Impact of Temperature on Anodic Kinetics

The impact of temperature was isolated by comparing anodic kinetics in ANCIT solution at 52°C and at room temperature. The results in Figure 3.12 show that in ANCIT solution, an increase in temperature from 24°C to 52°C caused an increase in anodic kinetics for both tempers.

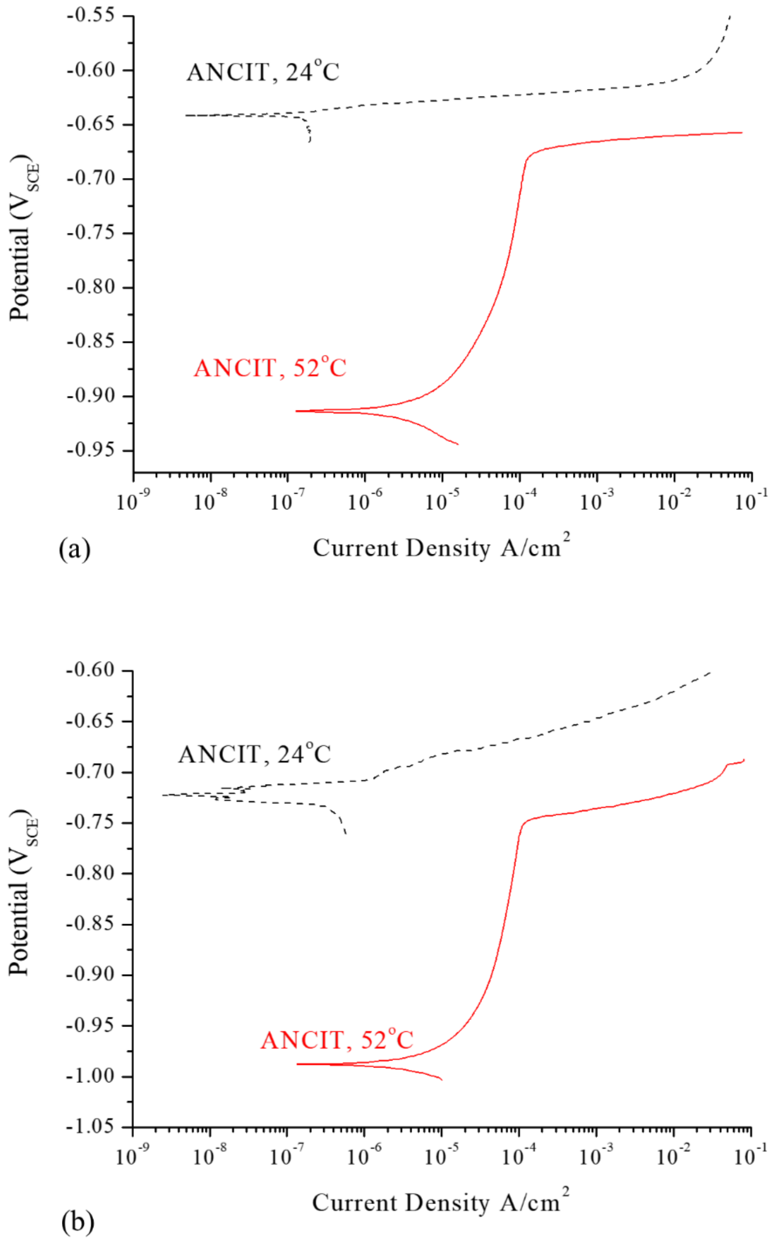

Figure 3.12: Anodic polarization scans for (a) AA2060-T3 and (b) AA2060-T86 in ANCIT solution at room temperature and at 52°C.

The impact of temperature on anodic kinetics of the exfoliation-susceptible -T3 temper was further demonstrated by comparing kinetics and immersion results for ANCIT solution at high and low temperatures. The increase in temperature from 30°C to 52°C caused a simultaneous decrease in E_{corr} and increase in $1/R_p$ (directly proportional to i_{corr}) indicating that the anodic kinetics had increased as expected (Figure 3.13a). After 7 days of exposure to both of these environments, severe exfoliation formed in the sample exposed at 52°C, but no blisters visible to the naked eye were observed on the sample exposed at 30°C.

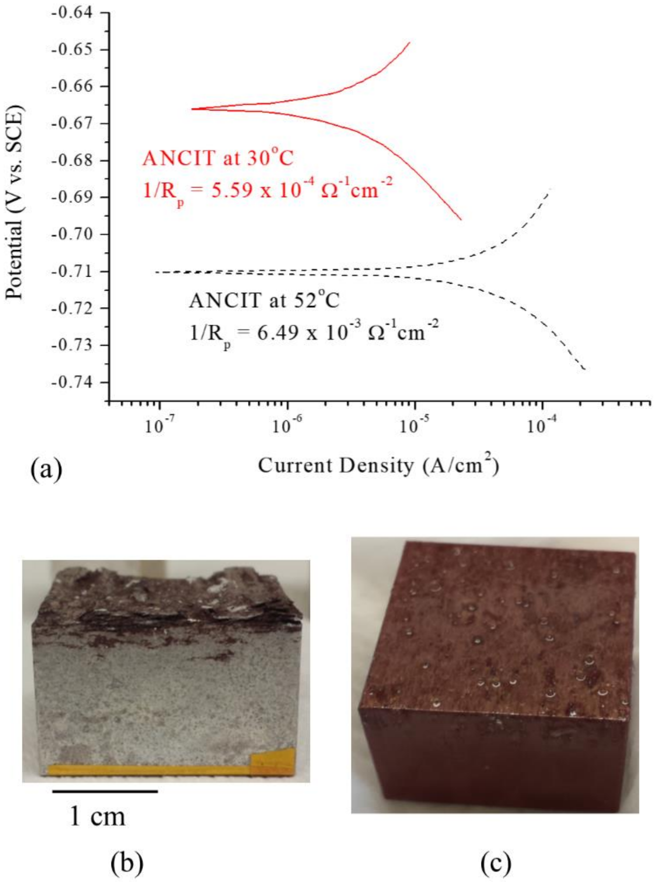

(a)

(b)

(c)

Figure 3.13: (a) Linear polarization scans for AA2060-T3 in standard ANCIT (52°C) and low temperature ANCIT (30°C). Increasing testing temperature led to an increase in anodic kinetics. (b) AA2060-T3 after 7 days exposure to standard ANCIT (52°C). (c) AA2060-T3 after 7 days exposure to low temperature ANCIT (30°C).

3.4.6 Evolution of Testing Environment over Time

During ASTM G34 exposures, a solution volume-to-metal surface area ratio between 10 to 30 ml/cm^2 is required per the standard to ensure that a specific evolution of solution chemistry occurs over time.[6] For example, Figure 3.14 shows that although the pH of ASTM G34 started very low, within 24-h it reached about the same pH as ANCIT.

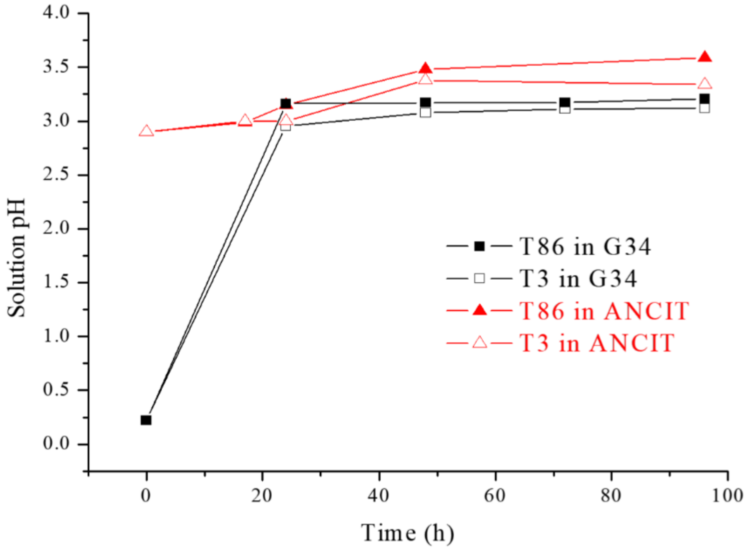

Figure 3.14: Evolution of solution pH in ASTM G34 and ANCIT over time.

Cathodic kinetics were measured on freshly prepared samples in ASTM G34 and ANCIT solution recovered after a 24 immersion test. The purpose of this experiment was to show the changes in cathodic kinetics due to the evolution in solution pH and consumption of NO_3^- during the first 24-h of exposure. Figure 3.15(a) shows that cathodic kinetics on AA2060-T3 decreased for both ASTM G34 and ANCIT after the 24-h immersion. At the start of testing, cathodic kinetics were higher for ASTM G34 than for ANCIT. However, the reduction in kinetics after 24-h was more significant for ASTM G34 than ANCIT, and ANCIT cathodic kinetics were faster at this point. A similar trend was observed for AA2060-T86 (Figure 3.15[b]).

Table 3.6 summarizes E_{corr}, R_p, and $1/R_p$ for AA2060-T3 and -T86 in fresh and “used” ASTM G34 and ANCIT solutions. In each case, a significant reduction in $1/R_p$ (directly proportional to i_{corr}) was observed when the fresh solution was compared to the “used” solution that was recovered after a 24-h immersion.

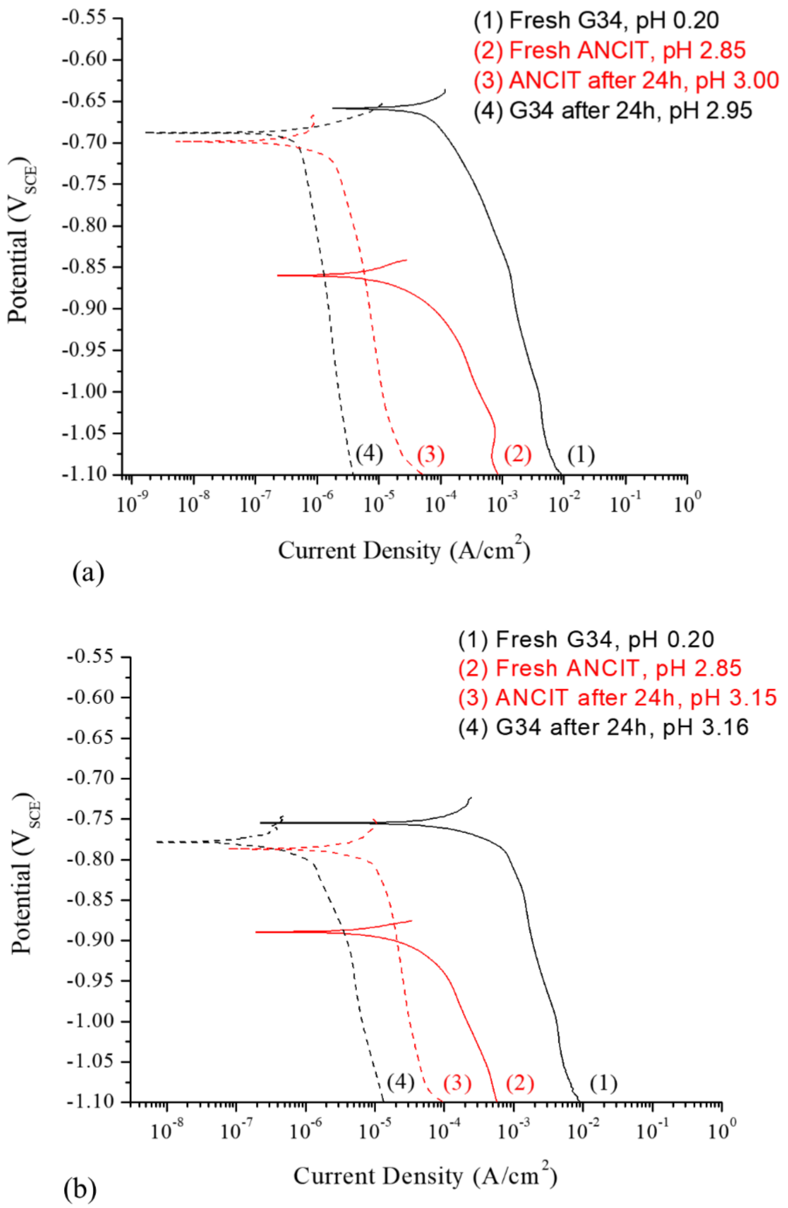

Figure 3.15: Comparison of cathodic kinetics on (a) AA2060-T3 and (b) AA2060-T86 using fresh solution (black dashed line for G34 and solid red line for ANCIT) and using solution after a 24-h immersion (solid blue line for G34).

Table 3.6: Comparison of E_{corr}, R_p, and $1/R_p$ for AA2060-T3 and -T86 in fresh and "used" ASTM G34 and ANCIT solution.

	Solution	**E_{corr} (V_{SCE})**	**R_p (Ω-cm^2)**	**$1/R_p$ (Ω^{-1}-cm^{-2})**
AA2060-T3	Fresh G34	-0.659	145	6.90×10^{-3}
	"Used" G34	-0.690	12,194	8.20×10^{-5}
	Fresh ANCIT	-0.859	806	1.24×10^{-3}
	"Used" ANCIT	-0.698	15,000	6.67×10^{-5}
AA2060-T86	Fresh G34	-0.755	70.3	1.42×10^{-2}
	"Used" G34	-0.777	30,207	3.31×10^{-5}
	Fresh ANCIT	-0.890	571	1.75×10^{-3}
	"Used" ANCIT	-0.787	1,912	5.23×10^{-4}

While measuring kinetics on a freshly prepared sample provides insight into solution chemistry changes over time, it does not account for changes in surface condition of the exposed sample. An attempt to capture the impact of the evolution of surface condition was made by measuring open circuit potential and polarization resistance during G34 and ANCIT immersion testing of full sized samples (2.54 cm x 2.54 cm x 1.75 cm). Figure 3.16(a) shows that $1/R_p$ for the AA2060-T3 sample increased for the first 4.1 hours of testing, then began to decrease. In contrast, $1/R_p$ for AA2060-T3 exposed to ANCIT was stable at low value during the full 24-h period. OCP was higher for the sample exposed to ASTM G34 at for the 24-h period (Figure 3.16[b]).

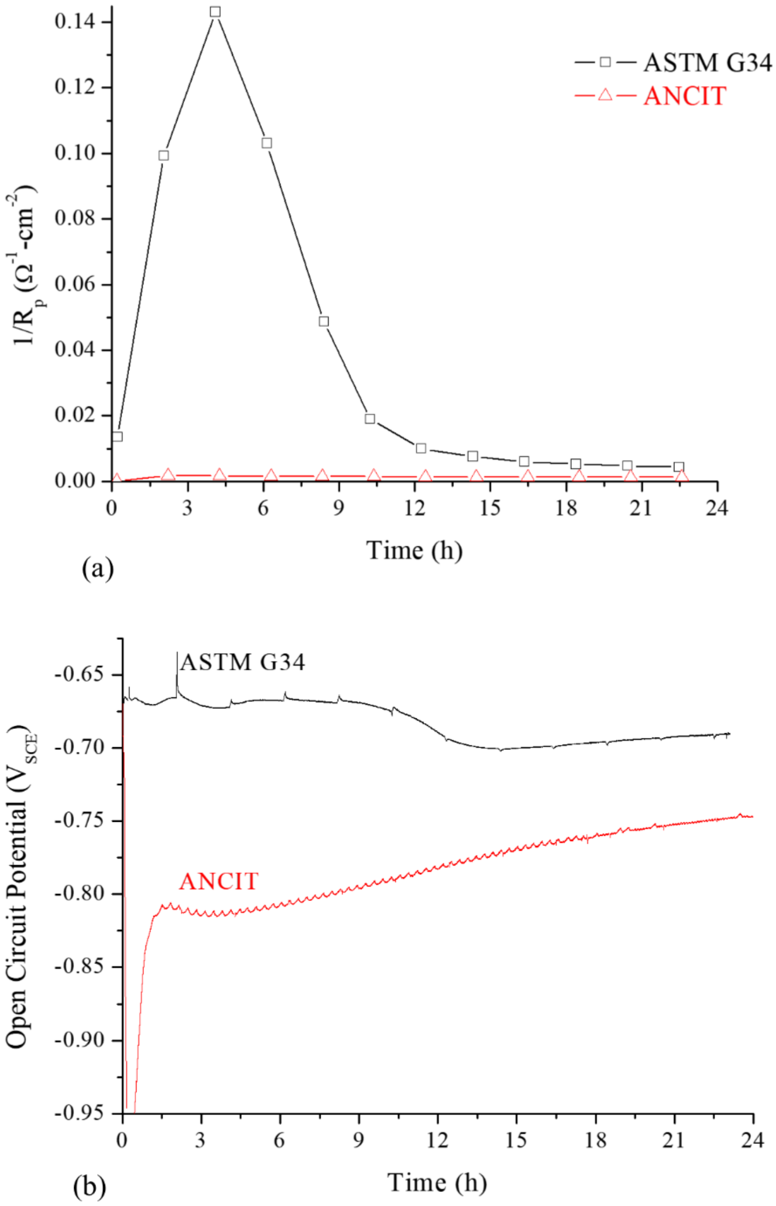

Figure 3.16: (a) $1/R_p$ and (b) OCP for AA2060-T3 the first 24-h of immersion in ASTM G34 and ANCIT.

3.5 Discussion

Previous work in this area showed that for AA2060-T3, exfoliation blisters formed within 7 days in ANCIT, but 4 weeks were required for exfoliation to form in ASTM G34. The difference in behavior between these two tests was determined to be in the rate of attack rather than the type of attack. When the exfoliation-resistant AA2060-T86 temper was exposed to these tests, an unrealistic degree of attack occurred.[8] The purpose of the current work was to deconstruct ASTM G34 and ANCIT and explain why these unexpected results developed. Understanding the electrochemical role of each component of the testing environment will allow better design of future immersion tests, reducing the need for trial and error.

3.5.1 Evolution of Solution pH

In the ASTM G34 standard, a volume-to-metal surface area ratio of 10 to 30 mL/cm^2 is required to ensure that a specific evolution in solution chemistry occurs over time.[6] Lee et al. examined the impact of volume-to-metal surface area ratio on solution chemistry over a 48 hour period by using ratios of 10, 15, 24, and 30 mL/cm^2 during the exposure of AA7150.[7] Solution pH increased with time for each volume-to-metal surface area ratio, and lower ratios led to faster changes in pH. For a ratio of 15 mL/cm^2, pH increased to 3.0 within the first 9 hours and stabilized at 3.2 within 24-h.

In the current study, a similar evolution of pH was observed. A solution volume-to-metal surface area ratio of 16 mL/cm^2 was used for this work. Figure 3.14 shows that the pH in ASTM G34 increased during the first 24-h and stabilized between 3.0 and 3.25. Anodic and cathodic reactions that occurred during immersion in ASTM G34 solution most likely were responsible for the changes in solution pH. Hydrolysis of the Al^{3+} ion produced during anodic dissolution of Al (Equation 3.1) would increase the H^+ concentration, creating a more acidic environment (Equation 3.2). However, H^+ would also be consumed during cathodic reactions such as proton reduction (Equation 3.3) or oxygen reduction (Equation 3.4). For each electron accepted during H^+ or O_2 reduction, one H^+ ion is consumed. However, each electron produced during the oxidization of Al only produces 1/3 Al^{3+} and 1/3 H^+ through the hydrolysis of the Al^{3+}. Even though the dissolution of Al acts to decrease pH through hydrolysis, the rate of H^+ consumption via cathodic reactions would exceed that of H^+ production, and overall the pH would be expected to rise as long as cathodic kinetics remain fast.

Equation 3.1[19]

$$Al \rightarrow Al^{3+} + 3e^-$$

Equation 3.2[18]

$$Al^{3+} + H_2O \rightarrow AlOH^{2+} + H^+$$

Equation 3.3[19]

$$2H^+ + 2e^- \rightarrow H_2$$

Equation 3.4[19]

$$O_2 + 4H^+ + 4e^- \rightarrow 2H_2O$$

The starting pH in ANCIT (2.8 - 3.2) was higher than in ASTM G34 (0.2 - 0.4), and the pH of fresh ANCIT solution was established by the addition of 0.0224 M $AlCl_3$. When this salt dissociated in an aqueous solution, the Al^{3+} underwent hydrolysis according to Equation 3.1 and created an acidic environment. Unlike ASTM G34 solution, ANCIT solution only increased slightly during testing. Consequently, after the first 24-h of exposure, solution pH was very similar for both ASTM G34 and ANCIT. The evolution of pH during ASTM G34 and ANCIT meant that corrosion kinetics measured in fresh solution may not be representative of kinetics later in testing. The following discussion is divided into several sections describing kinetics in fresh testing solution (representative of early exposure times) and in "used" solution (solution recovered after a 24-h immersion test).

3.5.2 Cathodic Kinetics in Fresh ASTM G34 and ANCIT Solution

3.5.2.1 Distinguishing Between H^+ and NO_3^- Reduction

In the literature regarding the development of ASTM G34 and ANCIT, only one mechanism for the role of nitrate was proposed. Work by Keddam et al. suggested that NO_3^- reduction provided a fast cathodic reaction to support the dissolution of Al during ASTM G34 testing,[9] but no data were provided to distinguish the NO_3^- reduction reaction from the H^+ reduction reaction. ASTM G34 operates at an extremely low solution pH (0.2 - 0.4), and the H^+ reduction reaction must be considered at this pH. Cathodic kinetics for AA2060-T3 and AA2060-T86 in fresh ASTM G34 solution are shown in Figure 3.3(a) and (b) respectively, but from these data alone it was difficult to identify the dominant reduction reaction in either test.

The cathodic kinetics of H^+ reduction at pH 0.27 were measured on AA2060-T86 using a solution of 3.9 M NaCl and 0.1 M HCl. The concentration of NaCl was reduced in this solution to maintain an overall Cl^- concentration of 4 M. Figure 3.4 presents a comparison of this cathodic line and the cathodic line for AA2060-T86 in ASTM G34 solution (4 M NaCl, 0.6 M NO_3^-, pH 0.24), and cathodic kinetics were not significantly different. NO_3^- reduction may have contributed slightly to the cathodic kinetics in ASTM G34 testing, but H^+ was the primary oxidizer.

ANCIT operated at a more moderate solution pH (2.8 – 3.2), so it was expected that H^+ reduction would be slower in this test than in ASTM G34. Cathodic kinetics for AA2060-T3 and AA2060-T86 in ANCIT were slower than in ASTM G34 as shown in Figure 3.3. To determine which cathodic reactions were controlling in ASTM G34, kinetics were measured in several nitrate containing and nitrate-free solutions (Figure 3.5). O_2 reduction kinetics were investigated by cathodically polarizing samples in a neutral 4 M NaCl solution. In neutral NaCl, the low H^+ concentration caused the diffusion limited current for H^+ reduction to be low, making O_2 reduction the dominant cathodic reaction. O_2 reduction kinetics were similar for both tempers. When 0.6 M KNO_3 was added to the test solution, a marked increase in cathodic kinetics was observed. Lowering solution pH to 2.85 did not alter NO_3^- reduction kinetics significantly, indicating that even at pH 2.85 H^+ reduction was too slow to contribute to the cathodic kinetics.

Overall, it was observed that cathodic kinetics were faster in fresh ASTM G34 solution than in ANCIT solution, and $1/R_p$ (directly proportional to i_{corr}) was higher in ASTM G34 solution than in ANCIT solution for both tempers (Figure 3.3, Table 3.4). The low solution pH in ASTM G34 provided a high H^+ concentration and a high diffusion limited current for H^+ reduction. In ANCIT, the fastest available cathodic reaction was NO_3^- reduction, which was not as powerful an oxidizer as H^+ was in fresh ASTM G34 solution.

3.5.2.2 Impact of $AlCl_3$ on Cathodic Kinetics

The small amount of $AlCl_3$ (0.0224 M) included in ANCIT may seem insignificant, but this addition had an impact on cathodic kinetics. Cathodic kinetics in ANCIT solution (4 M NaCl, 0.6 M KNO_3, 0.0224 M $AlCl_3$, pH 2.85) are compared to kinetics in 4 M NaCl, 0.6 M KNO_3 (pH 2.85) in Figure 3.9. Although both solutions contained the same amount of NO_3^-, $1/R_p$ was higher in the solutions containing $AlCl_3$ (Table 3.5). Additionally, the slope of the cathodic line was different in the two tests indicating a possible change in mechanism. When cathodic kinetics were measured with and without $AlCl_3$ on a Pt wire, the presence of $AlCl_3$ caused the i_{lim} H^+ reduction to increase such that it was faster than O_2 kinetics below a potential of -0.4 V_{SCE} (Figure 3.10). In addition, recent work by Khullar has shown that increasing $AlCl_3$ concentration led to an increase in i_{lim} for the H^+ reduction reaction on Pt.[25]

Nitrate reduction can occur via several mechanisms, each of which uses different amounts of H^+ (Equation 3.5 - Equation 3.8).[26] If the presence of $AlCl_3$ can impact the cathodic kinetics of H^+ reduction so significantly, $AlCl_3$ may impact the mechanism by which NO_3^- is reduced by increasing the amount of H^+ available for reaction with NO_3^-.

Equation 3.5

$$NO_3^- + 2H^+ + e^- \rightarrow \frac{1}{2}N_2O_{4(g)} + H_2O$$

Equation 3.6

$$NO_3^- + 3H^+ + 2e^- \rightarrow HNO_2 + H_2O$$

Equation 3.7

$$NO_3^- + 4H^+ + 3e^- \rightarrow NO_{(g)} + 2H_2O$$

Equation 3.8

$$NO_3^- + 10H^+ + 8e^- \rightarrow NH_4^+ + 3H_2O$$

The apparent ability of $AlCl_3$ to influence H^+ reduction kinetics is not yet well understood. The hydrolysis of Al^{3+} (Equation 3.2) does increase H^+ concentration, but in each of the tests described above, pH was adjusted in the $AlCl_3$ to match the pH of the $AlCl_3$ containing solution. HCl was used for all pH adjustments. After the pH adjustments, H^+ concentration should have been the same in $AlCl_3$ free and $AlCl_3$ containing solutions. This phenomena has been observed on multiple materials (AA2060, AA5083, AA7075, Pt),[25,27] indicating that the mechanism was not surface dependent. Khullar has suggested that $AlCl_3$ acts as a buffer in the test solution, which leads to an increased flux of H^+ to the electrode surface when H^+ is depleted at the surface during cathodic polarization.[25] In contrast, Liu proposed that the mechanism involves the formation of an adsorbed hydrated $Al(OH)_3$ layer on the electrode surface.[27] Both theories require more investigation before a definitive mechanism is identified.

3.5.3 Anodic Kinetics in Fresh ASTM G34 and ANCIT Solution

3.5.3.1 Impact of NO_3^- on Anodic Kinetics

In a publication describing the development of ASTM G34,[1] Sprowls et al. suggested that using the correct Cl^-:NO_3^- ratio was important to obtain the desired corrosion morphology, but no explanation was given for this phenomenon. In the current work, it was found that altering the Cl^-:NO_3^- ratio impacted E_{corr}. Figure 3.7 shows that decreasing the Cl^-:NO_3^- ratio caused E_{corr} to increase. The impact of Cl^- on corrosion kinetics is well known, and increases in $[Cl^-]$ would be expected to increase anodic kinetics due to the interaction of the Cl^- ion with the protective oxide film on Al. However, NO_3^- can counteract the impact of Cl^- by competing for adsorption sites in the oxide film.[14]

At some Cl^-:NO_3^- ratios, NO_3^- has been shown to act as an inhibitor. The criterion for NO_3^- to prevent pitting in Al was described by Bohni et al. in an empirical the following empirical relationship:[12]

Equation 3.9

$$\log[Cl^-] = 0.65\ \log[NO_3^-] - 0.78$$

According to Equation 3.9, the 0.6 M NO_3^- present in ASTM G34 and ANCIT solutions would only inhibit pitting for a maximum $[Cl^-]$ of 0.12 M. The actual $[Cl^-]$ in these tests is much higher (4 M), but it was shown that the presence of nitrate still had an impact on anodic kinetics. Figure 3.8(a) and (b) show anodic polarization scans for AA2060-T3 and AA2060-T86 respectively in 4 M NaCl and 4 M NaCl, 0.6 M KNO_3. Anodic kinetics slowed with the addition of NO_3^- for both tempers, but the impact was most significant for the -T3 temper. The passive current density (i_{pass}) and breakdown potential (E_{br}) could not be observed in the anodic scans in Figure 3.8, but in general, a decrease in i_{pass} would be expected to accompany a significant slowing of anodic kinetics. If this was the case for NO_3^- containing solutions, NO_3^- may have helped promote the formation of exfoliation by reducing the passive dissolution rate experienced by surface grains. Exfoliation corrosion occurs when corrosion proceeds along grain boundaries, but if the rate of general corrosion is too high, even IGC susceptible materials may not exhibit EC. For example, when AA2060-T3 was exposed to ASTM G110,[28] an accelerated corrosion test that uses hydrogen peroxide (H_2O_2) as an oxidizing agent, IGC was observed, but no exfoliation blisters formed.[29] H_2O_2 is a strong oxidizing agents and can provide very fast cathodic kinetics, but the general corrosion of surface grains prevented the trapping of corrosion products in IGC fissures which is required for exfoliation formation. If NO_3^- reduces the general corrosion rate of surface grains which are still passive, trapping of corrosion products in IGC fissures would be easier. This role of NO_3^- may be even more important during ANCIT testing where the elevated temperature may act to increase i_{pass}.

Regardless of the influence of NO_3^- on i_{pass}, this ion clearly can play an important role in tuning E_{corr} in chloride containing solutions. For some Al alloys, different attack morphologies form at different potentials.[30] The ability to choose the appropriate E_{corr} in an accelerated test to match that observed during service could be helpful when updating and improving immersion tests for new generation alloys.

3.5.3.2 Impact of Temperature on Anodic Kinetics

Previous work in this study showed that neither ASTM G34 nor ANCIT produced exfoliation in the susceptible temper in the standard exposure time. Extended testing time showed that only 7 days were required for exfoliation formation in ANCIT, while 4 weeks were needed in ASTM G34.[8] The factor that caused faster formation of exfoliation in ANCIT was not identified. In the current work, it was found that the anodic kinetics for the exfoliation-susceptible -T3 temper were faster in ANCIT than in ASTM G34 (Figure 3.6). When anodic kinetics for AA2060-T3 and AA2060-T86 were measured in ANCIT solution at both 25^{o}C and 52^{o}C, the anodic kinetics were slower for the samples exposed at the lower temperature (Figure 3.12). This result indicated that the fast anodic kinetics in ANCIT were due to the high testing temperature (52^{o}C) compared to ASTM G34 (25^{o}C).

The impact of temperature on anodic kinetics of the exfoliation-susceptible -T3 temper was further demonstrated by comparing kinetics and immersion results for ANCIT solution at high and low temperatures. The increase in temperature from 30^{o}C to 52^{o}C caused a simultaneous decrease in E_{corr} and increase in $1/R_p$ (directly proportional to i_{corr}) indicating that the anodic kinetics had increased as expected (Figure 3.13[a]). After 7 days of exposure to these environments, severe exfoliation formed in the sample exposed at 52^{o}C, but no blisters visible to the naked eye were observed on the sample exposed at 30^{o}C. While there are several differences in solution chemistry in ASTM G34 and ANCIT, the temperature difference may actually be the most important factor. As shown in the next section, solution chemistry evolved during exposure. Factors such as solution pH may change during testing, but temperature was always higher for ANCIT exposure than for ASTM G34 exposures. The influence of temperature on anodic kinetics, especially for the susceptible -T3 temper, may have had a more important influence than the other factors.

3.5.4 Cathodic Kinetics in "Used" ASTM G34 and ANCIT Solution

The changes in solution pH during ASTM G34 exposure had an impact on cathodic kinetics. Cathodic kinetics were very fast in freshly made solution (Figure 3.3), but were much slower after 24-h of exposure. Figure 3.15(a) and (b) show that cathodic kinetics in all tests were slower in the "used" solution. Values of $1/R_p$ (directly proportional to i_{corr}) were also smaller in the "used" solution than in the fresh solution (Table 3.6). The cathodic kinetics presented in Figure 3.15 were all measured on freshly prepared samples, but the scans labeled "ANCIT after 24h" and "G34 after 24h" were measured in "used" solution recovered after a standard 24-h immersion test. The most obvious reason for the slowing of cathodic kinetics in ASTM G34 solution was the lowered diffusion limited current for H^+ due to the increase in pH. At the more moderate pH, cathodic kinetics may have been dominated by NO_3^- reduction rather than H^+ reduction.

Cathodic kinetics were also reduced after 24-h of exposure in ANCIT solution, but ANCIT kinetics were faster than ASTM G34 after 24-h. Observed trends were similar for both tempers. The pH change was not significant in ANCIT solution over this period, but cathodic kinetics were most likely reduced because of the depletion in NO_3^-, which was the fastest oxidizing agent in the fresh solution.

Even though the solution pH was very similar for both ASTM G34 and ANCIT in the "used" solution, the cathodic kinetics were faster in ANCIT than in ASTM G34. One possible reason for this result is the impact of testing temperature on cathodic kinetics. The higher exposure temperature during ANCIT (52^{o}C) may have increased i_{lim} by increasing the diffusion coefficient of NO_3^-.

3.5.5 In-Situ Measurements in ASTM G34 and ANCIT

While measuring kinetics on a freshly prepared sample in “used” solution provided insight into solution chemistry changes over time, it did not account for changes in surface condition of the exposed sample. An attempt to capture the impact of the evolution of surface condition was made by measuring open circuit potential (OCP) and polarization resistance (R_p) during ASTM G34 and ANCIT immersion testing of full sized samples (2.54 cm x 2.54 cm x 1.75 cm). Due to the nature of this measurements and possible issues with current distribution on a cubic sample, this data was only used to qualitatively to observe trends in kinetics. Figure 3.16(a) and (b) show $1/R_p$ and OCP for AA2060-T3 in ASTM G34 and ANCIT. In ASTM G34, $1/R_p$ increased during the first few hours of exposure. Over time, however, $1/R_p$ decreased and stabilized at a value similar to the $1/R_p$ in ANCIT. OCP was higher in ASTM G34 than ANCIT during the full 24-h period (Figure 3.15[b]). The changes in $1/R_p$ during ASTM G34 exposure could be rationalized by considering the evolution of solution pH. At the start of ASTM G34 testing, kinetics increased as local anodes initiated. The fast cathodic kinetics H^+ provided at pH 0.2 could support a large number of anodes. However, as H^+ was consumed in reduction reactions and cathodic kinetics slowed, fewer anodes could be supported and some may have stifled. Kinetics continued to decrease until the pH stabilized and a steady state was reached. In ANCIT, solution pH did not change significantly during the first 24-h of exposure, so corrosion kinetics were stable during the full testing period.

3.5.6 Possible Directions for Improvement

The purpose of this work was to provide an understanding of the electrochemical role of testing parameters in ASTM G34 and ANCIT. Differences between ASTM G34 and ANCIT testing protocol included testing temperature, solution pH, and the addition of $AlCl_3$ to the ANCIT solution. While the development of a new immersion test for exfoliation susceptibility was not a direct objective in this work, several observations and recommendations are outlined below.

There was no advantage to the low solution pH in ASTM G34, which provided fast H^+ reduction kinetics. Although there was a peak in $1/R_p$ during the first few hours of exposure the desired attack morphology did not form during this period, and kinetics began to drop after 4.1 hours due to increasing solution pH.

The addition of $AlCl_3$ to ANCIT solution did cause an increase in $1/R_p$ compared to a solution with the same NaCl and KNO_3 concentration and the same pH. While the mechanism for $AlCl_3$ is not yet well understood, it may be a useful tool in accelerated corrosion testing of Al alloys.

The presence of NO_3^- played a role in both anodic and cathodic kinetics. While H^+ reduction dominated the cathodic kinetics in ASTM G34 in fresh solution, NO_3^- kinetics most likely became an important provider of cathodic current after the pH increased. The pH in ANCIT was never low enough to provide fast H^+ reduction kinetics, and NO_3^- was the dominant cathodic reaction in this test. The presence of NO_3^- also slowed anodic kinetics. This effect was much greater for the -T3 temper, and may have supported exfoliation formation by reducing the general corrosion rate of surface grains.

The elevated testing temperature (52°C) for ANCIT caused an increase in anodic kinetics that led to the formation of exfoliation in the susceptible -T3 temper of AA2060. This was the only factor that could be directly linked to exfoliation formation in AA2060-T3, so the impact of temperature should be considered in any future test development.

A significant problem with both tests that was not addressed in this paper was the high degree of attack experienced by the exfoliation-resistant -T86 temper. In natural environments, exfoliation forms in AA2060-T3 while only minor attack develops in AA2060-T86. Reproducing attack morphology observed during natural atmospheric exposure using a full immersion test can be challenging, but future efforts should be aimed at reducing severity towards the exfoliation-resistant tempers.

3.6 Conclusions

The findings of this study are summarized below:

- The solution pH in ASTM G34 increased significantly during the first 24-h of exposure, but only a small increase in pH was observed for ANCIT.
- The evolution of pH over time caused cathodic kinetics to slow in both tests. The slowing of cathodic kinetics was more dramatic in ASTM G34, most likely because the change in pH was more significant in this test.

- At the start of testing, pH was so low in the ASTM G34 testing solution that H^+ reduction dominated cathodic kinetics. As pH increased in ASTM G34, NO_3^- reduction most likely became the primary provider of cathodic current. In ANCIT, pH was more moderate, and NO_3^- reduction dominated. The presence of $AlCl_3$ may have had an impact on the NO_3^- reduction mechanism.
- The addition of $AlCl_3$ caused a change in slope of the cathodic line and an increase in $1/R_p$ compared to the $AlCl_3$ free solution. On a Pt surface, $AlCl_3$ appeared to enhance the H^+ reduction reaction, but the mechanism for Al^{3+} is not yet understood.
- The presence of NO_3^- caused a decrease in anodic kinetics, but this effect was more significant for the -T3 temper than for the -T86 temper. The impact of NO_3^- on anodic kinetics may have promoted formation of exfoliation in the susceptible -T3 temper.
- Elevated temperature caused an increase in anodic kinetics for AA2060-T3 and -T86 exposed to ANCIT solution. Temperature was found to be the critical difference between ASTM G34 and ANCIT. In ANCIT, the fast anodic kinetics due to elevated temperature caused exfoliation to form in the susceptible -T3 temper faster than in ASTM G34.

3.7 Acknowledgements

This work was supported by Rolls-Royce and the Office of the Undersecretary of Defense Corrosion University Pilot Program, Contract #: W911NF-14-2-0005.

3.8 References

1. D.O. Sprowls, J.D. Walsh, M.B. Shumaker, “Simplified Exfoliation Testing of Aluminum Alloys,” in Localized Corrosion – Cause of Metal Failure, STP 516 (Philadelphia, PA: ASTM, 1971), p. 38-65.
2. M.J. Robinson, *Corrosion Sci.* 22, 8 (1982): p. 775-790.
3. M.J. Robinson, *Corrosion Sci.* 23, 8 (1983): p. 887-899.
4. M.J. Robinson, *Corrosion Sci.* 41, 5 (1999): p. 1013-1028.
5. E.M. Zaretskii, A.F. Kireeva, Zavodskaya Laboratoriya 29, 9 (1963): p. 1098-1101.
6. ASTM G34-1, “Standard Test Method for Exfoliation Corrosion Susceptibility in 2XXX and 7XXX Series Aluminum Alloys” (West Conshohocken, PA: ASTM International, 2001), p. 1-7.

7. S. Lee, B.W. Lifka, "Modification of the EXCO Test Method for Exfoliation Corrosion Susceptibility in 7XXX, 2XXX, and Aluminum-Lithium Alloys," in New Methods for Corrosion Testing of Aluminum Alloys, eds. V.S. Agarwala, G.M Ugiansky, STP 1134 (West Conshohocken, PA: ASTM International, 1992), p. 1-19.
8. M.E. Parker, R.G. Kelly, *Corrosion* 72, 11 (2016): p. 1342-1350.
9. M. Keddam, C. Kuntz, H. Takenouti, D. Schuster, D. Zuili, Electrochimica Acta 42, 1 (1997): p. 87-97.
10. A.M. McKissick, A.A. Adams, R.T. Foley, J. Electrochem. Soc. 117, 11 (1970): p. 1459-1460.
11. B.W. Samuels, K. Sotoudeh, R.T. Foley, *Corrosion* 37, 2 (1981): p. 92-97.
12. H. Bohni, H.H. Uhlig, J. Electrochem. Soc. 116, 7 (1969): p. 906-910.
13. S. Pyun, S. Moon, *J. Solid State Electrochem* 3 (1999): p. 331-336.
14. R. Ambat, E.S. Dwarakadasa, *Corrosion Sci*. 33, 5 (1992): p. 681-690.
15. K.R. Cooper, R.G. Kelly, *J. Chromatogr. A* 850 (1999): p. 381-389.
16. C.B. Crane, R.G. Kelly, R.P. Gangloff, *Corrosion* 72, 2 (2016): p. 242-263.
17. K. Sotoudeh, T.H. Nguyen, R.T. Foley, B.F. Brown, *Corrosion* 37, 6 (1981): p. 358 – 362.
18. McCafferty, E. *Introduction to Corrosion Science*. Springer 2010, p. 188.
19. Z.A. Foroulis, M.J. Thubrikar, Materials and Corrosion 26, 5 (1975): p. 350 – 355.
20. A.Y. El-Etre, *Corrosion Sci.* 45 (2003): p. 2485-2495.
21. J.P. Moran, F.S. Bovard, J.D. Chrzan, P. Vandenburgh, "Corrosion Performance of New Generation Aluminum-Lithium Alloys for Aerospace Applications," 13th Int. Conf. on Aluminum Alloys, held June 3-7, 2012 (Hoboken, NJ: John Wiley & Sons, Inc., 2012).
22. N. Ott, Y. Yan, S. Ramamurthy, S. Kairy, N. Birbilis, *Scrip. Mater.* 119 (2016): p. 17-20.
23. N. Ott, S.K. Kairy, Y. Yan, N. Birbilis, *Metallurgical Materials Trans. A* 48, 1 (2017): p. 51-56.
24. R.J. Rioja, J. Liu, *Metal. Mater. Trans. A* 43 (2012): p. 3325-3337.
25. P. Khullar, *Cathodic Control of Intergranular Corrosion in Sensitized AA5083-H131*. PhD Dissertation (2018): p. 163-188.
26. P.C. Hayes, *Process Principles in Minerals and Materials Production*. Hayes Publishing (1993): p. 663.
27. C. Liu, Personal Communication (2017).

28. ASTM G110-92, “Standard Practice for Evaluating Intergranular Corrosion Resistance of Heat Treatable Aluminum Alloys by Immersion in Sodium Chloride + Hydrogen Peroxide Solution” (West Conshohocken, PA: ASTM International, 2003), p. 1-3.
29. M.E. Parker, R.G. Kelly, *Materials Science Forum* 794 (2014): p. 223-228.
30. W. Zhang, G.S. Frankel, *Electrochimica Acta* 48 (2003): p. 1193–1210.

4. The Role of H_2O_2, and $K_2S_2O_8$ as Oxidizing Agents in Accelerated Corrosion Testing

Summary:

In this chapter, the role of two oxidizing agents, hydrogen peroxide (H_2O_2) and potassium persulfate ($K_2S_2O_8$), in accelerated corrosion testing was investigated. Oxidizing agents are commonly used to accelerate corrosion kinetics during immersion testing, but different oxidizing agents can have different impacts on Al alloys. For example, KNO_3 acted as an oxidizing agent during ANCIT testing and generated faster cathodic kinetics than the oxygen reduction reaction, but KNO_3 also caused the anodic kinetics of AA2060 to slow. Investigating the impact of other oxidizing agents on the corrosion behavior of AA2060 provided a deeper understanding of the behavior of Al-Li alloys during immersion testing. H_2O_2 was found to be a powerful oxidizing agent, but it decomposed after being added to a test solution and could not be stored for more than a few hours before the concentration measurably decreased. $K_2S_2O_8$ was stable for days after mixing, but cathodic kinetics were not as fast for this species as they were for H_2O_2. The cathodic kinetics of $K_2S_2O_8$ were manipulated by decreasing solution pH and adding aluminum chloride ($AlCl_3$). Both of these changes increased cathodic kinetics, but the under-aged and near peak-aged tempers could not be distinguished after exposure to the solution containing $AlCl_3$ as they both formed pitting. In other solutions, intergranular corrosion (IGC) developed in the under-aged temper rather than pitting. Neither H_2O_2 nor $K_2S_2O_8$ were found to be appropriate for exfoliation testing of Al-Li alloys, but these oxidizers could be used to quickly distinguish between intergranular corrosion (IGC) and pitting susceptibility.

4.1 Abstract

In this work, the application of two oxidizing agents hydrogen peroxide (H_2O_2) and potassium persulfate ($K_2S_2O_8$) to accelerated corrosion testing was considered. H_2O_2 is already used as an accelerant in ASTM G110, and $K_2S_2O_8$ is an oxidizing agent that shows promise for corrosion testing applications. A Koutecky-Levich approach was used to investigate the cathodic kinetics of both oxidizing agents as well as dissolved oxygen (O_2). Cathodic kinetics for O_2, H_2O_2, and $S_2O_8^{2-}$ were faster when measured on a Pt electrode than when measured on an AA2060-T3 electrode. This difference was attributed to the additional limit to cathodic kinetics posed by the

protective oxide film on aluminum. H_2O_2 was a more potent accelerant than $K_2S_2O_8$ at a concentration of 0.1 M due to the faster cathodic kinetics of H_2O_2 on aluminum. However, $K_2S_2O_8$ was more convenient to use in a laboratory setting due to its stability during storage. The severity of tests using $K_2S_2O_8$ was increased by lowering the solution pH to 2.28. At the low solution pH, cathodic kinetics and extent of attack increased. Adding 0.022 M $AlCl_3$ to the test solution also increased the cathodic kinetics in tests using $K_2S_2O_8$, but the attack morphology looked similar for both tempers, and the tempers could not be distinguished.

4.2 Introduction

Accelerated corrosion testing plays a critical role in alloy and temper design, material selection, and lot acceptance. As new generation high-strength aluminum alloys are being produced, many standardized tests designed for legacy alloys are failing to reproduce service results for the new alloys.[1-3] Improved corrosion testing protocol is needed, but data to guide changes is lacking. Without a foundation of understanding of the roles of different accelerating agents, accelerated test development must proceed by trial and error. The long service times of interest make validation of accelerated testing expensive, so clear mechanistic connections are important.

4.2.1 The Role of Oxidizing Agents in Accelerated Corrosion Testing

There are many approaches for accelerating corrosion in a laboratory environment, but one of the most effective for high-strength aluminum alloys is to add an oxidizing species that will provide faster cathodic kinetics than oxygen does. In most aqueous solutions, oxygen reduction (ORR) dominates cathodic kinetics for aluminum alloys at near neutral pH, but the solubility of oxygen is low in sodium chloride (NaCl) solutions, and the cathodic kinetics tend to be limited by the diffusion of oxygen.[4] Figure 4.1 shows the O_2 solubility in various salt solutions.

Jakab et al. used the Koutecky-Levich approach to study the oxygen reduction reaction (ORR) on AA2024-T3, high-purity aluminum, and high-purity copper.[5] Charge-transfer, mixed, and mass-transfer controlled regimes were observed for ORR at different potentials on the AA2024-T3 electrode. It was found that ORR occurred at a lower rate on AA2024-T3 compared to pure copper, but the lowest ORR rate was measured on pure aluminum.[5] The rate determining step for ORR on pure aluminum is thought to be impacted by the protective oxide film on Al. If cathodic reactions occur at the metal-oxide film interface, the oxidizing species must diffuse through the oxide film before reacting. If cathodic reactions occur at the oxide film-electrolyte interface, electrons must migrate through the oxide film to react. Pryor and Keir reported that the low ORR rate on pure Al was due to the high electronic resistance of aluminum oxide, which prevented electronic migration through the film except at "weak" points in the film.[6] ORR kinetics are much faster on pure Cu than on pure Al, and Cu-rich sites that arise from Cu-replating on AA2024-T3[5,7] can enhance ORR on this alloy, leading to accelerated corrosion.

One way to increase cathodic kinetics during accelerated corrosion testing of aluminum alloys is to add an additional oxidizing agent. Several oxidizing agents are already used in standard accelerated corrosion tests (KNO_3 in ASTM G34, H_2O_2 in ASTM G110),[8,9] but there are many other oxidizing species that have not yet been explored for this purpose.

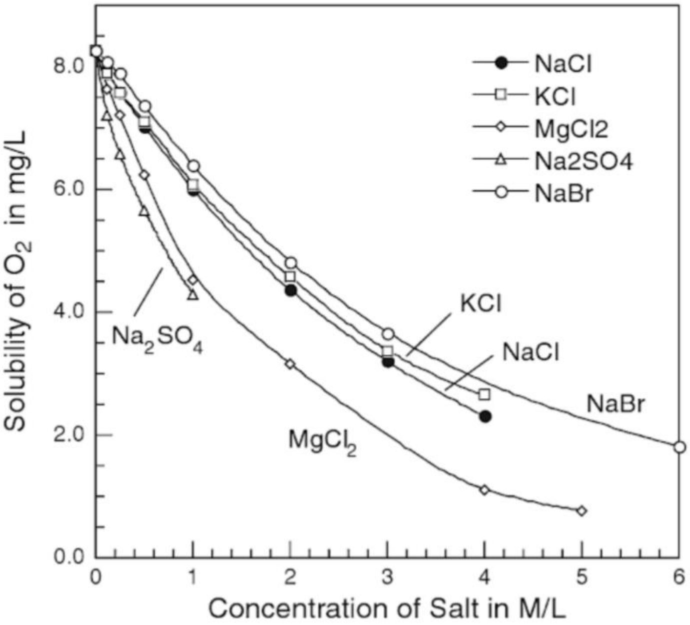

Figure 4.1: Solubility of O_2 decreases with increasing NaCl concentration. From reference 4.

4.2.2 ASTM G110 Immersion Testing

One standard immersion test for localized corrosion in high-strength Al alloys is ASTM G110.[9] This test contains a high concentration of NaCl (~1.0 M), operates at a slightly elevated temperature (30°C), and contains the oxidizing agent H_2O_2 (~0.1 M) to provide fast cathodic kinetics. Samples are fully immersed in the test solution for a minimum of 6 hours, with longer exposures allowed if deemed appropriate by the experimenters. After exposure, samples are prepared for examination with optical microscopy, where the type and extent of localized corrosion is evaluated.

In some ways, H_2O_2 is an ideal oxidizing agent for aluminum corrosion testing. It has full miscibility with water and its reaction products are non-toxic. The drawback of this oxidizing agent is its poor stability when exposed to light or heat. Impurities in the solution can induce homogenous decomposition of H_2O_2 as well. Yazici et al. reported that decomposition of 800 mg/L H_2O_2 accelerated greatly at a temperature of 50^{o}C. The presence of dissolved $CuSO_4$ also increased the rate of decomposition.[10] Care must be taken when storing H_2O_2 to prevent a reduction in concentration, and test solutions must only be mixed immediately before testing begins.

Long testing times are required for some tests, but the fast cathodic kinetics provided by the added oxidizing species are expected to slow over time as reduction reactions deplete the supply of oxidizer. For tests that last several days, it can be beneficial to replenish the oxidizing species at a regular interval. However an understanding of the depletion rate is necessary to set an appropriate schedule. If the oxidizer is replenished too early, high concentrations may accumulate.

4.2.3 Alternative Oxidizers for use in Accelerated Corrosion Testing

H_2O_2 is not the only oxidizing agent available for use in accelerated corrosion testing, but many oxidizers, such as $KMnO_4$, $Ca(ClO)_2$, and $K_2S_2O_8$, are still unexplored for this application. Unlike H_2O_2, which is near neutral when dissolved in NaCl solutions, $KMnO_4$ forms a basic solution and $K_2S_2O_8$ forms an acidic solution. The impact of pH on aluminum alloys during accelerated testing is significant, so pH must be considered when exploring alternative oxidizing agents. In this study, several oxidizing agents were screened, but $K_2S_2O_8$ was chosen for further investigation due to its moderate acidity (pH~3.5). Acidic, neutral, and alkaline solutions can be used for accelerated corrosion testing, but acidic environments are more common in standard corrosion tests for aluminum (ASTM G34, ASTM G85-A2, ANCIT).[8,11,12]

4.2.4 Al-Cu-Li Alloys in Accelerated Corrosion Testing

The materials chosen for this study included an under-aged (T3) temper and a near peak-aged (T86) temper of a third-generation aluminum-copper-lithium (Al-Cu-Li) alloy AA2060. These two tempers were chosen because their localized corrosion behavior during seacoast exposure has already been documented. The under-aged T3 temper experiences intergranular corrosion (IGC) while the near peak-aged temper T86 undergoes pitting.[1] The transition from IGC to pitting susceptibility is due to microstructural changes that occur during thermomechanical treatments that produce the near-peak aged heat treatment.[13,14] It is critical that accelerated corrosion tests can distinguish between different forms of localized corrosion susceptibility for different alloy tempers.

The following work presents a comparison of the stability, kinetics, and immersion corrosion testing results for two oxidizing agents. The first, H_2O_2 has already been utilized in standard testing procedure (ASTM G110), and the second, $K_2S_2O_8$, will be presented as an alternative that could be used in new accelerated corrosion tests.

4.3 Experimental Procedures

4.3.1 Electrochemical Measurements

Unless indicated otherwise, all electrochemical measurements were performed using a standard three electrode flat cell with a saturated calomel reference electrode (SCE), a platinum mesh counter electrode, and a 1 cm^2 exposure window for the working electrode. A scan rate of 0.5 mV/s was used in all polarization measurements. Measurements were made with a Biologic poteniostat, and IR compensation was used. IR compensation was performed by averaging 4 impedance measurements at a frequency of 100 kHz. Data measured during linear polarization was compensated at 85%.

4.3.2 Sample preparation

In all cases, AA2060-T3 and -T86 samples were ground to a 1200 grit finish before electrochemical measurements or immersion testing. After grinding, the samples were cleaned ultrasonically in DI water and rinsed with ethanol. AA2060 composition is presented in Table 4.1.[15]

Table 4.1: Composition of AA2060 (w/w%).[15]

Li	Cu	Mg	Ag	Zr	Mn	Zn	Al
0.75	3.95	0.85	0.25	0.11	0.30	0.40	Bal.

4.3.3 Monitoring Oxidizer Concentration

A method was devised to monitor the concentration of oxidizing species in a test solution by measuring the diffusion limited current (i_{lim}) of the oxidizer on a 1 mm diameter platinum wire working electrode. The i_{lim} is related to bulk oxidizer concentration (C_b) according to Equation 4.1,[4] where δ is the thickness of the diffusion layer, n is the number of electrons transferred during reduction, F is Faraday's constant, and D is the diffusion coefficient for the oxidizing species.

Equation 4.1[4]

$$|i_{lim}| = \frac{nFDC_b}{\delta}$$

With the assumption that n, F, D, and δ were constant, a linear relationship was determined between i_{lim} and C_b by measuring i_{lim} in several solutions with known H_2O_2 or $K_2S_2O_8$ concentration. These data were then used to construct a calibration curve to determine unknown oxidizer concentrations from a measured i_{lim}.

Calibration curves were constructed for both H_2O_2 and for $K_2S_2O_8$ using solutions of 1 M NaCl and various concentrations of the oxidizing species as shown in Table 4.2.

Table 4.2: Oxidizer concentrations used for constructing calibration curve

Oxidizing Species	Bulk Oxidizer Concentration, C_b (M)					
H_2O_2	0.015	0.025	0.035	0.050	0.075	0.10
$K_2S_2O_8$	0.015	0.025	0.030	0.050	0.075	0.10

To measure i_{lim}, the Pt wire working electrode was polarized cathodically from +0.05 V vs. OCP to -1.1 V vs. SCE. The cathodic polarization began after a short period of time, usually 5 minutes, to allow the OCP to stabilize. Testing temperature was maintained at 30^{o}C using a temperature control chamber. This temperature was chosen because it is the testing temperature used in the ASTM G110 standard. Diffusion-limited current density was taken at a potential of -0.6 V_{SCE}. When all of the added oxidizer was consumed from the test solution, ORR became the dominant cathodic reaction. The presence of the ORR reaction meant that the detection limit for this method was approximately 0.01 M.

Once the calibration curves were completed, i_{lim} measurements were used to track changes in oxidizer concentration during two scenarios. The first was intended to imitate the conditions during solution storage, and the second was to imitate the conditions during immersion testing. In the first scenario, only the Pt wire working electrode, Pt mesh counter electrode, and SCE reference electrode were inserted into the testing solution. In the second scenario, an AA2060 sample with a surface area of 13.0 cm^2 was inserted into the test solution in addition to the working, counter, and reference electrodes. Note that the Pt wire was still used as the working electrode in the second scenario. The purpose of the AA2060 sample was simply to support corrosion processes that would consume the oxidizing species as occurs during immersion testing. The starting solution for each scenario was 1 M NaCl and 0.1 M H_2O_2 or $K_2S_2O_8$, and testing temperature was 30^{o}C. For all tests, i_{lim} was measured daily on the platinum working electrode. Solution volume to surface area ratio was no less than 11 mL/cm^2. The Pt wire was still the working electrode in this test, but the AA2060 sample dissolution allowed for changes in solution chemistry to occur as they would during an accelerated corrosion test.

4.3.4 Rotating Disk Electrode Measurements

A rotating disk electrode (RDE) system was used to obtain an understanding of the cathodic kinetics for O_2, H_2O_2, and $K_2S_2O_8$. The RDE setup allows measurements to be made under controlled conditions where the diffusion layer is determined by the rotation speed (ω) of the disk electrode. The diffusion limited current density (i_{lim}) is related to the oxidizing species diffusivity (D) according to Equation 4.2,[16] where v is the kinematic viscosity.

Equation 4.2[16]

$$i_{lim} = 0.620nFD^{2/3}v^{-1/6}C_b\omega^{1/2}$$

If n, F, and v are known, the diffusion coefficient of the oxidizing species can be determined from the slope of the line obtained when i_{lim} is plotted against $\omega^{0.5}$. Relevant parameters such as v, and O_2 concentration were obtained using OLI solution modeling.[*] For calculations relevant to O_2 and H_2O_2, the MSE (H_3O+ ion) database. $K_2S_2O_8$ was not included in the MSE (H_3O+ ion database, so the AQ (H+ ion) database was used for $K_2S_2O_8$ calculations.

---

[*] OLI version 9.5.4 was used for this work.

For cathodic reactions that exhibit mixed control (both activation control and mass transfer control influence current), a Koutecky-Levich analysis can be used to calculate the activation controlled current density (i_{act}) and the diffusion limited current density (i_{lim}) from the total measured cathodic current (i_T). A Koutecky-Levich plot is constructed by plotting the inverse of the total measured current ($1/i_T$) at a particular potential against the inverse square root of the rotation rate ($\omega^{-1/2}$).[5] The y-intercept of the linear trend lines associated with data obtained at a particular potential is related to the i_{act} according to Equation 4.3. The i_{lim} can then be calculated from the total measured current and the activation controlled current according to Equation 4.4. It can be seen from Equation 4.4 that the total measured current (i_T) will be dominated by the smaller of the i_{act} and i_{lim}. When cathodic over potential is high, i_{act} will also be high and i_T is approximately equal to i_{lim}.

Equation 4.3[5]

$$y_{intercept} = \frac{1}{i_{act}}$$

Equation 4.4[5]

$$\frac{1}{i_T} = \frac{1}{i_{act}} + \frac{1}{i_{lim}}$$

Measurements were made using both a platinum RDE and an AA2060-T3 RDE. For tests on the Pt electrode, a solution of 1.0 M NaCl was used, with 0.1 M oxidizing species added when needed. For tests on the AA2060-T3 electrode, a Cl^- free environment was used to avoid excessive attack on the aluminum electrode during measurements. A supporting electrolyte of K_2SO_4 was used when measuring the kinetics of O_2 and H_2O_2, but Na_2SO_4 had to be used when measuring the kinetics of $K_2S_2O_8$ to avoid reaching the maximum solubility of K^+ in solution. To correct for any impact of the change in supporting electrolyte on the diffusivity of the oxidizing species, OLI was used to determine the best concentration of the substitute supporting electrolyte. For example, a solution of 0.56 M K_2SO_4 results in a similar O_2 diffusivity and similar O_2 concentration as a 1.0 M NaCl solution. For measuring H_2O_2 kinetics on AA2060-T3, a solution of 0.41 M $K_2S_2O_8$ and 0.1 M H_2O_2 was used. When measuring $K_2S_2O_8$ kinetics on AA2060-T3, a solution of 0.32 M Na_2SO_4 and 0.1 M $K_2S_2O_8$ was used. A mercury-mercurous sulfate (MMS) reference electrode was used for the Cl^- free tests.

After period to allow the OCP to stabilize, usually 5 - 15 minutes, cathodic polarization was used to measure i_{lim}. For Pt samples, the scan started at 0 V vs. SCE, and ended at -1.2 V vs. SCE. For the AA2060-T3 samples, the scan started at +0.01 V vs. OCP, and ended at -2.0 V vs. MMS. i_{lim} was measured for rotation rates of 30, 60, 100, 300, 600, and 1000 rpm. The pH of each solution was measured before testing began.

4.3.5 Immersion Testing and Cathodic Kinetics under Quiescent Conditions

Immersion testing was carried out on AA2060-T3 and AA2060-T86 samples with geometry as shown in Figure 4.2. The testing procedure followed the ASTM G110 testing protocol with one minor modification. The G110 standard calls for an etching/cleaning procedure of where samples are immersed in a solution of nitric acid (HNO_3) and hydrofluoric acid (HF) at high temperature (93^oC). Due to environmental and safety concerns, this step was omitted from the testing procedure. All other steps, including the 1 minute immersion in concentrated HNO_3, were followed as described by the G110 standard.

Each sample was placed in a separate beaker, and the beakers were placed in a water bath to maintain a temperature of 30^oC. Samples were placed on top of small inverted beakers to prevent them from touching the bottom of the larger beaker as shown schematically in Figure 4.3. An exposure time of 12 hours was chosen to provide time for significant localized corrosion to develop. Testing was carried out using the ASTM G110 solution of 1 M NaCl and 0.1 M H_2O_2, but also with a substitution of 0.1 M $K_2S_2O_8$ for the standard oxidizer. Several modifications to the immersion test with $K_2S_2O_8$ were explored for the purpose of understanding the impact of oxidizer concentration and solution pH on immersion testing severity. Other immersion testing environments considered in this work include: 1 M NaCl, 0.125 M $K_2S_2O_8$, solution pH 2.28 and 1 M NaCl, 0.1 M $K_2S_2O_8$, 0.022 M $AlCl_3$, solution pH 3.2. Temperature was 30^oC in both tests.

After immersion testing, samples were cleaned ultrasonically in DI water to remove excess corrosion products, cross-sectioned, mounted, and polished to a 1 μm finish for examination with optical microscopy.

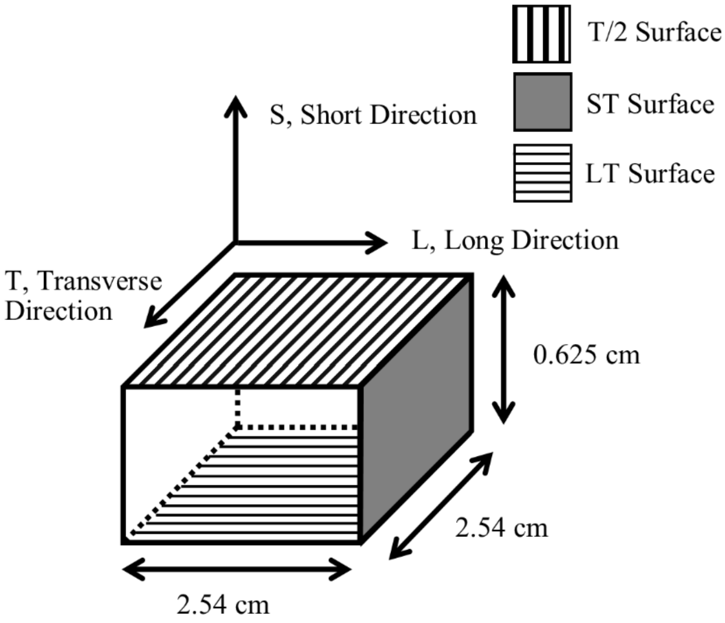

Figure 4.2: Schematic showing geometry of AA2060-T3 and -T86 immersion samples.

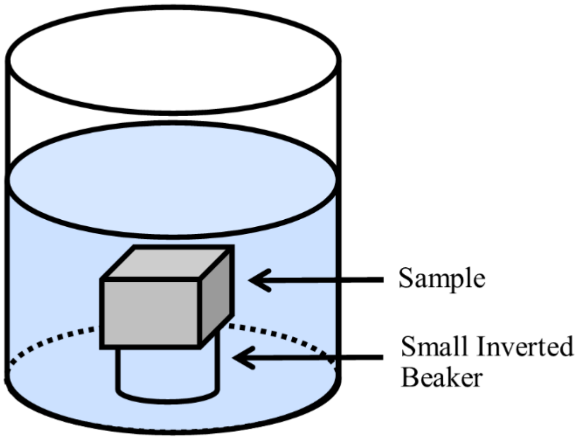

Figure 4.3: Schematic showing the immersion testing apparatus. The sample was supported by a small inverted beaker.

Cathodic kinetics under quiescent conditions were measured on AA2060-T3 and AA2060-T86 using linear polarization in each of the solutions used for immersion testing. Scans began at +0.025 V vs. OCP and ended at -1.0 V vs. SCE after a 15 min period for the OCP to stabilize.

These scans were performed in the standard ASTM G110 test solution of 1 M NaCl and 0.1 M H_2O_2 or 0.1 M $K_2S_2O_8$, as well as in several modified solutions.

4.4 Results

4.4.1 Stability of H_2O_2 and $K_2S_2O_8$ during Storage and Immersion Testing

A linear relationship between i_{lim} and oxidizer concentration (C_b) was established by measuring i_{lim} in several solutions of known H_2O_2 or $K_2S_2O_8$ concentration. Linear regression was used to establish a mathematical expression for this relationship. The data and trend lines can be seen in Figure 4.4.

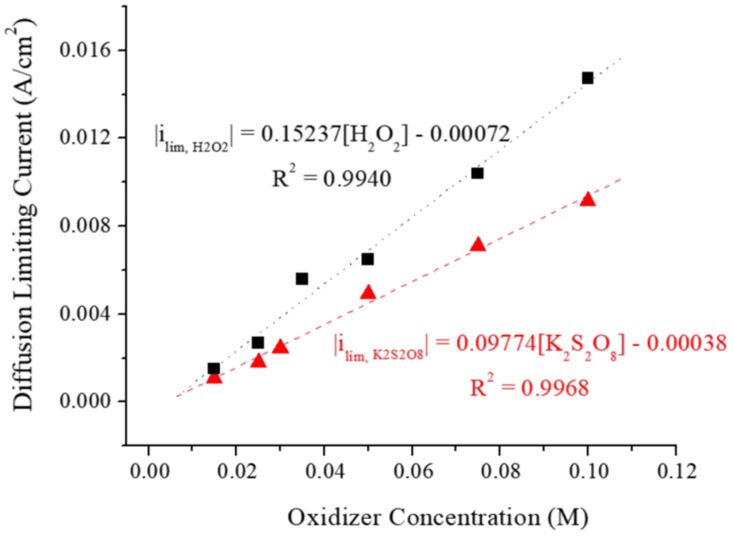

Figure 4.4: Relationship between oxidizer concentration and i_{lim} for H_2O_2 and $K_2S_2O_8$ on a platinum electrode at 30^{o} in a solution of 1 M NaCl.

The empirical relationship between oxidizer concentration and i_{lim} (Equation 4.5, Equation 4.6) was used to monitor oxidizer concentration over time during two test scenarios. The first scenario was intended to imitate conditions during solution storage prior to immersion testing. In the second scenario, an AA2060 sample was placed in the test solution to imitate conditions during immersion testing.

Equation 4.5

$$[H_2O_2] = \frac{|i_{lim,H2O2}| - 0.00072}{0.15237}$$

Equation 4.6

$$[K_2S_2O_8] = \frac{|i_{lim,K2S2O8}| - 0.00038}{0.09774}$$

The results for both oxidizing agents in the two test scenarios are shown in Figure 4.5. The test imitating storage conditions (no AA2060 sample present in the test solution) showed that the concentration of H_2O_2 decreased rapidly over time due to homogenous decomposition. This decomposition was partly due to the slightly elevated testing temperature (30^{o}C), but reported decomposition for H_2O_2 in the literature was similar at 20^{o}C and 30^{o}C.[10] NaCl has been reported to have very little impact on H_2O_2 decomposition, and in some cases Cl^- inhibited H_2O_2 decomposition by reacting with other species that would otherwise catalyze the breakdown of H_2O_2.[17-19] H_2O_2 is extremely sensitive to light, especially UV radiation.[17,18] Although most of the this test was performed in a closed temperature control chamber with little light exposure, the test solution was periodically exposed to light during the set up for each measurement.

In contrast, solutions containing $K_2S_2O_8$ were very stable over time. These results indicate that test solutions containing H_2O_2 should only be mixed right before testing begins. In contrast, solutions containing $K_2S_2O_8$ may be made as much as a week ahead of time and stored.

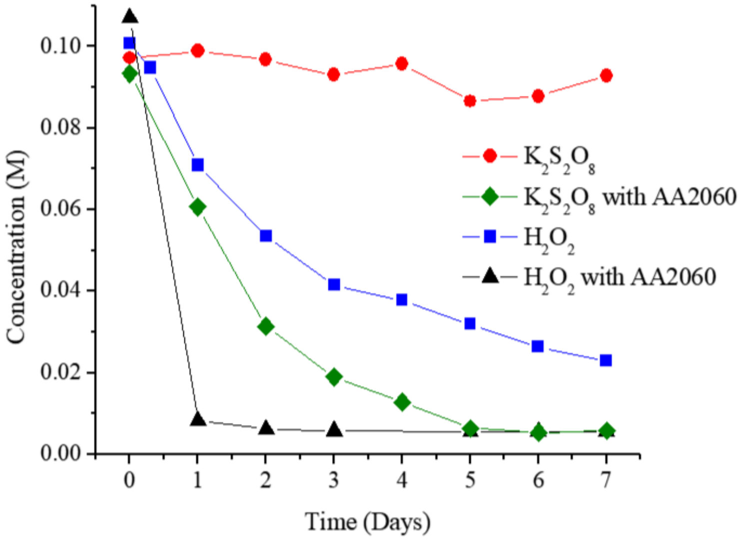

Figure 4.5: Concentrations of H_2O_2 and $K_2S_2O_8$ over time in 1 M NaCl at 30ºC. The starting oxidizer concentration in each case was 0.1 M.

In the scenario imitating immersion testing conditions (AA2060 sample was present in solution), concentration for both oxidizers dropped over time. This decrease was due to the consumption of oxidizing species in reduction reactions as the aluminum corroded. The concentration of H_2O_2 decreased faster than $K_2S_2O_8$, which could partly be accounted for by the homogenous reactions in solution that occurred even in the absence of AA2060, but may also have been an indication that reaction rate for H_2O_2 reduction was faster than the reaction rate for $S_2O_8^{2-}$ reduction.

4.4.2 Measuring Diffusion Coefficients

RDE tests were used to gain a better understanding of reduction kinetics for oxygen (O_2), H_2O_2, and $K_2S_2O_8$ and to calculate diffusion coefficients for each of the oxidizing agents. Table 4.3 summarizes relevant parameters such as the type and concentration of supporting electrolyte, the solution pH, and the number of electrons transferred during reduction. The reduction reactions that were assumed for each oxidizer are shown in Equation 4.7 - Equation 4.10.[20] At a solution pH of ~3.5, $S_2O_8^{2-}$ may be reduced by two different mechanisms (Equation 4.9, Equation 4.10). If pH increases, the reaction will tend to proceed by Equation 4.9, but if the pH decreases, Equation 4.10 will become more dominant.

The kinematic viscosity (*v*) and O_2 concentration that were calculated in OLI are also included in Table 4.3. These parameters were necessary to calculate diffusivity. For tests utilizing an AA2060-T3 working electrode, excessive attack formed when the tests were performed in a Cl^- containing environment. To avoid access attack during the measurement of cathodic kinetics on AA2060-T3, these tests were carried out in Cl^- free environments with supporting electrolytes such as K_2SO_4 or Na_2SO_4.

Table 4.3: Parameters for RDE Testing

Species	Electrode	ν (m^2/s)	C_b (M)	n	Supporting Electrolyte	pH
O_2	Pt	1.01×10^{-6}	0.00021	2	1 M NaCl	4.71
H_2O_2	Pt	1.01×10^{-6}	0.1	2	1 M NaCl	5.30
$S_2O_8^{2-}$	Pt	9.95×10^{-7}	0.1	2	1 M NaCl	3.50
O_2	2060-T3	9.84×10^{-7}	0.00020	2	0.56 M K_2SO_4	6.37
H_2O_2	2060-T3	9.80×10^{-7}	0.1	2	0.41 M K_2SO_4	6.12
$S_2O_8^{2-}$	2060-T3	1.03×10^{-6}	0.1	2	0.32 M Na_2SO_4	3.50

Equation 4.7

$$O_{2(g)} + 4H^+_{(aq)} + 4e^- \rightarrow 2H_2O$$

Equation 4.8

$$H_2O_{2(aq)} + 2H^+_{(aq)} + 2e^- \rightarrow 2H_2O$$

Equation 4.9

$$S_2O^{2-}_{8(aq)} + 2e^- \rightarrow 2SO^{2-}_{4(aq)}$$

Equation 4.10

$$S_2O^{2-}_{8(aq)} + 2H^+ + 2e^- \rightarrow 2HSO^-_{4(aq)}$$

Figure 4.6 shows the cathodic kinetics of dissolved O_2 on Pt and AA2060-T3 electrodes. On the Pt electrode, cathodic kinetics appeared to be diffusion limited below a potential of -0.3 V_{SCE} (Figure 4.6[a]). With every increase in RPM, an increase in i_{lim} was observed. Cathodic kinetics of O_2 on the AA2060-T3 electrode appeared to be under mixed control (Figure 4.6[b]). Rotation rate did not influence cathodic current significantly.

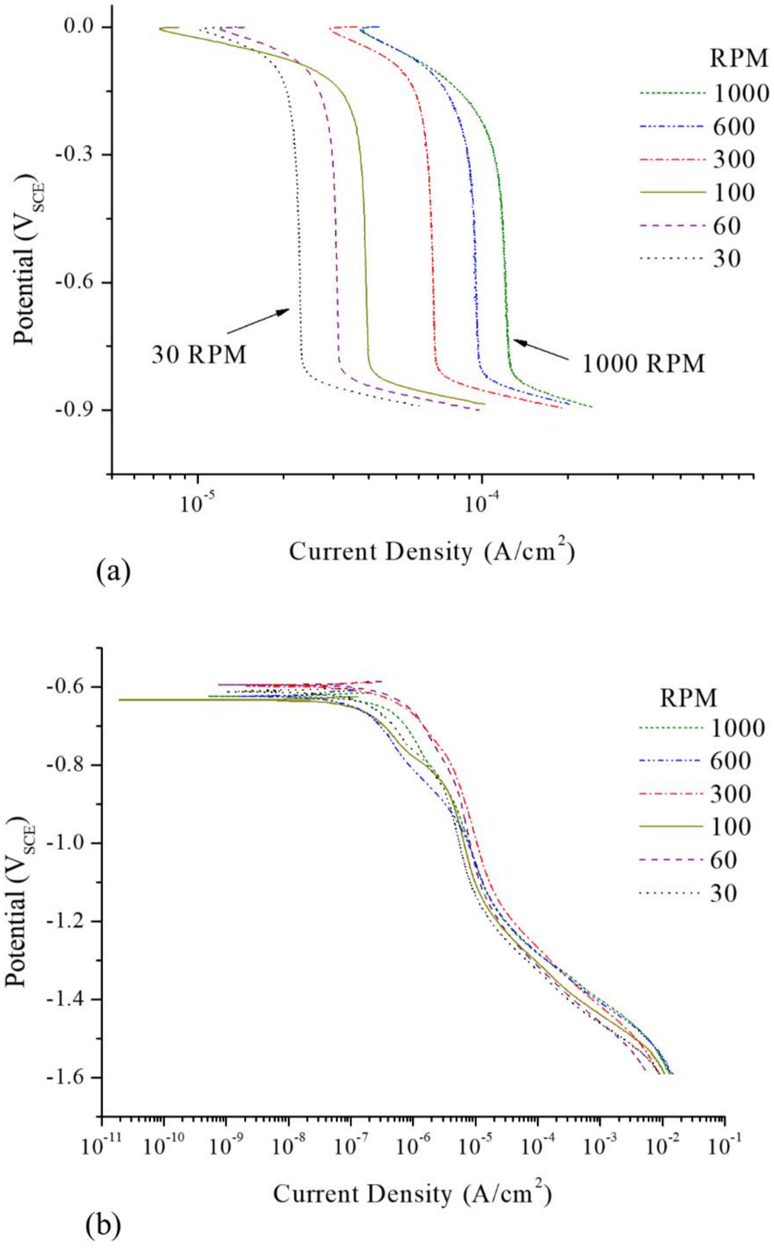

(a)

(b)

Figure 4.6: Cathodic polarization scans at various rotation rates showing cathodic kinetics of dissolved O_2 on (a) a Pt electrode and (b) an AA2060-T3 electrode.

A Koutechky-Levich analysis was applied to all RDE to determine an accurate value for i_{lim}. In a Koutechky-Levich plot, the dependence of $1/i_T$ on $\omega^{-1/2}$ is shown for several different potentials. The i_{act} at each potential can be obtained from the y-intercept of trend lines associated with data at each potential (Equation 4.3). Figure 4.7(a) and (b) show the Koutecky-Levich plot for the reduction of dissolved O_2 on Pt and the reduction of $S_2O_8^{2-}$. For potentials of -0.6 V_{SCE}, -0.7 V_{SCE}, and -0.8 V_{SCE}, the relationship between i_T and ω was independent of potential, indicating that the system was diffusion limited at all of these potentials. A slight potential dependence of i_T was observed for $S_2O_8^{2-}$ reduction kinetics from -0.6 V_{SCE} to -0.8 V_{SCE}, and the y-intercept for lines constructed at these potentials increased with increasing potential. Below -0.8 V_{SCE}, cathodic kinetics were unaffected.

Values for i_{lim} and i_{act} were calculated for each oxidizing agent and electrode material. The ratios of i_{lim} / i_{act} are presented in Figure 4.8. When the value of i_{lim} / i_{act} was near zero, this indicated that $i_{lim} << i_{act}$. Based on Equation 4.4, when $i_{lim} << i_{act}$, the value of i_{lim} is approximately equal to i_T. For O_2, H_2O_2, and $S_2O_8^{2-}$ kinetics measured on Pt as well as H_2O_2 kinetics measured on AA2060-T3, this approximation was used to construct Levich plots. For O_2 and $S_2O_8^{2-}$ kinetics measured on AA2060-T3, this approximation could not be applied, and the i_{lim} calculated from the Koutecky-Levich plot was used instead.

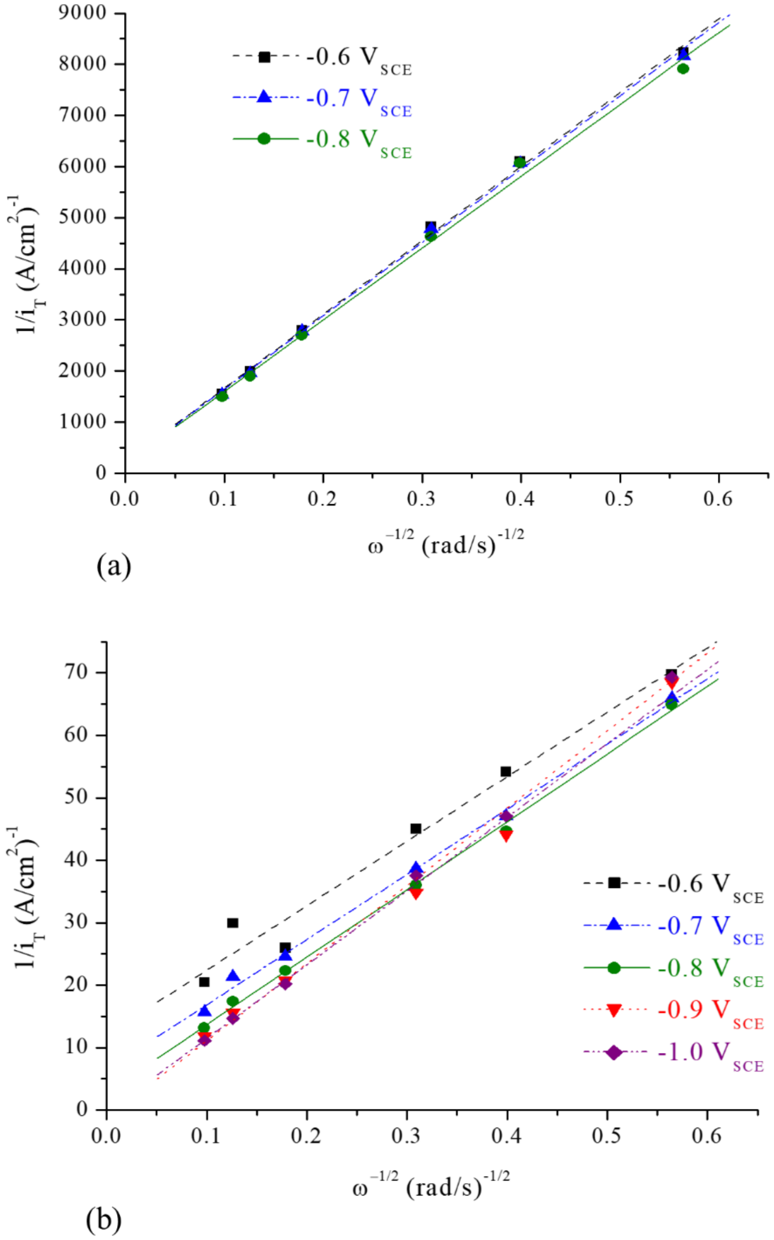

Figure 4.7: Koutecky-Levich plots for (a) reduction of dissolved O_2 and (b) reduction of 0.1 M $S_2O_8^{2-}$. 1.0 M NaCl was also present in both solutions.

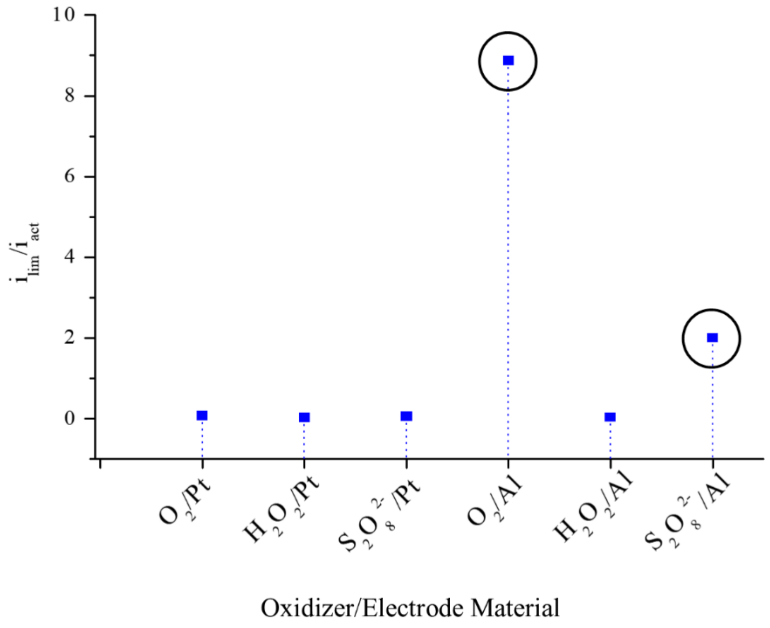

Figure 4.8: Summary of the ratio of i_{lim} / i_{act} for each oxidizer and electrode material combination. The two circled data points had a high value of i_{lim} / i_{act}, which indicated that mixed control was present in these tests. i_{lim} and i_{act} were calculated using a Koutechy-Levich analysis. i_{lim} was taken at 300 RPM and a potential of -1.0 V_{SCE} for every test except for dissolved O_2 on Pt. In this case, a higher potential (-0.8 V_{SCE}) was used to avoid the H_2O reduction reaction.

Figure 4.9 and Figure 4.9 shows the Levich plots for dissolved O_2 and the added oxidizing agents on Pt and AA2060-T3. In general, diffusivities calculated on the Pt surface were slightly lower than reported literature values (Table 4.4).

The i_{lim} measured for O_2 reduction was much lower for AA2060-T3 than it was for Pt (Figure 4.9). In addition, rotation rate (ω) had virtually no impact on i_{lim} on the AA2060 sample. The apparent diffusivity calculated from the data calculated on AA2060-T3 was 3.64 x 10^{-13} m^2/s. This number was significantly lower than the diffusivity calculated using the Pt working electrode. The apparent diffusivity measured on the AA2060-T3 may have been slowed by the extra diffusion barrier posed by the protective oxide film on aluminum.

The Levich plots for H_2O_2 on a Pt surface and on an AA2060-T3 surface are shown in Figure 4.10(a). Similarly to O_2 reduction, i_{lim} was lower on the AA2060-T3 surface than it was on the Pt surface in the H_2O_2 solution. However, i_{lim} did have a dependence on rotation rate even on the AA2060-T3 surface. The apparent H_2O_2 diffusivity measured on the AA2060-T3 surface was 2.39 x 10^{-10} m^2/s.

Figure 4.10(b) shows the Levich plots for $K_2S_2O_8$ on a Pt surface and on an AA2060-T3 surface. As for the other oxidizers, i_{lim} was lower on the AA2060-T3 surface than it was on the Pt surface. The apparent $S_2O_8^{2-}$ diffusivity measured on AA2060-T3 was 2.39 x 10^{-11} m^2/s.

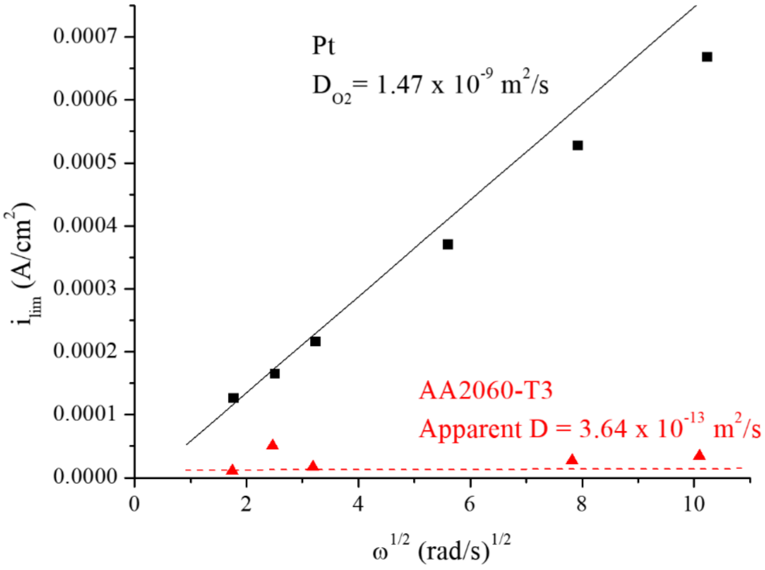

Figure 4.9: Levich plot comparing O_2 reduction on a platinum surface and on an AA2060-T3 electrode in 1.0 M NaCl. i_{lim} was measured at -0.8 V for the Pt electrode and -1.0 V for the AA2060-T3 electrode.

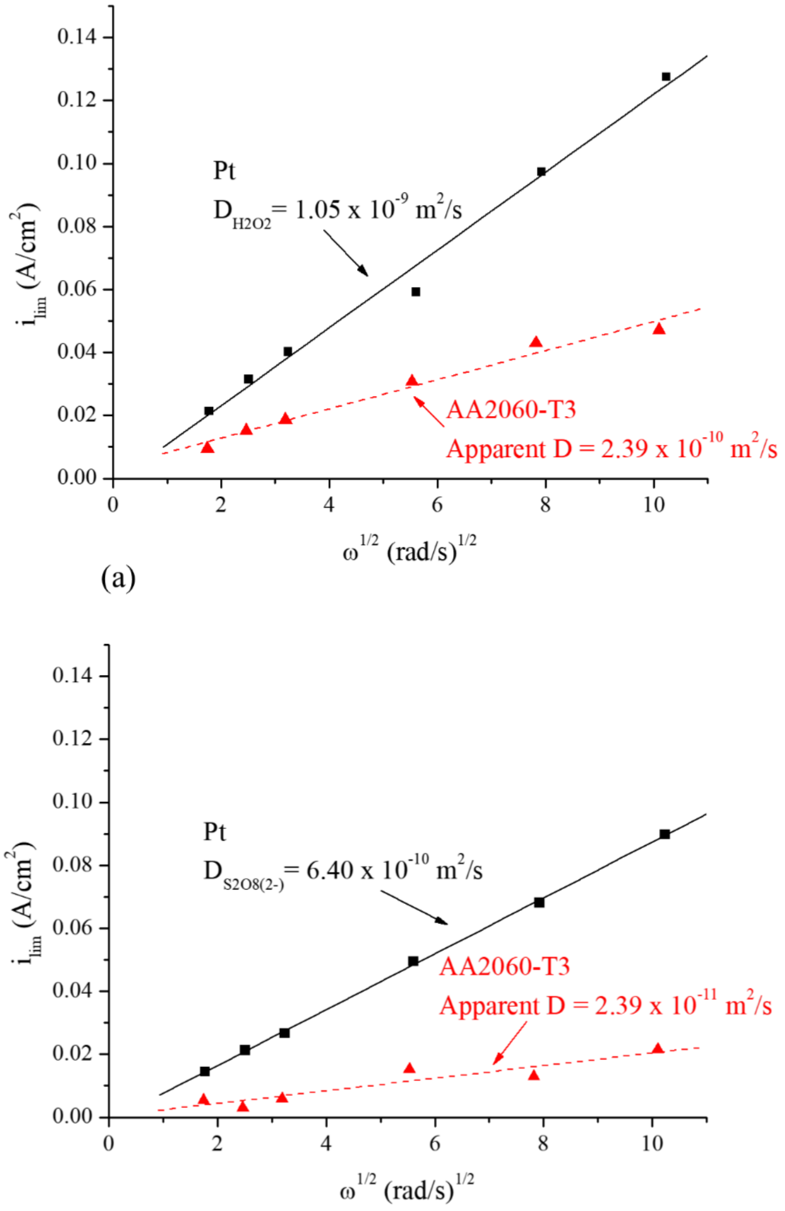

(a)

(b)

Figure 4.10: Levich plots showing the reduction of (a) H_2O_2 and (b) $K_2S_2O_8$ on Pt and AA2060-T3 electrodes in 1.0 M NaCl + 0.1 M oxidizer. i_{lim} was measured at -1.0 V_{SCE} in each case.

Table 4.4: Diffusivity (m^2/s) at room temperature

Species	**Literature Value**[21,22]	**Measured on Pt**	**Measured on AA2060-T3**
O_2	1.9×10^{-9}	1.47×10^{-9}	3.64×10^{-13}
H_2O_2	1.4×10^{-9}	1.05×10^{-9}	2.39×10^{-10}
$S_2O_8^{2-}$	8×10^{-10}	6.40×10^{-10}	2.39×10^{-11}

4.4.3 Constant Immersion Testing Results

4.4.3.1 Electrochemical Measurements

Cathodic kinetics were measured for H_2O_2 and $K_2S_2O_8$ on AA2060 under quiescent conditions at 30°C (exposure temperature for ASTM G110), and it was found that cathodic kinetics were significantly higher for H_2O_2 compared to $K_2S_2O_8$ for both tempers (Figure 4.11[a] and [b]). Table 4.5 presents $1/R_p$ (directly proportional to i_{corr}) for each test. These values show that the faster cathodic kinetics in the H_2O_2 solution compared to $K_2S_2O_8$ led to a higher corrosion rate as well.

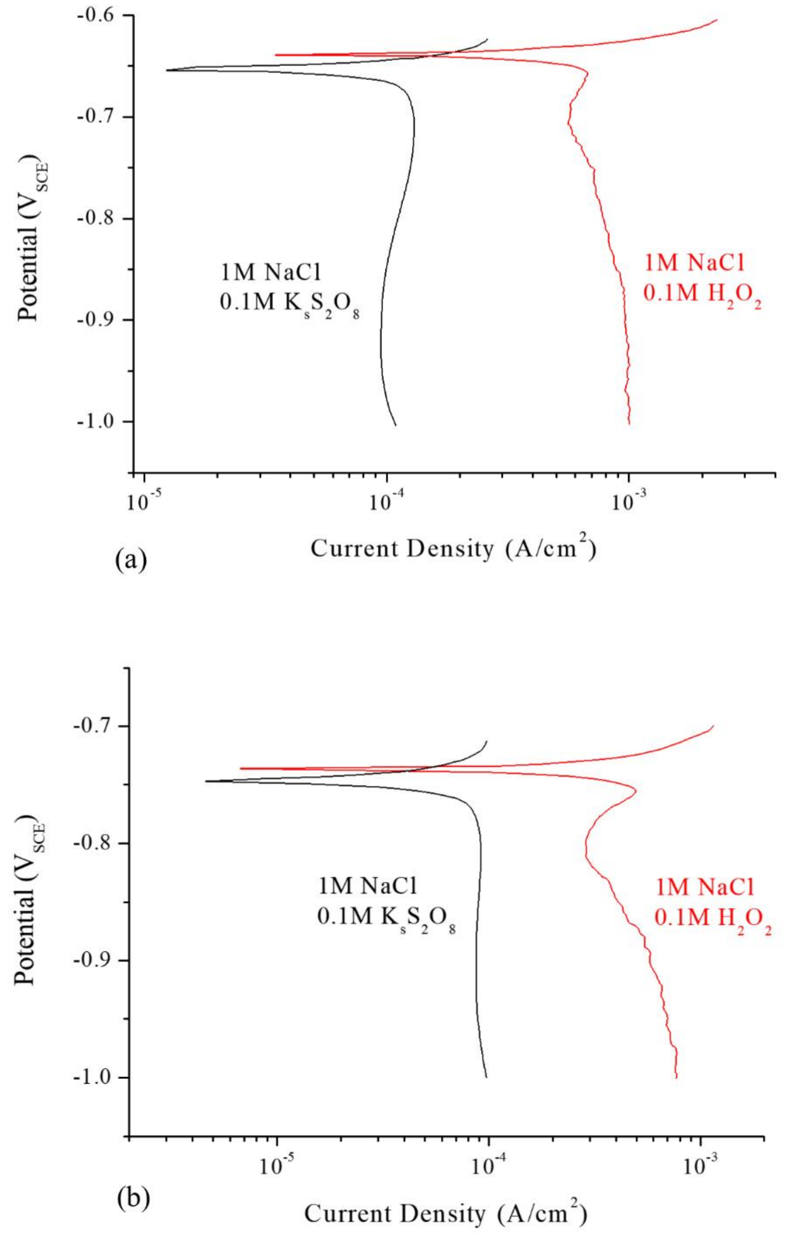

Figure 4.11: Cathodic polarization scans showing the difference in diffusion limited current density and corrosion current between 0.1 M H_2O_2 and 0.1 M $K_2S_2O_8$ solutions in 1 M NaCl at 30^{o}C for (a) AA2060-T3 and (b) AA2060-T86.

Table 4.5: $1/R_p$ (Ω^{-1}-cm^{-2}) for AA2060-T3 and -T86 measured in solutions of 1 M NaCl and 0.1 M oxidizing agent at 30°C.

AA2060 Temper	0.1 M $K_2S_2O_8$	0.1 M H_2O_2
T3	1.10×10^{-2}	7.14×10^{-2}
T86	5.10×10^{-3}	3.85×10^{-2}

4.4.3.2 Immersion Results

Figure 4.12 shows AA2060-T3 after exposure to 0.1 M H_2O_2 and 0.1 M $K_2S_2O_8$ for 12 hours. Both solutions also contained 1.0 M NaCl, and both tests were performed at a constant temperature of 30°C. AA2060-T3 experienced intergranular corrosion in both solutions, but IGC fissures were deeper and more frequent in the solution containing H_2O_2.

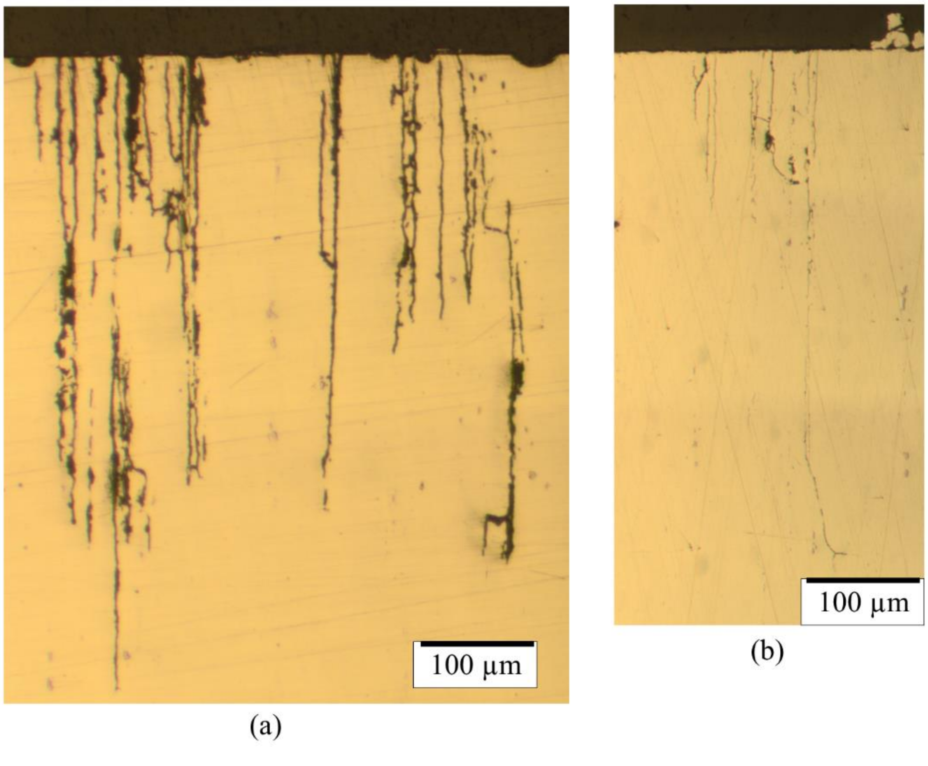

(a)
(b)

Figure 4.12: AA2060-T3 after exposure to (a) a solution of 0.1 M H_2O_2 and 1 M NaCl at 30°C for 12 hours and (b) a solution of 0.1 M $K_2S_2O_8$ and 1 M NaCl at 30°C for 12 hours. The exposed surface was ST.

In contrast, the AA2060-T86 developed deep pits after exposure to both 0.1 M H_2O_2 and 0.1 M $K_2S_2O_8$. Attack was more severe in the H_2O_2 solution, as shown in Figure 4.13.

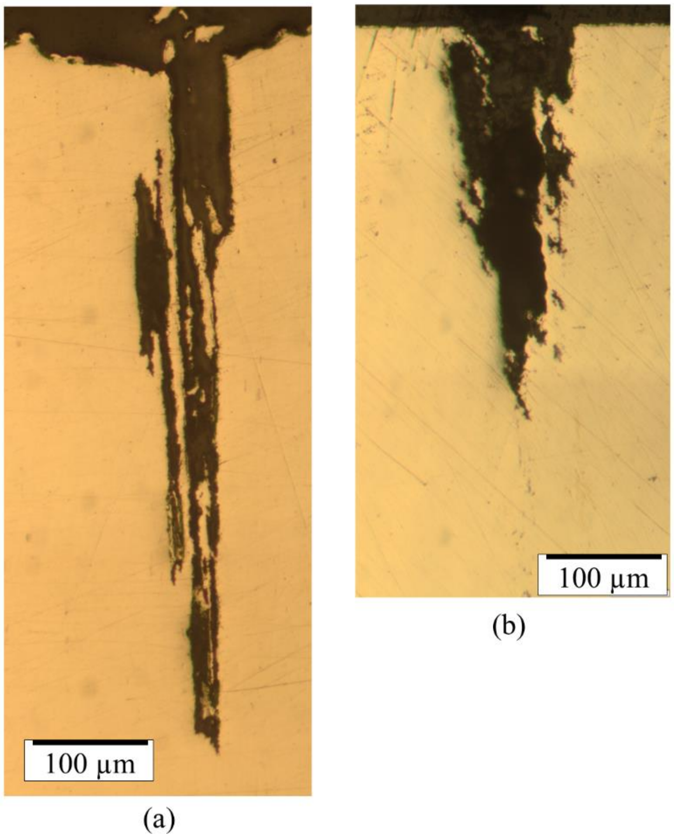

Figure 4.13: AA2060-T86 after exposure to (a) a solution of 0.1 M H_2O_2 and 1 M NaCl at 30°C for 12 hours and (b) a solution of 0.1 M $K_2S_2O_8$ and 1 M NaCl at 30°C for 12 hrs. The exposed surface was ST.

4.4.4 Adjusting the Severity of Accelerated Tests Using Solution pH

4.4.4.1 Electrochemical Measurements

The most common approach used to increase the cathodic kinetics provided by an oxidizing agent that operates under primarily mass transport limited conditions is to increase the concentration. However, $K_2S_2O_8$ solubility in water is limited to 0.22 M at room temperature.[23] Instead, the cathodic kinetics of the $K_2S_2O_8$ solution where manipulated by lowering solution pH. Figure 4.14 shows an increase in cathodic kinetics for AA2060-T3 and AA2060-T86 when the solution pH was decreased from 3.5 to 2.28. The values for $1/R_p$ (directly proportional to i_{corr}) are summarized in Table 4.6, which also reflect the order of magnitude increase in cathodic current density at the lower pH.

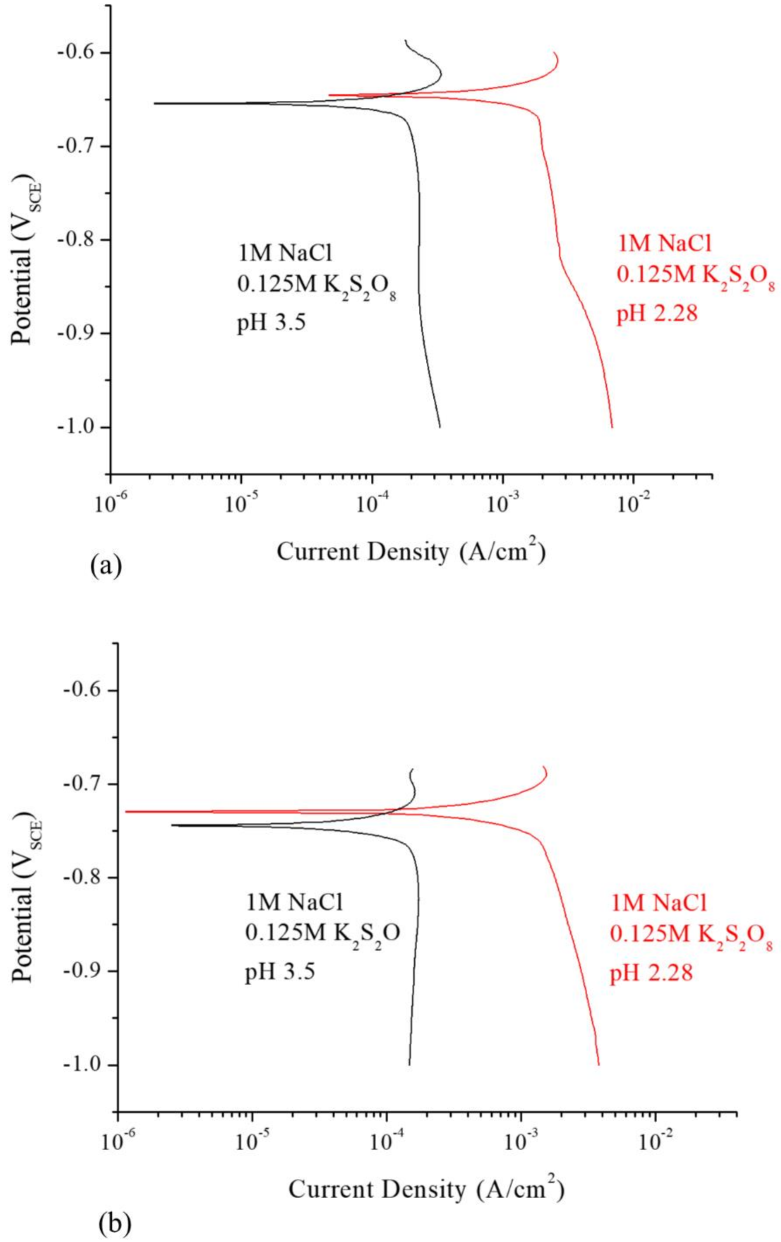

Figure 4.14: Cathodic polarization scans showing the impact of pH on the reduction kinetics of $K_2S_2O_8$ on (a) AA2060-T3 and (b) AA2060-T86.

Table 4.6: $1/R_p$ (Ω^{-1}-cm^{-2}) for AA2060-T3 and -T86, measured in solutions of 1 M NaCl and 0.125 M $K_2S_2O_8$ at pH 3.5 and pH 2.28.

AA2060 Temper	**0.125 M $K_2S_2O_8$, pH 3.5**	**0.125 M $K_2S_2O_8$, pH 2.28**
T3	1.51×10^{-2}	1.13×10^{-1}
T86	7.87×10^{-3}	4.90×10^{-2}

4.4.4.2 Immersion Results

The samples exposed to $K_2S_2O_8$ at reduced pH (2.28) formed extensive attack in both tempers (Figure 4.15[a] and [b]). Fine IGC fissures formed in the -T3 temper (Figure 4.13[a]), but wide fissures were also observed near the surface of the sample. This result may have been due to grain fall out during sample preparation. Grain fall out occurs sometimes when IGC has weakened most or all the grain boundary area surrounding the grain. During polishing, the gritty paper can pull these grains out of the sample. Pitting was observed in the -T86 temper (Figure 4.15[b]).

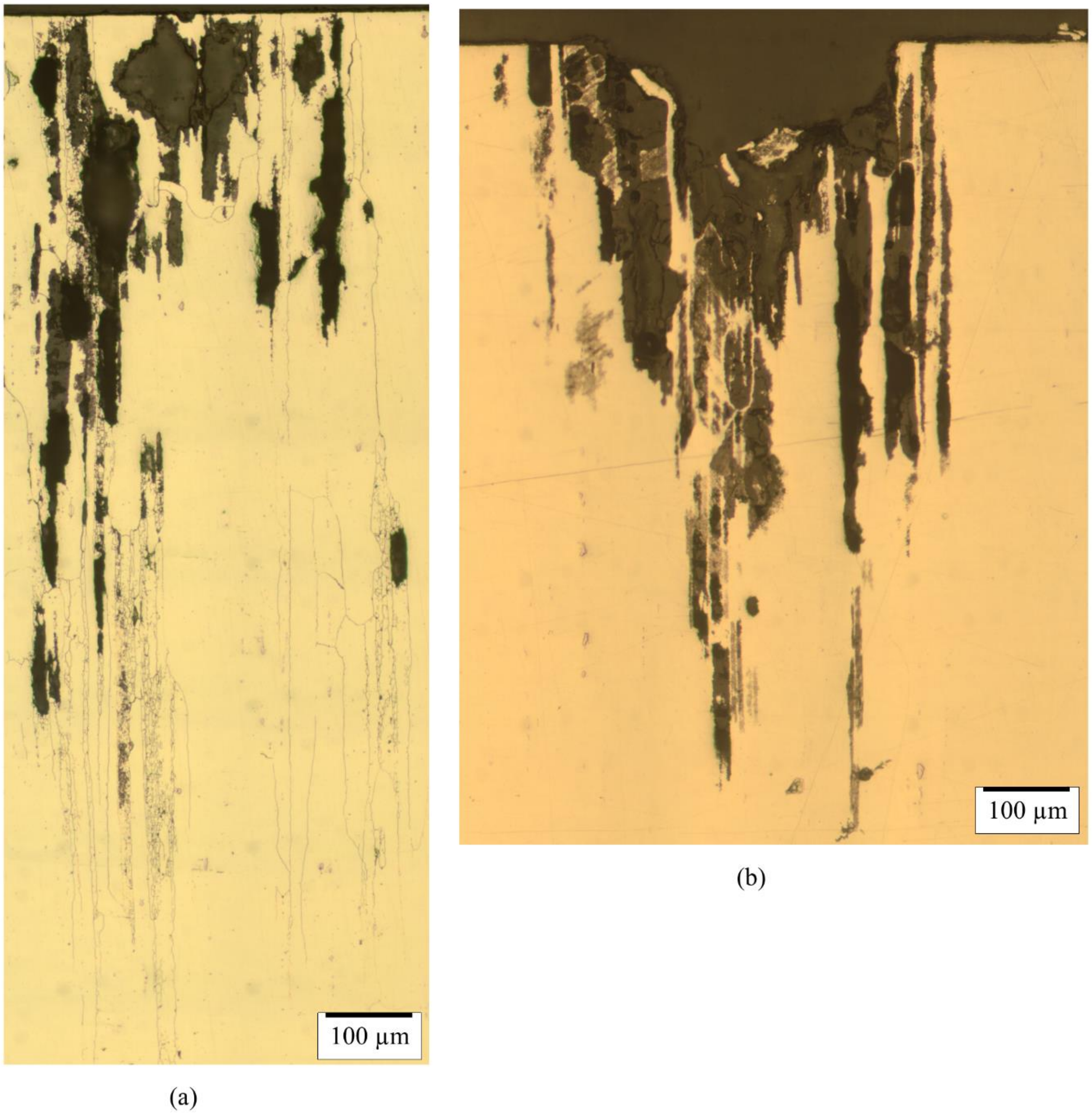

Figure 4.15: (a) AA2060-T3 and (b) AA2060-T86 after a 12 hour exposure to 1 M NaCl, 0.125 M $K_2S_2O_8$ with solution pH 2.28.

4.4.5 Adjusting Severity of Testing with $AlCl_3$

A second approach was used to manipulate the cathodic kinetics. Previous work showed that the addition of small $AlCl_3$ concentrations could increase the corrosion rate of AA2060 during accelerated corrosion testing.[24]

4.4.5.1 Electrochemical Measurements

The addition of just 0.0224 M $AlCl_3$ caused a significant increase in cathodic kinetics for AA2060-T3 and -T86 in a solution of NaCl and $K_2S_2O_8$ (Figure 4.16[a] and [b]). The addition of $AlCl_3$ caused a small reduction in solution pH (3.2), so the pH of the $AlCl_3$ free solution was adjusted with HCl to match. Table 4.7 presents $1/R_p$ values (directly proportional to i_{corr}) for each solution, which reflect significant increase in cathodic current density with the addition of $AlCl_3$ to the testing solution.

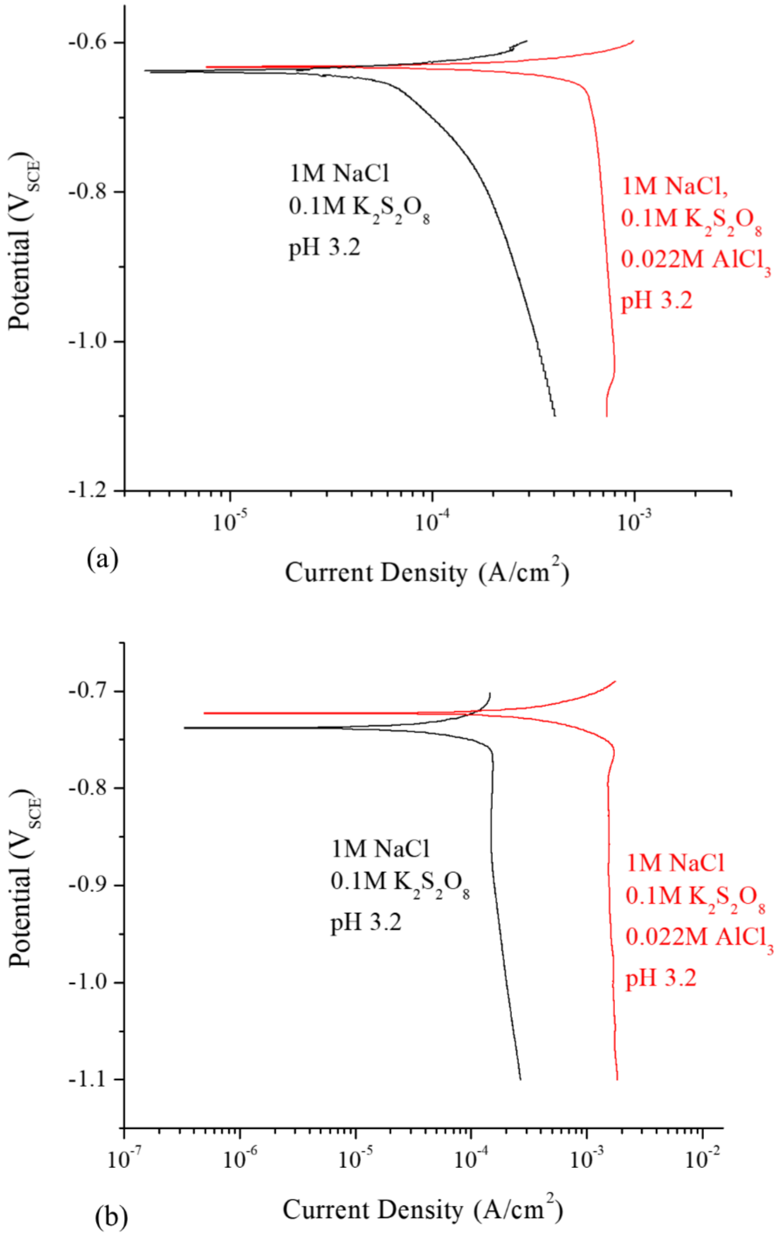

Figure 4.16: Cathodic scans for (a) AA2060-T3 and (b) AA2060-T86 in $AlCl_3$ free and $AlCl_3$ containing solutions.

Table 4.7: $1/R_p$ (Ω^{-1}-cm^{-2}) for AA2060-T3 and -T86 in solutions of 1 M NaCl, 0.1 M $K_2S_2O_8$ with and without 0.022 M $AlCl_3$ at pH 3.2.

AA2060 Temper	**0.1 M $K_2S_2O_8$**	**0.1 M $K_2S_2O_8$, 0.022 M $AlCl_3$**
T3	4.74×10^{-3}	3.30×10^{-2}
T86	7.81×10^{-3}	5.35×10^{-2}

4.4.5.2 Immersion Results

Samples exposed to the test solution containing $AlCl_3$ could not be distinguished by temper (Figure 4.17[a] and [b]). The -T8 temper formed deep pitting as in other tests, but very little IGC was visible in the -T3 temper. The wide fissures observed in the -T3 temper could be partially due to grain fall out during sample preparation, but the lack of visible IGC at the base of the fissures make this theory unlikely.

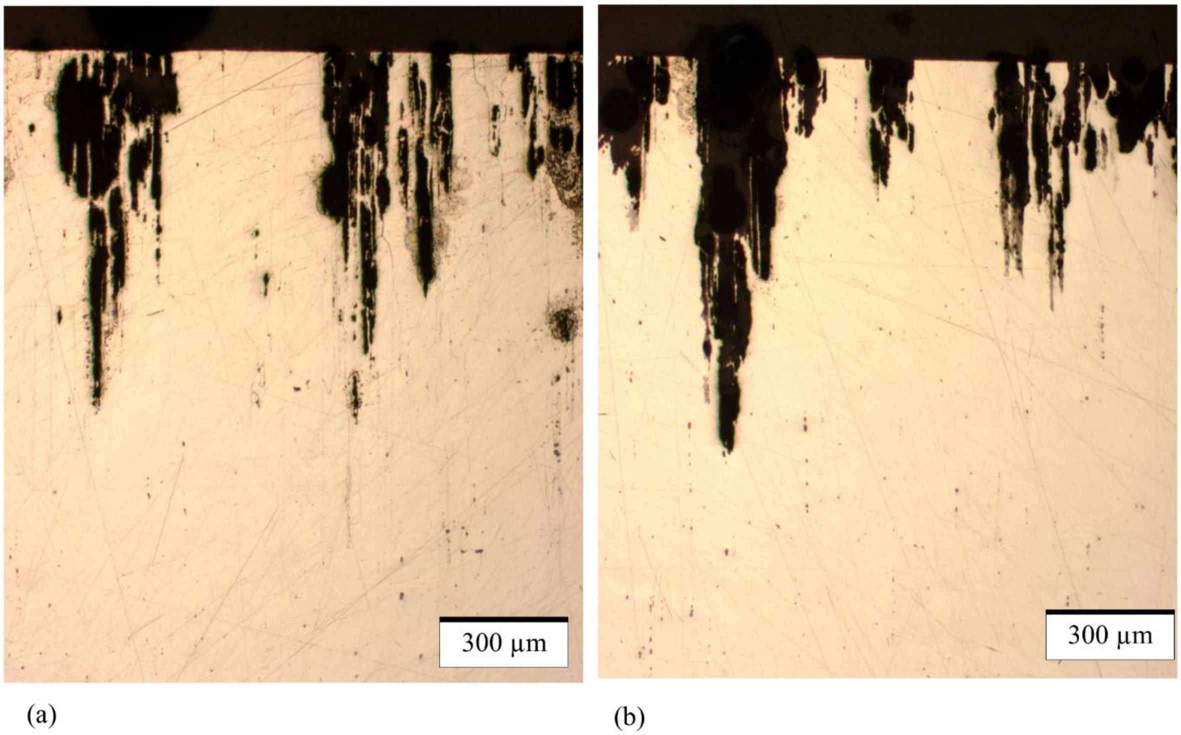

Figure 4.17: (a) AA2060-T3 and (b) AA2060-T86 after 12 hours of exposure to a solution of 0.1 M K2S2O8, 1 M NaCl, 0.022 M AlCl3 at 30oC. Solution pH was 3.2.

4.5 Discussion

In this work, the application of two oxidizing agents (H_2O_2 and $K_2S_2O_8$) to accelerated corrosion testing was considered. H_2O_2 is already used as an accelerant in ASTM G110, and $K_2S_2O_8$ is an oxidizing agent that shows promise for corrosion testing applications. H_2O_2 was a more potent accelerant than $K_2S_2O_8$ at a concentration of 0.1 M due to the faster cathodic kinetics of H_2O_2 on aluminum. However, $K_2S_2O_8$ was more convenient to use in a laboratory setting due to its stability during storage. The severity of tests using $K_2S_2O_8$ was increased by lowering the solution pH to 2.28. The severity of a corrosion test utilizing $K_2S_2O_8$ could conceivably be adjusted by selecting a solution pH between 3.5 and 2.0 in order to meet the needs of a particular application. Both H_2O_2 and $K_2S_2O_8$ are effective tools for accelerating corrosion in aluminum alloys, but they each have their own advantages and disadvantages.

4.5.1 Stability of H_2O_2 and $K_2S_2O_8$

When performing accelerated laboratory tests in large numbers, it can be convenient to mix large volumes of testing solution to use over several days. However the ASTM G110 standard stipulates that hydrogen peroxide must be added to the test solution immediately before testing begins to avoid loss of concentration. The data shown in Figure 4.5 supports this requirement as the H_2O_2 concentration was shown to decrease from 0.1 M to 0.008 M over a 24-h period of storage. In contrast, $K_2S_2O_8$ concentration was stable over a period of 7 days indicating that it may be a more convenient oxidizing agent for use in accelerated corrosion tests.

Oxidizer concentration during actual immersion testing dropped significantly over time due to reduction of the oxidizing species on the aluminum surface. It was observed that the H_2O_2 concentration decreased more quickly than the $K_2S_2O_8$ concentration, indicating that the reduction rate of H_2O_2 may have been faster. This conclusion was supported by later data showing that i_{lim} was higher for H_2O_2 during exposures at 30^{o}C (Figure 4.11) and that the extent of attack was more significant for samples tested in H_2O_2 containing solutions (Figure 4.12, Figure 4.13). RDE results showed that the effective diffusivity measured on AA2060-T3 was an order of magnitude higher for H_2O_2 than for $S_2O_8^{2-}$ (Table 4.4), which caused i_{lim} to be higher in tests containing H_2O_2. Another important observation was that for H_2O_2 containing solutions, the concentration of H_2O_2 dropped to near zero levels after 24-hours of immersion testing. Some loss was due to the natural decomposition of H_2O_2, and the rest of the H_2O_2 was consumed in reduction reactions on the surface of aluminum. Researchers using this test solution for long term tests (longer than 24-h) should be aware of the loss of oxidizing agent over time and consider monitoring and replenishing the solution if necessary for their application.

4.5.2 Electrochemical Kinetics of H_2O_2 and $K_2S_2O_8$

A Koutecky-Levich approach was used to gain a better understanding of cathodic kinetics for oxygen (O_2), H_2O_2, and $K_2S_2O_8$ and to calculate diffusion coefficients for each of the oxidizing agents. Table 4.3 summarizes relevant parameters such as the type and concentration of supporting electrolyte, the solution pH, and the number of electrons transferred during reduction. The kinematic viscosity (v) and O_2 concentration that were calculated in OLI are also included in Table 4.3. These parameters were necessary to calculate diffusivity.

For each oxidizer, reduction kinetics were much faster on the Pt electrode than on the AA2060-T3 electrode. Levich plots for O_2, H_2O_2, and $K_2S_2O_8$ solutions can be seen in Figure 4.9 and Figure 4.10. The diffusivities calculated from the Pt data agreed reasonably well with literature values (Table 4.4), but values measured here were slightly lower than literature values. This may have been due to the slightly low room temperature (22°C) in the laboratory where these tests were conducted. Measurements on AA2060-T3 were performed in Cl^- free solutions where the supporting electrolyte was either K_2SO_4 or Na_2SO_4. The Cl^- free environment was used to prevent excessive attack during the measurement.

The apparent diffusivity of O_2 measured on AA2060-T3 was very low (3.64×10^{-13} m^2/s), and there was no dependency on rotation rate. Similar behavior has been reported for pure aluminum, where the rate limiting step was thought to be migration of electrons through the oxide film on Al rather than mass-transfer of O_2.[6,25] Al-Cu-Li alloys can include Cu-rich constituent particles and intermetallic compounds in their microstructure.[26] Cu-containing intermetallic compounds have been found to enhance ORR on AA2024-T3,[5] but this enhancement did not occur for AA2060-T3 when exposed to dissolved O_2 in a solution of 0.56 M K_2SO_4. Little to no corrosion would be expected to occur in this solution, so no Cu redeposition was expected to occur.

Cathodic kinetics on AA2060-T3 were faster for H_2O_2 and $S_2O_8^{2-}$ than for dissolved O_2. When just H_2O_2 and $S_2O_8^{2-}$ were compared, H_2O_2 was found to have the faster cathodic kinetics on AA2060-T3. The apparent diffusivity as measured on AA2060-T3 was 2.39×10^{-10} m^2/s for H_2O_2 and 2.39×10^{-11} for $S_2O_8^{2-}$. These numbers are significantly lower than the diffusivities measured on Pt, most likely due to the impact of the protective oxide film on aluminum.

When cathodic kinetics were measured on AA2060-T3 and -T86 under quiescent conditions (i.e. no stirring), cathodic kinetics were faster for the samples exposed to 0.1 M H_2O_2 than for samples exposed to 0.1 M $K_2S_2O_8$. This result agreed with the finding that H_2O_2 cathodic kinetics were faster than $S_2O_8^{2-}$ cathodic kinetics under controlled stirring conditions. The faster apparent diffusivity of H_2O_2 on AA2060 compared to $S_2O_8^{2-}$ produced a greater i_{lim} even under quiescent conditions.

The cathodic kinetics of $S_2O_8^{2-}$ were manipulated by decreasing the solution pH and by adding 0.022 M $AlCl_3$. Usually concentration would be increased to obtain faster cathodic kinetics for an oxidizing agent under mass-transport control, but the solubility of $K_2S_2O_8$ in water is limited.[23] When solution pH was lowered from 3.5 to 2.28, a significant increase in cathodic kinetics was observed (Figure 4.14). The protective oxide film on aluminum becomes unstable at low pH, so the limiting impact of the oxide film on $S_2O_8^{2-}$ became less significant at the lower solution pH. Cathodic kinetics also increased with the addition of 0.022 M $AlCl_3$ (Figure 4.16), but the reason for this impact was less clear. $AlCl_3$ does impact solution pH though the hydrolysis of Al^{3+}, but pH did not seem to play a significant role as cathodic kinetics in the $AlCl_3$ solution were faster even compared to an $AlCl_3$ free solution with pH adjusted to match that of the $AlCl_3$ containing solution. The impact of Al^{3+} on cathodic kinetics is currently a topic of study in several projects, and a more in-depth discussion of possible mechanisms can be found elsewhere.[24,27,28]

4.5.3 Correlation between Electrochemical Kinetics and Attack Morphology

The fast cathodic kinetics provided by 0.1 M H_2O_2 in a chloride containing solution corresponded to a greater extent of attack compared to AA2060-T3 and -T8 samples exposed to 0.1 M $S_2O_2^{2-}$. IGC was observed in AA2060-T3 in both tests (Figure 4.12[a] and [b]), but the attack was more prominent in the sample exposed to H_2O_2. Pitting was observed in the -T86 temper (Figure 4.13[a] and [b]), but attack depth was greater for the sample exposed to H_2O_2.

When the cathodic kinetics of $S_2O_2^{2-}$ were manipulated by lowering solution pH to 2.28, the severity of attack increased for both tempers (Figure 4.15[a] and [b]). However, the fine line IGC observed in the -T3 temper was accompanied by some wider fissures, which may have appeared due to grain fall out during sample preparation. Grains can get pulled out of the sample during polishing if the grain boundaries have been sufficiently weakened by IGC.

Although the addition of $AlCl_3$ increased cathodic kinetics for AA2060-T3 and -T86 (Figure 4.16[a] and [b]), the presence of $AlCl_3$ did not improve the performance of the accelerated test. In the solution containing 0.022 M $AlCl_3$, the attack morphology looked very similar for both tempers (Figure 4.17[a] and [b]). Very little IGC was observed on the -T3 temper, but wide fissures resembling pitting were present. The impact of $AlCl_3$ on the electrochemical kinetics of aluminum alloys is not yet well understood, and it is difficult to speculate why this change in attack morphology for AA2060-T3 was observed when $AlCl_3$ was included in the testing solution. Other accelerated testing has shown that IGC developed in AA2060-T3 when exposed to a solution of 4 M NaCl, 0.6 M KNO_3, and 0.0224 M $AlCl_3$ (pH 3.2),[24,29] and it is unclear why a different morphology developed when this alloy was exposed to 1 M NaCl, 0.1 M $K_2S_2O_8$, 0.022 M $AlCl_3$ (pH 3.2). The impact of $AlCl_3$ requires additional study before the governing mechanisms can be explained.

4.6 Conclusions

This work has shown that H_2O_2 and $K_2S_2O_8$ can both be used to increase cathodic kinetics during accelerated corrosion testing. They have different benefits and drawbacks, which should be considered when designing a laboratory test. Key conclusions from this work are listed below.

- H_2O_2 test solutions were not stable during storage and should be mixed directly before testing begins. In contrast, $K_2S_2O_8$ was stable for up to 7 days of storage.
- Cathodic kinetics for each oxidizing agent as well as dissolved O_2 were faster when measured on Pt compared to AA2060-T3. The protective oxide film on aluminum acted as an addition limit to cathodic kinetics.
- Cathodic kinetics for the oxidizing agents were ranked $H_2O_2 > S_2O_8^{2-}$ based on i_{lim} measurements on AA2060-T3 under a controlled diffusion layer.
- The faster cathodic kinetics provided by 0.1 M H_2O_2 compared to 0.1 M $S_2O_8^{2-}$ corresponded to a greater extent of attack in the H_2O_2 solution.
- Cathodic kinetics in $S_2O_8^{2-}$ solutions could be manipulated by decreasing solution pH and by adding 0.022 M $AlCl_3$. When solution pH was decreased to 2.28, cathodic kinetics increased and extent of attack for exposed AA2060 samples as well. Cathodic kinetics also increased with the addition of $AlCl_3$, but the attack morphology was very similar for both tempers. Instead of developing IGC, the AA2060-T3 temper developed a morphology that looked similar to pitting.

4.7 Acknowledgements

This work was supported by Rolls-Royce and the Office of the Undersecretary of Defense Corrosion University Pilot Program, Contract #: W911NF-14-2-0005. Thank you to Srishti Shrivastava and Russell Repasky for running laboratory experiments.

4.8 References

1. J.P. Moran, F.S. Bovard, J.D. Chrzan, P. Vandenburgh, “Corrosion Performance of New Generation Aluminum-Lithium Alloys for Aerospace Applications,” 13th Int. Conf. on Aluminum Alloys, held June 3-7, 2012 (Hoboken, NJ: John Wiley & Sons, Inc., 2012).
2. S. Lee, B.W. Lifka, “Modification of the EXCO Test Method for Exfoliation Corrosion Susceptibility in 7XXX, 2XXX, and Aluminum-Lithium Alloys,” in New Methods for Corrosion Testing of Aluminum Alloys, eds. V.S. Agarwala, G.M Ugiansky, STP 1134 (West Conshohocken, PA: ASTM International, 1992), p. 1-19.
3. M.E. Parker, R.G. Kelly, Corrosion 72, 11 (2016): p. 1342-1350.
4. McCafferty, E. *Introduction to Corrosion Science*. Springer 2010, p. 188.
5. M.A. Jakab, D.A. Little, J.R. Scully, *J. Electrochem. Soc.* 152, 8 (2005): p. B311-B320).
6. M.J. Pryor, D.S. Keir, *J. Electrochem. Soc.* 102, 10 (1955): p. 605-607.
7. R.G. Buchheit, R.K. Boger, M.C. Carroll, R.M. Leard, C. Paglia, J.L Searles, *JOM* 53, 7 (2001): p. 29-33.
8. ASTM G34-1, “Standard Test Method for Exfoliation Corrosion Susceptibility in 2XXX and 7XXX Series Aluminum Alloys” (West Conshohocken, PA: ASTM International, 2001), p. 1-7.
9. ASTM G110-92, “Standard Practice for Evaluating Intergranular Corrosion Resistance of Heat Treatable Aluminum Alloys by Immersion in Sodium Chloride + Hydrogen Peroxide Solution” (West Conshohocken, PA: ASTM International, 2003), p. 1-3.
10. E.Y. Yazici, H. Deveci, “Factors Affecting Decomposition of Hydrogen Peroxide.” XIIth International Mineral Processing Symposium, held October 6-8, 2010, p. 609-616.
11. ASTM G85-02, “Standard Practice for Modified Salt Spray (Fog) Testing” (West Conshohocken, PA: ASTM International, 2002), p. 1-14.
12. S. Lee, B.W. Lifka, “Modification of the EXCO Test Method for Exfoliation Corrosion Susceptibility in 7XXX, 2XXX, and Aluminum-Lithium Alloys,” in New Methods for Corrosion Testing of Aluminum Alloys, eds. V.S. Agarwala, G.M Ugiansky, STP 1134 (West Conshohocken, PA: ASTM International, 1992), p. 1-19.
13. N. Ott, Y. Yan, S. Ramamurthy, S. Kairy, N. Birbilis, *Scrip. Mater.* 119 (2016): p. 17-20.

14. N. Ott, S.K. Kairy, Y. Yan, N. Birbilis, *Metallurgical Materials Trans. A* 48, 1 (2017): p. 51-56.
15. R.J. Rioja, J. Liu, *Metal. Mater. Trans. A* 43 (2012): p. 3325-3337.
16. J.L. Town, F. MacLaren, H.D. Dewald, *J. Chemical Education* 68, 4 (1991): p. 352-354.
17. J.E.F. Moraes, F.H. Quina, C.A.O. Nascimento, D.N. Silva, O. Chiavone-Filho, *Environ. Sci. Technol.* 38 (2004): p. 1183-1187.
18. J.J. Pignatello, *Environ. Sci. Technol.* 26 (1992): p. 944-951.
19. A.J. Luna, C.A.O. Nascimento, O. Chiavone-Filho, *Brazilian J. Chem. Eng.* 23, 3 (2006): p. 341-349.
20. M. Pourbaix, "Atlas of Electrochemical Equilibria in Aqueous Solutions" NACE (1974).
21. Biezen, S.A.M, Everaerts, F.M., Janssen, L.J.J, Tacken, R.A. *Diffusion coefficients of oxygen, hydrogen peroxide and glucose in a hydrogel.* Analytica Chimica Acta, 273 (1993) 553-560.
22. J. Desilvestro, M. J. Weaver, *J. Electroanalytical Chem.* 234 (1987): p. 237-249.
23. A. Apelblat, E. Korin, E. Manzurola, *J. Chem. Thermodynamics* 33 (2001): p. 61-69.
24. M.E. Parker, R.G. Kelly, "Deconstructing the Electrochemical Basis of ASTM G34 and ANCIT Immersion Tests," Unpublished work.
25. G.O. Ilevbare, J.R. Scully, *J. Electrochem. Soc.* 148, 5 (2001): p. B196-B207.
26. R.G. Buchheit, J.P. Moran, G.E. Stoner, *Corrosion* 46, 8 (1990) p. 610-617.
27. K. Sotoudeh, T.H. Nguyen, R.T. Foley, B.F. Brown, *Corrosion* 37, 6 (1981): p. 358 – 362.
28. P. Khullar, *Cathodic Control of Intergranular Corrosion in Sensitized AA5083-H131.* PhD Dissertation (2018): p. 163-188.
29. M.E. Parker, R.G. Kelly, *Corrosion* 72, 11 (2016): p. 1342-1350.

5. Deconstructing DB ASTM G85-A2 Testing Environment with In-Situ Measurements

Summary:

In this chapter, the behavior of AA2060-T3 and -T86 in dry bottom (DB) ASTM G85-A2 was characterized. Several techniques for measuring properties in-situ were presented, and the impact of relative humidity (RH) on time of wetness (TOW) and potential was investigated. It was found that the RH during DB ASTM G85-A2 dropped very low (17% - 20.5%) during the dry air purge and dwell periods of the repeating 6 hour cycle. The TOW sensor showed that drying did not occur instantaneously, and moisture was detected on the sensor until 1.5 - 4 hours after the start of the dry air purge. It should be noted, however, that salt accumulation on the sensor was much greater than on the AA2060 samples. It was difficult to determine the TOW specifically for the AA2060 samples, but visually these samples appeared to be dry 5 - 10 minutes after the start of the dry air purge. Open circuit potential (OCP) measurements showed that a transition in OCP profile occurred from day 2 to day 8 of the test. After 2 days, the OCP was stable during the salt spray cycle and decreased during the dry cycle. After 8 days of exposure, however, a potential peak was measured about 10 minutes into the dry air purge. It was hypothesized that this potential peak was a sign of increasing oxygen reduction kinetics as the electrolyte film on the sample decreased. The measurement techniques presented in this chapter were used to further deconstruct the ASTM G85-A2 test in Chapter 6.

The work presented in this chapter has been reported in the following publication:

- M.E. Parker, R.G. Kelly. “Deconstructing DB ASTM G85-A2 Testing Environment with In-Situ Measurements” Corrosion 2017, (NACE International, 2017).

5.1 Abstract

Accelerated corrosion testing is an important tool for understanding the corrosion behavior of aerospace alloys, but many standardized accelerated tests do not correlate well with seacoast exposures, and results can be drastically different from test-to-test. Previous testing of aluminum lithium alloy 2060 has shown that DB ASTM G85-A2 correctly distinguishes between exfoliation-susceptible and resistant tempers. In the current study, in-situ measurements were used to

deconstruct the testing environment of DB ASTM G85-A2 to provide an understanding of what makes this test successful when others are not. Time of wetness measurements showed that complete drying of the sensor did not occur until 1.5 – 4 hours after the dry air purge began. After 2 days, the open circuit potential of AA2060 was stable during the salt spray cycle and decreased during the dry cycle. After longer testing time (8 days), the potential was lower, due to activation of more localized corrosion sites. In addition, a peak in potential was observed at around 10 minutes into the dry air purge after 8 days of testing. This change in potential was attributed to the impact of relative humidity on electrolyte film thickness and cathodic kinetics.

5.2 Introduction

Accelerated laboratory testing is an important tool for understanding and predicting the corrosion behavior of aerospace alloys that are exposed to salt aerosols in the atmosphere during service. For accelerated testing to be useful, the results must correlate well with the corrosion behavior during service and be easily reproducible between different laboratories. Many standardized accelerated tests are currently used for high-strength aluminum alloys (ASTM standards G34, G85, G110, and B117), but these tests do not always correlate well with seacoast exposures and results can be drastically different from test-to-test. This disagreement limits accelerated testing utility and hampers alloy and temper development. The purpose of this study is to deconstruct accelerated testing mechanisms to understand why certain tests are successful and others are unsuccessful. This work will also provide a basis for improved accelerated test design.

ASTM G85 Annex 2 is an acidified salt spray test used for aerospace alloys. There are two versions of this test, one called wet bottom (WB) where several inches of water are maintained on the bottom of the salt spray chamber, and one called dry bottom (DB) where the chamber is allowed to dry for portions of the test. Moran et al. showed that the DB version of the test correlates well with seacoast exposures (1.2 years) for Al-Cu-Li alloys.[1] Figure 5.1 shows the exfoliation ratings (ED is severe exfoliation, EA is mild exfoliation, P is no exfoliation as defined by ASTM G34)[2] for several AA2060 tempers after 1.2 years of seacoast exposure and after 4 weeks of ASTM G85-A2 testing. Under aged tempers displayed susceptibility to exfoliation both at seacoast and in the accelerated test, whereas near peak aged tempers were resistant.

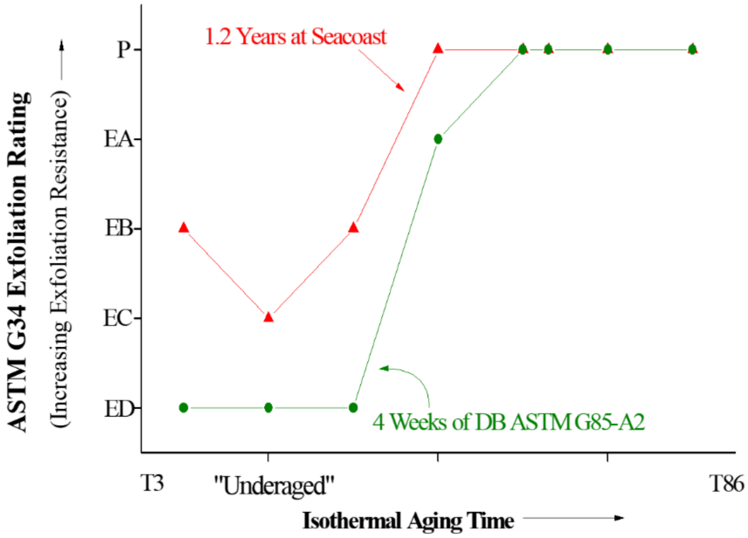

Figure 5.1: Exfoliation ratings for various AA2060 tempers after 1.2 years of seacoast exposure and after 4 weeks of DB ASTM G85-A2 testing. Adapted from reference 1.

In contrast to constant salt spray tests like ASTM B117, ASTM G85-A2 uses wet and dry cycling to create periods of high and low relative humidity (RH). The purpose of wet dry cycling is to better represent service conditions where an alloy may be exposed to a broad range of environmental conditions. It has been suggested by Lyon et al.[3] that the most important part of the test may actually be the transition from wet to dry. As RH decreases, the equilibrium NaCl concentration increases and the electrolyte film thickness decreases. A thinner electrolyte film also means easier access to oxygen. Both changes could lead to an increase in corrosion rate. This phenomenon is shown schematically in Figure 5.2.

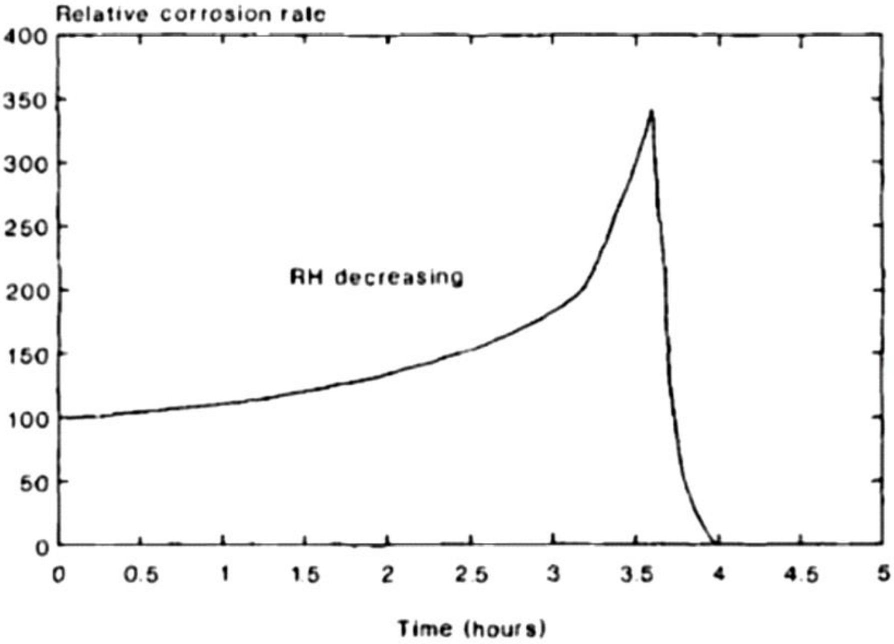

Figure 5.2: Schematic representation of changes in relative corrosion rate during drying (decreasing RH). From reference 3.

ASTM G85-A2 is composed of a repeating 6 hour, 3 part cycle that includes a salt spray period, a dry air purge, and a dwell. Although the standard requires that each part of the cycle run for a specified time, there is no guarantee that the resulting RH will be the same in every laboratory. Differences in the humidity of the air used to purge the chamber and other seemingly minor operational inconsistencies can lead to a variety of RH profiles during the standard wet and dry cycle.[4,5]

In the current work, in-situ measurements were used to deconstruct DB ASTM G85-A2. A particular focus was given to investigate the impact of RH on time of wetness (TOW) and open circuit potential (OCP).

5.3 Experimental Procedures

The material used in this study was Al-Cu-Li alloy 2060. Both the under aged condition (T3 temper) and the near peak aged condition (T86 temper) were considered. The alloy composition is listed in Table 5.1.[6]

All measurements were made according to ASTM G85-A2 under DB conditions in a Q-Fog CCT 1100 testing chamber. This test used a repeating 6 hour cycle including 45 minutes of salt spray, 2 hours of dry air purge, and a 3 hour and 15 minute dwell period. The testing temperature was 49 °C, and the testing solution was 0.9 M NaCl with the pH adjusted using acetic acid to a range of 2.8 – 3.0.

Table 5.1: AA2060 Composition (wt. %)

Li	Cu	Mg	Ag	Zr	Mn	Zn	Al
0.75	3.95	0.85	0.25	0.11	0.30	0.40	Bal.

Samples were positioned at 15° from the vertical during testing. A Dino-Lite digital microscope was placed in the testing chamber during select cycles to observe salt films as they wet and dry.

The AA2060 samples were cut in such a way that the half thickness plane (Figure 5.3) was the exposed surface. Sample preparation included grinding to a 1200 grit finish, cleaning ultrasonically in deionized water, and rinsing with ethanol.

In order to deconstruct the testing conditions, relative humidity (RH), time of wetness (TOW), and open circuit potential (OCP) were measured in-situ. An Omega USB-2-LCD-PLUS sensor was used to measure RH. This instrument is reported (by the manufacturer) to have an accuracy of ±4.0% RH within the range of 20 – 80% RH. Unfortunately, salt spray can contaminate electronic RH sensors and affect their operation. In order to determine the impact of salt spray on the RH sensor, deionized water was substituted for the acidified salt solution during some measurements. When salt solution was used, a protective plastic cone (approximates 12 inches in diameter) was placed over the sensor to prevent salt droplets from landing directly on the sensor. The presence of this cone was not found to have any impact on RH measurements.

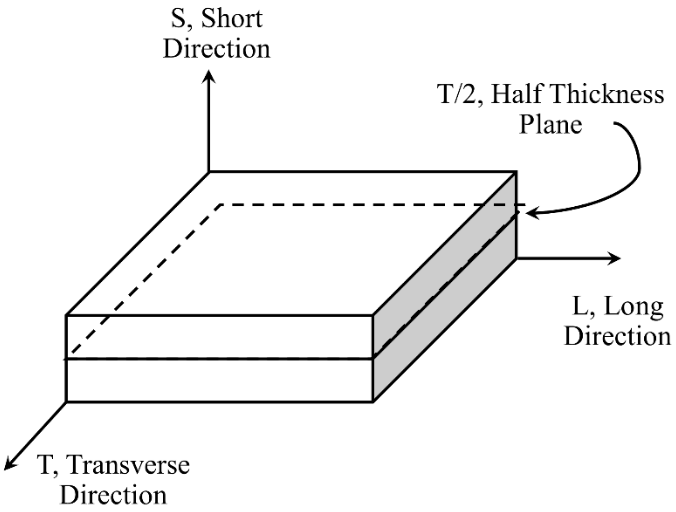

Figure 5.3: Schematic showing sample orientation.

TOW was detected by measuring the impedance of a Wetcorr sensor (Innovation NILU), which was constructed of interdigitated gold electrodes separated by 130 μm on an aluminum oxide substrate. Impedance measurements were made at a frequency of 29 kHz. When the sensor was dry, impedance was very high (~50,000 Ω), and when the sensor was wet, impedance was between 3 – 6 Ω. The sensor was positioned at 15° from the vertical during testing just as the AA2060 samples were, but it should be noted that the wetting behavior of the sensor surface was not exactly the same as the aluminum samples. A thicker salt film formed on the sensor compared to the AA2060 samples. Furthermore, corrosion products began to build up on the aluminum samples after a few days of testing. Despite those differences, the TOW sensor was still a useful tool to observe the wetting and drying behavior of salt films during RH cycling.

The open circuit potential (OCP) of AA2060 samples was measured during select salt spray cycles with the internal reference of an Orion flat tip pH electrode. The internal reference was tested for sensitivity to pH and chloride concentration of the test solution, and it was found to be very stable. Figure 5.4 shows an image of this electrode. The plastic fibers at the tip allowed ionic conduction between the reference electrode and the thin electrolyte film present on the sample during wet cycles through capillary action. By touching these fibers to the sample surface, OCP could be measured when a thin electrolyte film was present on the sample surface.

Figure 5.4: (a) The Orion flat tip pH electrode. (b) Magnified view of the polymer fibers (circled) on the tip of the electrode.

5.4 Results

5.4.1 Exposure Results

AA2060-T3 and -T86 were exposed to DB ASTM G85-A2 for 4 weeks. The -T3 temper formed mild exfoliation as seen in Figure 5.5(a), and no exfoliation was observed on the -T86 temper (Figure 5.5[b]).

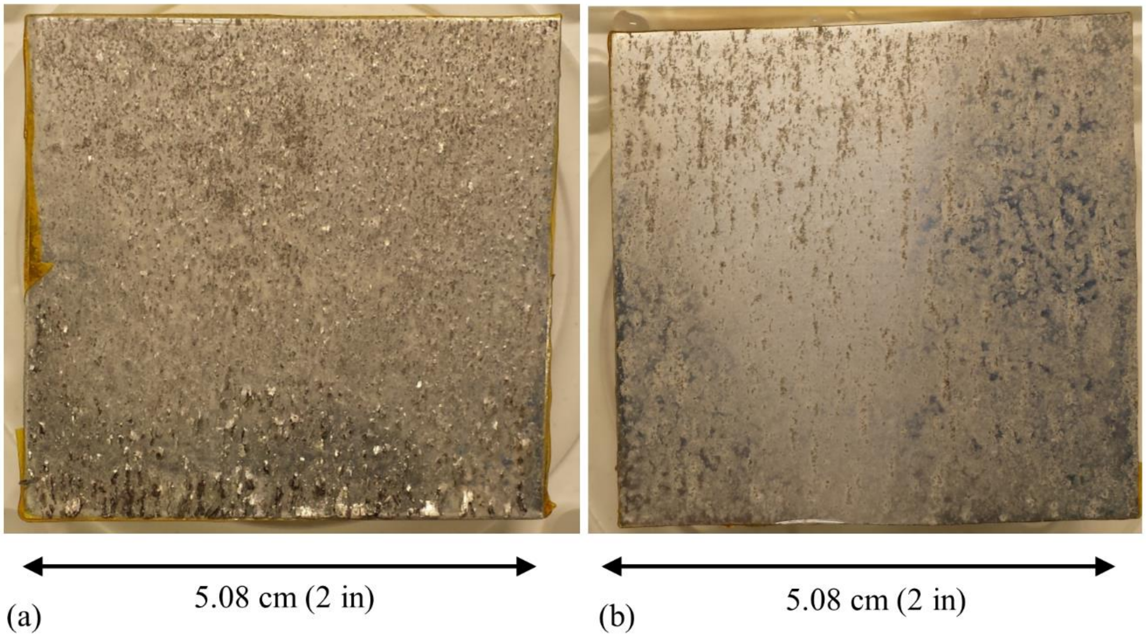

Figure 5.5: (a) AA2060-T3 after 4 weeks of DB ASTM G85-A2. (b) AA2060-T86 after 4 weeks of DB ASTM G85-A2. Mild exfoliation formed on the -T3 temper, and no exfoliation was observed on the -T86 temper.

The degree of exfoliation on AA2060-T3 was expected to be greater because this same alloy temper was rated ED (severe exfoliation) after 4 weeks of DB ASTM G85-A2 testing in work done by Moran et al.[1] This inconsistency in the extent of attack may be due to differences in the actual RH achieved by different salt fog chamber running the same standard cycle.

5.4.2 RH and TOW Measurements

Relative humidity during four consecutive cycles was measured during DB ASTM G85-A2. Figure 5.6 compares RH measurements when DI water was used as the testing solution and when acidified salt solution was used. Time zero on the horizontal axis represents the start of salt spray during the first cycle. Periods of high humidity were measured during the 45 minute salt spray, and the RH rapidly dropped once the 2 hour dry air purge began. RH only increased slightly during the dwell period.

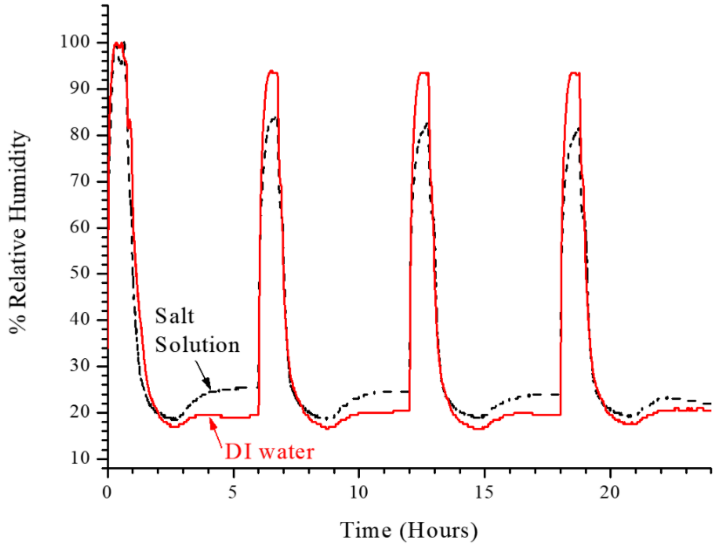

Figure 5.6: Relative humidity measurements during the first four cycles of DB ASTM G85-A2. The solid red line shows the results when test solution was deionized water, and the dashed black line shows the results when acidified salt solution was used.

The use of acidified salt solution seemed to affect sensor operation. RH measured during the first salt spray cycle was near 100%, but the RH for subsequent salt spray cycles were low (~84%). This difference was most likely due to contamination of the sensor with NaCl and acetic acid after the first cycle.

During TOW measurements, an impedance of approximately 50,000 Ohm indicated that the sensor was dry, and an impedance of 3 – 6 Ω indicated that the sensor was wet. The start of drying was defined as the point at which impedance exceeded 6 Ohm, and the end of drying was defined as the point at which impedance exceeded 49,000 Ohm. Sensor drying usually initiated between 13 – 17 minutes after the dry air purge began, but as shown in Figure 5.7, the time to finish drying was not the same for every cycle. This time ranged from 1.5 – 4 hours.

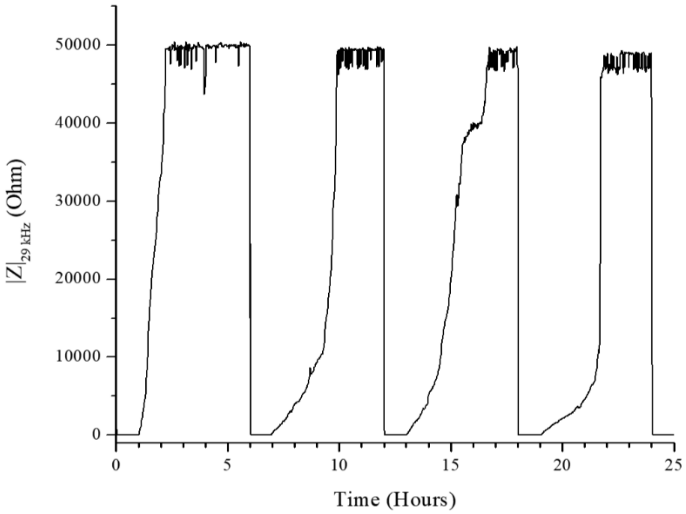

Figure 5.7: TOW measurements for DB ASTM G85-A2. An impedance of 50,000 Ω indicated a dry sensor and an impedance near zero indicated a wet sensor.

Figure 5.8 shows a closer view of the RH and TOW measurements during the second cycle. Drying began 13 minutes after the dry air purge started. According to measurements made with DI water, RH was 44.5% at this time. This value is lower than the efflorescence point for NaCl reported by Schindelholz et al.[7] (49 – 51%), but those measurements were made during gradual changes in RH (1% RH step every 30 minutes). The discrepancy in efflorescence point may be due to the low accuracy of the sensor used in this study (±4.0%) or the impact of a rapid RH drop on efflorescence kinetics. Furthermore, the impact of acetic acid on the efflorescence kinetics of NaCl is not yet known and could have played a role.

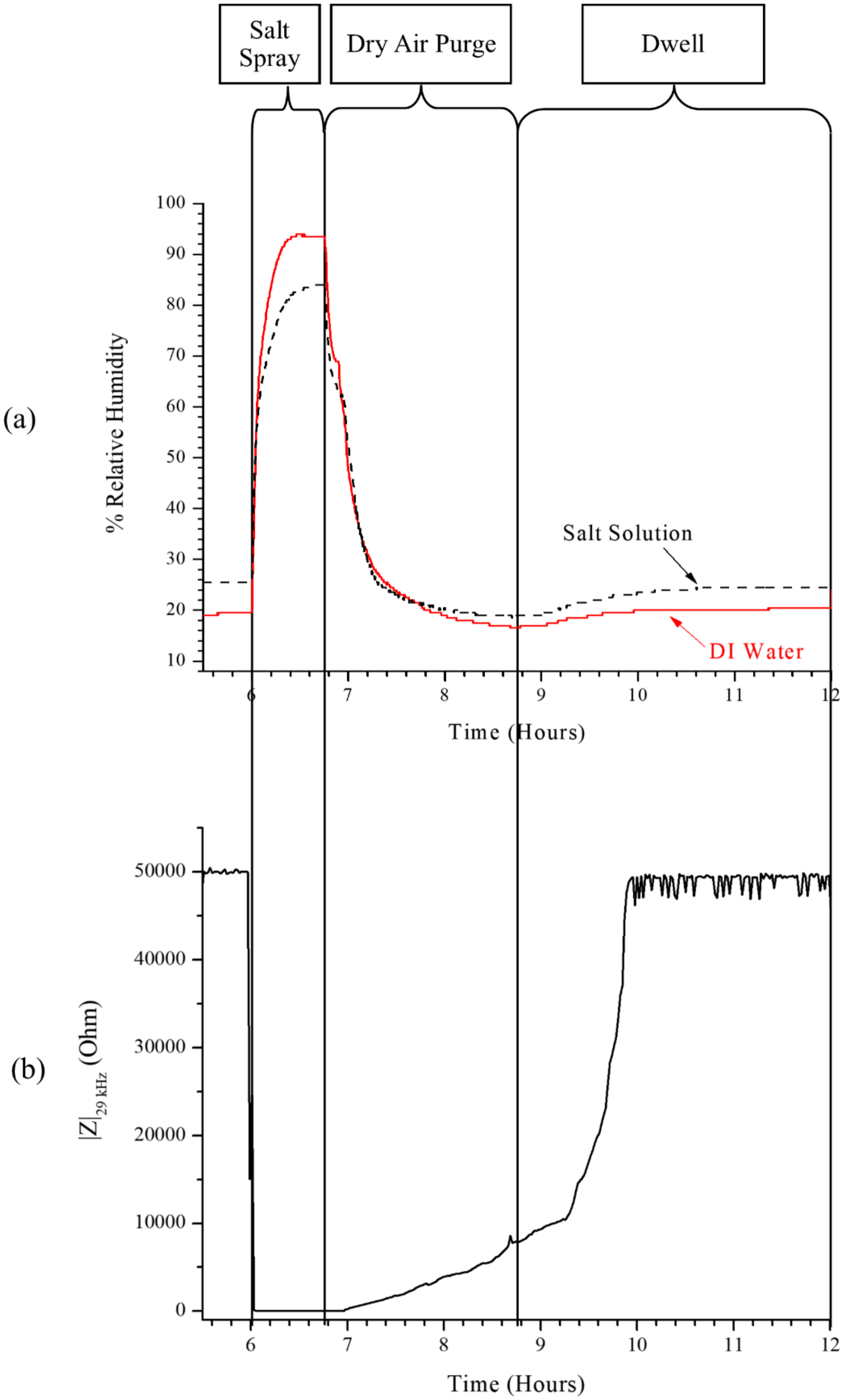

Figure 5.8: (a) RH and (b) TOW measurements for a single 6 hour cycle of DB ASTM G85-A2.

5.4.3 Potential Measurements

Open circuit potential (OCP) of AA2060-T3 and -T86 samples was measured during the salt spray period and the first 40 minutes of the dry air purge. After a short time in the chamber (2 days), the OCP of AA2060-T3 was stable at an average of -0.73 V_{SCE} during salt spray as shown in Figure 5.9a. The decline in potential during the dry air purge was associated with thinning of the electrolyte layer. Figure 5.10(c) shows an image of the sample 10 minutes into the dry air purge. The sample appeared dry, but as seen from the TOW results, there may still have been moisture trapped in the salt film at this time.

After longer a testing time (8 days), the average potential of AA2060-T3 during salt spray was -0.77 V_{SCE} (Figure 5.9[b]), which was lower than the potential after 2 days of testing. Figure 5.10(d) shows corrosion product buildup on the sample after 8 days of testing, and corrosion sites (circled) can be seen in Figure 5.10(e). The potential after 8 days was lower than after 2 days due to the activation of more localized corrosion sites.

Another feature of the OCP after longer testing time was the peak in potential at 10 minutes into the dry air purge. Although the sample appeared to be dry after 5 minutes of purging (Figure 5.10[f]), there could have been moisture trapped within corrosion fissures and under the salt film at this point, and the changing cathodic kinetics for these very thin electrolyte films may have been responsible for the changes in OCP. As the film thinned during drying, the diffusion path for oxygen to reach the metal-electrolyte interface would decrease, resulting in faster cathodic kinetics and higher OCP. At some point, however, the increasing solution resistance of the salt film would reduce access to cathode area, which would slow cathodic kinetics and decrease OCP. Measurements of polarization resistance would be needed to confirm this hypothesis, and this topic will be an area of future work.

Potential for the AA2060-T86 temper was consistently lower than for the -T3 temper during the salt spray cycle, but the patterns in OCP were similar. The potential after 2 days was stable during wetting, and a peak in potential was observed during drying after 8 days of testing.

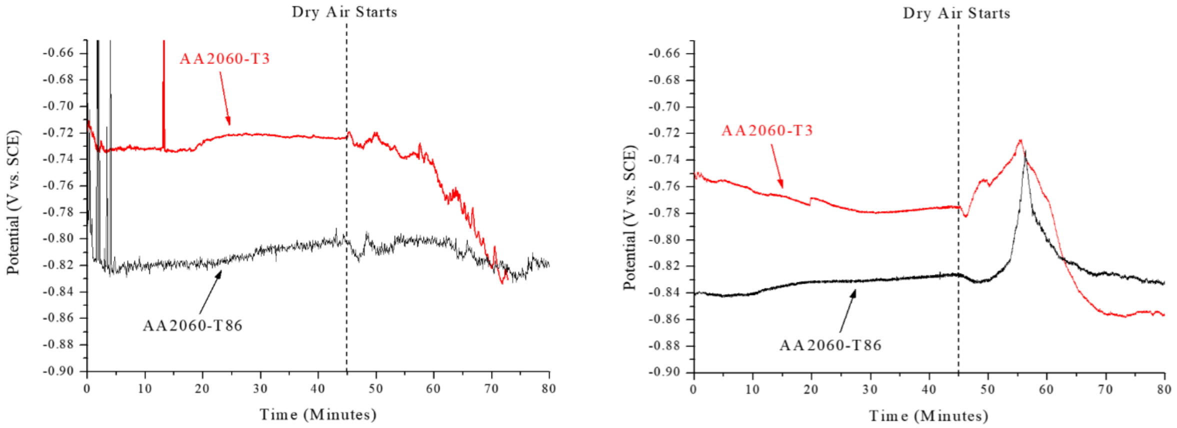

(a) (b)

Figure 5.9: (a) Potential measurements on AA2060-T3 and -T86 after 2 days of ASTM G85-A2. (b) Potential measurements of AA2060-T3 after 8 days of ASTM G85-A2 and AA2060-T86 after 9 days of ASTM G85-A2.

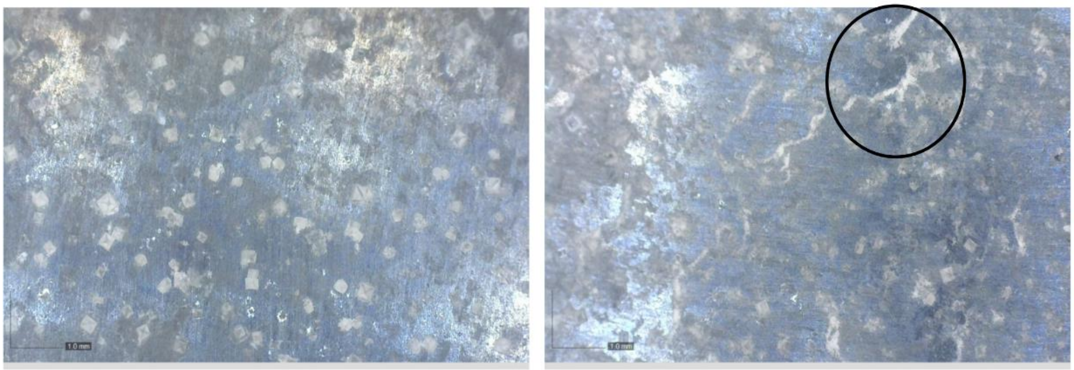

(a) Before Salt Spray, Day 2

(d) Before Salt Spray, Day 8

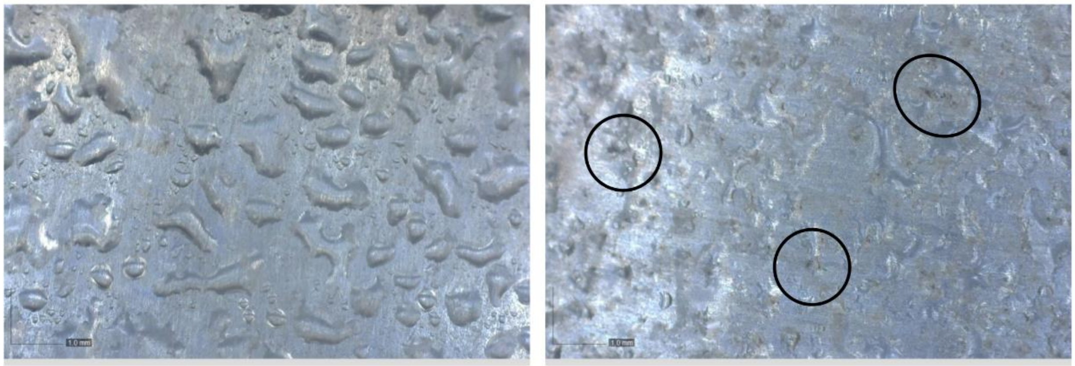

(b) 10 Minutes of Salt Spray, Day 2

(e) 10 Minutes of Salt Spray, Day 8

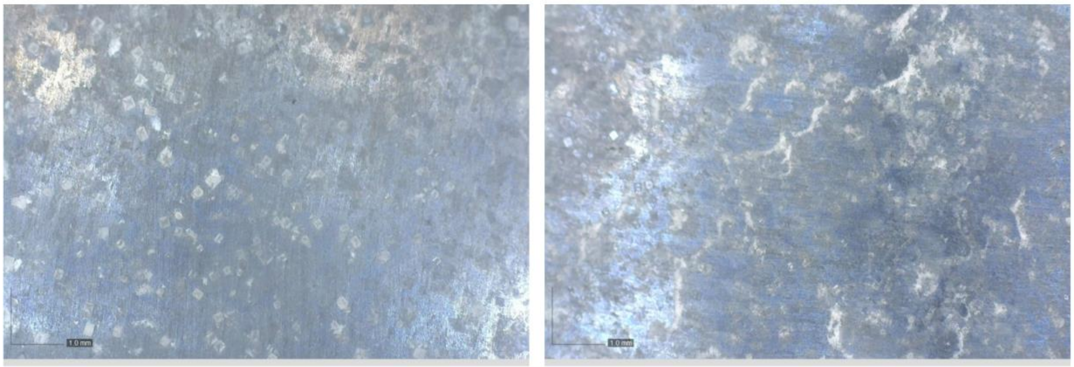

(c) 10 Minutes of Dry Air, Day 2

(f) 5 Minutes of Dry Air, Day 8

2 mm

Figure 5.10: Images of AA2060-T86 captured during wetting and drying. (a – c) Images showing the sample surface on the second day of testing. (d – f) images showing the sample surface on the eighth day of testing. The circle on (f) indicates an area with corrosion product buildup. Circles on (e) show corrosion sites.

5.5 Conclusions

In this work, DB ASTM G85-A2 was deconstructed in order to determine the impact of RH on TOW and potential. The AA2060-T3 sample exposed to DB ASTM G85-A2 for 4 weeks formed exfoliation as expected, but it was not as severe as the exfoliation reported for this alloy elsewhere[1]. Inconsistencies in cyclic salt spray testing results have been reported before[4] and can be attributed to differences in salt spray chamber operation.

Drying of the TOW sensor began at 13 minutes into the dry air purge when the RH was 44.5%, but the sensor did not finish drying until later in the cycle (between 1.5 – 4 hours depending on the cycle) even though the RH dropped below 20% during the dry air purge. The process of efflorescence was not instantaneous, and it seemed that some moisture remained in the salt film during the dry air and dwell periods even at low RH.

Potential measurements showed that a transition in OCP profile occurred from day 2 to day 8 of the test. After 2 days, the OCP was stable during the salt spray cycle and decreased during the dry cycle. The average potential was lower after 8 days of testing, which was due to activation of more localized corrosion sites. Rather than decreasing during the dry cycle, the potential increased until a peak was reached 10 minutes into the dry air purge. This peak may have been due to changes in cathodic kinetics as the electrolyte film decreased in thickness. At the start of drying, cathodic kinetics would be expected to increase as the diffusion path for oxygen became smaller. An increase in cathodic kinetics would lead to higher potential and higher corrosion current. However, there would be a critical electrolyte layer thickness where the impact of increasing solution resistance would dominate and slow cathodic kinetics. More work is needed to confirm this theory, but the current results show a path forward for improved test design.

These results suggest that the highest corrosion rate may not occur during the wet cycle, but may actually be reached during the early stages of the dry air purge. However, when the electrolyte film decreased to a critical thickness (after approximately 10 minutes into the dry air), cathodic kinetics slowed. The long period of time at low RH (20%-25%) during the dry air purge and dwell is not an effective use of testing time, because the corrosion rate is very slow. This test may be more effective if the dry air purge was shortened to prevent the RH from dropping this low. The optimum RH range for the dry air and dwell periods is not currently known, but it could be determined with the tools outlined in this paper. Many modern salt spray chambers have the capability to control RH during wet and dry cycles, but the ideal RH range could also be achieved in older chambers by tuning the time of the dry air purge to reach the desired RH. Using a standard RH in cyclic salt fog tests rather than a required dry air purge time would provide more consistency in testing results between laboratories.

5.6 Acknowledgements

The authors would like to recognize the Office of Undersecretary of Defense University Pilot Program under the direction of Mr. D. Dunmire, and Rolls Royce for their support of this work. The authors would also like to thank Drs. Jim Moran and Jenifer Locke (previously at the Alcoa Technical Center) for guidance and material.

5.7 References

1. J.P. Moran, F.S. Bovard, J.D. Chrzan, P. Vandenburgh, "Corrosion Performance of New Generation Aluminum-Lithium Alloys for Aerospace Applications," 13th International Conference on Aluminum Alloys, (John Wiley & Sons, 2012).

2. ASTM G34, "Standard Test Method for Exfoliation Corrosion Susceptibility in 2XXX and 7XXX Series Aluminum Alloys (EXCO Test)" (West Conshohocken, PA: ASTM).

3. S.B. Lyon, G.E. Thompson, J.B. Johnson, *New Methods for Corrosion Testing of Aluminum Alloys,* STP 1134 (West Conshohocken, PA: ASTM, 1992), p. 20-31.

4. F. Bovard, J. Tardiff, T. Jafolla, D. McCune, G. Courval, K. A. Smith, F. Lee, J. Repp, S. Ramamurthy, R. J. Shaffer, F. M. Vartolas, "Development of an Improved Cosmetic Corrosion Test for Finished Aluminum Autobody Panels," paper no. 2007-01-0417, *SAE International* (2007).

5. ASTM G85, Annex 2, "Standard Practice for Modified Salt Spray (Fog) Testing" (West Conshohocken, PA: ASTM).

6. R.J. Rioja, J. Liu, "The Evolution of Al-Li Base Products for Aerospace and Space Applications," *Metal. Mater. Trans. A* 43 (2012): p. 3325-3337.

7. E. Schindelholz, L. Tsui, R. G. Kelly, "Hygroscopic Particle Behavior Studied by Interdigitated Array Microelectrode Impedance Sensors," *J. Phys. Chem. A*, 118 (2014): 167-177.

6. Improved Atmospheric Corrosion Testing for High-Strength Aluminum Alloys

Summary:

This chapter presents a detailed comparison of the testing conditions and corrosion morphology after exposure to dry bottom (DB) and wet bottom (WB) ASTM G85-A2 using two different types of salt spray chambers. RH was found to play a critical role the formation of exfoliation. AA2060-T3 exfoliation under DB conditions was more severe in chamber Brand 1, which generated a moderate RH (72.9% to 79.9%) during the dry air and dwell periods when running DB ASTM G85-A2. In chamber Brand 2, RH during the dry air purge and dwell period was low (17% - 20.5%), and this caused corrosion kinetics to slow significantly. Under WB conditions in chamber Brand 1, RH was very high (86.5% - 87.8%) even during the dry air purge and dwell periods. Under these conditions, the no exfoliation blisters formed on the susceptible -T3 temper. At the very high RH, rinsing prevented corrosion products from accumulating on the sample and along grain boundaries, which was needed for exfoliation formation in AA2060-T3. After learning the importance of RH control during ASTM G85-A2 testing, two modified cyclic salt spray tests were designed. Both RH profiles utilized a 1 minute dry air purge and operated under WB conditions, but performing this program in two different chambers (both Brand 2) produced slightly different RH profiles. Mod WB 1 had an average RH of 61.5% during the dwell period, and Mod WB 2 had an average RH of 74% during the dwell period. Both modified tests produced exfoliation in the susceptible temper after just 12 days of exposure. This was much faster than the 4 weeks required by the standard test. AA7075 and AA2024 samples were also exposed to the modified tests, and both tests could distinguish between exfoliation-resistant and susceptible tempers.

6.1 Abstract

In this work, the testing environment of generated during ASTM G85-A2 exposure was deconstructed for two different salt spray chamber brands. It was found that RH control was critical to obtaining consistent results among different salt spray chamber brands, small differences in chamber operation could have a significant impact on RH profile. When RH was too high during the dwell period of the wet-dry cycle, as for ASTM B117 and WB ASTM G85-A2 (chamber Brand

1), rinsing of the sample prevented the accumulation of corrosion products along grain boundaries, which was necessary for exfoliation formation. When RH during the dwell period was too low, anodes stifled during the dry air purge and corrosion rate was very low for most of the repeating 6 hour cycle. Two modified tests were developed in this work (herein referred to as Mod WB 1 and Mod WB 2) with different average RH during the dwell period. Both tests produced moderate exfoliation in AA2060-T3 after just 12 days. Other high-strength aluminum alloys (AA7075, AA2024) were exposed to the modified tests, and both tests could correctly differentiate exfoliation resistance. An average RH between 77% and 61% during the dwell period was found to produce exfoliation in the susceptible temper within just 12 days. Electrochemical measurements were made in both standard and modified tests, and these data were used to propose electrochemical mechanisms that occur during wetting and drying in atmospheric corrosion testing.

6.2 Introduction

Atmospheric corrosion testing plays an important role in aluminum alloy and temper design. A well designed salt spray test can better represent service conditions than immersion tests such as ASTM G34 or ASTM G110,[1-2] but the required testing time is usually longer for salt spray testing than for immersion testing. A wide variety of salt spray tests exist (ASTM B117, ASTM G85, ASTM B368, ASTM D5894),[3-6] which range in complexity from a simple constant spray of neutral NaCl[3] to alternating exposures between a salt spray cabinet and a UV/condensation cabinet.[6] These tests fill different roles in atmospheric corrosion testing, and each test works only for specific alloys and specific applications.

6.2.1 Limitations of ASTM B117 and the development of ATSM G85-A2

ASTM B117 is a constant salt spray test that uses neutral 5% NaCl and operates at 35°C.[3] This test is used for general assessment of the corrosion resistance of metals and coatings, but it is not usually considered predictive of performance in natural environments.[3,7-11] As a constant salt spray test, ASTM B117 is over simplified compared to actual service conditions. During service, coated and uncoated metals cycle through a range of temperature, relative humidity (RH), and solution chemistry, all of which change depending on time of day, season of the year, and exposure site. No laboratory test can encompass the complexity of nature, but several modifications have been found to improve correlation with outdoor exposure results.[11,12] For example, an acidified cyclic salt spray test was developed in 1966 to reveal exfoliation susceptibility in high-strength aluminum alloys (AA2024, AA7075).[12] Before the development of this test, no salt spray test had been developed that could satisfactorily reproduce the exfoliation morphology observed after exposure to natural environments for these alloys. It was believed that exposure at a continuously high relative humidity prevented insoluble hydrates from forming along grain boundaries, which were needed to exert pressure between grains and form exfoliation blisters.

Various wet-dry cycles and solution chemistries were explored, and the optimum cycle was defined as a repeating 6 hour cycle with 45 minutes of 5% NaCl salt spray, 2 hours of dry air purge, and a 3 hour 15 minute soak period. Operating at an elevated temperature of 49^{o}C and adjusting solution pH to ~3 with acetic acid were found to increase the rate of exfoliation formation, but excessive general attack was observed when temperature was increased to 60^{o}C and when pH was reduced to 2.5. Consequently, 49^{o}C and pH 3 were chosen for the final testing protocol. Exposure results for AA7075 and AA2024 in this test were found to correlate well with seacoast exposures. This testing protocol later became the ASTM G85-Annex 2 standard,[4] and is also known by the acronym MASTMAASIS (Modified ASTM Acetic Acid Salt Intermittent Spray).

The ASTM G85-A2 test is defined by the length of each segment of the cycle (45 min salt spray, 2 h dry air purge, 3 h 15 min soak) rather than a target relative humidity for each segment. The researchers who designed the test generated the dry air purge in their chamber by redirecting the compressed air to enter the chamber without passing through the saturation tower. The 2 hour dry air purge reduced RH in the chamber to values between 40 and 70%, and RH slowly increased to values between 65 and 95% during the 3 hour 15 minute soak period due to the presence of a solution reservoir in the cabinet.[12]

6.2.2 Atmospheric corrosion testing for aluminum-lithium alloys

Like many high-strength aluminum alloys, aluminum-lithium (Al-Li) alloys can be susceptible to a form of localized corrosion known as exfoliation. Exfoliation corrosion (EC) occurs in sheet, plate, and extruded alloys that have a laminar grain structure. When attack occurs along grain boundaries or other susceptible microstructural features parallel to the material surface, corrosion products accumulate under the remaining grains and the pressure causes blisters to form.[13-15]

EC has been observed in several Al-Li alloy tempers at seacoast. Moran et al. reported that under-aged tempers of AA2199 sheet and AA2060 plate were susceptible to EC during seacoast exposure at Point Judith, RI.[16] The under-aged tempers of AA2199 and AA2060 were susceptible to intergranular corrosion (IGC), which developed into EC as corrosion products accumulated along grain boundaries. The commercial T8x tempers did not form IGC or EC during seacoast exposure. Figure 6.1 presents cross-sections and photographs of under-aged AA2060 and the commercial T8e86 temper after 1.2 years of exposure at Point Judith RI.[16]

The standard test for exfoliation susceptibility is ASTM G34 (EXCO), but this test was found to overestimate EC susceptibility in the commercial T8x tempers and underestimate susceptibility in the under-aged Al-Li tempers.[16,17] Researchers have reported that while the ASTM G34 test does not predict exfoliation behavior at seacoast for Al-Li alloys, the acidified cyclic salt spray test ASTM G85-Annex 2 was predictive of seacoast exposures.[16,17]

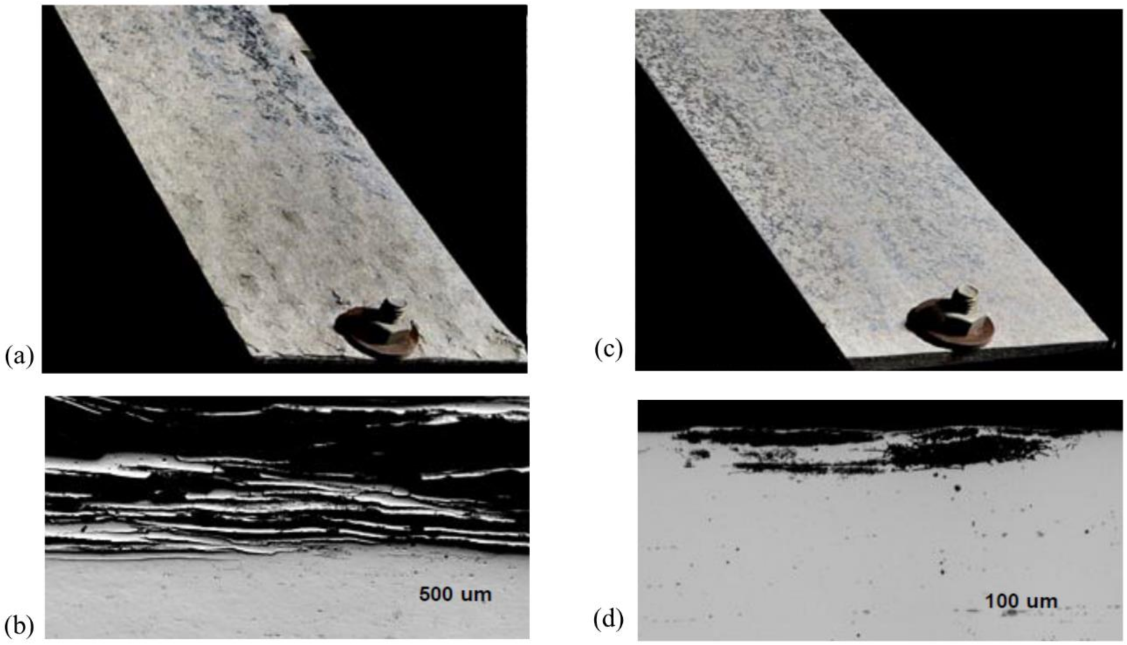

Figure 6.1: AA2060 in the under-aged condition (a-b) and in the commercial T8e86 temper (c-d) after 1.2 years of exposure at Point Judith RI. From reference 16.

6.2.3 Discrepancies in ASTM G85-A2 results among laboratories

Even when a salt spray test is developed that correlates well with outdoor exposures, the issue of consistency in testing environment remains. Bovard et al. reported significant variation in results for several painted aluminum alloys (AA6111-T4PD, AA6016-T4, AA6022-T43, and AA2036-T4) after exposure to ASTM G85-A2 at different laboratories.[18] These inconsistencies were attributed to misinterpretations of the standard protocol as well as differences in testing equipment. Older chambers originally designed to run continuous salt spray tests used compressed air to perform the dry air purge. It was this type of chamber used to develop the ASTM G85-A2 standard.[12] However, many modern CCT chambers create the dry air purge by drawing ambient air through a heater into the test chamber using a fan. While these differences may seem trivial, inconsistencies in testing equipment can have a significant impact on actual relative humidity during exposure.

6.2.4 Impact of relative humidity on salt films

Standardizing the relative humidity during each part of the repeating 6 hour ASTM G85-A2 cycle may be the key to generating consistent corrosion results regardless of equipment brand or laboratory. The solution used in this test is 5% NaCl with pH adjusted to ~3.0 with acetic acid, but the solution chemistry on the sample surface will evolve with changes in relative humidity. Figure 6.2 shows the evolution of several parameters relevant to localized corrosion with changes in RH.[19] During drying (RH decreasing), the equilibrium NaCl concentration increases. Parameters like oxygen (O_2) solubility and solution conductivity which depend on NaCl concentration are also impacted. Changes in NaCl concentration may impact anodic kinetics of aluminum as pitting potential and pit initiation time tend to decrease with increasing [Cl^-].[20,21] Cathodic kinetics may be affected by changes in O_2 concentration. Dolgikh et al. reported that oxygen reduction currents measured for Pt under an evaporating electrolyte film increased at first due to the improved access to O_2 under the thinning film. As the concentration of Cl^- increased in the evaporating film, O_2 solubility and O_2 reduction currents decreased.[22] Solution conductivity (κ) matters for cathodic kinetics because κ determines how much cathode area around an anode is accessible to provide current. Chen et al. modelled the cathode capacity of SS 304L under atmospheric conditions and found that the cathodic current provided by a circular cathode of radius r_L increased with increasing κ.[23] The model showed that increasing the electrolyte layer thickness (WL) would also increase cathodic current. WL would decrease and κ would increase during drying, but overall Chen et al. showed that cathodic current would fall with decreasing RH.

During full immersion tests like ASTM G34 and ASTM G110,[1,2] the rate of cathodic kinetics could be easily controlled through the use of oxidizing agents (H_2O_2, NO_3^-) or solution pH.[49-50] However, the cathodic kinetics during laboratory atmospheric testing will be dependent on the RH. In addition to the impact of RH on O_2 solubility and diffusion distance, RH will control the sample area available to support cathodic reactions. When RH is high, electrolyte droplets will be large, and the cathode area will be at its maximum. As RH decreases during drying, the electrolyte droplets will shrink, reducing the amount of area available to support cathodic reactions.

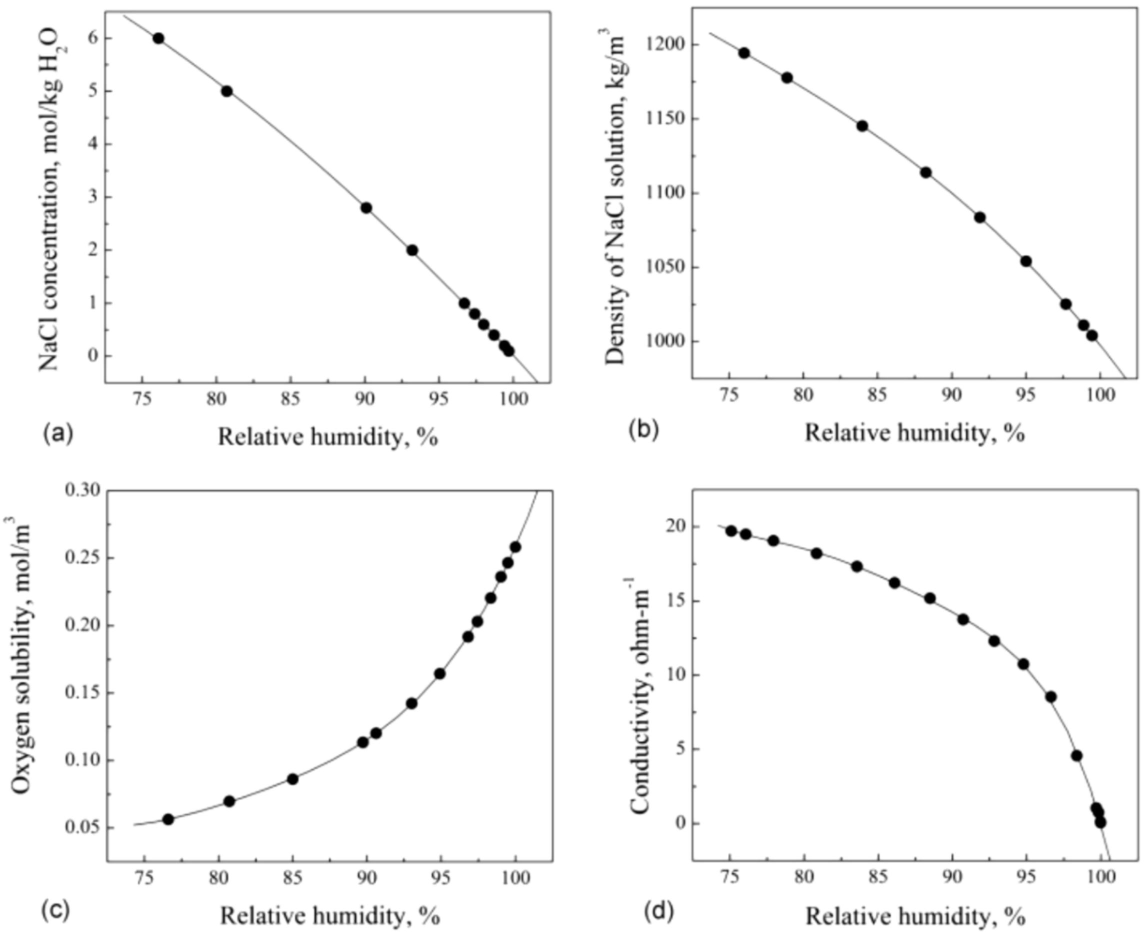

Figure 6.2: Impact of relative humidity on (a) NaCl concentration, (b) Density of NaCl solution, (c) O_2 solubility, and (d) solution conductivity. From reference 19.

The wetting and drying of soluble salts like NaCl are controlled by the deliquescence RH (DRH) and the efflorescence RH (ERH). The DRH is the relative humidity at which water vapor is absorbed by a soluble salt during wetting. During drying, a hysteresis exists such that re-crystallization (efflorescence) occurs at a lower RH than the DRH. The efflorescence process requires that the energy barrier for nucleation be overcome, which delays the process of drying to lower RH.[24] The presence of impurities may reduce the energy barrier by providing an avenue for heterogeneous nucleation. Han et al. found that the efflorescence point of $(NH_4)_2SO_4$ was increased by the presence of internally mixed insoluble particles.[25] Efflorescence of pure $(NH_4)_2SO_4$ occurred at 35% RH, but this value was increased to 57%, 59%, and 65% when the $(NH_4)_2SO_4$ particles were mixed with particles of Al_2O_3, ZrO_2, or TiO_2 respectively.[25]

The DRH and ERH reported in literature for pure NaCl were 74 - 77% (DRH) and 43% - 51% (ERH).[26-29] The measurement method varied among these reports, and measured ERH was slightly lower for techniques that used droplets suspended in air (43%-45%)[27,28] as opposed to deposited on a surface (49-51%)[29]. Both of these scenarios are relevant when studying corrosion processes.

While the DRH and ERH of pure NaCl are relevant for corrosion studies, aerosols found in nature may contain multiple salts. The addition of other salts to NaCl can have a significant impact on the deliquescence and efflorescence behavior.[30-34] The DRH for a simple mixed-chloride system like NaCl-KCl is based on the water activity at the eutonic point of the NaCl-KCl-H_2O system.[34] Tang et al. measured a mutual deliquescence point of 72.7% for NaCl-KCl mixtures.[31]

Even more relevant for ASTM G85-A2 exposures is the impact of acetic acid on wetting/drying behavior. NaCl is the main component of ASTM G85-A2 test solution, but a small amount of acetic acid is added to attain a solution pH between 2.8 and 3.0. No data pertaining to the impact of acetic acid on the DRH and ERH of NaCl could be found in literature, but there were reports on the impact of other organic species. Choi et al. studied the impact of glycerol, succinic acid, malonic acid, citric acid, and glutaric acid on the crystallization and deliquescence behavior of NaCl. Mixtures contained a 1:1 mole ratio of NaCl to the organic species with the exception of glutaric acid, which was a 1:1 ratio by mass. The authors reported that glycerol and succinic acid had no significant impact on the DRH of NaCl, but malonic acid and citric acid containing solutions exhibited a lower DRH than pure NaCl. Glutaric acid caused the deliquescence process to start at a low RH (57.3%), but deliquescence occurred gradually and the final DRH (70.7% RH) was only slightly lower than the reported DRH of pure NaCl (75% RH).[35]

6.2.5 New tools for *in-situ* corrosion monitoring

Monitoring corrosion during atmospheric corrosion testing is a difficult task. The electrodes used for measuring corrosion kinetics in bulk solution are too large for use in thin electrolyte films, and the highly corrosive environment inside a salt spray chamber is damaging to sensors.

Several sensors for corrosion monitoring that utilize electrochemical impedance spectroscopy (EIS) measurements in a two-electrode system have come into use recently.[36-38] For coated materials, impedance measurements for noble metal electrodes embedded in the coating can reveal moisture ingress during exposure.[37] Other sensors are available for monitoring corrosion rates of bare metals. These sensors use two interdigitated electrodes made of the alloy of interest (such as AA2024 or AA7075). Impedance measurements made at high and low frequency values are used to measure polarization resistance (R_p) during accelerated testing or exposure to natural environments.[38]

In the current work, the testing environment of ASTM G85-A2 was deconstructed for two different salt spray chamber brands. Commercial sensors and as well as specially constructed AA2060 samples were used to measure RH, TOW, R_p, and open circuit potential (OCP) in-situ. The understanding gained from studying ASTM G85-A2 was used to design a modified cyclic salt spray test, which successfully distinguished between exfoliation-resistant and susceptible tempers of a wide range of alloys after short exposure times.

6.3 Experimental Procedures

6.3.1 Materials

The primary alloys of concern in this study were the under-aged (T3) and near peak-aged (T86) tempers of the Al-Cu-Li alloy 2060. This material was in the form of 3.5 cm thick plate. The nominal AA2060 composition is presented in Table 6.1.[39] A limited number of exposures were also carried out with AA7075-T651, AA7075-T7351, AA7075-T7651 and AA2024-T3.

Table 6.1: Composition of AA2060[39]

Li	Cu	Mg	Ag	Zr	Mn	Zn	Al
0.75	3.95	0.85	0.25	0.11	0.30	0.40	Bal.

6.3.2 Sample Preparation

All samples were polished to a 1200 grit surface before testing. After grinding, samples were cleaned ultrasonically in deionized water and rinsed with ethanol.

The half-thickness plane, shown in Figure 6.3, was the exposed surface during all testing with AA2060. All other surfaces were masked with Kapton tape. Sample dimensions were 5 cm x 5 cm x 1.75 cm for atmospheric testing. A limited number of exposures were performed on AA2024-T3, AA7075-T651, AA7075-T7351, and AA7075-T7651.

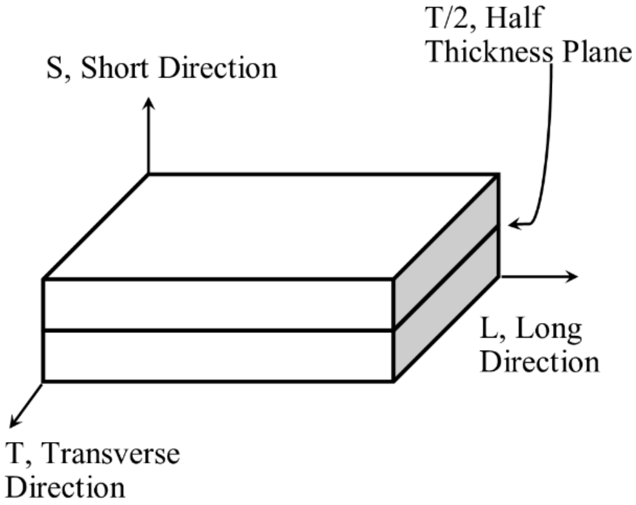

Figure 6.3: Schematic showing sample orientation.

6.3.3 Atmospheric Corrosion Tests

Two different salt spray chamber brands were used in this work. The cabinet identified as chamber Brand 1 was water jacketed and used a stream of compressed air to create a dry air purge. Chamber Brand 2 was a cyclic corrosion testing (CCT) chamber that used heating plates below the exposure zone and performed the dry air purge by blowing heat air into the chamber.

Three standard atmospheric corrosion tests were performed, including ASTM B117, wet bottom (WB) ASTM G85-A2, and dry bottom (DB) ASTM G85-A2. ASTM B117, which is a continuous salt spray test that operates at a temperature of 35°C,[3] was performed only in chamber Brand 2. This test uses a 5% salt solution, and samples were supported on a rack at an angle of 15° from the vertical. Exposure lasted for 4 weeks.

ASTM G85-A2 is a cyclic acidified salt spray test that has been shown to be effective for predicting the exfoliation behavior of Al-Li alloys,[4] and this test was performed in both chamber Brand 1 and 2. This test was carried out according to the standard in the “dry bottom” (DB) condition and “wet bottom” (WB) condition. Under DB conditions, the chamber drain was left open, allowing the chamber to fully dry during the 2 hour dry air purge. For WB conditions, the drain was closed and several inches of water were added to the bottom of the cabinet to ensure that a reservoir of water was available during all portions of the cycle. ASTM G85-A2 consisted of a repeating 6 hour cycle including 45 minutes of salt spray, 2 hours of dry air purge, and a 3 hour and 15 minute dwell period. The testing temperature was 49°C, and the solution was 0.9 M NaCl with the pH adjusted to 2.8 -3.0 with acetic acid. In practice, 23 – 25 ml of glacial acetic acid per 10 L of solution were required to reach a pH of 2.9. The resulting concentration of acetic acid ranged from 0.04 M to 0.0435 M. In chamber Brand 1, sample racks were oriented to hold samples at 45° from the vertical during testing. In chamber Brand 2, sample racks were oriented to hold samples at 15° from the vertical. The difference in sample angle between the two chamber brands was not intentional, and the potential impact of this difference must be considered. Samples at the steeper angle (in chamber Brand 2) would experience more solution run off compared to the samples exposed at the less steep angle (chamber Brand 1). This difference could lead to a greater accumulation of salt and corrosion products over time for samples exposed to chamber Brand 1. The ASTM G85-A2 does not stipulate a particular sample angle, but requires that samples be supported or suspended between 6° and 45° from the vertical.[4] Exposure lasted 4 weeks for all DB and WB ASTM G85-A2.

Exposures were also performed in modified versions of ASTM G85-A2. Modifications included altering the dry air purge time to produce different relative humidity profiles during the dry air and dwell periods of the test. All modified tests were performed in chamber Brand 2 with the standard ASTM G85-A2 test solution and an exposure temperature of 49°C. Sample racks were oriented to hold samples at an angle of 15^o from the vertical. Testing time varied. Additional details for the modified testing parameters can be found in section 6.4.6.

An effort was made to use a consistent salt solution deposition rate for each exposure. Salt deposition rates are generally required to fall within the range 1.0 to 2.0 mL/h over an 80 cm^2 area.[3,4] This large range of collection rate is allowed because it can be difficult to achieve a constant collection rate across the whole salt spray chamber. In chamber Brand 2, samples were tested in small batches so that only a quarter of the chamber was used at once. Over this area of the chamber, it was possible to achieve a collection rate range between 1.5 and 1.7 mL/h.

After exposure, samples were visually rated according to the ASTM G34 exfoliation rating system. The rating system includes several designations, which are summarized in Table 6.2. Photographs were taken directly after samples were removed from the test as well as after rinsing in either deionized (DI) water or nitric acid to remove salt deposits and corrosion products. Some samples were cross-sectioned and prepared for optical microscopy. Etched samples were prepared using Kellar's etch.

Table 6.2: Summary of exfoliation ratings from ASTM G34 and ASTM G112 standards[1,40]

Rating	Attack Type
N	No appreciable attack
IG	Intergranular attack
P	Pitting
EA	Mild exfoliation
EB	Moderate exfoliation
EC	Severe exfoliation
ED	Very severe exfoliation

6.3.4 In-Situ Measurements

6.3.4.1 Relative Humidity and Time of Wetness

Relative humidity and temperature in chamber Brand 2 were measured using a commercial sensor with a manufacturer reported accuracy of ±4.0% RH within the range 20 – 80% RH and ±0.1°C within the range -35 - 80°C. Measurements were performed when DI water was used as the spray solution rather than NaCl because it was determined in previous work that NaCl solution interfered with the performance of the sensor.[41] RH measurements in chamber Brand 1 were made with a different commercial sensor, but details regarding this sensor were not available.

Time of wetness (TOW) was determined by measuring impedance of a gold interdigitated sensor (~300 μm spacing) at a frequency of 26 kHz. Impedance at high frequency correlates with solution resistance (R_s),[38] and a low value of the 26 kHz impedance measurement would indicate R_s was low (i.e. wet sensor). Similarly, a high impedance measurement would R_s was high (i.e. dry sensor). Figure 6.4 shows a combined TOW sensor and corrosion rate sensor produced by Luna Innovations (Charlottesville, VA). The left side of the sensor contained an AA2024-T3 interdigitated sensor and the right side contained the gold interdigitated sensor.

A different brand TOW sensor (Wetcorr) had been used in a previous section of this work, and it was noted by Parker et al. that a thicker salt film formed on the Wetcorr sensor compared to the AA2060 samples.[41] In fact, a continuous salt film was observed on the sensor after 12 days of exposure (Figure 6.5). While salt accumulation over time is expected, a continuous salt film was not observed on the AA2060 that early in testing. Using a sensor with a salt accumulation rate similar to the aluminum samples was important because this factor impacts the TOW measurement. A large salt film takes longer to dry out than discrete salt crystals. The Luna TOW sensor used in the current work accumulated discrete salt crystals (Figure 6.29) more representative the salt film observed on AA2060.

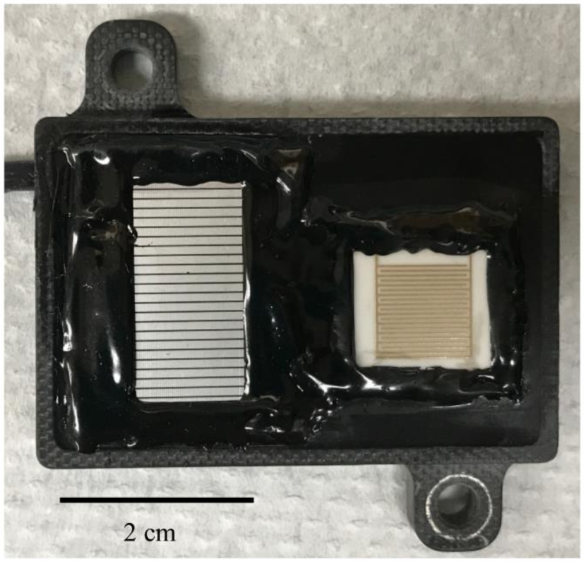

Figure 6.4: Interdigitated electrodes made with AA2024-T3 (Left) and gold (Right).

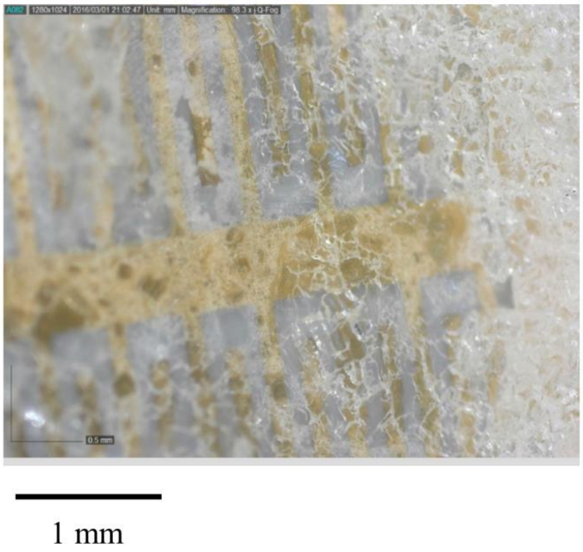

Figure 6.5: A continuous salt film was observed on the Wetcorr sensor after about 12 days exposure in DB ASTM G85-A2.

6.3.4.2 Electrochemical Measurements

Open circuit potential (OCP) was measured using the internal reference of an Orion flat tip pH electrode. The use of this electrode is described in more detail elsewhere.[41]

Electrochemical impedance spectroscopy (EIS) was used to determine polarization resistance (R_p). A cylindrical 5 mm diameter working electrode (either AA2060-T3 or AA2060-

T86) was embedded in the large 5.08 cm x 5.08 cm sample of the same material. The internal reference of an Orion flat tip pH electrode was used as the reference electrode, and a thin Pt wire was inserted into the fill solution of the Orion flat tip electrode to serve as a counter electrode. Impedance was measured from 200 kHz to 100 mHz. Figure 6.6 shows a typical Bode plot from the EIS measurements.

In general, the impedance at very high frequency is related to the solution resistance (R_s), and impedance measured at very low frequency is related to the sum of solution resistance (R_s) and polarization resistance (R_p).[42] These relationships are shown in Equation 6.1 and Equation 6.2. Highly accurate values of R_s and R_p can be determined by applying an equivalent circuit analysis to the experimental data, but the purpose of this test was to simply identify trends in electrochemical kinetics. $Z_{\omega\rightarrow\infty}$ was measured at a high frequency, usually 12.9 kHz, and $Z_{\omega\rightarrow 0}$ was measured at a low frequency, usually 0.2 Hz. These frequencies are shown in the Bode plots in Figure 6.6. Impedance values were multiplied by the electrode area surface area (0.79 cm^2), and Equation 6.1 and Equation 6.2 were used to estimate R_p. EIS spectra were measured at regular intervals during the test cycle, and the total number of spectra collected depended on how quickly each sample dried during the dwell period.

Equation 6.1[42]

$$Z_{\omega\rightarrow 0}(\omega) = R_p + R_s$$

Equation 6.2[42]

$$Z_{\omega\rightarrow\infty}(\omega) = R_s$$

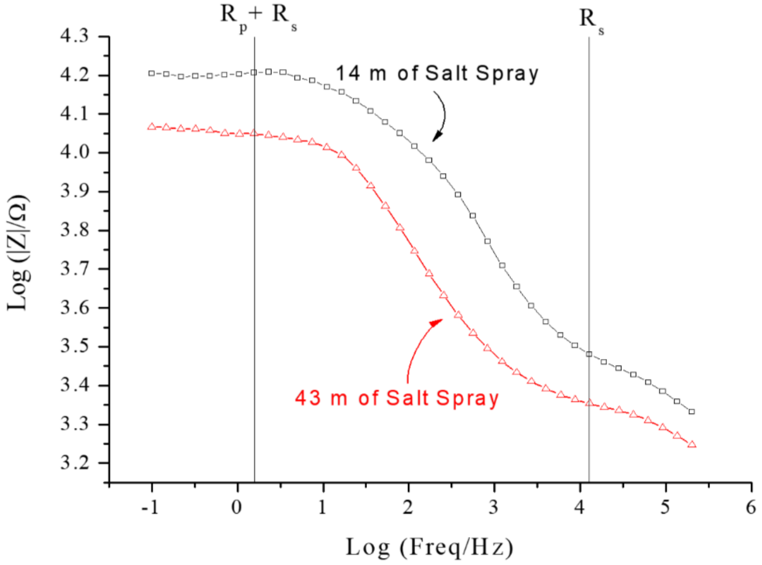

Figure 6.6: Bode plots for AA2060-T3 after 14 minutes and 43 minutes of salt spray on day 2 of DB ASTM G85-A2. Lines show typical frequency used to determine R_s and R_p.

EIS was also used to determine R_p for an AA2024-T3 interdigitated electrode sensor manufactured by Luna Innovations. In this case, impedance was measured from 200 kHz to 10 mHz. For every spectrum, $Z_{\omega\rightarrow\infty}$ was measured at 300 kHz and $Z_{\omega\rightarrow 0}$ was measured at 109 mHz. Typical Bode plots during the salt spray period and during the dwell period in DB ASTM G85-A2 (chamber Brand 2) are shown in Figure 6.7. Due to the large surface area of the sensor (about 2.5 cm^2), the area covered by droplets at any one given time could not be known. Consequently, units of Ω are were used for data collected with this sensor rather than $\Omega\text{-}cm^2$. Once these data were collected, R_p was calculated using Equation 6.1 and Equation 6.2.

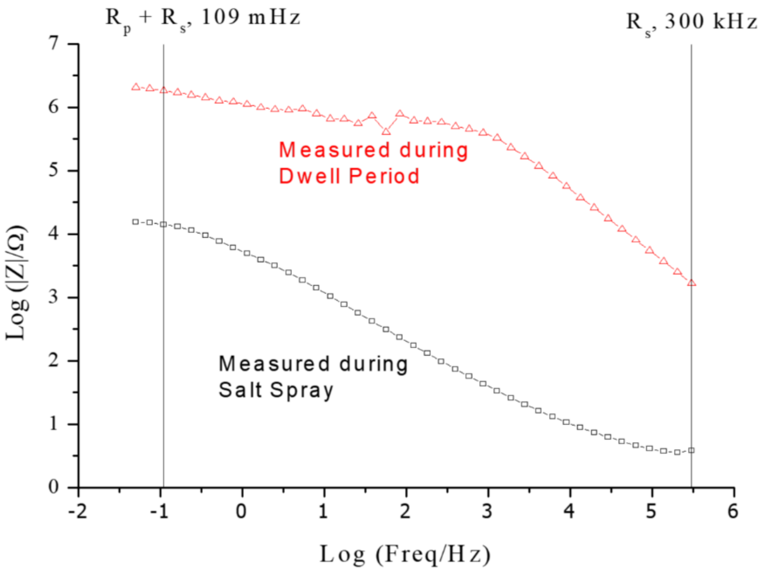

Figure 6.7: Bode plot showing the Log|Z| over a range of frequencies for an EIS spectra measured during the salt spray period (high humidity) and during the dwell period (low humidity) in DB ASTM G85-A2. Frequencies used to estimate R_s (300 kHz) and $R_p + R_s$ (109 mHz) are indicated on the plot.

6.3.5 Solution Chemistry Modelling

OLI studio stream analyzer (OLI Systems, Hanover, NJ) is a commercial software package for calculating physical properties of specified solution chemistries. This software was used to predict changes in chloride concentration, oxygen concentration, oxygen diffusivity, and solution conductivity as a function of relative humidity. OLI version 9.5.4 was used for this work.

The starting solution chemistry included 0.9 M NaCl at 49°C. Calculations were performed with and without the addition of 0.06 M acetic acid (needed to achieve a solution pH of 2.9 in the model). The amount of acetic acid used in the model was slightly higher than the concentration used in the actual testing solution (0.04 M), but the purpose of adding acetic acid was to adjust pH to a particular value. The pH predicted by the model when 0.04 M acetic acid was slightly higher than 2.9, so a little more acetic acid was added to the model to achieve the target pH.

The RH was varied by performing a survey of H_2O composition. While OLI does not report the relative humidity directly, it can be determined using the activity of water, which OLI does report. RH can be defined as the ratio of water vapor pressure to the water vapor pressure at the saturation point (Equation 6.3) where p_{H2O} is the vapor pressure of water, p^{*}_{H2O} is the saturated vapor pressure of water at temperature T, and a_{H2O} is the activity of water.[43.44,45]

Equation 6.3

$$\%RH = \frac{p_{H2O}}{p^{*}_{H2O}(T)} * 100 = a_{H2O} * 100$$

Calculations were performed using the MSE (H_3O+ ion) database in OLI. To simulate water evaporation, the moles of H_2O in the system were varied between 55 and 0. An increment of 0.1 mol was used for calculations within the range 55 to 3, and a smaller increment (0.001 M) was necessary for H_2O content below 3 mol. RH was calculated from the reported activity of water at each water concentration.

Experimental measurements of efflorescence and deliquescence for NaCl solutions with and without acetic acid were measured using the interdigitated gold Luna TOW sensor (Figure 6.4). In each case, a 9-drop array of 2-µl droplets was used. The solution used to make the droplets contained 1.0 M NaCl. For droplets containing acetic acid, solution pH was 2.9. For droplets containing only NaCl, pH was neutral. The sensor was placed in an RH control chamber so that the droplets could be exposed to gradually increasing (for deliquescence measurements) or decreasing (for efflorescence measurements) RH. A 30-minute period was used for every 1% step in RH to allow the droplets to reach steady state at each RH. Salt droplets with and without acetic acid were deposited on the sensor using a pipette, and then exposed to decreasing RH until completely dry. The dried salt crystals were then exposed to increasing RH to measure DRH. Figure 6.8 shows droplets at various stages during the drying process.

Two additional efflorescence measurements were carried out where the chamber was set to produces the fastest drop in RH it was capable of generating. This test was designed to measure the impact of drying rate on efflorescence.

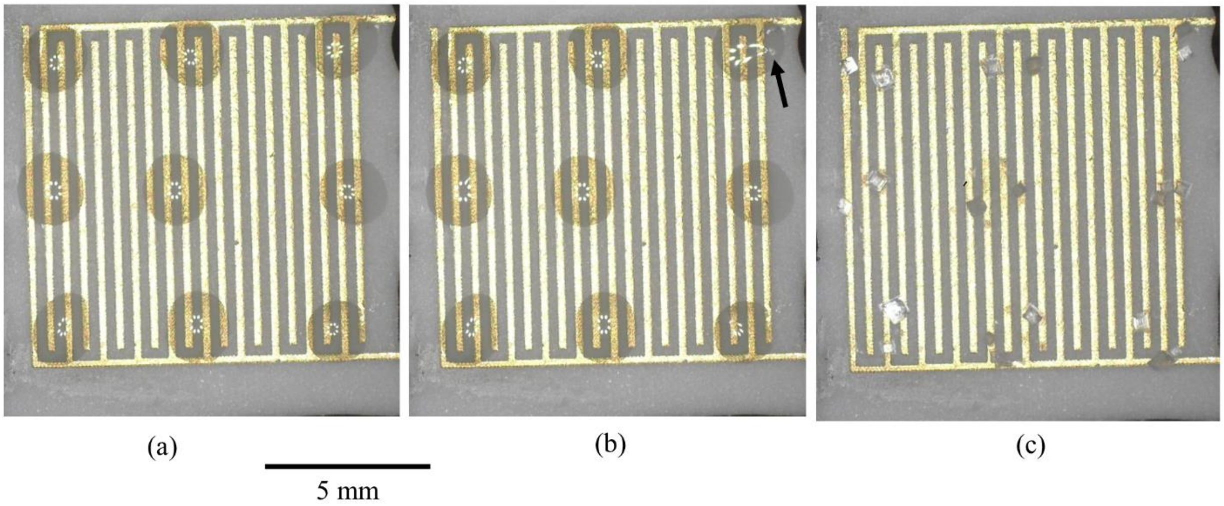

Figure 6.8: NaCl droplets with acetic acid at various stages in the drying process. RH and $|Z|_{26kHz}$ during each image were (a) 75.5%, 68 Ω (b) 74%, 69 Ω and (c) 70%, 41741 Ω. The arrow in image (b) shows the first crystalized NaCl visible with the camera. The circle of white dots within each droplet in (a) and (b) are the reflection of the LED from the camera.

6.4 Results

6.4.1 ASTM B117

After 4 weeks of exposure to ASTM B117 in chamber Brand 2, the appearance of the under-aged -T3 temper and the near peak-aged -T86 temper were indistinguishable. Figure 6.9(a) and (b) show the -T3 and -T86 tempers immediately after being removed from the test. Very little corrosion product or salt accumulated on the sample surfaces, so rinsing samples did not change the appearance significantly (Figure 6.9[c] and [d]). These samples would be rated P based on the descriptions in Table 6.2.

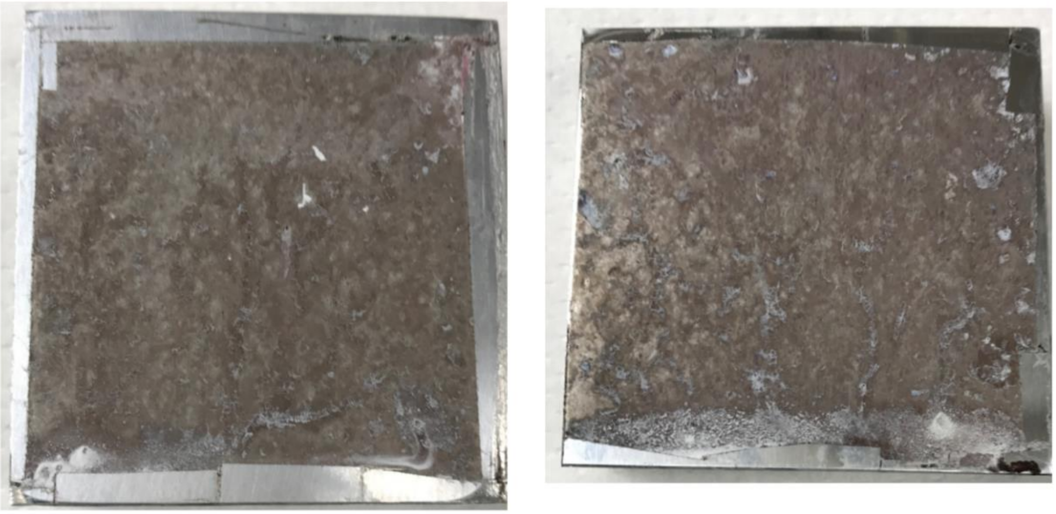

(a) AA2060-T3, No Rinse

(b) AA2060-T3-86, No Rinse

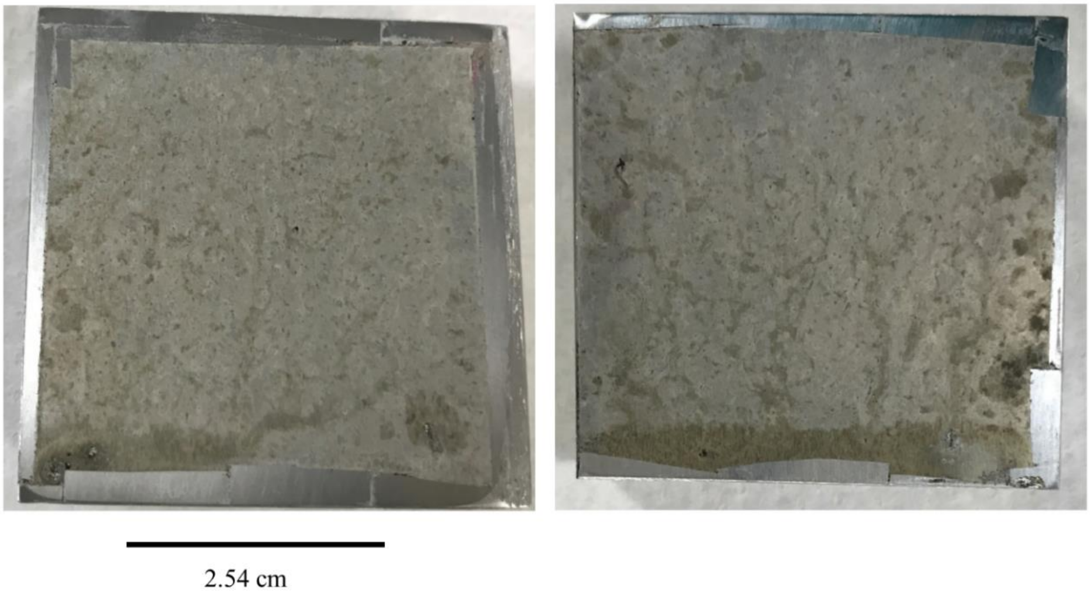

(c) AA2060-T3, With Rinse

(d) AA2060-T3-86, With Rinse

Figure 6.9: (a) AA2060-T3 and (b) AA2060-T86 after 4 weeks of ASTM B117 testing with no rinsing. (c) AA2060-T3 and (b) AA2060-T86 after 4 weeks of ASTM B117 testing with a DI water rinse.

6.4.2 DB and WB ASTM G85-A2

Dry bottom ASTM G85-A2 was more successful at distinguishing between tempers than ASTM B117, but there were significant differences in the extent of attack when testing was performed with different salt spray chamber brands.

Using chamber Brand 1, the tempers were easily distinguished after 4 weeks of exposure. Figure 6.10(a) and (b) show the -T3 and -T86 tempers directly after being removed from the test chamber, and Figure 6.10(c) and (d) show the tempers after rinsing in nitric acid to remove corrosion products. Large exfoliation blisters can be seen in the -T3 temper (Figure 6.10[a] and [c]), and this sample was rated EB for moderate exfoliation. The -T86 temper was rated P for pitting (Figure 6.10[b] and [d]). It should be noted that significant exfoliation had already formed on the -T3 temper in chamber Brand 1 even after just 2 weeks of exposure. Figure 6.11 shows AA2060-T3 after 2 weeks of exposure to DB ASTM G85-A2. Exfoliation blisters were less prominent at 2 weeks than at 4 weeks, but enough exfoliation had formed to rate the sample EB after just 2 weeks.

However, after 4 weeks of exposure to DB ASTM G85-A2 using chamber Brand 2, the extent of attack was noticeably lower compared to testing in chamber Brand 1. Exfoliation blisters on the -T3 temper were too small to see beneath the layer of salt and corrosion products present directly after removing from the test chamber (Figure 6.12[a]), but small blisters were visible after cleaning (Figure 6.12[c]). This sample was rated EA for mild exfoliation. The -T86 temper was rated P for pitting (Figure 6.12[b] and [d]). Cross-sections confirmed that the extent of attack was more severe after testing in chamber Brand 1. Figure 6.13(a) and (b) show blisters and grain lifting representative of the -T3 sample after exposure in chamber Brand 1 and 2 respectively. Both samples experienced IGC, but grain lifting was more significant for the sample exposed in chamber Brand 1.

After 4 weeks of exposure to WB ASTM G85-A2 in chamber Brand 1, the two alloy tempers were indistinguishable. Figure 6.14 shows the -T3 and -T86 temper directly after being removed from the chamber (a-b) and after rinsing in nitric acid (c-d). No exfoliation blisters were observed on the -T3 temper (Figure 6.14[a] and [c]), but this sample was rated I because IGC was observed after cross-sectioning (Figure 6.15[a]).

In contrast, the samples exposed to WB ASTM G85-A2 in chamber Brand 2 could be distinguished by temper. In fact, the samples exposed to this test looked similar to the samples exposed to DB ASTM G85-A2 in chamber Brand 2. The -T3 temper was rated EA for mild exfoliation (Figure 6.16[a] and [c]), and the -T86 temper was rated P for pitting (Figure 6.16[b] and [d]). Exfoliation ratings are summarized in Table 6.3.

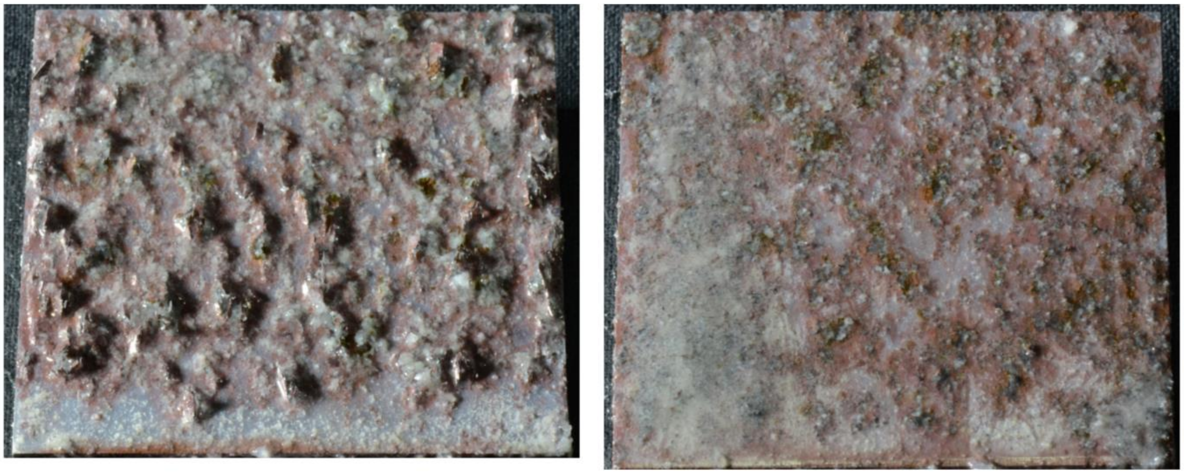

(a) AA2060-T3, No Rinse

(b) AA2060-T3-86, No Rinse

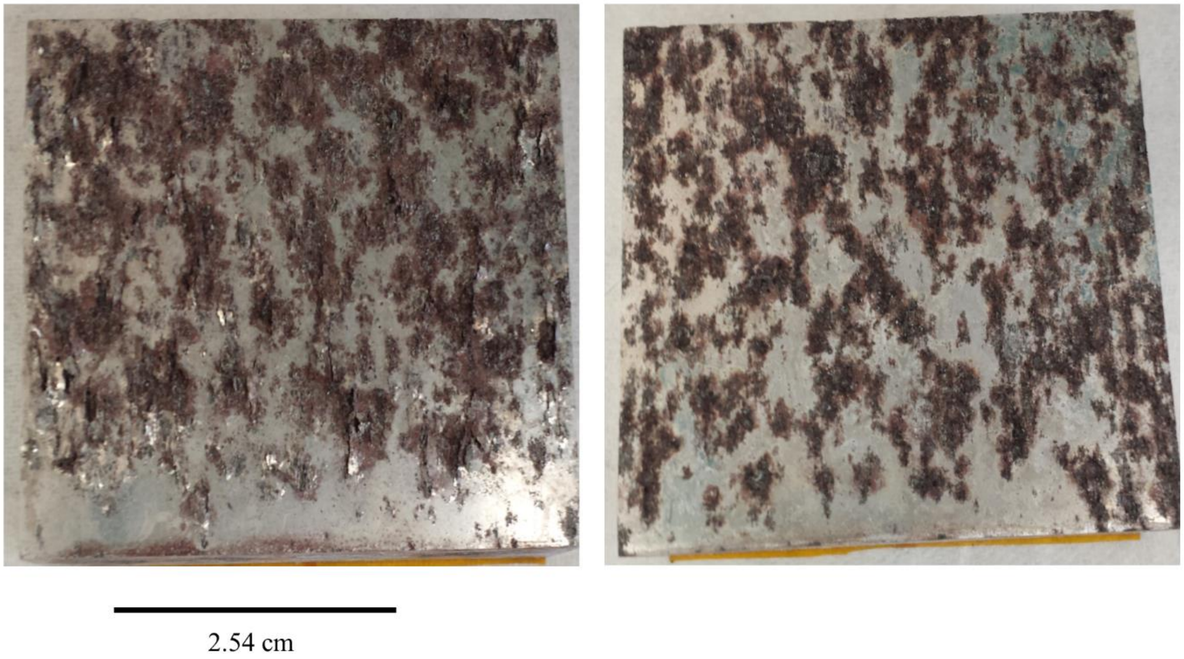

(c) AA2060-T3, With Rinse

(d) AA2060-T3-86, With Rinse

Figure 6.10: (a) AA2060-T3 and (b) AA2060-T86 after 4 weeks of DB ASTM G85-A2 testing using chamber Brand 1 without any rinsing of the sample. (b) AA2060-T3 and (c) AA2060-T86 after 4 weeks of DB ASTM G85-A2 testing after cleaning in nitric acid.

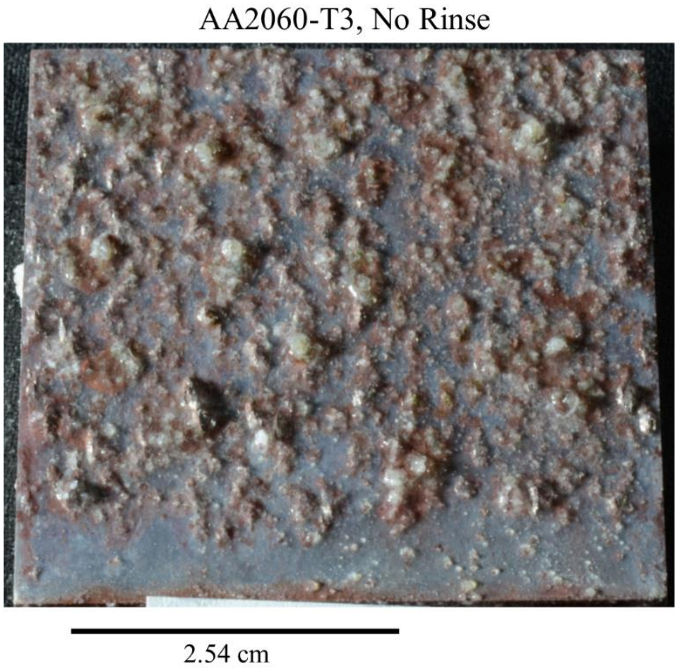

Figure 6.11: Exfoliation blisters rated EB formed on AA2060-T3 after just 2 weeks of exposure to DB ASTM G58-A2 in chamber Brand 1.


(a) AA2060-T3, No Rinse

(b) AA2060-T3-86, No Rinse

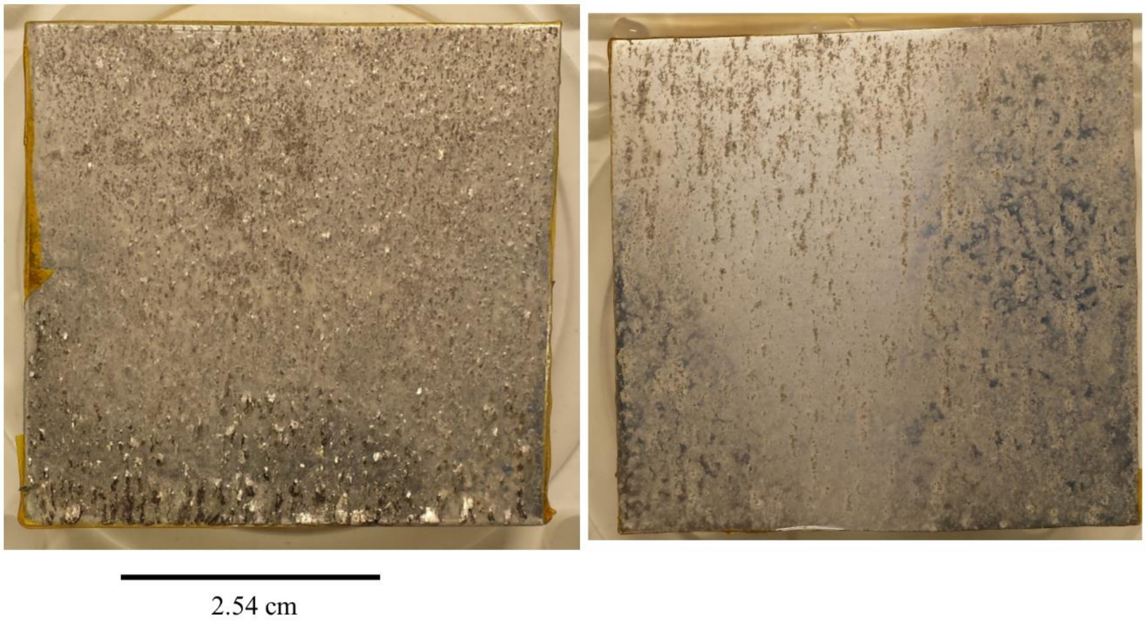
(c) AA2060-T3, With Rinse

(d) AA2060-T3-86, With Rinse

Figure 6.12: (a) AA2060-T3 and (b) AA2060-T86 after 4 weeks of DB ASTM G85-A2 using chamber Brand 2 without any rinsing. (b) AA2060-T3 and (b) AA2060-T86 after 4 weeks of DB ASTM G85-A2 with a rinse in DI water. These results have been published in reference 41.

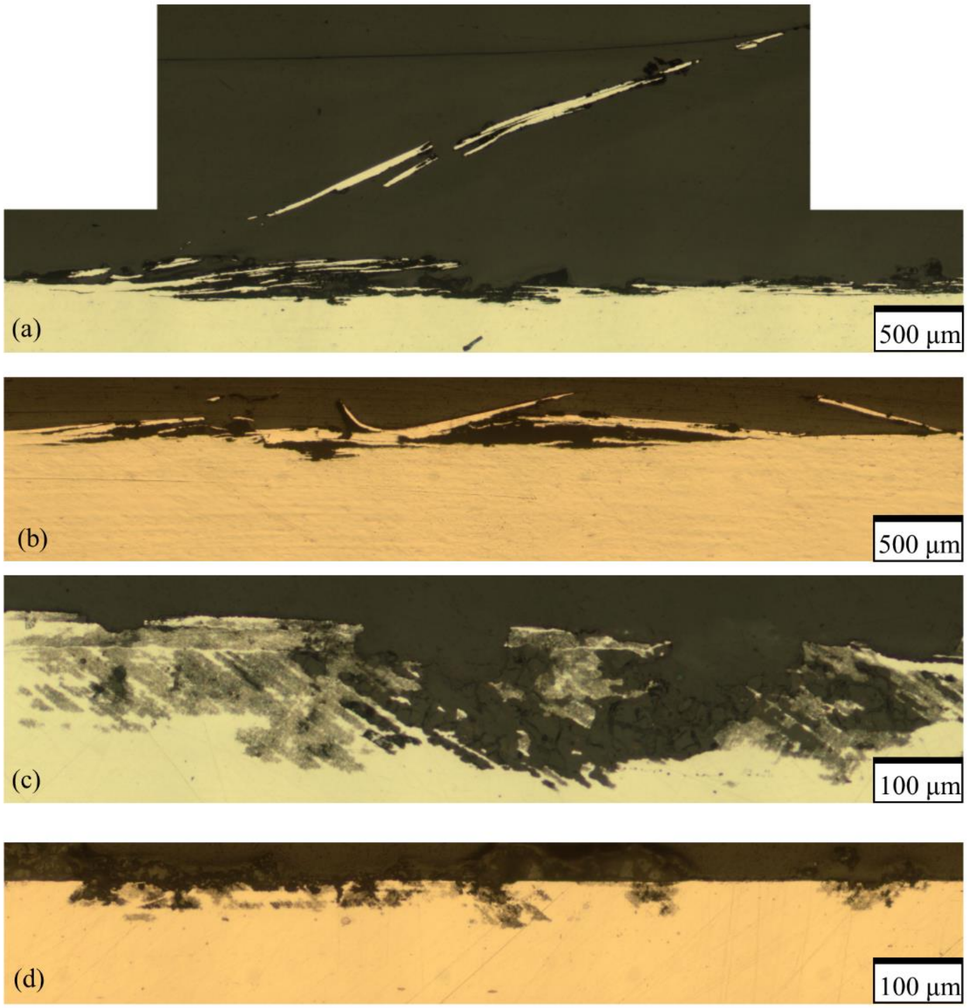

Figure 6.13: AA2060-T3 after 4 weeks of DB ASTM G85-A2 at (a) chamber Brand 1 and (b) chamber Brand 2. AA2060-T86 after 4 weeks of DB ASTM G85-A2 using (b) chamber Brand 1 and (b) chamber Brand 2.

(a) AA2060-T3, No Rinse (b) AA2060-T3-86, No Rinse

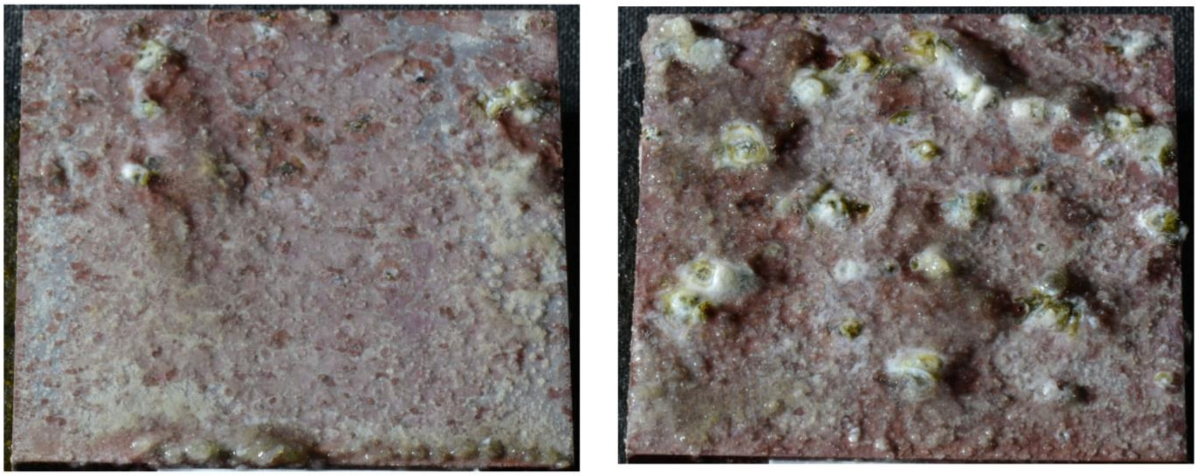

(c) AA2060-T3, With Rinse (d) AA2060-T3-86, With Rinse

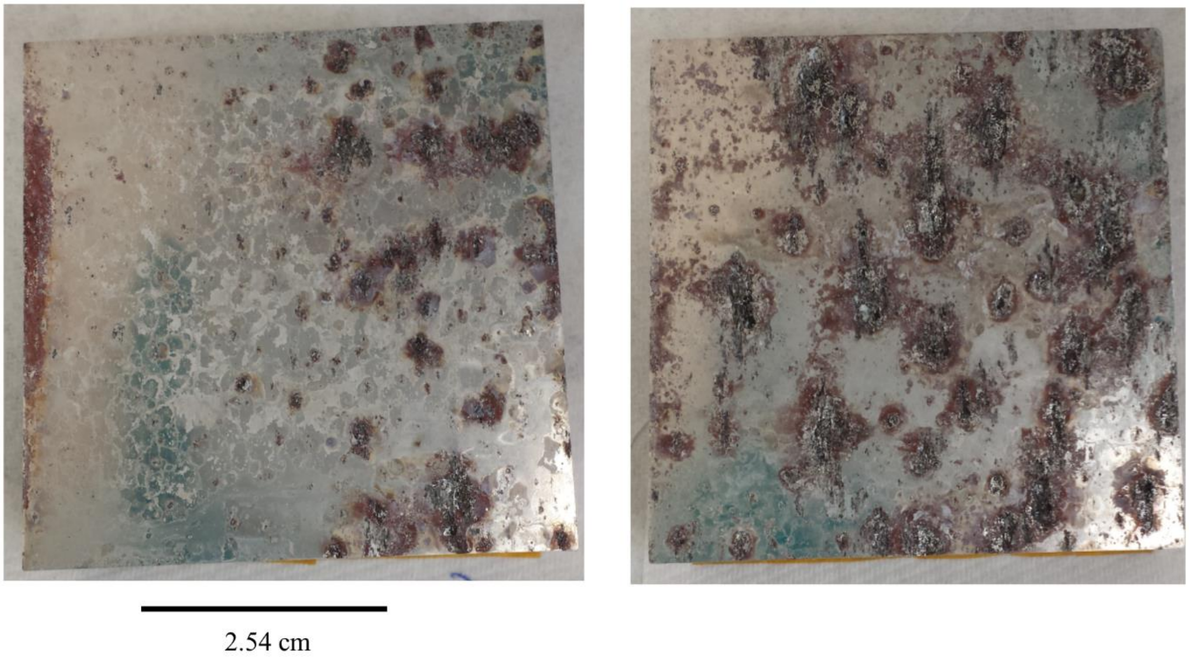

Figure 6.14: (a) AA2060-T3 and (b) AA2060-T86 after 4 weeks of WB ASTM G85-A2 in chamber Brand 1 with no rinsing. (b) AA2060-T3 and (b) AA2060-T86 after 4 weeks of WB ASTM G85-A2 in chamber Brand 1 with nitric acid rinse.

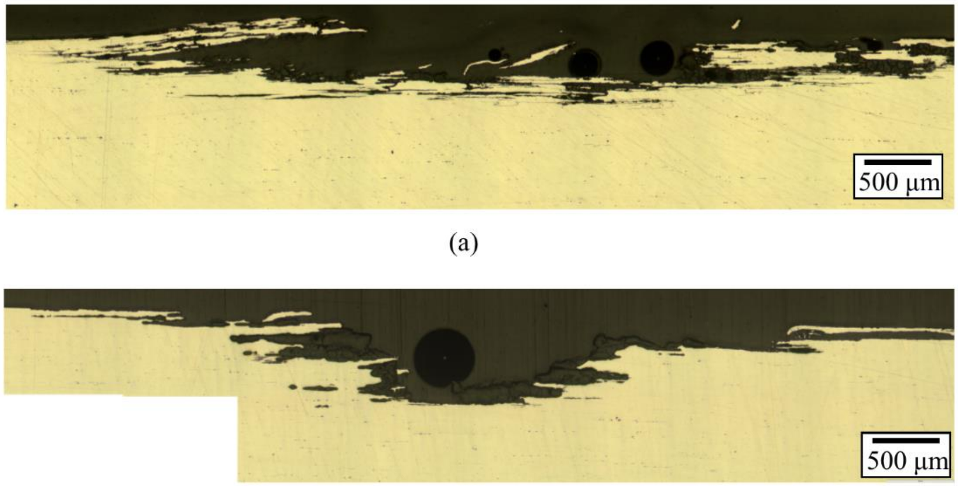

Figure 6.15: Cross-sections of (a) AA2060-T3 and (b) AA2060-T86 after 4 weeks of exposure to WB G85-A2 in chamber Brand 1.

(a) AA2060-T3, No Rinse

(b) AA2060-T3-86, No Rinse

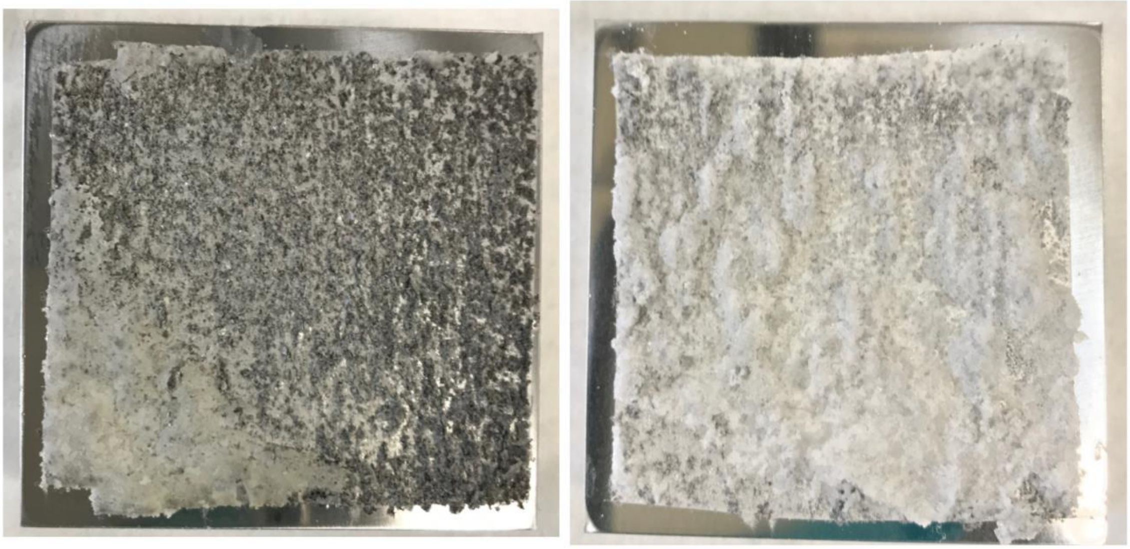

(c) AA2060-T3, With Rinse

(d) AA2060-T3-86, With Rinse

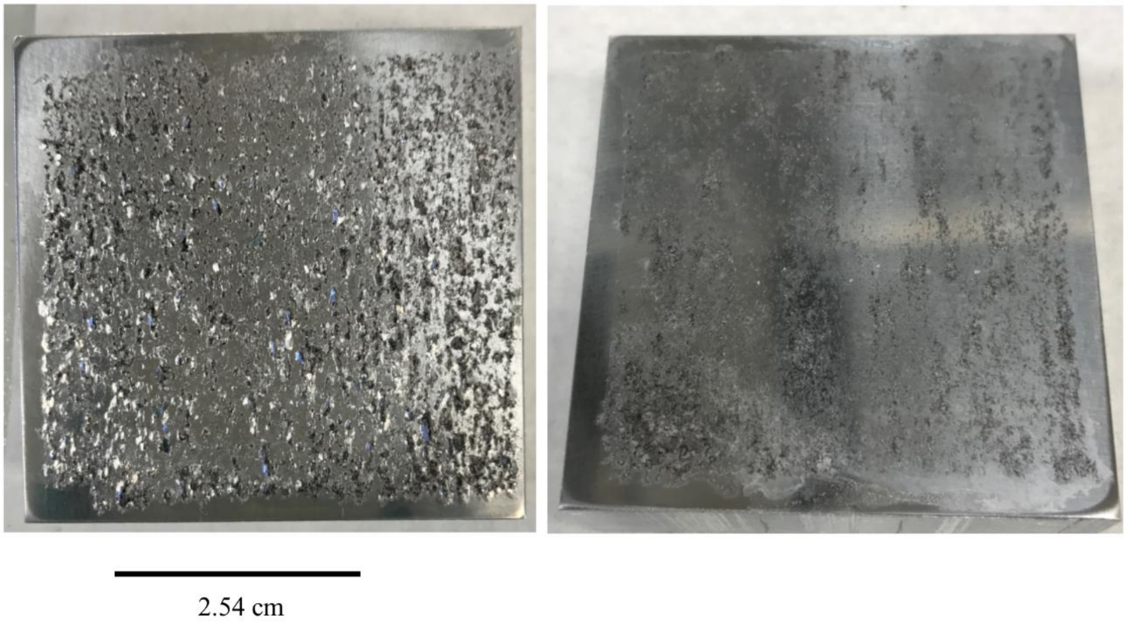

Figure 6.16: (a) AA2060-T3 and (b) AA2060-T86 after 4 weeks of WB ASTM G85-A2 in chamber Brand 2 with no rinsing. (c) AA2060-T3 and (d) AA2060-T86 after 4 weeks of WB ASTM G85-A2 in chamber Brand 2 after nitric acid rinse.

Table 6.3: Summary of exfoliation ratings for WB and DB ASTM G85-A2

	AA2060-T3		**AA2060-T86**	
	DB	WB	DB	WB
Chamber Brand 1	EB	I	P	P
Chamber Brand 2	EA	EA	P	P
Point Judith RI[16]	EB	EB	P	P

6.4.3 Relative Humidity and Time of Wetness

6.4.3.1 Comparing RH in chamber Brands 1 and 2

Relative humidity in chamber Brands 1 and 2 for DB and WB ASTM G85-A2 is shown in Figure 6.17(a) and (b) respectively. Relative humidity was high during the 45 minute salt spray period at the start of each 6 hour cycle regardless of the testing equipment. However, RH varied significantly during the dry air purge and dwell period based on chamber brand and test type (WB or DB).

Under DB conditions, RH decreased during the dry air purge in both chamber brands, but the decrease was more significant in chamber Brand 2. During the dry air purge in chamber Brand 2, RH dropped to 17%, but 72.9% was the lowest RH during the dry air purge in chamber Brand 1. During the dwell period RH increased slightly in both chambers. The highest RH reached during the dwell period was 79.9% in chamber Brand 1 and 20.5% in chamber Brand 2.

For WB conditions, RH decreased to 23% during the dry air purge in chamber Brand 2, but only dropped to 86.5% in chamber Brand 1. During the dwell period, RH increased slightly to 87.8% in chamber Brand 1. The change in RH during the dwell period was more significant in chamber Brand 2, but a maximum RH of only 53% was reached during this period.

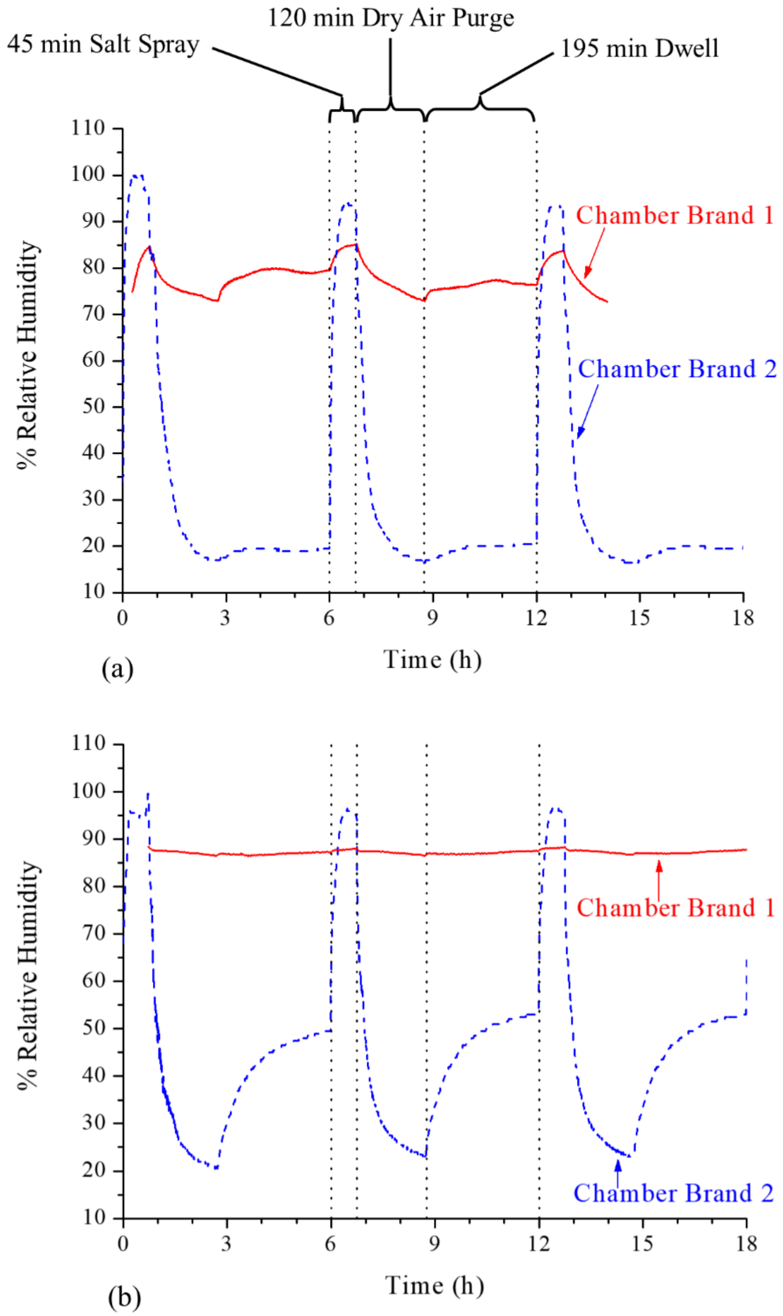

Figure 6.17: Relative humidity in chamber Brand 1 and 2 for (a) DB ASTM G85-A2 and (b) WB ASTM G85-A2.

Access to chamber Brand 1 was limited during this study, but additional measurements were made in chamber Brand 2. Figure 6.18 presents impedance measurements from an interdigitated time of wetness (TOW) sensor during DB and WB ASTM G85-A2 in chamber Brand 2. A low impedance value indicated that the sensor was wet. As soon as the sensor dried, impedance increased until the baseline dry sensor value (~54,000 Ω) was reached. Even though RH was higher under WB conditions during the dwell period than under DB conditions, the TOW was very similar for both versions of the test. In both WB and DB G85-A2, once the sensor dried, it did not re-wet until the next salt spray cycle began. Average time after the start of the dry air purge to reach the baseline dry impedance value was 13.5 min for DB G85-A2 and 20.3 min for WB ASTM G85-A2.

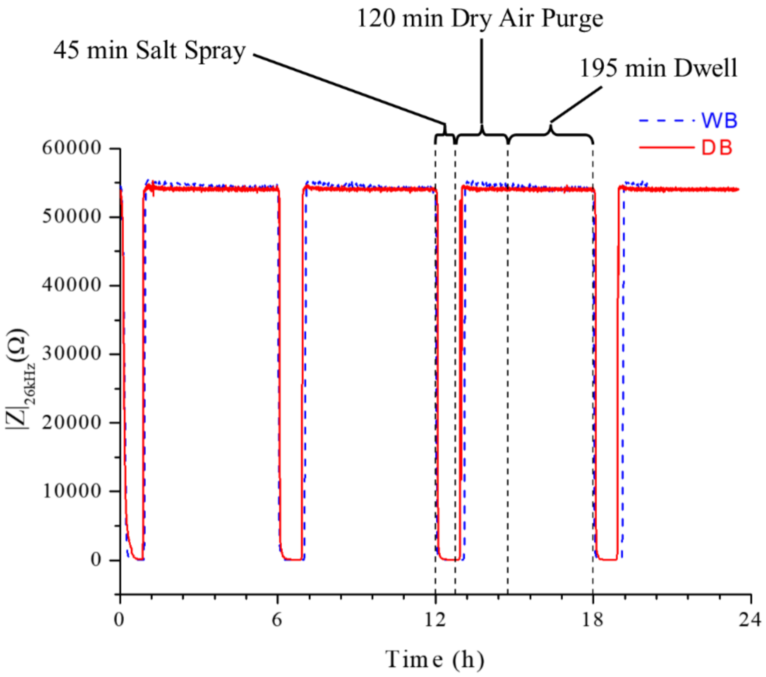

Figure 6.18: Impedance of TOW sensor for 4 cycles of DB ASTM G85 (solid red line) and WB ASTM G85 (dashed black line) in chamber Brand 2.

6.4.3.2 Relationship between Temperature and RH in Chamber Brand 2

The maximum relative humidity reached during the dwell period under wet bottom conditions in chamber Brand 2 was only 53% RH, which was surprising considering a large water reservoir was present on the bottom of the chamber. RH and temperature were measured during a long dwell period (29 hours) after a 45 minute wet cycle to determine the steady state RH at several positions within chamber Brand 2 under wet bottom conditions. Figure 6.19(a) shows temperature measurements at locations above, below and within the exposure zone during a 30 hour dwell period under WB conditions. Even though the chamber was set to run at 49^{o}C, temperature varied throughout the chamber. This particular chamber brand used metal heating plates below the exposure zone to maintain chamber temperature. Below the exposure zone, temperature was high (61^{o}C) due to the close proximity to the heating plates. Temperature decreased as distance from the heating places increased, falling to 51^{o}C within the exposure zone and 47.5^{o}C above the exposure zone. The chamber temperature sensor was located about 15 cm above the exposure zone, which may explain why temperature within the exposure zone was higher than the set temperature for the chamber.

Figure 6.19(b) shows that RH also varied above, within, and below the exposure zone during a long dwell period under WB conditions. %RH was lowest at the bottom of the chamber, averaging 35% RH from hour 20 to 30 of the measurement. Over the same time period, % RH within the exposure zone averaged 54%, and % RH above the exposure zone averaged 64%.

Relative humidity was also measured when the chamber set temperature was 24^{o}C (room temperature) under WB conditions (Figure 6.19[b]). With a set temperature of 24^{o}C, the heating plates never needed to turn on and chamber temperature should have been uniform. Under these conditions, % RH quickly increased to high values, reaching an average of 99% from hour 20 to hour 30 of the long dwell period (Table 6.4).

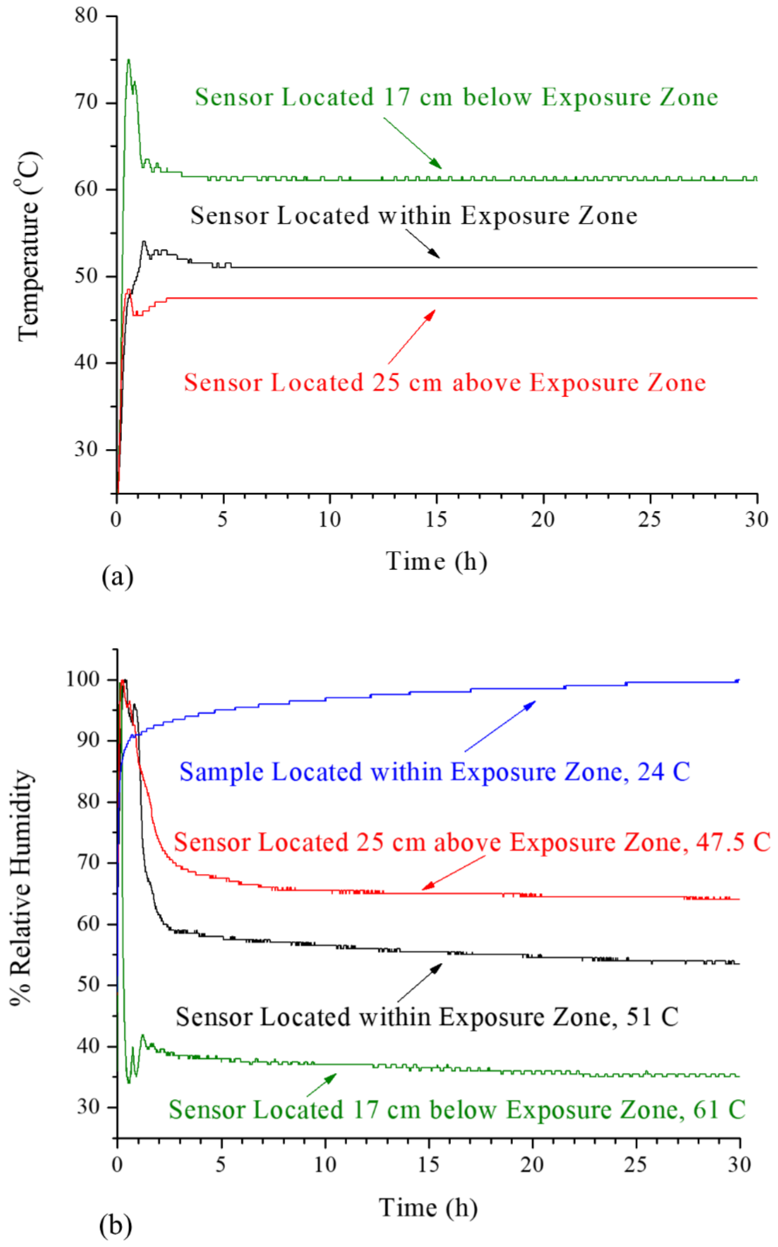

Figure 6.19: (a) Temperature measurements and (b) relative humidity measurements at various locations in the salt spray chamber.

Table 6.4: Actual temperature and relative humidity (average from hour 20 to hour 30) at various locations within the salt spray chamber

Sensor Location	Temperature Setting	Actual Temperature	Actual RH
25 cm Above Exposure Zone	49°C	47.5°C	64%
In Exposure Zone	49°C	51°C	54%
17 cm Below Exposure Zone	49°C	61°C	35%
In Exposure Zone	24°C	24°C	99%

6.4.4 Impact of Acetic Acid on Deliquescence/Efflorescence

6.4.4.1 OLI modeling

OLI solution modeling was used to obtain a better understanding of possible changes in solution chemistry during wetting and drying. Figure 6.20 shows the calculated relationship between chloride concentration ($[Cl^-]$) and relative humidity for NaCl with and without acetic acid present. The model predicted that deliquescence of neutral NaCl would occur around 74.9% RH, which was consistent with experimentally determined values in literature.[26-29]

When 0.06 M acetic acid (CH_3COOH) was added to the model, NaCl began to crystalize 74.3% RH, but complete drying was delayed to much lower RH. Even at RH as low as 3.2%, the model predicted a small amount of liquid would remain. Figure 6.21 presents the predicted volume of liquid during dehumidification, with an assumed starting volume of 2 μL. For the solution containing only NaCl, the volume of liquid dropped suddenly at 74.9% due to loss of water at RH below the thermodynamic DRH of NaCl. For the solution containing both NaCl and acetic acid, however, very small volumes of liquid were predicted to be present even at an RH of 3.2%. Table 6.5 shows the predicted remaining volume at three values of RH for a droplet containing NaCl and acetic acid with a starting volume of 2 μL. The radius of the droplets was calculated using the predicted solution volume with the assumption that droplets were perfect hemispheres.

The model also predicted that acetic acid would evaporate during dehumidification. The amount of acetic acid in the liquid phase decreased very slowly between 97% RH and 74.2% RH, and evaporated rate increased below 74.2% (Figure 6.21[b]). At 27.5% RH, most of the acetic acid was in the vapor phase, but a small amount of liquid acetic acid remained.

Pure acetic acid is a liquid at room temperature. During drying, both water and acetic acid were predicted to evaporate from the liquid phase. In the fresh test solution, the ratio of liquid acetic acid to liquid water in the electrolyte was very small (0.06 mol acetic acid to 55 mol H_2O), but water was predicted to evaporate faster than the acetic acid. As the electrolyte dried, the ratio of liquid acetic acid to liquid water (mol/mol) increased. Figure 6.22(a) shows changes in the ratio of acetic acid to water (mol/mol) during drying. The calculated solubility of NaCl in pure water was significantly higher than the solubility of NaCl in pure acetic acid (Figure 6.22[b]). OLI calculations predicted a NaCl solubility limit of 5.5 M in pure water and just 0.036 M in pure acetic acid. A temperature of 49°C was used for the calculations.

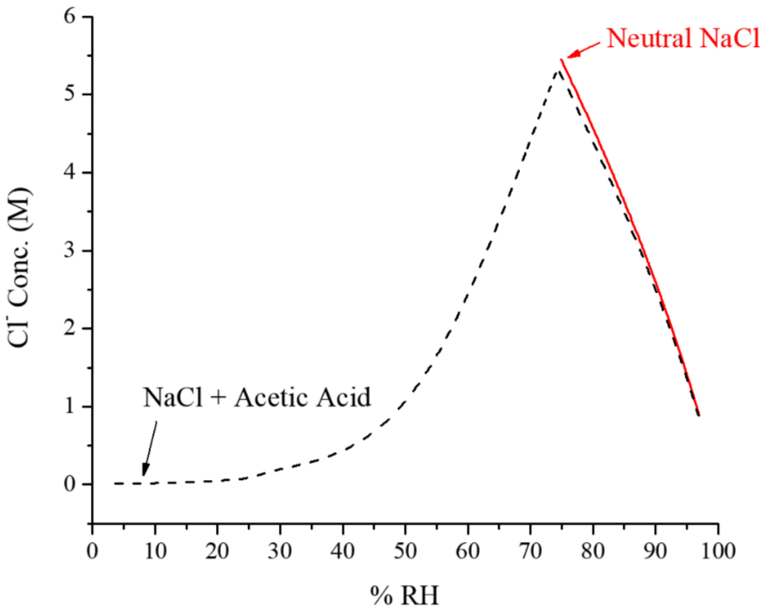

Figure 6.20: Cl^- concentration as a function of RH for neutral NaCl and NaCl with 0.06 M acetic acid.

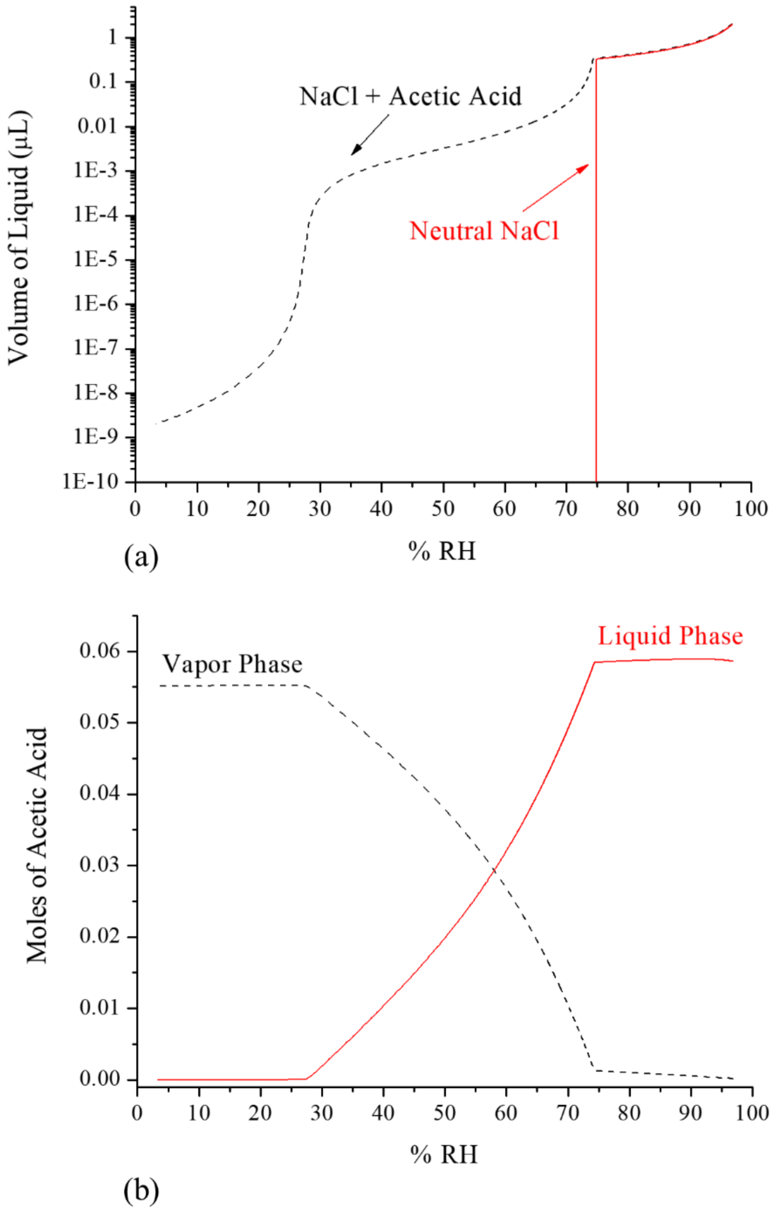

Figure 6.21: (a) Predicted solution volume changes (starting condition was 2 uL) during dehumidification with and without acetic acid. (b) Predicted phase change of acetic acid during dehumidification.

Table 6.5: Predicted volume of liquid and droplet radius for NaCl + acetic acid solution at various RH. Starting liquid volume was 2 μL, and droplets were assumed to have a perfect hemispherical shape.

% RH	60	30	20
Liquid Volume (nL)	7.4	0.25	3.6×10^{-5}
Droplet Radius (μm)	153	49	2.6

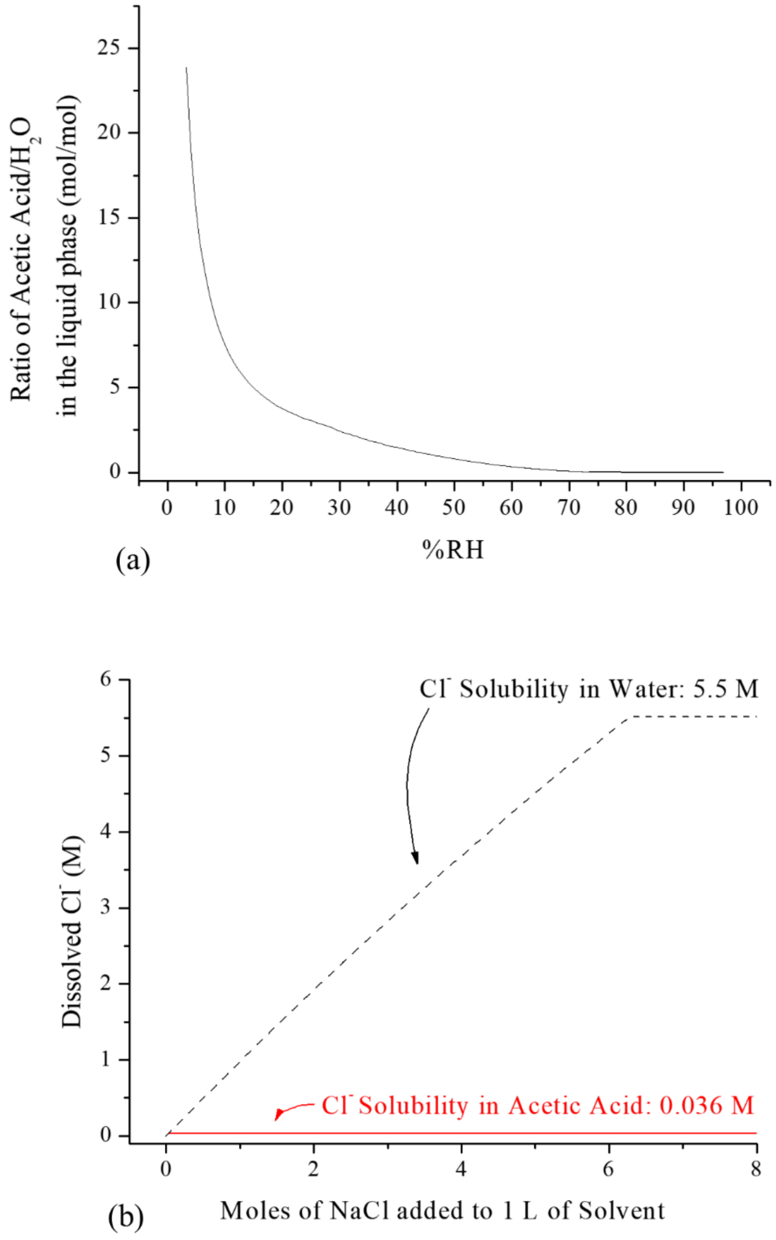

Figure 6.22: (a) Changes in ratio of acetic acid to H_2O in the liquid phase during dehumidification. (b) Predicted solubility limits for NaCl in pure water and pure acetic acid at 49°C.

6.4.4.2 Efflorescence/Deliquescence Measurements

Experimental measurements of efflorescence and deliquescence for NaCl solutions with and without acetic acid were carried out to validate the OLI modelling presented above. In each case, a 9-drop array of 2-μl droplets was used. Figure 6.8 shows droplets at various stages during the drying process.

The deliquescence point was measured by monitoring the impedance of dry salt crystals on a TOW sensor in an RH chamber while slowly increasing the relative humidity (30 minutes for every 1% step in humidity). Figure 6.23(a) shows that measured deliquescence point was consistently 74.5% for several replicate experiments for NaCl with and without acetic acid. This value agreed with published experimental values of NaCl DRH.[26-29] Measured efflorescence point was not as reproducible as the deliquescence point, and ranged between 69% and 73.5% RH regardless of the presence or absence of acetic acid.

When the rate of dehumidification was increased to a level more comparable to that generated during the dry air purge in DB ASTM G85-A2, the efflorescence point was depressed significantly. Impedance began increasing at 50% RH (with acetic acid) and 52% RH (without acetic aicd). The baseline dry sensor impedance was reached at 40.5% RH (with acetic acid) and 43.5% RH (without acetic acid). A comparison of the dehumidification profile used for this experiment to the dehumidification profile in DB ASTM G85-A2 is shown in Figure 6.24.

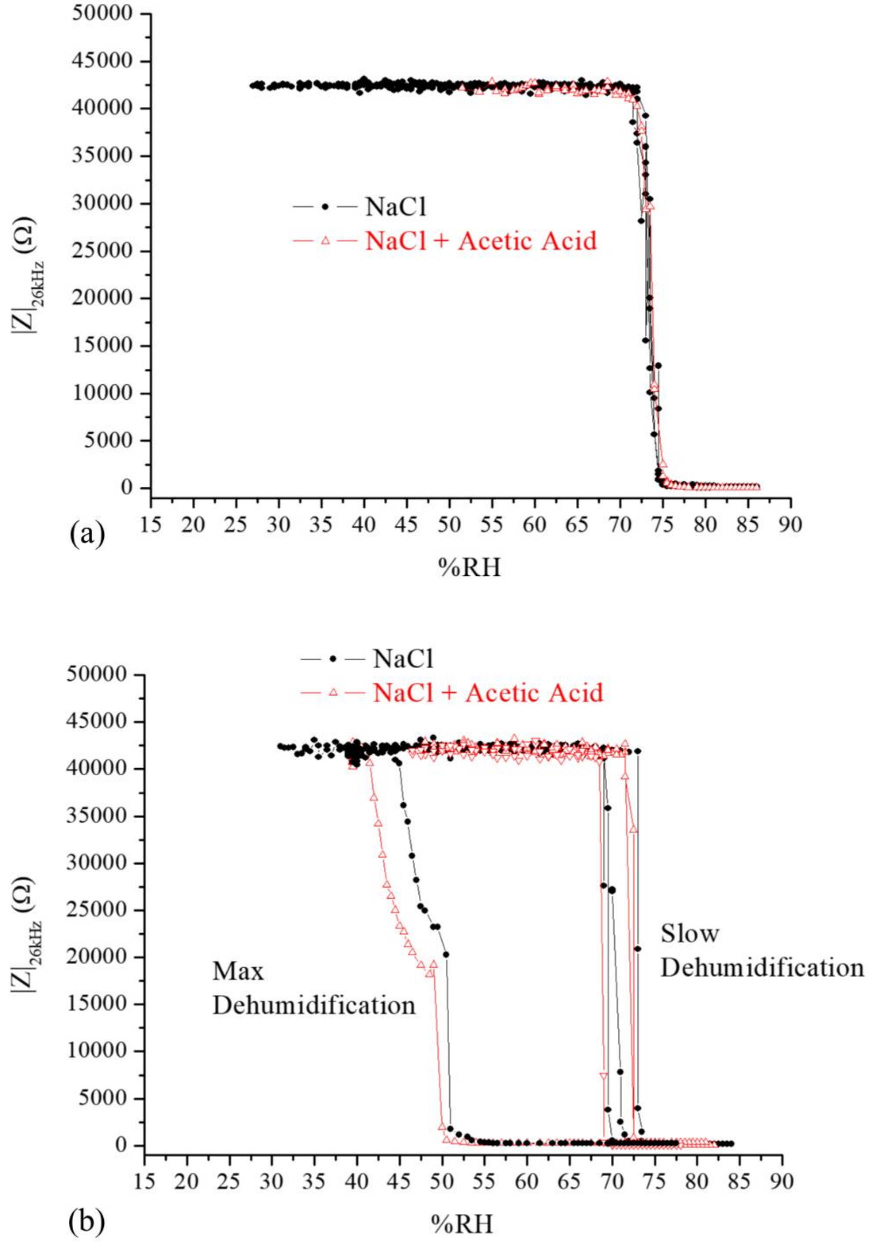

Figure 6.23: (a) Humidification and (b) dehumidification of a 9 drop array of 2 µl droplets deposited on a time of wetness sensor. Humidification was performed in increments of 1% RH every 30 minutes. Dehumidification was performed in two ways: slow dehumidification (steps of 1% RH every 30 minutes) and max dehumidification. In the second case, dry air into the chamber was set at a maximum to produce the fastest decrease in RH achievable in the chamber.

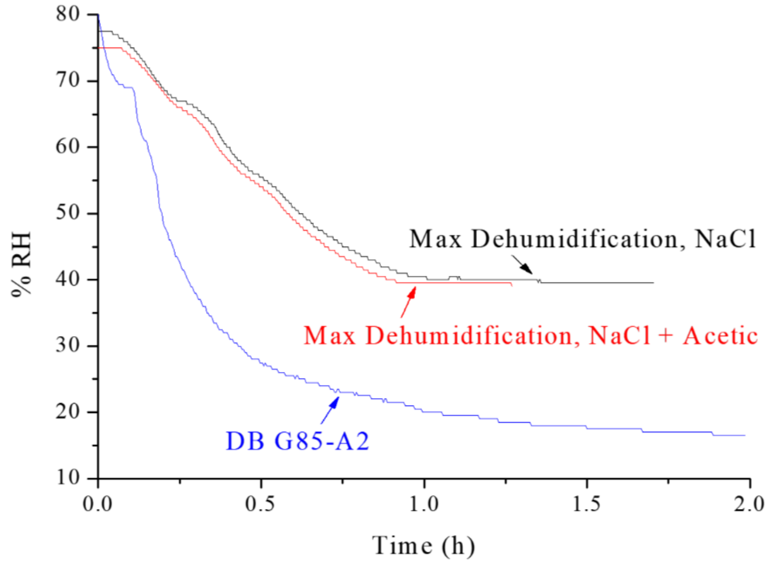

Figure 6.24: The “max dehumidification” profiles used when measuring time of wetness for NaCl droplets (black) and NaCl + acetic acid droplets (red). The drying profile in DB ASTM G85-A2 is shown in blue.

6.4.5 In-Situ Electrochemical Measurements

6.4.5.1 Potential Measurements

Figure 6.25 presents a comparison of potential measurements in DB and WB ASTM G85-A2 at short and long exposure times for AA2060-T3 and -T86. After a short exposure time, the potential was flat during the wet cycle, and no potential peak was observed upon drying (Figure 6.25[a] and [c]). The high level of noise in the measurements for AA2060-T86 in WB ASTM G85-A2 on day 1 was caused by a poor connection between the reference electrode and the thin electrolyte film on the working electrode. After a longer exposure time (8-9 days), a potential peak during the drying was measured. The maximum potential was measured 11 minutes after the dry air purge began in DB ASTM G85-A2 and 14 minutes after the dry air purge in WB ASTM G85-A2.

The presence of the external reference electrode used to make OCP measurements caused additional buildup of salt and corrosion product compared to a samples that was never in contact with the external reference electrode. Figure 6.26 shows images of AA2060-T3 samples that were both exposed to DB ASTM G85-A2 in chamber Brand 2 for 4 weeks. The sample that was used for OCP measurements could be easily identified by the accumulation of corrosion product in the area the reference electrode was placed. The reference electrode was only used on this sample 6 times for 1.5 - 2 h periods during the 4 week exposure.

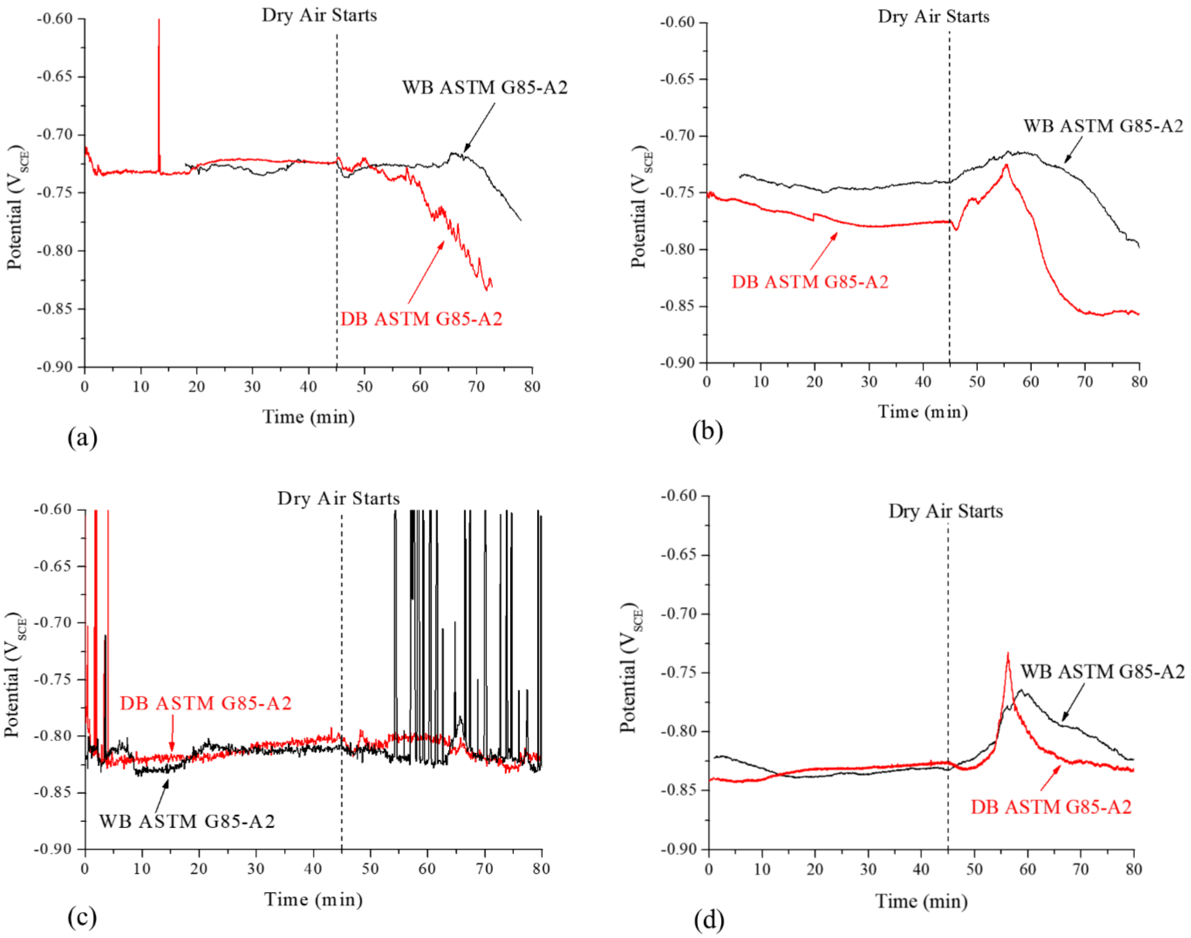

Figure 6.25: Potential measurements for AA2060-T3 in DB and WB ASTM G85-A2 (a) at a short exposure time (day 2 of exposure) and (b) at a long exposure time (day 8 of exposure). Potential measurements for AA2060-T86 in DB and WB ASTM G85-A2 (c) at a short exposure time (day 1 of exposure for WB, day 2 of exposure for DB) and (d) at a long exposure time (day 8 of exposure for WB, day 9 of exposure for DB). OCP measurements in DB ASTM G85-A2 were previously published in reference 41.


(a) AA2060-T3, No Rinse

(b) AA2060-T3, No Rinse, With Electrode

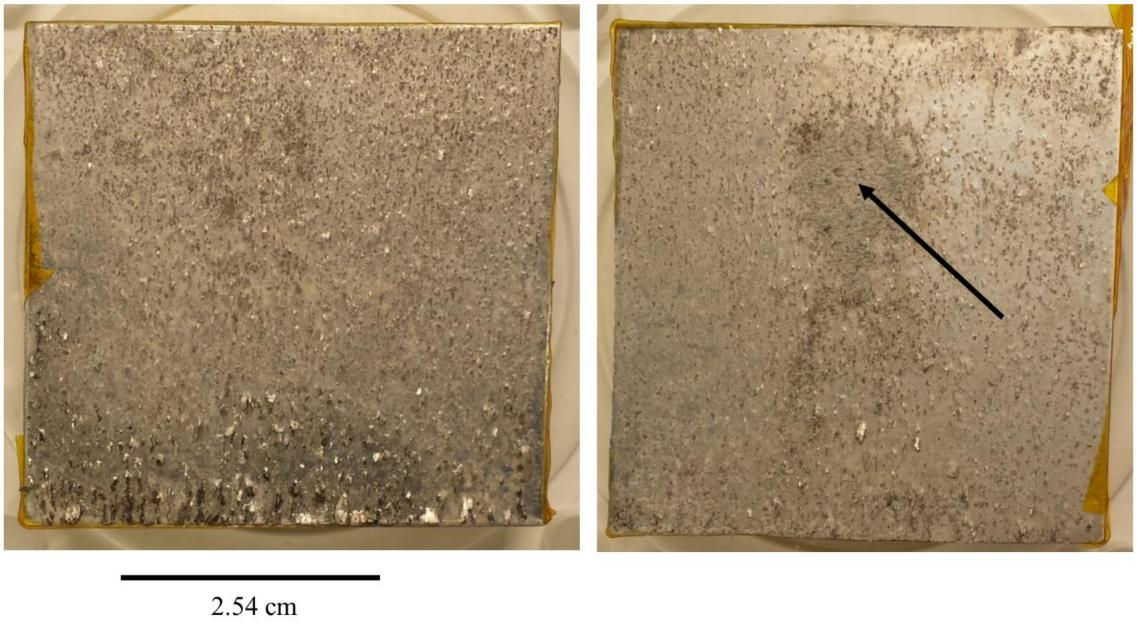
(c) AA2060-T3, With Rinse

(d) AA2060-T3, With Rinse, With Electrode

Figure 6.26: Comparison of an AA2060-T3 sample that did not ever have contact with an external reference electrode (a,c) to an AA2060-T3 sample that was used for several potential measurements (b,d) Arrows show the placement of the external reference electrode for cycles that OCP was measured. A buildup of corrosion products is visible around the area that the reference electrode was placed.

.

6.4.5.2 Polarization Resistance Measurements

Polarization resistance was estimated for AA2060 in DB ASTM G85-A2 using EIS measurements on a 5 mm working electrode embedded in the standard 5.08 cm x 5.08 cm exposure sample.

Figure 6.30(a) and (b) show results for AA2060-T3 and -T86 respectively. Time zero represented the start of the first salt spray cycle on each day. The dry air purge started at time 0.75 h. For both tempers, the $1/R_p$ (proportional to dissolution rate) peaked during the salt spray cycle and dropped low after the dry air purge started. The peak value of $1/R_p$ reached during the wet cycle also increased with increasing exposure time/cycles. There were fewer data points collected for day 2 because the sample dried more quickly, making R_p impossible to measure. For both tempers, the sample dried more slowly with increasing exposure time, allowing additional data points to be collected. Surprisingly, for day 5 and day 8 $1/R_p$ for the -T86 temper recovered after the initial fall at the start of the dry air purge, indicating a rise in corrosion rate at about 1.3 hours into the cycle.

Figure 6.28 shows the sample surface of AA2060-T86 before and after the $1/R_p$ measurement on day 2 of exposure in DB ASTM G85-A2. A dried salt film was visible around the electrode tip after the measurement.

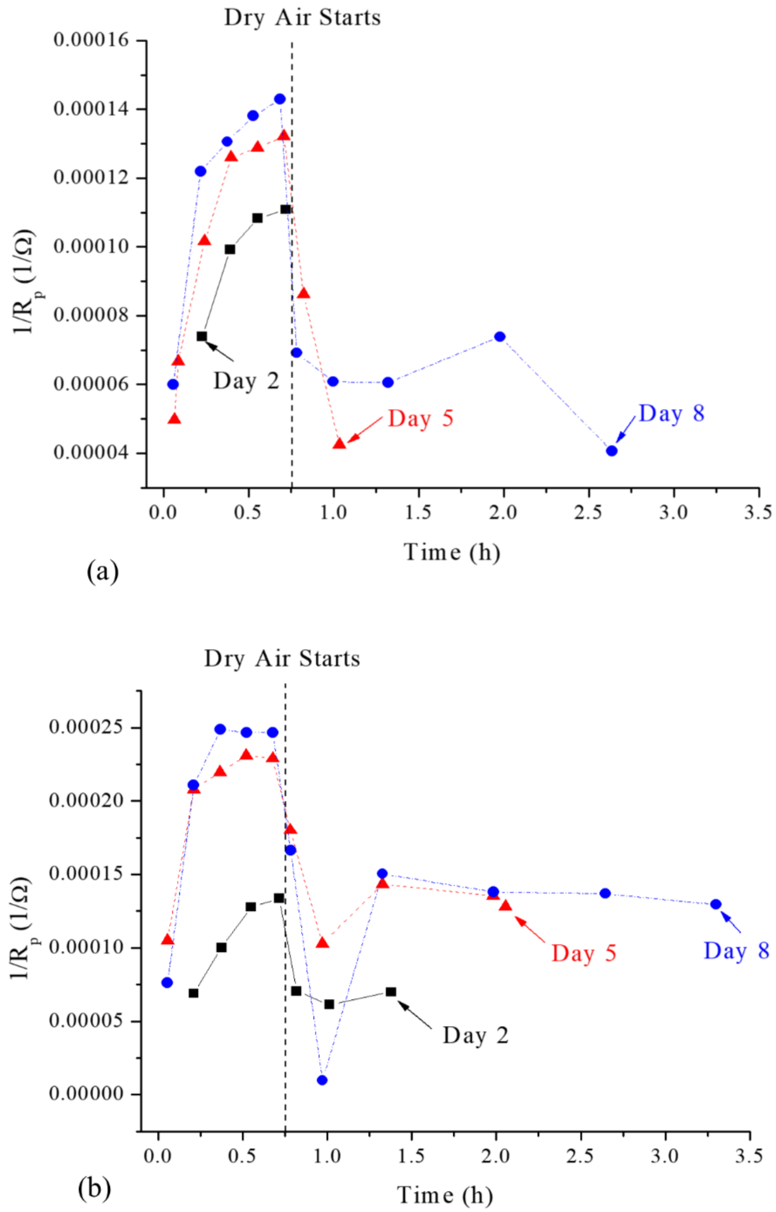

Figure 6.27: 1/R$_p$ (directly proportional to i$_{corr}$) measurements for (a) AA2060-T3 and (b) AA2060-T86 during DB ASTM G85-A2 after 2 days, 5 days, and 8 days of exposure.

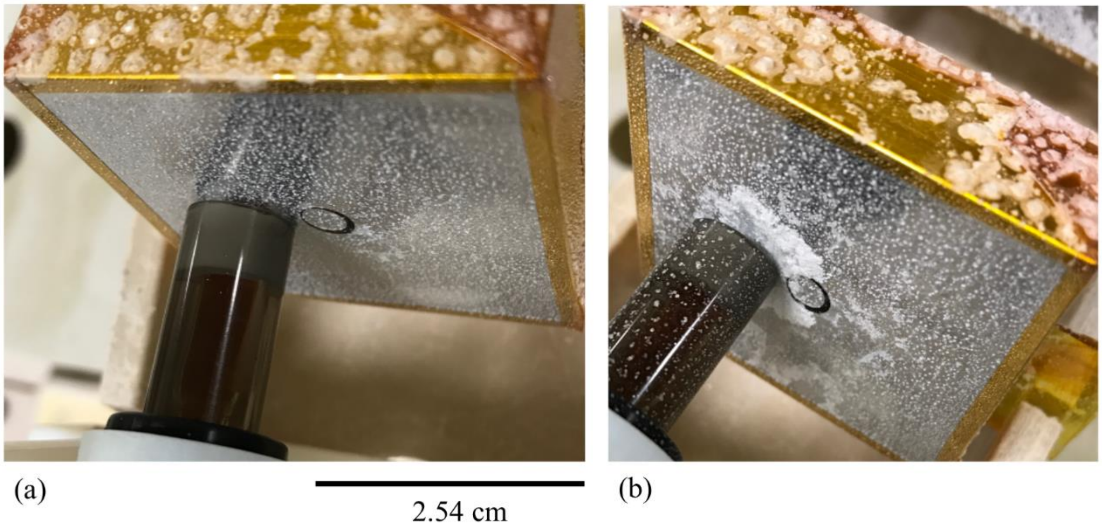

Figure 6.28: AA2060-T86 on day 2 of DB ASTM G85-A2 exposure (a) before 1/Rp measurements and (b) after $1/R_p$ measurements.

6.4.5.3 AA2024-T3 Interdigitated Sensor

An interdigitated sensor made with two AA2024-T3 electrodes was used to obtain an estimate of polarization without the influence of an external reference electrode. EIS measurements were performed using a two electrode system in which one of the AA2024-T3 electrodes was the working electrode and the other acted as both the counter and reference electrode. An image of this sensor on day 2 of exposure in DB ASTM G85-A2 can be seen in Figure 6.29. Figure 6.30 shows $1/R_p$ measurements on day 2 of exposure in DB ASTM G85-A2 and WB ASTM G85-A2. In both cases, $1/R_p$ (directly proportional to corrosion current) was high during the 45 minute salt spray period of each cycle and dropped low during the dry air purge and dwell periods.

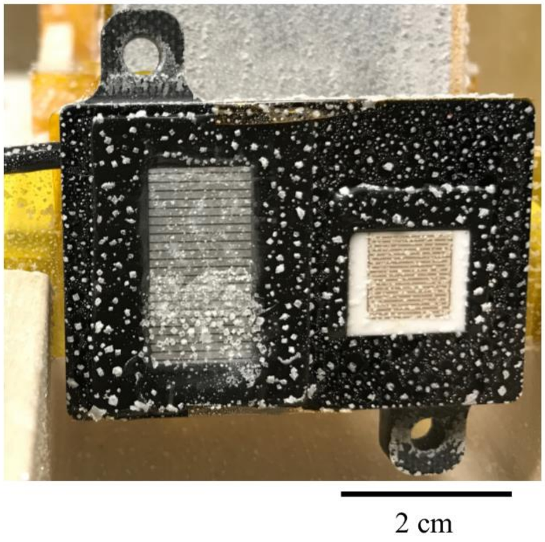

Figure 6.29: Luna interdigitated sensors constructed with AA2024-T3 electrodes (left) and gold electrodes (right).

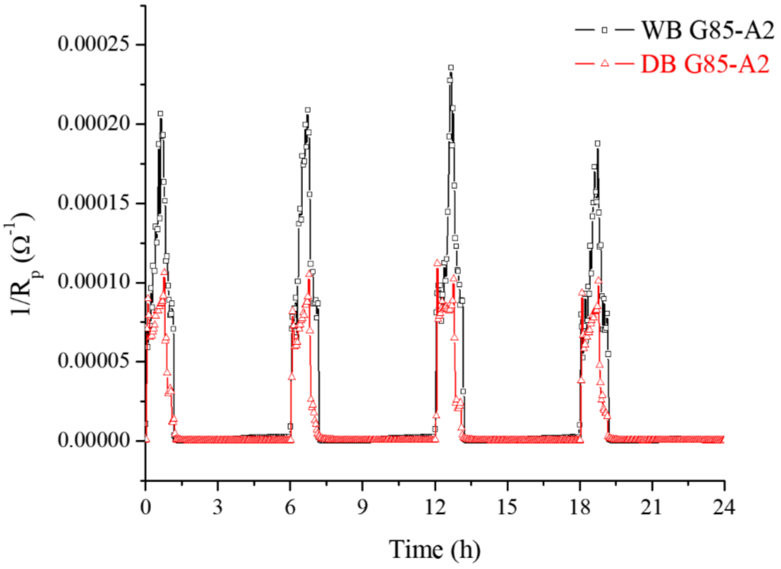

Figure 6.30: Estimate of $1/R_p$ (directly proportional to i_{corr}) for 4 cycles of WB ASTM G85-A2 (black squares) and DB ASTM G85-A2 (red triangles) on day 2 of exposure.

6.4.6 Modified Testing Protocol in Chamber Brand 2

Based on the TOW and $1/R_p$ measurements in DB and WB ASTM G85-A2 (chamber Brand 2), the 2 hour dry air purge and 3.25 hour dwell period are not an efficient use of testing time due to the very low corrosion rate at low relative humidity. Improved testing protocol should incorporate wet-dry cycling, but protocol should include a lower bound of RH that does not reduce corrosion rate to trivial levels.

6.4.6.1 Modified Relative Humidity Profiles and TOW

RH during the dwell period was adjusted by changing the dry air purge time. Figure 6.31 shows that when the dry air purge was reduced to 10 minutes, RH during the dwell period was significantly higher than when the dry air purge was the standard 2 hours. RH during the dwell period was even higher when a 1 minute dry air purge was used. These measurements were made under DB conditions, and a cycle length of 6 hours was maintained by extending the dwell time to compensate for the reduction of dry air purge time.

When the modified dry air purge was used under WB conditions, the RH during the dwell period was more stable, which allowed a more specific RH to be targeted. A modified sequence with 45 min salt spray, 1 min dry air purge, and 5.23 h dwell was tested in two different chambers that were both chamber Brand 2, and different RH profiles were obtained. Figure 6.32 compares the modified test sequence in the two different chambers under WB conditions (Mod WB 1 and Mod WB 2) with the RH in DB ASTM G85-A2.

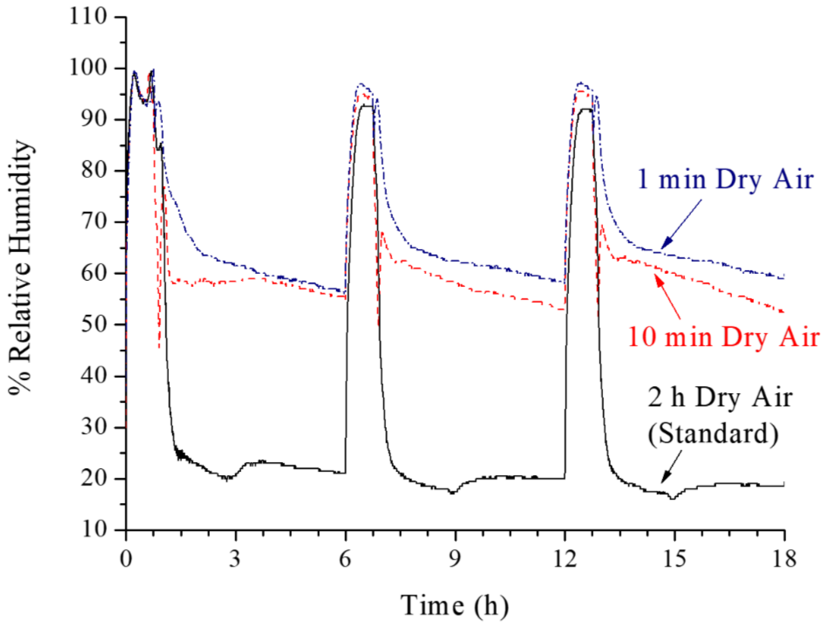

Figure 6.31: Impact of dry air purge time on RH during dwell period. For the tests with modified dry air time, the dwell period was extended to maintain cycle length of 6 hours.

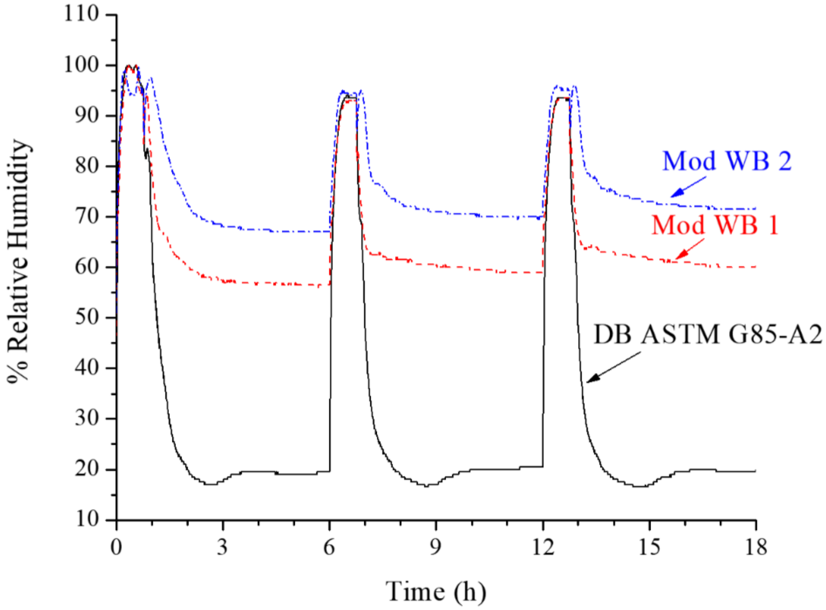

Figure 6.32: Two modified RH profiles were chosen for study. The first was achieved using 1 minute of dry air purge in Q-Fog Chamber 2 (blue) and the second was achieved by using 1 minute of dry air purge in Q-Fog Chamber 1 (red). These produce much higher RH during the dwell period compared to standard DB ASTM G85-A2 (black).

As expected, TOW was much longer in Mod WB 1 and Mod WB 2 than in ASTM G85-A2 due to the short dry air purge (1 minute). Figure 6.33 shows that TOW was initially longer for the sensor exposed to the modified WB 1 test, but TOW increased over time for both tests. Unfortunately, there was an accidental interruption in the measurement at hour 13.5, but the measurement resumed at hour 23. By cycle 5 (beginning at hour 24), the sensor remained wet during the full 6 hour cycle in both Mod WB 1 and 2.

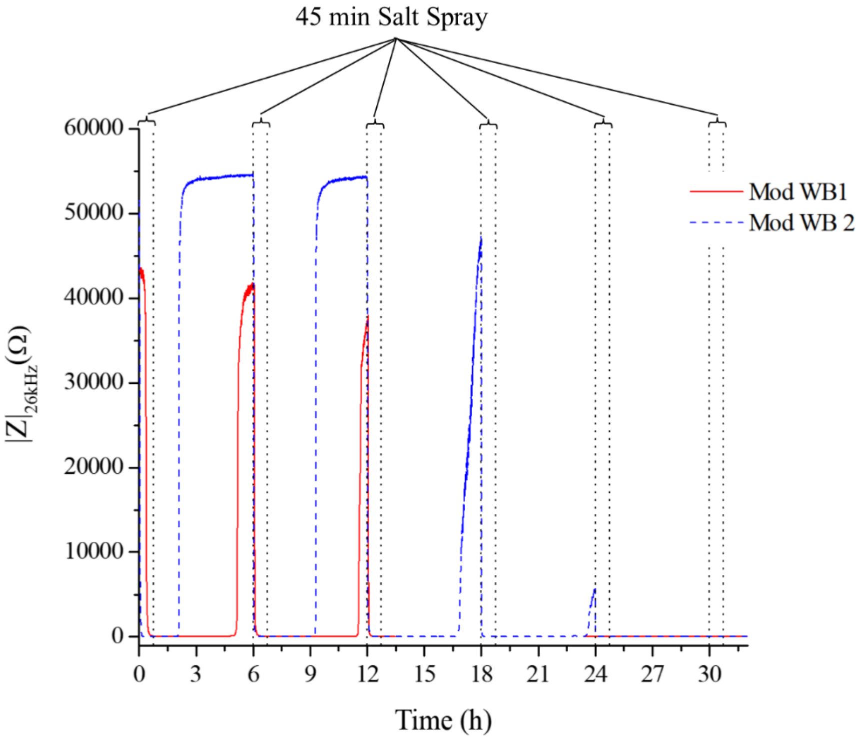

Figure 6.33: Impedance measured on interdigitated gold time of wetness sensor for modified WB 1 and modified WB 2. Time zero was the start of the first salt spray cycle that sensors were exposed to. There was an interruption in the measurement for Mod WB 1 from hour 13.5 to hour 23.

6.4.6.2 Exposure Results

AA2060-T3 and -T86 samples were exposed to modified WB 1 and 2. Testing only lasted for 12 days, because exfoliation in the susceptible -T3 temper reached an EB rating within this time. The results were similar for both tests, but attack seemed to be slightly more severe after exposure to Mod WB 1 (Figure 6.34) than to Mod WB 2 (Figure 6.36). However both of these modified tests were far more successful than either standard WB or DB ASTM G85-A2 (chamber Brand 2), because the exfoliation-resistant and susceptible tempers were clearly and quickly distinguishable. A comparison of cross-sections from modified WB 1, standard DB G85-A2, and seacoast exposures are shown in Figure 6.35.

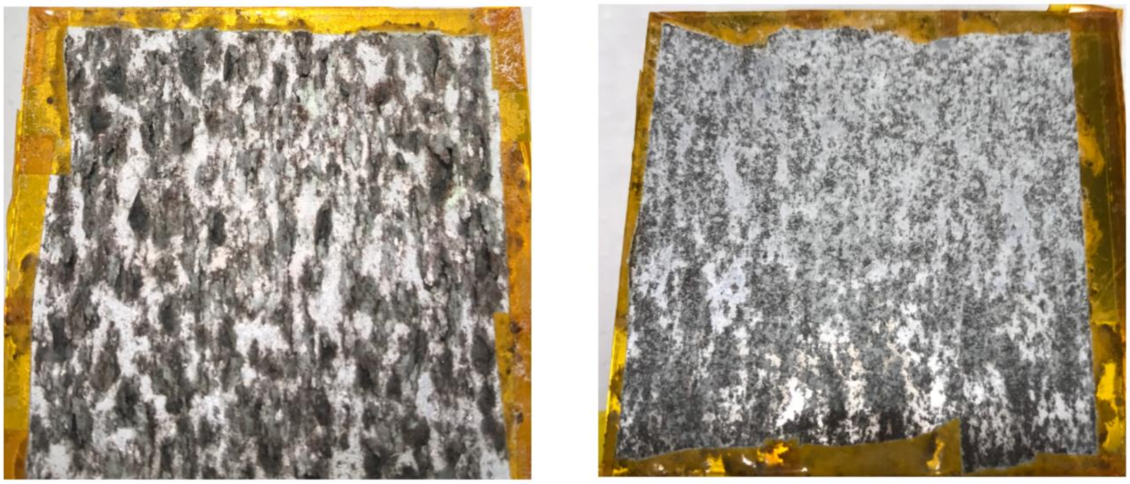
(a) AA2060-T3, No Rinse

(b) AA2060-T3-86, No Rinse


(c) AA2060-T3, With Rinse

(d) AA2060-T3-86, With Rinse

Figure 6.34: (a) AA2060-T3 and (b) AA2060-T86 after 12 days of Modified WB 1 exposure with no rinsing. (c) AA2060-T3 and (d) AA2060-T86 after 12 days of Modified WB 1 exposure with nitric acid rinse.

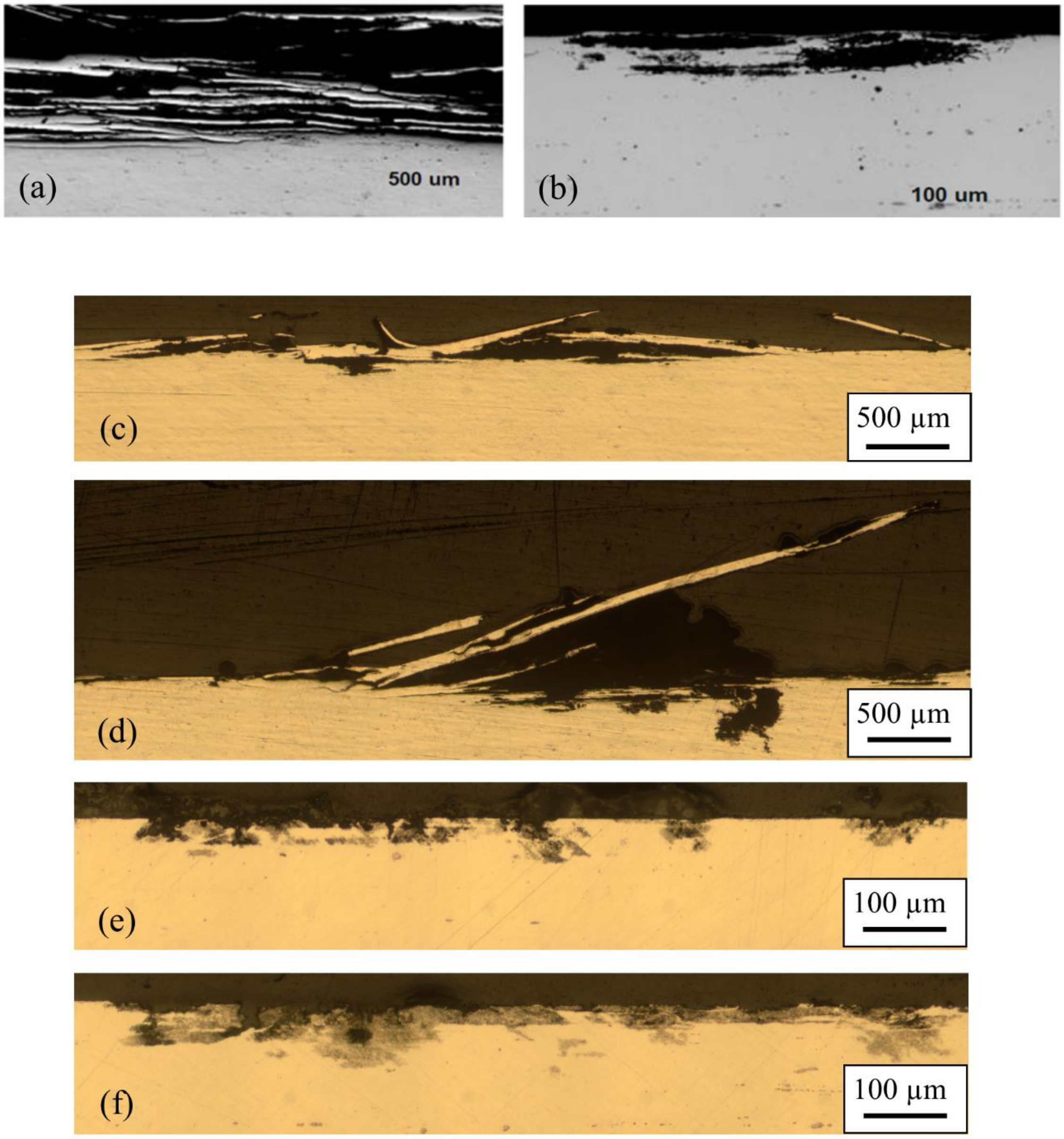

Figure 6.35: Comparison of AA2060-T3 after (a) 1.2 years of exposure at Point Judith RI (c) DB ASTM G85-A2 and (d) Modified WB 1. Comparison of AA2060-T86 after (b) 1.2 years of exposure at Point Judith RI (e) DB ASTM G85-A2 and (f) Modified WB 1.

(a) AA2060-T3, No Rinse (b) AA2060-86, No Rinse

(c) AA2060-T3, With Rinse (d) AA2060-86, With Rinse

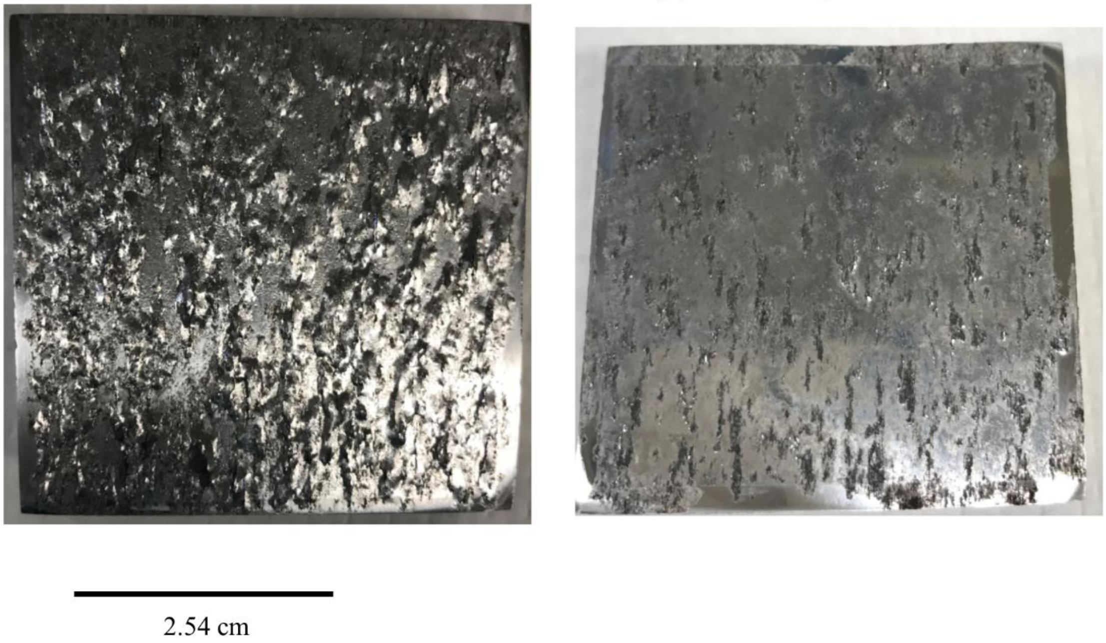

Figure 6.36: (a) AA2060-T3 and (b) AA2060-T86 after 12 days of Modified WB 2 exposure with no rinsing. (c) AA2060-T3 and (d) AA2060-T86 after 12 days of Modified WB 2 exposure with nitric acid rinse.

6.4.6.3 Polarization Resistance Measurements in Mod WB 1

Figure 6.37 compares $1/R_p$ for (a) AA2060-T3 and (b) AA2060-T86 in Mod WB 1 and DB ASTM G85-A2 on day 2 or 3 of exposure. Not only were the $1/R_p$ measurements higher in Mod WB 1 than DB ASTM G85-A2, data could be collected during the whole cycle because the sample did not dry in Mod WB 1. In Mod WB 1, $1/R_p$ increased during the salt spray period and decreased during the dwell period.

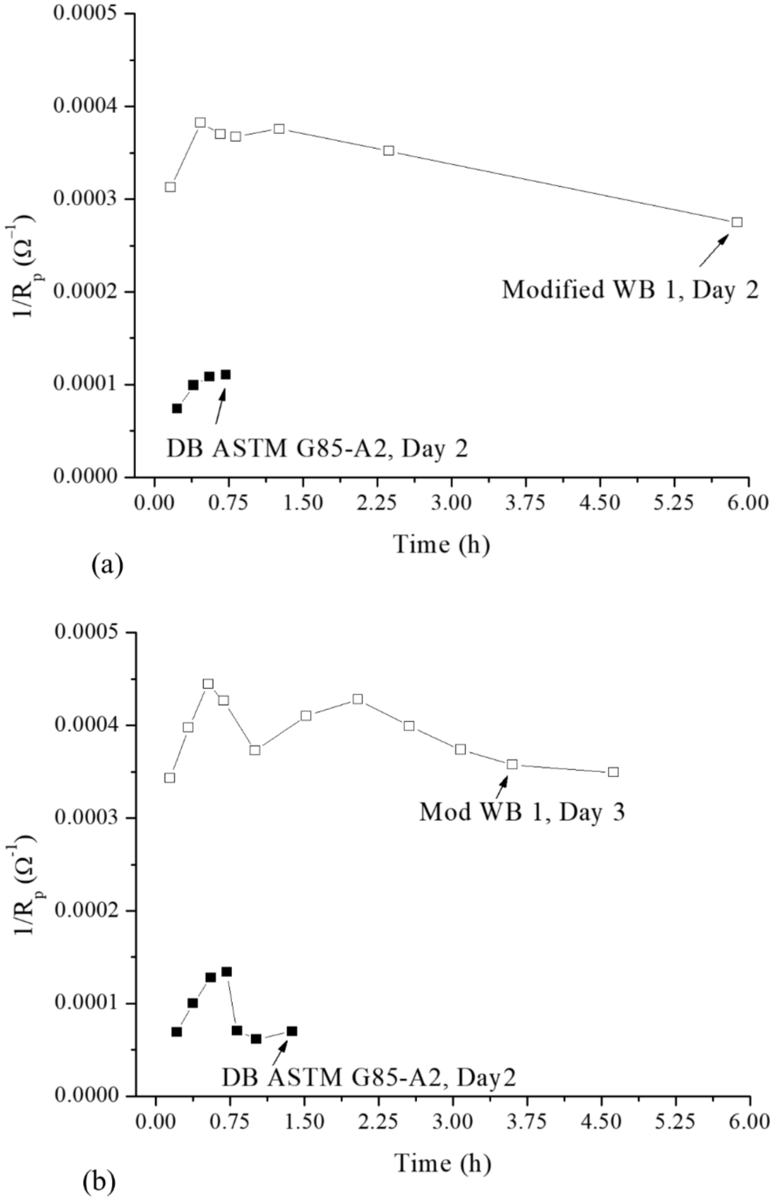

Figure 6.37: Estimates of $1/R_p$ for (a) AA2060-T3 and (b) AA2060-T86 on day 2 or 3 of exposure in DB ASTM G85-A2 (closed symbols) and modified WB 1 (open symbols).

6.4.6.4 Interdigitated AA2024 Sensor

Figure 6.38 presents a comparison of $1/R_p$ measured on an interdigitated AA2024-T3 sensor in DB G85, Mod WB 1, and Mod WB 2. The $1/R_p$ dropped to very low values during the dry air purge and dwell period in DB G85-A2, but $1/R_p$ remained high during the dwell period in modified WB 1. In modified WB 2, there was an initial drop in $1/R_p$ but then a peak later in the dwell period. This peak consistently occurred at an RH between 73 and 74%.

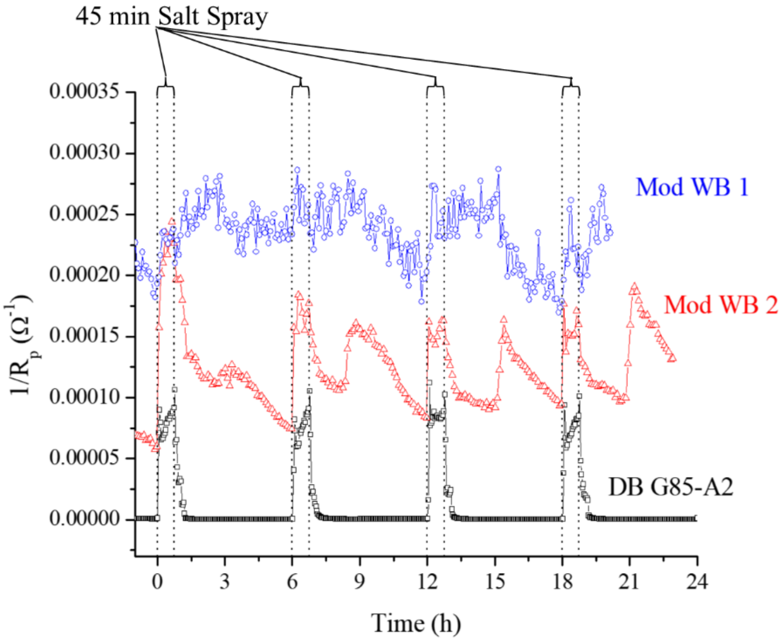

Figure 6.38: Estimate of $1/R_p$ of interdigitated AA2024 sensor during day 2 of exposure to DB G85-A2 (Black), modified WB 1 (Blue), and modified WB 2 (Red).

Figure 6.39 presents the 1/R$_p$ measurement for the AA2024-T3 interdigitated electrode in Mod WB 2 with potential measured on a AA2060-T3 plate in the same test. During the salt spray period, both OCP and 1/R$_p$ increased, suggesting an increase in cathodic kinetics. During the first hour and 15 minutes of the dwell OCP and 1/R$_p$ decreased, but then a peak in 1/R$_p$ occurred. This peak was most likely due to increasing anodic kinetics because potential decreased slightly during this period. When 1/R$_p$ began to decrease towards the end of the cycle, potential increased, indicating that anodic kinetics were slowing down at this point.

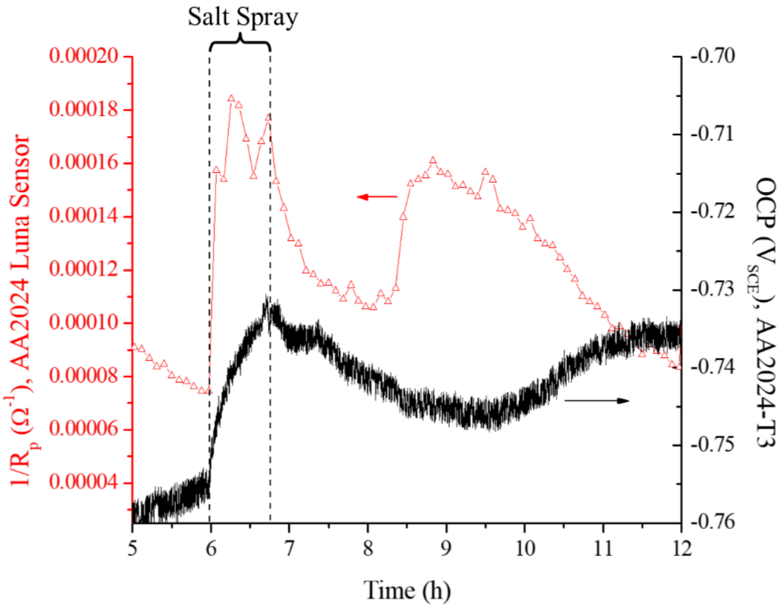

Figure 6.39: 1/R$_p$ of AA2024-T3 Luna sensor and open circuit potential of AA2024-T3 on day 2 of Mod WB 2 exposure.

6.4.7 Exposure of AA7075 and AA2024 to Mod WB 1 and 2

Exfoliation-susceptible (-T651) and exfoliation-resistant (-T7351 and -T7651) AA7075 tempers were exposed to Mod WB 1 and Mod WB 2. Exfoliation-susceptible AA2024-T3 was also exposed to both tests. Figure 6.40 shows samples directly after being removed from the Mod WB 1. Even before rinsing, the exfoliation-susceptible tempers (Figure 6.40[a] and [d]) could be distinguished from the exfoliation-resistant tempers (Figure 6.40[b] and [c]). After rinsing samples in concentration nitric acid, tempers were even easier to distinguish because the corrosion products and salt deposits had been removed (Figure 6.41). Exfoliation-susceptible and resistant tempers could also be distinguished after exposure to Mod WB 2 before and after cleaning (Figure 6.42 and Figure 6.43). Exfoliation blisters are more easily viewed from an angle, so a side view of each susceptible sample (AA7075-T651, AA2024-T3) is provided in Figure 6.44.

(a) AA7075-T651, No Rinse

(b) AA7075-T7351, No Rinse

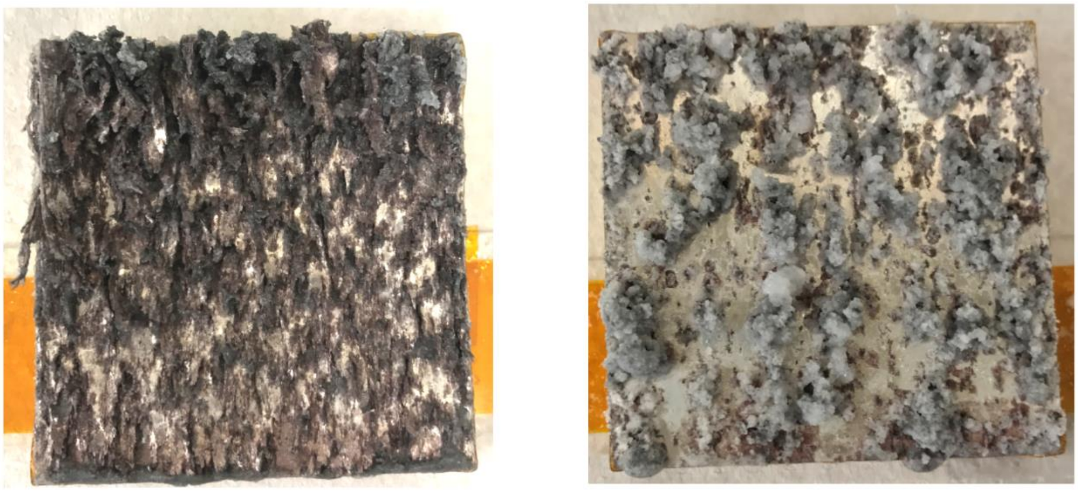

(c) AA7075-T7651, No Rinse

(d) AA2024-T3, No Rinse

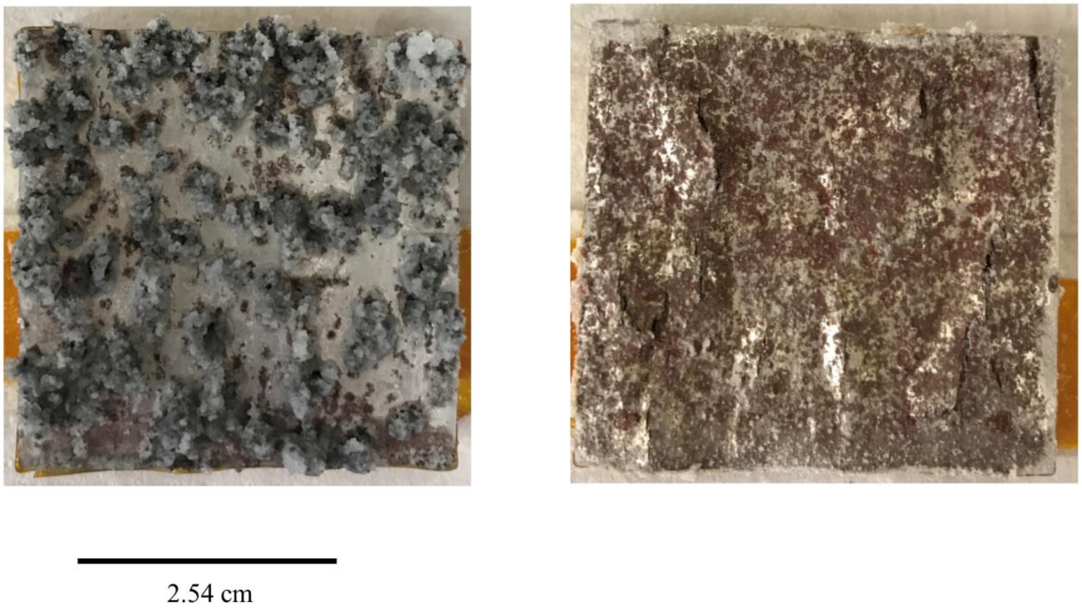

Figure 6.40: (a) AA7075-T651, (b) AA7075-T7351, (c) AA7075-T7651, and (d) AA2024-T3 directly after being removed from Mod WB 1 with no rinsing.

(a) AA7075-T651, With Rinse

(b) AA7075-T7351, With Rinse

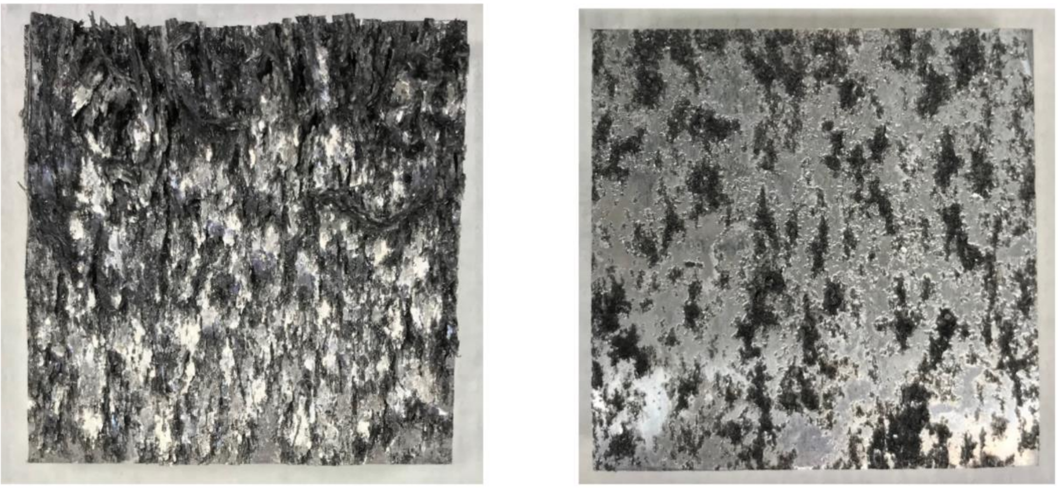

(c) AA7075-T7651, With Rinse

(d) AA2024-T3, With Rinse

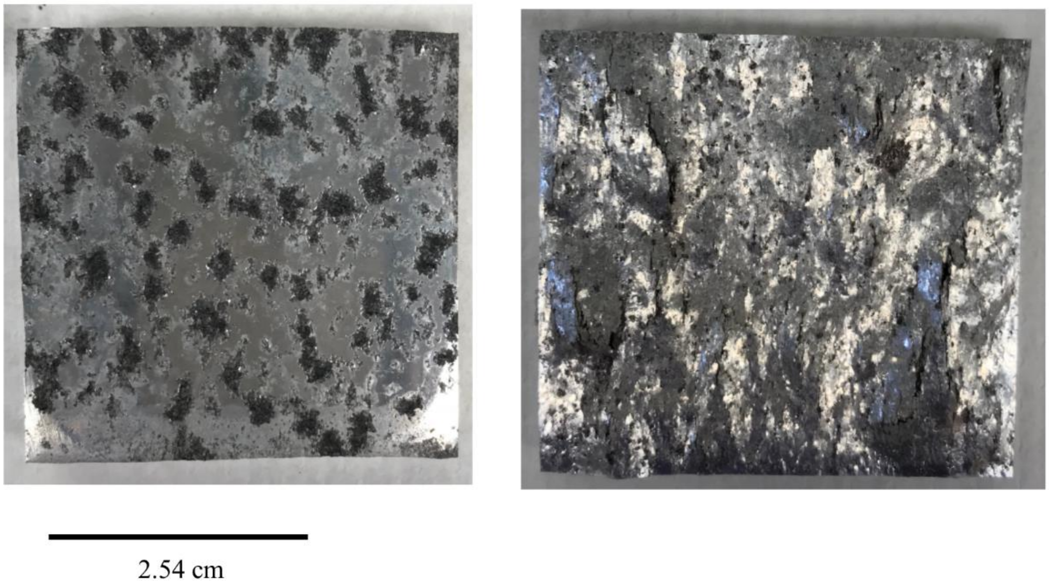

Figure 6.41: (a) AA7075-T651, (b) AA7075-T7351, (c) AA7075-T7651, and (d) AA2024-T3 after exposure to Mod WB 1 and nitric acid rinse.

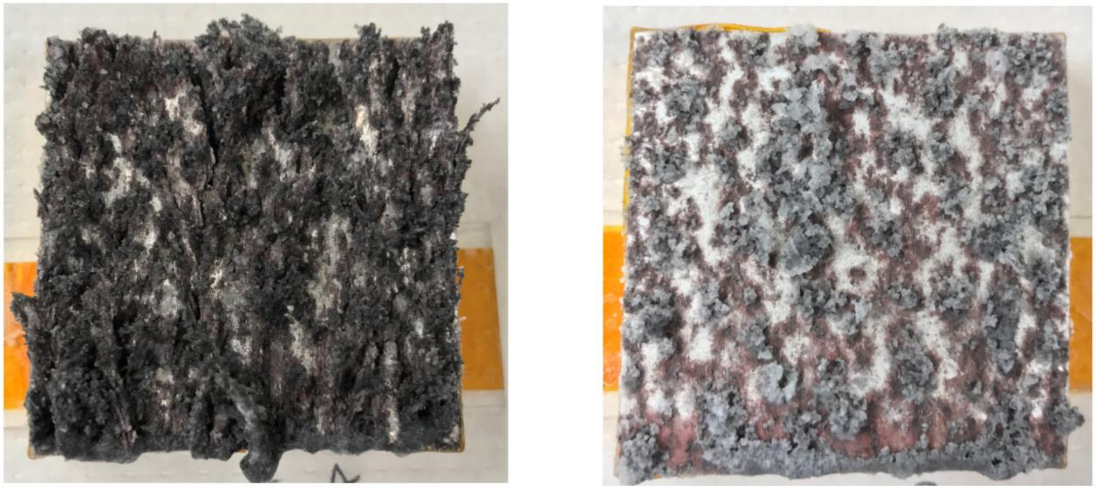

(a) AA7075-T651, No Rinse

(b) AA7075-T7351, No Rinse

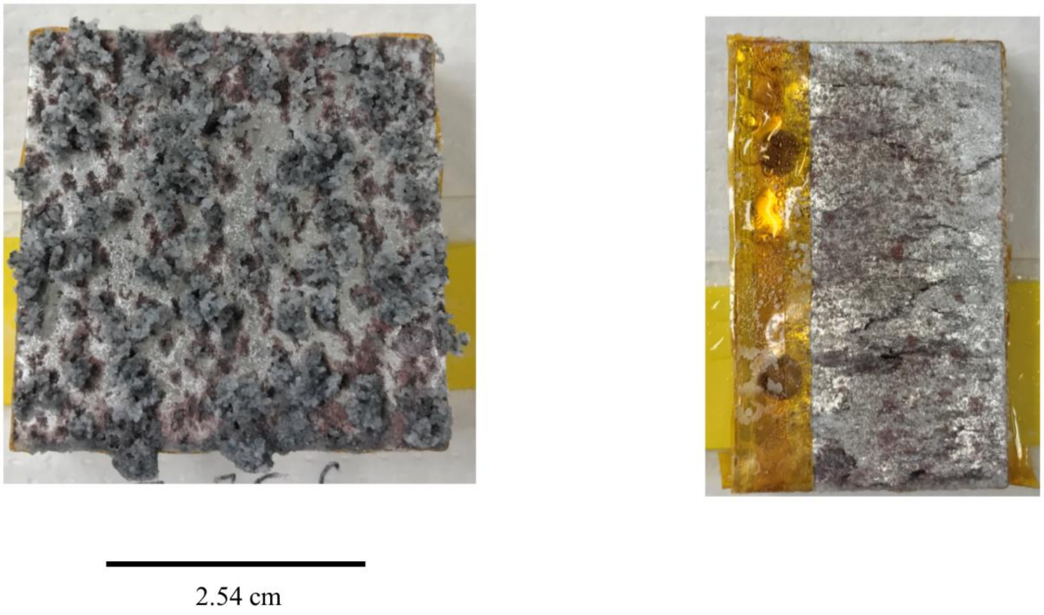

(c) AA7075-T7651, No Rinse

(d) AA2024-T3, No Rinse

Figure 6.42: (a) AA7075-T651, (b) AA7075-T7351, (c) AA7075-T7651, and (d) AA2024-T3 directly after being removed from Mod WB 2 with no rinsing.

(a) AA7075-T651, With Rinse

(b) AA7075-T7351, With Rinse

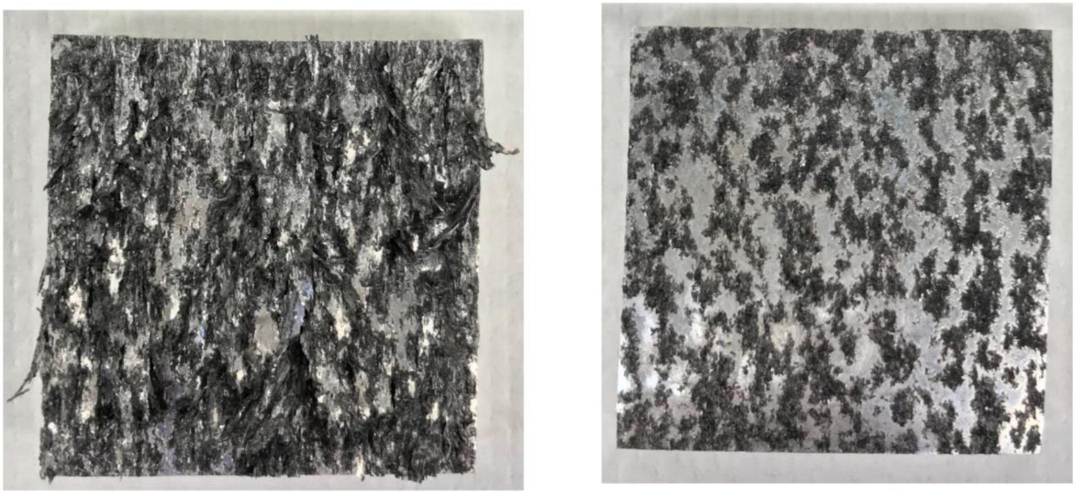

(c) AA7075-T7651, With Rinse

(d) AA2024-T3, With Rinse

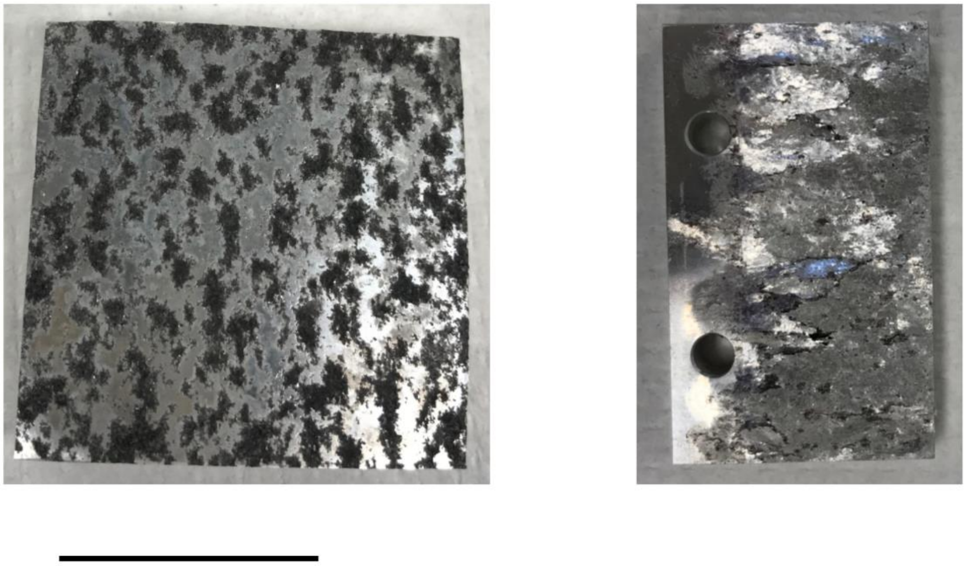

Figure 6.43: (a) AA7075-T651, (b) AA7075-T7351, (c) AA7075-T7651, and (d) AA2024-T3 directly after exposure to Mod WB 2 and DI water rinse.

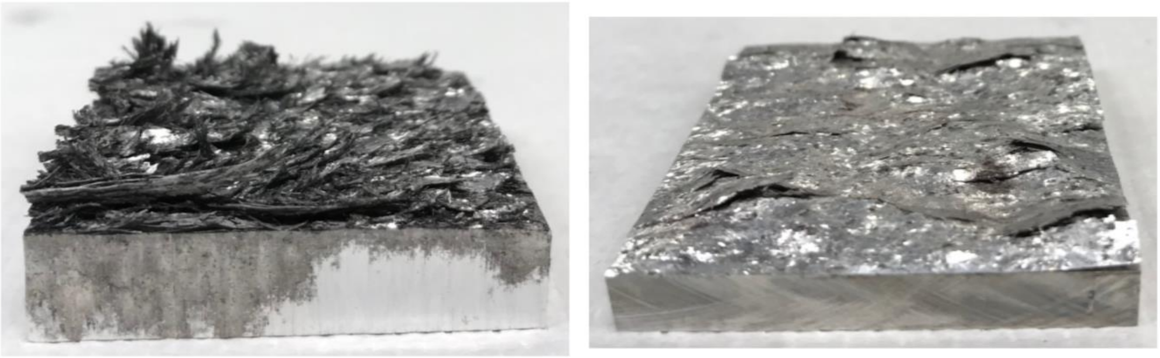

(a) AA7075-T651, Mod WB 1

(b) AA2024-T3, Mod WB 1

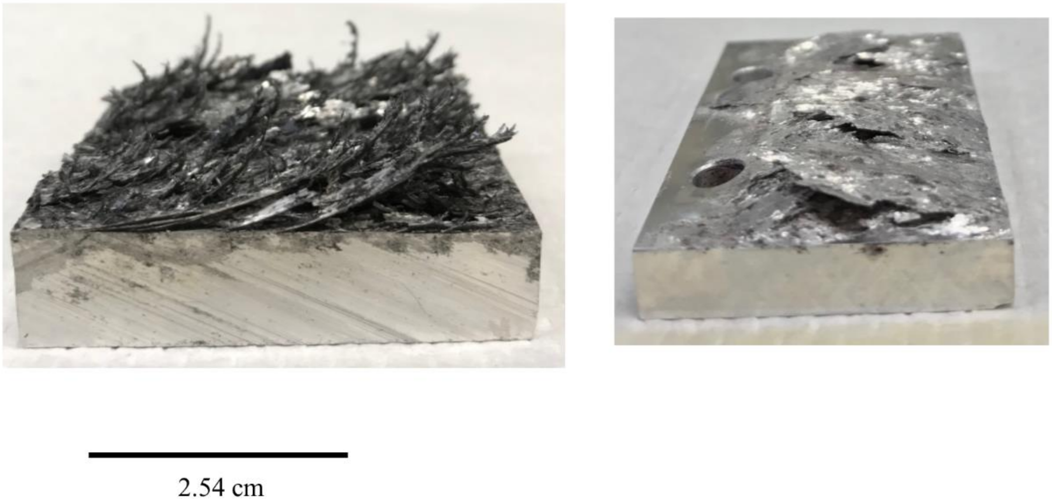

(c) AA7075-T651, Mod WB 2

(d) AA2024-T3, Mod WB 2

Figure 6.44: Another view of exfoliation-susceptible tempers (AA7075-T651 and AA2024-T3) after exposure to (a-b) Mod WB 1 and (c-d) Mod WB 2.

6.5 Discussion

In this work, the testing environment of generated during ASTM G85-A2 exposure was deconstructed for two different salt spray chamber brands. It was found that small differences in chamber operation could have a significant impact on RH profile and exposure results. These results suggested that better RH control during ASTM G85-A2 was necessary to improve consistency in exposure results among different equipment brands.

6.5.1 Importance of RH control during atmospheric corrosion testing

Extent of attack was different for AA2060-T3 and -T8 exposed to ASTM G85-A2 in chamber Brand 1 and chamber Brand 2. Under DB conditions, chamber Brand 1 seemed to be more aggressive as extent of attack was greater for both tempers in this chamber (Figure 6.10 and Figure 6.12). Cross-sections revealed greater grain lifting in the exfoliation-susceptible -T3 temper and deeper pitting in the exfoliation-resistant -T86 temper (Figure 6.13) in chamber Brand 1 under DB conditions. AA2060-T8 underwent deep pitting during exposure to WB conditions in chamber Brand 1, but no exfoliation was observed in the susceptible -T3 temper in this test (Figure 6.15). In contrast, exfoliation was observed in the susceptible temper during exposure to WB conditions in chamber Brand 2 (Figure 6.16).

The inconsistencies in exposure results for the two chamber brands may have been partially due to the difference in support angle of samples. In chamber Brand 1, samples were supported at 45° from vertical, but the sample angle in chamber Brand 2 was 15° from vertical. It was thought that the less steep angle in chamber Brand 1 would cause a greater accumulation of salt and corrosion products. However, visual examinations of the sample surface directly after being removed from testing did not reveal a consistent trend for salt/corrosion product film accumulation in the two chambers (Figure 6.10, Figure 6.12, Figure 6.14, and Figure 6.16).

RH was significantly different during the dry air purge and dwell periods of the G85-A2 cycle in the two chamber brands (Figure 6.17). Chamber Brand 1 operating under DB conditions, which generated more exfoliation in the susceptible -T3 temper than chamber Brand 2, had higher RH during the dry air and dwell periods than chamber Brand 2. In chamber Brand 1, RH ranged from 72.9% to 79.9% during the dry air purge and dwell period, while RH was significantly lower (17% to 20.5%) during the same period in chamber Brand 2.

RH was also higher for chamber Brand 1 than chamber Brand 2 during the dry air purge and dwell periods under WB conditions. For chamber Brand 2, RH ranged between 23% and 53% during this period, but RH was much higher (86.5% to 87.8%) in chamber Brand 1. Instead of accelerating the exfoliation process, the very high RH during WB ASTM G85-A2 in chamber

Brand 1 did not generate any exfoliation blisters in the susceptible -T3 temper (Figure 6.14). Exfoliation did form in the susceptible -T3 temper in WB ASTM G85-A2 in chamber Brand 2, which had a more moderate RH during the dry air purge and dwell.

The drastic differences in RH between the two chamber brands that were running the same ASTM G85-A2 cycle indicated that differences in chamber operation that may have seemed unimportant in the past could cause significant variation in test results. Bovard et al. also reported variation in ASTM G85-A2 exposure results for different laboratories using different types of salt spray chambers. The inconsistencies in exposure results were attributed to a combination of misinterpretation of the standard and differences in testing equipment.[18] For example, two different methods of temperature control are utilized in different types of salt spray chambers. Some chambers use water jackets while others include heating plates below the exposure zone. Another difference is the dry air purge methods. Older chambers that were adapted for wet-dry cycling may use compressed air to purge the chamber. Many new chambers which were specifically designed for humidity cycling use a fan to draw ambient or heated air into the chamber.

In the current study, chamber Brand 1 used a water jacket for heating and compressed air to purge the chamber. In contrast, chamber Brand 2 contained heating plates below the exposure zone and used a fan to blow heated air into the chamber during the dry air purge. The higher RH during the dry air purge in chamber Brand 1 (Figure 6.17) indicated that compressed air generated a less effective dry air purge than the heated air blower used in chamber Brand 2.

The difference in dry air purge method did not explain why under WB conditions, the RH did not approach 100% during the 3.25 hour dwell period in chamber Brand 2. Given enough time, the RH in a confined space such as a salt spray chamber should reach saturation if a large water supply is available. The maximum RH reached during the 3.25 hour dwell under WB conditions in chamber Brand 2 was only 53%. Temperature and RH measurements performed above, within, and below the exposure zone over a 30 hour period showed that the heating plates below the exposure zone in chamber Brand 2 created a temperature gradient (Figure 6.19[a]). The chamber was programed to maintain a temperature of 49°C, but near the heating plates (17 cm below exposure zone) the temperature was 61°C. Within the exposure zone temperature was 51°C, and temperature was 47.5°C at a location 25 cm above the exposure zone. The internal chamber temperature sensor was located about 15 cm above the exposure zone, so when the chamber was set to run at 49°C, the exposure zone was actually at a higher temperature as it was closer to the heating plates than the internal temperature sensor.

The temperature gradient created by the location of the heating plates in chamber Brand 2 also generated an RH gradient (Figure 6.19[b]). RH was low (35%) near the heating plates and increased with increasing distance from the heating plates. Within the exposure zone, the RH was 54%, which was just slightly higher than the maximum RH (53%) reached during the 3.25 hour dwell period in chamber Brand 2 under WB conditions.

The relationship between RH and temperature is based on the amount of water vapor needed to reach the saturation point at a given temperature. Relative humidity represents the amount of water vapor in air relative to the amount of water vapor required for saturation at a given temperature. This relationship is shown in Equation 6.3 where p_{H2O} is the vapor pressure of water and p^*_{H2O} is the saturation vapor pressure of water.

The value for p^*_{H2O} increases with increasing temperature, indicating that more water vapor is needed to reach saturation at high temperatures. The temperature gradient in chamber Brand 2 meant that the saturation point for water vapor in air (p^*_{H2O}) also varied throughout the chamber, where the highest values would be at the bottom of the chamber where temperature was high and the lowest values would be at the top of the chamber where temperature was low. If p_{H2O} is assumed to be approximately constant throughout the chamber, the variation in p^*_{H2O} due to the temperature gradient would explain why areas of high temperature corresponded to low RH and vice versa.

Standardization of laboratory tests is needed to ensure that data collected with different equipment brands and at different laboratories can be reasonably compared. However, following the standard protocol for ASTM G85-A2 was not sufficient to generate consistent results across different brands of equipment. The standard cycle was defined by the time spent in salt spray, dry air purge, and dwell, but it is really the relative humidity during each part of the cycle that matters. Due to seemingly small differences in chamber operation, the RH during the dry air purge and dwell period was significantly different for the two chamber brands. Many modern salt spray chambers have direct control over RH, which would allow the same RH to be used during each part of the cycle regardless of chamber brand or laboratory. However chambers with direct RH control are not yet widespread throughout laboratories, and other approaches to improving consistency in cyclic salt spray results are needed.

6.5.2 Ideal RH Range during Dry Cycle

After exposure to ASTM B117, AA2060-T3 and AA2060-T86 were indistinguishable (Figure 6.9). Exfoliation can only occur when corrosion products that form along grain boundaries can build up pressure and lift grains, but the constant rinsing during ASTM B117 prevented the buildup of salt and corrosion products on the sample. The inability of WB ASTM G85-A2 in chamber Brand 2, which ran at very high RH even during the dry air purge and dwell periods, to distinguish between AA2060 tempers (Figure 6.14) indicated that even in a wet-dry cyclic test, an upper limit of RH exists for the formation of exfoliation.

Figure 6.45 presents the correlation between exfoliation rating and average RH during the dwell period. As a continuous salt spray test, an RH value of 100% was assigned to ASTM B117 even though it technically does not have a dwell period. WB ASTM G85-A2 in chamber Brand 1 and ASTM B117 operated at the highest RH, and neither of these tests could distinguish exfoliation-susceptible and resistant AA2060 tempers. The highest degree of exfoliation occurred in DB ASTM G85-A2 in chamber Brand 1, which had an average RH during the dwell period just above the DRH of NaCl. DB and WB ASTM G85-A2 in chamber Brand 2 both had average RH during the dwell period significantly below the DRH of NaCl, and AA2060-T3 only developed mild exfoliation (EA) in these tests.

The impact of RH during the dwell period on exfoliation rating for the susceptible AA2060-T3 alloy indicated that there may be a range of optimum RH for exfoliation formation. At very low RH, corrosion rate may slow significantly. TOW measurements in DB and WB ASTM G85-A2 in chamber Brand 2 suggested that samples would be dry for most of the repeating 6 h cycle in these tests (Figure 6.18). At high RH, as in ASTM B117 and WB ASTM G85-A2 (chamber Brand 1), rinsing prevents the accumulation of corrosion products in IGC fissures. The ideal RH should be lower than 87% (average for WB G85 Brand 1), but higher than 46.7% (average for WB G85 Brand 2). This range is still quite large, a narrower range of RH could be determined with additional testing.

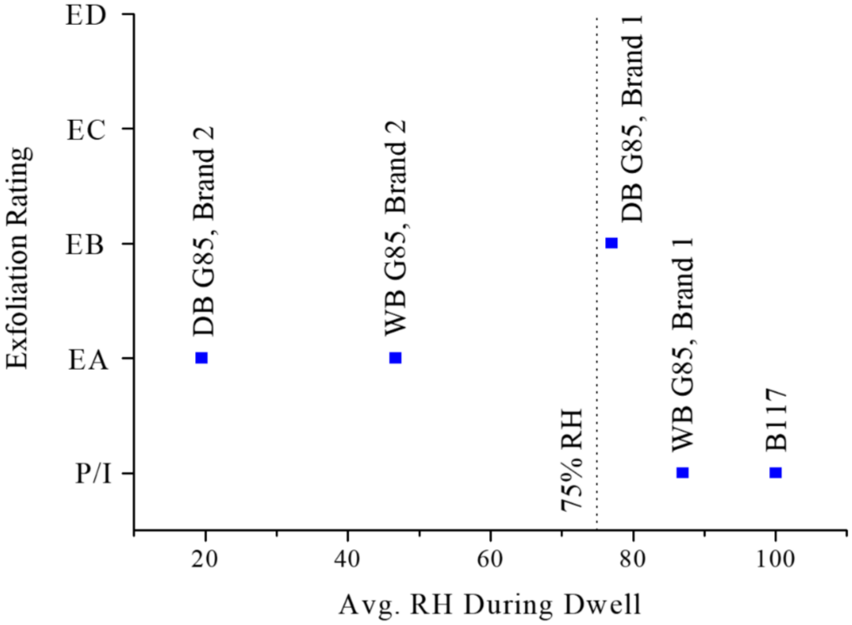

Figure 6.45: Impact of average RH during the dwell period on exfoliation ratings for AA2060-T3. Very high and very low RH both negatively impact exfoliation formation. P/I indicates either pitting or IGC was observed, but no exfoliation was visible. Exposure time was 4 weeks in each case.

6.5.3 Impact of Acetic Acid on DRH/ERH

RH measurements in chamber Brand 2 showed that RH dropped very low during the 2 h dry air purge portion of the repeating 6 h cycle in both WB and DB ASTM G85-A2 (Figure 6.18). TOW measurements suggested that samples would dry quickly once the dry air purge began, which may have caused the corrosion rate to slow significantly during the 3.25 h dwell period. Before an improved testing protocol could be designed, a better understanding of the impact of solution chemistry on drying kinetics was needed. The solution for ASTM G85-A2 was made up primarily of NaCl (0.9 M), but the pH was adjusted with acetic acid (CH_3COOH). Other work has shown that some organic species could impact the deliquescence behavior of NaCl,[35] but no data was available for the effect of adding acetic acid specifically.

6.5.3.1 OLI Solution Chemistry Modeling

OLI solution modeling was used to simulate the equilibrium drying behavior of neutral NaCl as well as NaCl with pH adjusted to 2.9 with acetic acid (0.06 M). The model predicted a deliquescence point of 74.9% for NaCl, which agreed with accepted literature values.[26-29] However, the addition of just 0.06 M acetic acid reduced the predicted deliquescence point to nearly zero. NaCl began to crystalize at 74.3% RH, but the acetic acid retained water until a much lower %RH. Acetic acid is a liquid in its pure form at room temperature, so it does not deliquesce/effloresce as a soluble salt would. The model predicted that acetic acid would evaporate slowly while RH was high, but evaporation rate would increase starting at 74.2% RH (Figure 6.21[b]). At 27.5% RH, nearly all the acetic acid was in the vapor phase, but a very small volume of liquid remained.

The total liquid volume (containing both acetic acid and water) during dehumidification is shown in Figure 6.21(a). For the solution containing only NaCl, the volume of liquid dropped abruptly to zero at RH lower than the DRH. This abrupt drop occurred because these calculations were made using thermodynamic data, and the model did not take into account the kinetics limitations of efflorescence. Liquid volume for the solution containing both NaCl and acetic acid was similar to the liquid volume of the NaCl solution until the DRH of NaCl was reached (74.9%). Rather than the abrupt drop of liquid volume to zero as was seen for the NaCl solution, liquid volume decreased more gradually. Although this model predicted the presence of some remaining liquid even at very low RH for solutions containing acetic acid, the amount of liquid present was trivial in some cases. Table 6.5 presents the calculated volume of liquid predicted to remain at various RH values when the starting point was a 2 μL electrolyte droplet. At 60% RH, only 7.4 nL of solution were predicted to remain. At 20% RH, which is close to the RH measured during the 3.25 h dwell period for DB ASTM G85-A2 (chamber Brand 2), only 3.36×10^{-5} nL were predicted to remain. Even though the OLI model suggested that TOW during drying would be extended greatly with the addition of acetic acid, the small liquid volumes calculated at low RH indicate that corrosion rate may drop low during periods of low RH even when acetic acid was present.

During the evaporation of an aqueous multi-salt solution, the concentration of the first salt to begin crystalizing would be expected to remain saturated for the remainder of the drying process. However, solution modelling predicted that NaCl concentration would reach saturation at 74.3%

RH, and then begin to decrease as RH continued to drop. This behavior was caused by the increasing ratio of acetic acid to water (mol/mol) in the liquid phase with decreasing RH (Figure 6.21[b]). NaCl solubility is lower in most organic solvents than in water, so the greater proportion of acetic acid in the electrolyte, the lower NaCl solubility would be. Data for the solubility limit of NaCl in acetic acid was not available in the literature, but the solubility limit calculated in OLI was 0.036 M, which was significantly lower than NaCl solubility in water (5.5 M).

6.5.3.2 Experimental Measurements of DRH/ERH

Although solution modelling predicted a severe decrease in mutual deliquescence point when acetic acid was added to NaCl, experimental measurements of DRH and ERH did not support this conclusion. DRH was consistently 74.5% and ERH ranged from 69% to 73.5% regardless of the presence of acetic acid (Figure 6.23[a] and [b]). It is difficult to know for certain why there was such a large disagreement between the experimental and simulated data, but it is possible that evaporation of the acetic acid occurred more quickly than predicted by OLI. When Peng et al. investigated the hygroscopic properties of several water-soluble organic compounds, acetic acid was said to be too volatile to be used in their measurements.[46] If the acetic acid evaporated at an RH above or at the ERH of NaCl, no impact on drying would be measured. Another possibility is that the spacing between the gold interdigitated electrodes (~300 μL) was too large to detect the very small volumes of electrolyte remaining below the ERH of NaCl. Droplets must touch at least two adjacent electrodes for impedance measurements to detect moisture. The predicted volume of liquid remaining at low RH was very small, and the moisture may not have been detected by this method.

Based on the modeled and experimental results discussed above, the role of acetic acid during RH cycling is still unclear. Solution modelling indicated that samples would be exposed to some moisture even at very low values of RH, but experimental results did not support this hypothesis as ERH and DRH were not impacted by the presence of acetic acid. However, the TOW sensor used in this work was not sensitive to very small liquid volumes due to the large spacing between the gold interdigitated electrodes. To provide a more complete picture of the impact of acetic acid, ERH and DRH should be measured using a sensor with much smaller spacing, or with equipment that does not rely on impedance measurements such as a tandem differential mobility analyzer (TDMA).[28]

The ERH points measured here for NaCl (69% - 73.5%) were higher than values found in literature. The lowest ERH values for NaCl in literature (43% - 45%)[27,28] were measured using electrolyte droplets flowing through clean air where opportunities for heterogeneous nucleation were rare. A higher ERH was measured for NaCl droplets deposited on a gold interdigitated time of wetness sensor (49 - 51%)[29] where the sensor surface could act as a site for heterogeneous nucleation. In this study, a gold interdigitated time of wetness sensor was used to monitor wetting and drying of electrolyte droplets, but the electrode spacing was larger (~300 μm) than for the sensor used in reference 22 (3 μm). A larger spacing makes the sensor less sensitive to droplets as they shrink because a droplet must overlap two adjacent electrodes for impedance measurements to sense moisture.

The crystallization process of NaCl could be monitored visually as well as using impedance in this study, and visually, NaCl crystallization was identified at RH as high as 74% (Figure 6.8[b]). The start of NaCl crystallization at an RH so near the DRH indicated that heterogeneous nucleation was very favorable. The surface roughness of the TOW sensor used in this study was not analyzed, but differences in surface condition between different brands of TOW sensors could be partially responsible for high value of ERH measured. On a corroding metal sample, there are many sites for heterogeneous nucleation. Even if samples are polished to a mirror surface before exposure, the precipitation of insoluble corrosion products will provide sites for NaCl nucleation. The ERH associated with the homogenous nucleation from a NaCl droplet is relevant when considering the behavior of salt aerosols, but once salt droplets have deposited on a metal surface, heterogeneous nucleation is a more likely scenario.

6.5.3.3 Impact of Drying Rate

During ASTM G85-A2, the decrease in RH is rapid. The impact of drying rate on ERH was investigated by setting the RH chamber to its maximum dehumidification setting. A comparison of the maximum dehumidification provided by the RH chamber to the RH profile in chamber Brand 2 during drying in DB ASTM G85-A2 is shown in Figure 6.24. ERH was greatly reduced compared to the equilibrium ERH measurement (Figure 6.23[b]). Nucleation is a kinetically limited process, and the rapid drop in RH did not allow enough time for salt crystals to nucleate at the equilibrium ERH even when it was thermodynamically possible.

Although the TOW sensor used in this work was not sensitive enough to fully explain the role of acetic acid during the drying of a NaCl droplet, the rate of drying clearly had an important impact. This result suggested that the rapid decrease in RH during the dry air purge in ASTM G85-A2 (chamber Brand 2) may have had a more significant role in the drying behavior of the electrolyte film on samples exposed to this test than did the presence of acetic acid in the test solution. Although the discussion above presented only a partial explanation for the drying behavior of electrolyte films containing NaCl and acetic acid, the modeling and experimental results can be used to aid in the interpretation of electrochemical mechanisms during wetting and drying.

6.5.4 Deconstructing Electrochemical Mechanisms

When studying electrochemical kinetics under full immersion conditions, many techniques are available. In a bulk electrolyte, dominant cathodic and anodic reactions can easily be measured using linear polarization. Under atmospheric conditions, however, electrochemical measurements can be challenging. Several techniques such as scanning kelvin probe (SKP) or other specialized set ups exist,[47] but these cannot be easily adapted for in-situ measurements during atmospheric corrosion testing due to spatial constraints as well as the harsh environment inside a salt spray chamber.

6.5.4.1 Mixed Potential Theory

In the current work, some in-situ electrochemical measurements were achieved in spite of the constraints posed by the challenges of making such measurements in a salt spray chamber. The internal reference electrode of a flat tip pH electrode was used to measure OCP, and EIS was used to monitor Rp on an embedded AA2060 sample as well as an interdigitated AA2024-T3 electrode. Although anodic and cathodic kinetics could not be measured directly using these tools, trends in corrosion kinetics could be proposed based on Mixed Potential Theory.[48] According to Mixed Potential Theory, changes in potential and corrosion current density (i_{corr}) can be correlated with increases or decreases in cathodic or anodic kinetics. R_p is inversely proportional to i_{corr},[42] so values of $1/R_p$ were used to infer qualitative trends in i_{corr} in this work. Figure 6.46 presents schematic representations of Mixed Potential Theory. When a simultaneous increase in potential and increase in $1/R_p$ is measured, this indicates that an increase in cathodic kinetics has occurred (Figure 6.46[a]). However, when an increase in $1/R_p$ is accompanied by a decrease in potential, anodic kinetics have increased (Figure 6.46[b]). If $1/R_p$ decreases while potential decreases, cathodic kinetics have decreased (Figure 6.46[c]), but a simultaneous decrease in $1/R_p$ and increase in potential indicates a decrease in anodic kinetics (Figure 6.46[d]). These rules are summarized in Table 6.6.

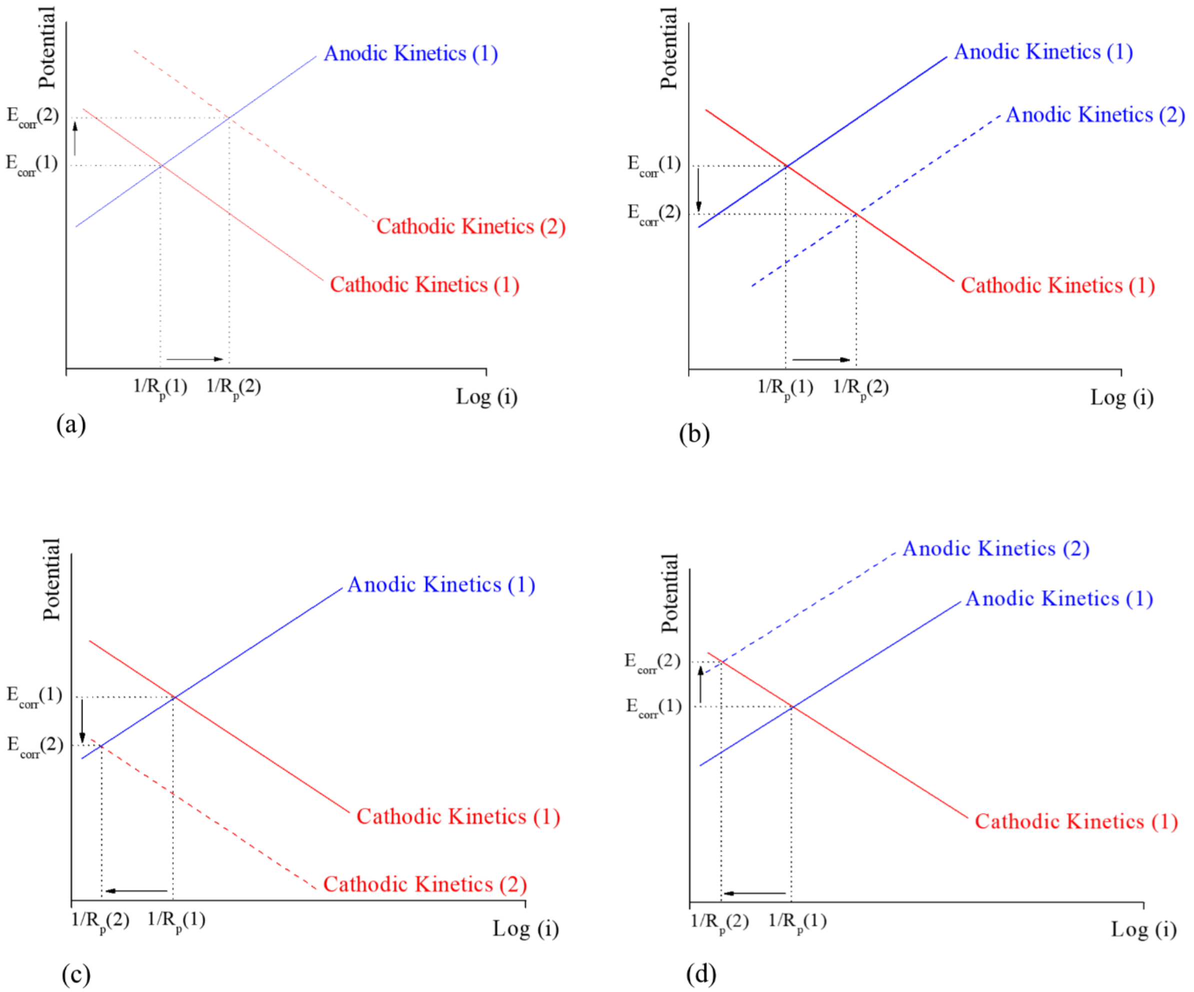

Figure 6.46: Schematic diagrams showing mixed potential theory for (a) increasing cathodic kinetics (b) increasing anodic kinetics (c) decreasing cathodic kinetics and (d) decreasing anodic kinetics.

Table 6.6: Summary of rules for Mixed Potential Theory

	OCP	**1/R_p**
Cathodic Kinetics Increase	↑	↑
Anodic Kinetics Increase	↓	↑
Cathodic Kinetics Decrease	↓	↓
Anodic Kinetics Decrease	↑	↓

6.5.4.2 Impact of Reference Electrode on Electrochemical Measurements

An external reference electrode was necessary for the in-situ potential and R_p measurements on AA2060. The internal reference of the Orion flat tip pH electrode was successful at maintaining ionic contact with the thin electrolyte film present on the metal samples, but some gradual leaking of the external electrode fill solution may have impacted measurements. During the discussion of OCP and R_p measurements, the possible impact of the reference electrode will be considered.

Potential measurements shown in Figure 6.25 started at the beginning of a new salt spray cycle and ended 35 min into the dry air purge. The ability to measure potential so far into the dry air purge was surprising, especially because the TOW sensor indicated that the average time to reach the baseline dry impedance was 13.5 minutes for DB G85-A2 and 20.3 minutes for WB G85-A2. The TOW measurements presented here only accounted for the first 24-h of exposure, and TOW would be expected to become longer with longer exposures as salt accumulated, but the ability to measure potential 35 minutes into the dry air purge even on day 2 of exposure was an indication that the reference electrode fill solution was influencing the measurement. The impact of the reference electrode on the sample condition can be seen in Figure 6.26. The sample shown in Figure 6.26(b) and (d) was exposed to DB ASTM G85-A2 (chamber Brand 2) for 4 weeks, and the external reference electrode was used on this sample 6 times for 1.5 – 2 h periods during the 4 week exposure. A significant build-up of corrosion product was visible in the area the reference electrode was place during OCP measurements.

Signs of electrode leakage were also observed in the R_p data. The number of data points that could be collected on day 2 was limited due to drying of the sample. However, with each additional day, more data points could be measured because the sample remained wet for longer (Figure 6.27). In addition, an unrealistic increase in $1/R_p$ late in the dry air purge was observed for AA2060-T86 on day 5 and day 8 (Figure 6.27[b]). R_p measurements performed using the interdigitated AA2024-T3 sensor, which did not require an external reference electrode, showed that $1/R_p$ decreased during the dry air purge and stayed low until the next salt spray cycle began (Figure 6.30). Physical signs of solution leakage were observed on AA2060-T86 after just one set of R_p measurements. Figure 6.28(a) and (b) show the sample surface of AA2060-T86 on day 2 of exposure before and after the R_p measurements for that day. Before the R_p measurement, a uniform layer of salt crystals was visible on the sample surface. After the R_p measurement, a thicker salt film was visible surrounding the tip of the reference electrode.

When the reference electrode was present on the sample, solution leaking from the electrode, particularly during periods of low humidity when dry salt around the electrode would provide a driving force for liquid to move out of the electrode, could artificially increase the TOW for the area just around the reference electrode. The solution being released from the electrode was KCl (the salt used for the fill solution of the reference electrode), and KCl most likely become incorporated into the salt film and remained there even when the reference electrode was not being used. The mutual DRH of the NaCl-KCl system has been reported to be 72.7%,[31] which is lower than the DRH of NaCl alone, so the TOW for the sample covered in a mixed NaCl-KCl salt film would be increased even when the reference electrode was not physically present on the sample.

6.5.4.3 Electrochemical Kinetics in DB and WB ASTM G85-A2

The impact of the leaking reference electrode must be taken into consideration when interpreting the OCP and R_p measurements. Potential measurements for AA2060-T3 and AA2060-T86 in DB and WB ASTM G85-A2 had already been reported in a previous publication.[41] These measurements showed that there was a transition between short exposure time (2 days) and long exposures time (8-9 days) where a potential peak during drying appeared only after long exposure time. The current work showed that potential measurements in WB ASTM G85-A2 were very similar to the previous measurements in DB G85 (Figure 6.25), and a potential peak was observed after 8-9 days of exposure time. For each testing condition, OCP was higher for the -T3 temper than for the -T86 temper. This observation was consistent with trends in E_{corr} for AA2060-T3 and

AA2060-T86 measured under full immersion conditions in a variety of solutions (NaCl, NaCl + KNO_3, NaCl + $K_2S_2O_8$, NaCl + H_2O_2).[49,50]

During the salt spray period in DB ASTM G85-A2 chamber Brand 2, dry salt particles deliquesced and grew in size as RH increased. The growth of the electrolyte volume would cause the NaCl concentration to decrease, but more cathode area would become available at the same time. Electrochemical measurements showed that OCP was stable during this time, and $1/R_p$ increased for both tempers on each measurement day (Figure 6.25, Figure 6.27). According to mixed potential theory, this behavior indicated a simultaneous and equivalent increase in anodic and cathodic kinetics. Although some leaking from the reference electrode may have occurred during the salt spray period, the ohmic drop through the electrolyte film would be lowest during this stage of the test when samples were wet. The low solution resistance of the electrolyte film during the salt spray period would allow the reference electrode to sense potential from a large sample area. Under these conditions, the impact of the leaking electrode on the potential measurement would be minimal.

During the dry air purge, the behavior at early exposure time and at later exposure time deviated. While $1/R_p$ always decreased during the first 10 to 15 minutes of the dry air purge regardless of temper or day, the measured OCP was different on day 2 and day 8/9. On day 2 of exposure, OCP continued to be stable for the first 15 minute of the dry air purge, but a potential peak was observed after longer exposure time (8 or 9 days). It was previously hypothesized that the peak in potential measured on day 8 and 9 was due to increasing cathodic kinetics as the diffusion distance for oxygen (O_2) from the atmosphere decreased.[41] A similar behavior was observed for ORR on a Pt electrode under an evaporating electrolyte film.[22] As film thickness decreased, an initial increase in current was measured due to the easy access to oxygen through the thin film. However, O_2 solubility was also decreasing during drying as the electrolyte became more concentration in Cl^-. At some point, the second mechanism overcame the first and measured current decreased.[22]

If a similar mechanism was responsible for the potential peak measured during drying on day 8 and 9 of exposure to DB and WB ASTM G85-A2, a peak in $1/R_p$ would be expected to occur alongside the peak in potential. This hypothesis was not supported by the data because no peak in $1/R_p$ was measured within the first 10 - 15 minutes of drying when the potential peak was measured. Even when R_p was measured on the interdigitated AA2024-T3 sensor where no external reference electrode was present to interfere with the measurement, no $1/R_p$ peak was observed 10 – 15 minutes into the dry air purge (Figure 6.30). Another problem with this hypothesis is the impact of aluminums protective oxide film on ORR. Measurements of the diffusion limiting current (i_{lim}) of O_2 on AA2060-T3 under controlled diffusion layers showed that current was independent of rotation rate (i.e. independent of the hydrodynamically controlled diffusion layer).[50] This independence was attributed to the additional barrier posed by the protective oxide film on Al. If the oxide film is the limiting factor for ORR on Al, the changes in electrolyte film thickness during drying would not significantly impact cathodic kinetics. As a Cu containing alloy, AA2060 can undergo Cu re-deposition in some environments. Cu is a better surface for ORR than aluminum, and Cu re-deposition on aluminum can significantly increase the rate of ORR.[51] If Cu deposited on the sample surface later in the exposure, the ORR rate would likely be impacted by changes electrolyte film thickness during wetting and drying. Cu re-deposition was not visible on AA2060 after short exposure times (e.g. 2 days), but it was observed after 4 weeks of exposure to ASTM B117 (Figure 6.9), and DB and WB ASTM G85 in chamber Brand 1 (Figure 6.10 and Figure 6.14). Cu re-deposition was not visible after a 4 week exposure to DB and WB ASTM G85 in chamber Brand 2 (Figure 6.12 and Figure 6.16). The reason for this difference was not determined in this study, but this result indicates that ORR kinetics may change over the course of a long test as Cu re-deposition may occur part of the way through.

If increasing cathodic kinetics were not responsible for the potential peak during drying in DB and WB ASTM G85-A2 (chamber Brand 2), an alternative explanation would be that a decrease in anodic kinetics caused potential to increase. Decreasing anodic kinetics during drying could have been caused by the stifling of local anodes as access to cathode area decreased.

The potential peak measured on day 8 and 9 of exposure to DB and WB ASTM G85-A2 was not observed on day 2 of exposure. Anodes would still be expected to stifle during drying on day 2 of exposure, so this difference in OCP must have been related to the interaction between the external reference electrode and exposed samples. In a previous section of this project, it was shown that very little corrosion products were present on samples on day 2, and the electrolyte in the form of discrete droplets rather than a continuous film.[41] Day 2 was also the first time the reference electrode had been placed on the samples, so there was no excess salt or corrosion product buildup around the reference electrode. During the salt spray period, a thin layer of adsorbed water between discrete droplets would allow the reference electrode to sense areas far away from the reference electrode, but communication between droplets would be lost as soon as drying began due to increasing solution resistance. Under these conditions, the potential measurements during drying would be representative only of the small area right around the reference electrode where the 3 M KCl leaking from the electrode allowed the sample to remain wet. Even if the potential of the bulk sample was increasing due to a reduction in anodic kinetics, the reference electrode would not be able to sense that change.

On day 8, corrosion products were visible on the sample surface,[41] which may have created a path for communication droplets via capillary forces during the early stages of the dry air purge. With the increased access to the bulk sample during early drying, the decrease in anodic kinetics could be sensed by the reference electrode. However, as drying proceeded, the reference electrode would eventually lose contact with anodes far away from the electrode, and the potential measurement would become dominated by the area right around the reference electrode.

A summary of the proposed mechanisms for the evolution of corrosion kinetics during wetting and drying in ASTM G85-A2 (chamber Brand 2) are shown in Figure 6.47. Although these mechanisms are difficult to prove with the limited tools available for in-situ electrochemical measurements, the mechanisms presented here are supported by the electrochemical data that was collected during ASTM G85-A2 exposures. As better sensors are developed for monitoring current and potential in-situ, addition data can be collected to shed more light on the mechanisms driving corrosion during atmospheric testing.

Day 2: Very little corrosion product present

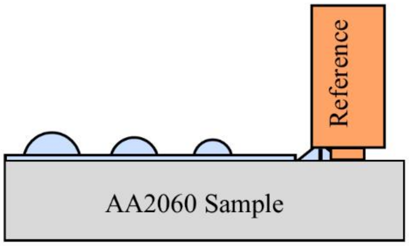

Stage 1: Salt Spray
1. RH increases from 20.5% (DB) or 53% (WB) to 96% RH
2. Droplets grow in size, causing cathodic kinetics to increase and local anodes to activate.

1/R_p increases and OCP remains stable

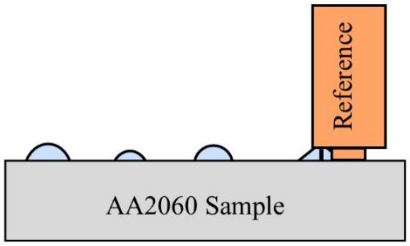

Stage 2: Drying
1. RH decreases from 96% RH to 17% (DB) or 23% (WB) over a 2 hr period
2. Droplets on sample quickly shrink, but area around reference electrode remains wet
3. Reference electrode only measures potential for area influenced by leaking

OCP measurement not representative of bulk sample

Day 8: Corrosion products visible on sample.

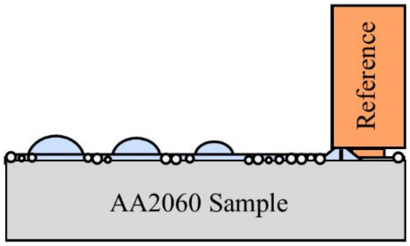

Stage 1: Salt Spray
1. RH increases from 20.5% (DB) or 53% (WB) to 96% RH
2. Droplets grow in size, causing cathodic kinetics to increase and local anodes to activate.

1/R_p increases and OCP remains stable

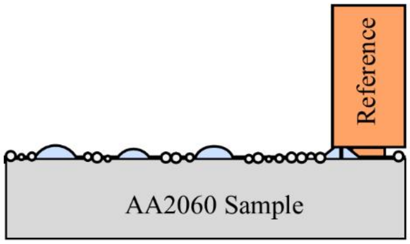

Stage 2: Drying
1. RH decreases from 96% RH to 17% (DB) or 23% (WB) over a 2 hr period
2. Droplets on sample shrink, reducing cathode area and causing anodes to stifle

1/R_p decreases and OCP increases

3. As sample dries out, reference electrode loses communication with bulk sample area

OCP measurement not representative of bulk sample

Figure 6.47: Proposed electrochemical mechanisms for wetting and drying in ASTM G85-A2 (chamber Brand 2) on day 2 and day 8 with consideration for the influence of the external reference electrode.

6.5.5 Modified Testing Protocol

The R_p measurements from the interdigitated AA2024-T3 sensor (which did not use an external reference electrode) showed that corrosion currents drop to low values during the dry air purge and dwell periods of DB and WB ASTM G85-A2 in chamber Brand 2 (Figure 6.30). The flow of heated air into chamber Brand 2 during the dry air purge produced very low RH, and TOW measurements indicated that samples would dry quickly in these conditions (Figure 6.18). RH did increase during the dwell period when the chamber was operated under WB conditions due to the large water reservoir in the bottom of the chamber, but the RH did not exceed the DRH for NaCl and samples did not re-wet. Although individual corrosion fissures may remain wet even at low RH, the dry conditions during the dry air purge and dwell periods caused the sample surface area available to support cathodic reactions to shrink and some anodes to stifle. It was hypothesized that an ideal RH for the dwell period would be lower than 87% (average for WB G85 Brand 1), but higher than 46.7% (average for WB G85 Brand 2). In the next section, the exposure results for two RH profiles within that range are discussed.

6.5.5.1 Exposure results

Two new RH profiles were tested using AA2060-T3 and -T86. Both RH profiles utilized a 1 minute dry air purge and operated under WB conditions. Performing this program in two different chambers (both Brand 2) produced slightly different RH profiles which are shown in Figure 6.32. The test called Mod WB 1 produced a lower RH during the dwell period (average of 61.5% during the dwell) than the test called Mod WB 2 (average of 74% during the dwell).

Both modified tests produced exfoliation blisters rated EB in the susceptible -T3 temper after just 12 days of exposure. The -T86 temper was rated P for pitting for both tests. Photographs of the samples can be viewed in Figure 6.34 and Figure 6.36. This increase in rate of exfoliation formation in these tests corresponded to an increase in TOW. The TOW sensor did dry, or at least start to dry, for the first few cycles, but by day 2 (cycle 5) the TOW sensor remained wet for the full 6 hour cycle (Figure 6.33). The change in drying behavior of the first 30 hours of exposure was most likely due to the accumulation of salt on the sensor.

Figure 6.48 shows the impact of average RH during the dwell period updated with the samples exposed to Mod WB 1 and Mod WB 2. It appears that the ideal RH range for the dwell period in exfoliation formation in atmospheric corrosion testing may fall between 77% (average during dwell for DB G85, Brand 1) and 61.5% (Mod WB 1). Attack after exposure to 12 days of Mod WB 1 and 2 was a more severe version of the EB rating than the attack after exposure to 2 weeks of DB G85 (Brand 1), but all three tests produced EB rated exfoliation in the susceptible -T3 temper in a reasonable time frame. It may be difficult to achieve the exact same RH profile in different laboratories using different equipment even with adjustments in the dry air purge time, so the existence of an acceptable range of RH during the dwell period is an encouraging result. ASTM G85-A2 exposure results would be more consistent among laboratories and equipment brands if the RH during the dwell period was required to fall between 77% and 61%.

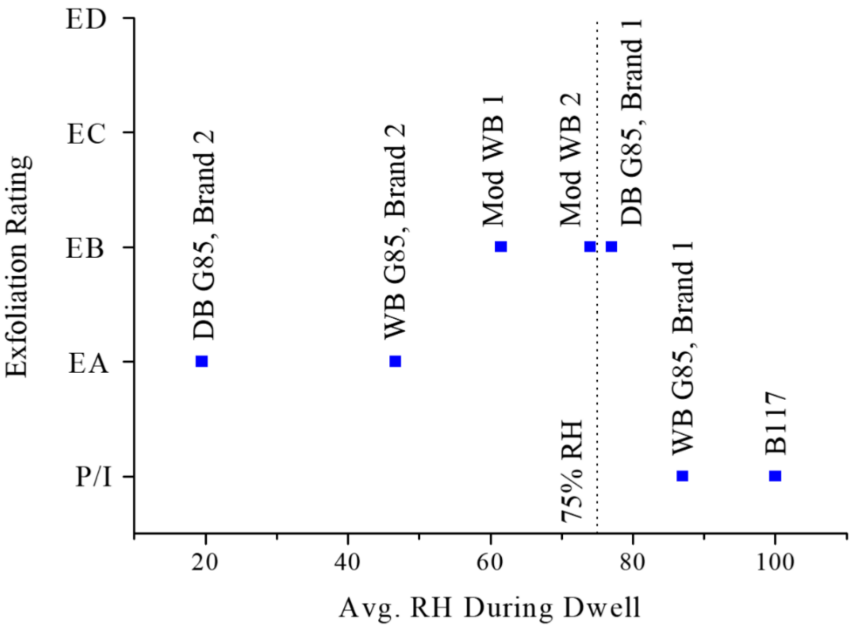

Figure 6.48: Impact of average RH during the dwell period on exfoliation ratings for AA2060-T3 updated to include the exposure results from Mod WB 1 and Mod WB 2. All exposures lasted for 4 weeks except for Mod WB 1 and 2, which lasted for 12 days.

6.5.5.2 Electrochemical Measurements in Mod WB 1 and Mod WB 2

$1/R_p$ measurements for AA2060-T3 and -T86 in Mod WB 1 were significantly higher than the $1/R_p$ measured in DB ASTM G85-A2. During the salt spray period, $1/R_p$ increased, and then $1/R_p$ decreased gradually during the 1 minute dry air purge and the 5.23 h dwell period (Figure

6.37). Similar trends were measured for the interdigitated AA2024-T3 sensor exposed to Mod WB 1 (Figure 6.39). The $1/R_p$ measured for the interdigitated AA2024-T3 sensor exposed to Mod WB 2 exhibited a different trend. $1/R_p$ was high during the salt spray period as expected, and then $1/R_p$ decreased during the first half of the dwell period. Halfway through the dwell period, a peak in $1/R_p$ was measured. Table 6.7 presents the %RH at which $1/R_p$ started to increase and then later decrease for three cycles.

The trends in $1/R_p$ and potential (OCP was measured on a regular AA2024-T3 sample not on the interdigitated sensor) are presented in Figure 6.39. During the salt spray period, both $1/R_p$ and OCP increased, which was most likely caused by increasing cathodic kinetics as the sensor wetted. During the first part of the dry air purge, both $1/R_p$ and OCP decreased, which indicated cathodic kinetics were decreasing. Even though electrolyte droplets did not dry as RH decreased from 97% RH to 75.5%, the size of droplets would be expected to decrease, which could reduce the area available to support cathodic reactions. Once RH reached values between 74.0 - 75.5%, $1/R_p$ began to increase again. The decreasing OCP during this period suggested that the increase in $1/R_p$ was caused by increasing anodic kinetics rather than a change in cathodic kinetics. The Cl^- concentration would be expected to be saturated or nearly saturated at RH ranging from 74.0 - 75.5%, and this very high Cl^- concentration may have been responsible for the increase in anodic kinetics. As RH continued to decrease, the $1/R_p$ began to decrease again at an RH between 73.0 - 74.0 %. Most likely the area available to support cathodic reactions decreased enough that anodes began to stifle.

Table 6.7: Summary of time and %RH associated with 1/Rp peak in Mod WB 2. Cycle numbers reflect the number of cycles since the start of exposure.

Cycle #	**$1/R_p$ Starts to Increase**		**$1/R_p$ Starts to Decrease**	
	Time into Dwell (h)	%RH	Time into Dwell (h)	%RH
6	1.79	74.5	2.85	73.0
7	1.42	75.5	2.08	74.0
8	2.08	74.0	2.65	73.0

In Mod WB 1, the peak in $1/R_p$ during drying was not observed, but $1/R_p$ remained quite high for most of the dwell cycle. It is possible that same mechanisms existed in both tests during drying (decreased cathodic kinetics electrolyte droplets shrink, increased anodic kinetics as $[Cl^-]$ becomes saturate), but the drop in RH was more rapid for Mod WB 1, which meant that the saturation point of $[Cl^-]$ was reached faster in this test. It is possible that the fast anodic kinetics produced by the high Cl^- concentration came into play earlier in the drying process in Mod WB 1, and the decrease in $1/R_p$ measured in Mod WB 2 was essentially skipped over.

Regardless of the governing mechanisms, corrosion rates were clearly higher in the modified tests compared to the standard WB and DB ASTM G85-A2 tests. The longer TOW in the modified tests prevented stifling of anodes during drying, and as a result, exfoliation formed more quickly in the modified tests than in the standard tests. Standardizing an appropriate RH for the dwell period of ASTM G85-A2 would provide a more consistent testing environment across different chamber brands, and it may also reduce the time needed to obtain results by increasing the TOW during the dwell period.

6.5.5.3 Applicability to other High-Strength Aluminum Alloys

A well designed atmospheric corrosion test for exfoliation should be applicable to more than one high-strength Al-alloy. AA7075 and AA2024 samples were exposed to Mod WB 1 and Mod WB 2, and both tests correctly distinguished between exfoliation-susceptible and resistant tempers. Although the exposure time to reveal exfoliation susceptibility would likely be different for different Al alloys, cyclic salt spray testing appears to be the nearest thing to a universal accelerated laboratory test for high-strength Al alloys. Unlike immersion tests which tend to be “over-designed” for just one type of Al-alloy, cyclic salt spray tests are a better approximation of nature and can be extended to a larger range of alloys. Currently, the most significant issue with ASTM G85-A2 is the lack of consistency in results across different types of equipment. If the standard was adjusted to require a specific range of RH during the dry air and dwell periods, consistency in results among different laboratories would be improved.

6.6 Conclusions

In this work, it was shown that RH control is critical to obtaining consistent results among different salt spray chamber brands. When RH is too high as for ASTM B117 and WB ASTM G85-A2 (chamber Brand 1), rinsing of the sample prevents the accumulation of corrosion products along grain boundaries, which is necessary for exfoliation formation. When RH is too low, anodes stifle during the dry air purge and corrosion rate is very low for bulk of each 6 hour cycle. However, an average RH between 77% and 61% during the dwell period was found to produce exfoliation in the susceptible temper in a reasonable amount of time. The two modified tests explored in this work (Mod WB 1 and Mod WB 2) produced different $1/R_p$ trends, but both tests produced high corrosion rates on the AA2024-T3 interdigitated sensor, and both tests produced moderate exfoliation for AA2060-T3 in just 12 days.

Several electrochemical mechanisms were proposed to explain the behavior of AA2060 in each of the cyclic salt spray tests. It was shown that measurement using the external reference electrode may have been influenced by leaking of the electrode fill solution, but this was considered when interpreting results. Upon wetting, $1/R_p$ always increased regardless of sample type or test. The degree of increase depended on the exact exposure conditions. The increase in corrosion rate seemed to be caused either by an increase in cathodic kinetics, or an increase in both cathodic and anodic kinetics. For most tests, $1/R_p$ decreased at the start of drying. For standard DB ASTM G85-A2 (Brand 2) where RH dropped very low during drying, local anodes appeared stifle, and corrosion rate remained low for the full dwell period. For Mod WB 2, $1/R_p$ decreased initially due to slowing cathodic kinetics, but $1/R_p$ increased again mid-way through the dwell cycle, possibly due to increasing anodic kinetics as Cl^- became saturated in the electrolyte droplets. In Mod WB 1, $1/R_p$ only decreased slightly during drying. This may have been because the saturation point of NaCl was reached faster in this test, which caused anodic kinetics to remain high during the full dwell period. In-situ measurements during salt spray exposures are challenging. The mechanisms proposed here are a starting point for an understanding of corrosion kinetics during atmospheric corrosion testing that will no doubt continue to evolve as more tools become available for this type of study.

6.7 Acknowledgements

This work was supported by Rolls-Royce and the Office of the Undersecretary of Defense Corrosion University Pilot Program, Contract #: W911NF-14-2-0005.

6.8 References

1. ASTM G34-1, "Standard Test Method for Exfoliation Corrosion Susceptibility in 2XXX and 7XXX Series Aluminum Alloys" (West Conshohocken, PA: ASTM International, 2001), p. 1-7.
2. ASTM G110-92, "Standard Practice for Evaluating Intergranular Corrosion Resistance of Heat Treatable Aluminum Alloys by Immersion in Sodium Chloride + Hydrogen Peroxide Solution" (West Conshohocken, PA: ASTM International, 2003), p. 1-3.
3. ASTM B117-16, "Standard Practice for Operating Salt Spray (Fog) Apparatus" (West Conshohocken, PA: ASTM International, 2016), p. 1-12.
4. ASTM G85-02, "Standard Practice for Modified Salt Spray (Fog) Testing" (West Conshohocken, PA: ASTM International, 2002), p. 1-14.
5. ASTM B368-09(2014), "Standard Test Method for Copper-Accelerated Acetic Acid-Salt Spray (Fog) Testing (CASS Test)" (West Conshohocken, PA: ASTM International, 2014), p. 1-4
6. ASTM D5894-16, "Standard Practice for Cyclic Salt Fog/UV Exposure of Painted Metal, (Alternating Exposures in a Fog/Dry Cabinet and a UV/Condensation Cabinet)" (West Conshohocken, PA: ASTM International, 2016), p. 1-4.
7. K.R. Baldwin, C.J.E. Smith, *Aircraft Eng. Aerospace Tech.* 71, 3 (1999): p. 239-244.
8. R.L. Howard, S.B. Lyon, J.D. Scantlebury. *Prog. Organic Coatings.* 37, 1-2 (1999): p. 91-98.
9. D. Liang, H.C. Allen, G.S. Frankel, Z.Y. Chen, R.G. Kelly, Y. Wu, B.E. Wyslouzil, *J. Electrochem. Soc.* 157, 4 (2010): p. C146-C156.
10. S.S. Pathak, M.D. Blanton, S.K. Mendon, J.W. Rawlins. *Corrosion Sci.* 52 (2010): p. 1453-1463.
11. Y. Wan, E.N. Macha, R.G. Kelly. *Corrosion*. 68, 3 (2012): p. 1-10.
12. B.W. Lifka, D.O. Sprowls. *Corrosion.* 22, 1 (1966): p. 7-15.
13. M.J. Robinson, *Corrosion Sci.* 22, 8 (1982): p. 775-790.

14. M.J. Robinson, *Corrosion Sci.* 23, 8 (1983): p. 887-899.
15. M.J. Robinson, *Corrosion Sci.* 41, 5 (1999): p. 1013-1028.
16. J.P. Moran, F.S. Bovard, J.D. Chrzan, P. Vandenburgh, "Corrosion Performance of New Generation Aluminum-Lithium Alloys for Aerospace Applications," 13th International Conference on Aluminum Alloys, (John Wiley & Sons, 2012).
17. E.L. Colvin, S.J. Murtha, "Exfoliation Corrosion Testing of Al-Li Alloys 2090 and 2091," 5th International Aluminum-Lithium Conference, (MCE Publications Ltd. 1989) p. 1251-1260.
18. F. Bovard, J. Tardiff, T. Jafolla, D. McCune, G. Courval, K.A Smith, F. Lee, J. Repp, S. Ramamurthy, R.J. Shaffer, F.M. Vartolas. "Development of an Improved Cosmetic Corrosion Test for Finished Aluminum Autobody Panels" (Warrendale, PA: SAE, 2007). SAE Paper 2017-01-0417.
19. Z.Y. Chen, F. Cui, R.G. Kelly. *J. Electrochem. Soc.* 155, 7 (2008): p. C360-C368.
20. B. Zaid, D. Saidi, A. Benzaid, S. Hadji, *Corrosion Sci.* 50 (2008): 1841-1847.
21. Z.A. Foroulis, M.J. Thubrikar, *J. Electrochem. Soc.* 122, 10 (1975) p. 1296-1301.
22. O. Dolgikh, A.C. Bastos, A. Oliveira, C. Dan, J. Deconinck, *Corrosion Science* 102 (2016): p. 338-347.
23. Z.Y. Chen, R.G. Kelly, *J. Electrochem. Soc.* 157, 2 (2010): p. C69-C78.
24. E. Schindelholz, R.G. Kelly. *Corrosion Reviews*. 30, 5/6 (2012): p. 135-170.
25. J.H. Han, S.T. Martin. *J. Geophysical Research.* 104, D3 (1999): p. 3543-3553.
26. M.D. Cohen, R.C. Flagan, J.H. Seinfeld. *J. Phys. Chem*. 91 (1987a): p. 4563-4574.
27. I.N. Tang. "Deliquescence properties and particle size change of hygroscopic aerosols" Paper presented at the Symposium on Biological Studies of Environmental Pollutants: Aerosol Generation and Exposure Facilities, Honolulu, Hawaii, 1979.
28. G. Biskos, A. Malinowski, L.M. Russell, P.R. Buseck, S.T. Martin. *Aerosol Sci. Tech.* 40 (2006): p. 97-106.
29. E. Schindelholz, L. Tsui, R.G. Kelly. *J. Physical Chem. A.* 118 (2014): p. 167-177.
30. M.D. Cohen, R.C. Flagan, J.H. Seinfeld. *J. Phys. Chem*. 91 (1987b): p. 4575-4582.
31. I.N. Tang, H.R. Munkelwitz. *J. Applied Meteorology.* 33 (1994): p. 791-796.
32. Z. Ge, A.S. Wexler, M.V. Johnston. *J. Colloid Interface Sci.* 183 (1996): p. 68-77.
33. J.P. Darr, S.Q. Davis, Y. Kohno, K. McKenna, P. Morales. *J. Aerosol Sci.* 77 (2014): p. 158-167.

34. I.N. Tang. "Phase Transformation and Growth of Hygroscopic Aerosols." Ch. 4 of *Aerosol Chemical Processes in the Environment*. ed. K.R. Spurny. (Boca Raton, Fl: CRC Press, 2000): p. 61-80.
35. M.Y. Choi, C.K. Chan, *Envrion. Sci. Technol.* 36 (2002): p. 2422-2428.
36. G.D. Davis, L.A. Krebs, C.M. Dacres, "Coating Evaluation and Validation of Accelerated Test Conditions Using an In-Situ Corrosion Sensor"
37. C. Grumbach, S. Pennell, K.S. Williams, K.A. Schultz, P. Kramer, F. Friedersdorf, A.J. Feickert, S.G. Croll, "Accelerated Testing of Aerospace Coating Systems Using Combined Mechanical Stress and Environmental Exposure," 2017 Department of Defense – Allied Nations Technical Corrosion Conference, Paper No. 2017-587411.
38. J. Demo, A. Steiner, F. Friedersdorf, M. Putic, "Development of a Wireless Miniaturized Smart Sensor Network for Aircraft Corrosion Monitoring," Aerospace Conference, (IEEE, 2010).
39. R.J. Rioja, J. Liu, *Metal. Mater. Trans. A* 43 (2012): p. 3325-3337.
40. ASTM G112-92, "Standard Guide for Conducting Exfoliation Corrosion Tests in Aluminum Alloys" (West Conshohocken, PA: ASTM International, 2015), p. 1-7.
41. M.E. Parker, R.G. Kelly, "Deconstructing DB ASTM G85-A2 Testing Environment with In-Situ Measurements," Corrosion 2017, (NACE International, 2017).
42. J.R. Scully, *Corrosion* 56, 2 (2000) p. 199-218.
43. R.H. Stokes, R.A. Robinson, *Ind. Eng. Chem.* 41 (1949) p. 2013.
44. I.N. Tang, H.R. Munkelwitz, *J. Geophysical R.* 99, D9 (1994): p. 18,801-18,808.
45. M. Starzak, M. Mathlouthi, *Food Chemistry* 96 (2006): p. 346–370.
46. C. Peng, M.N Chang, C.K. Chan, *Environ. Sci. Technol.* 35 (2001): p. 4495 – 4501.
47. D. B. Blucher, J.E. Svensson, L.Gl Johansson, M. Rohwerder, M. Stratmann, *J. Electrochem. Soc.* 151, 12 (2004): p. B621-B626.
48. R.G. Kelly, J.R. Scully, D.W. Shoesmith, R.G. Buchheit, "Electrochemical Techniques in Corrosion Science and Engineering." CRC Press (2002).
49. M.E. Parker, R.G. Kelly, "Deconstructing the Electrochemical Basis of ASTM G34 and ANCIT Immersion Tests," to be submitted for publishing in 2018.
50. M.E. Parker, R.G. Kelly, "The Role of H2O2, and K2S2O8 as Oxidizing Agents in Accelerated Corrosion Testing," to be submitted for publishing in 2018.
51. M.A. Jakab, D.A. Little, J.R. Scully, *J. Electrochem. Soc.* 152, 8 (2005): p. B311-B320).

7. Conclusions and Technological Impact

7.1 Conclusions

In this project, several accelerated tests for exfoliation corrosion of aluminum alloys were deconstructed. ASTM G34, a standard full immersion test for exfoliation, and ANCIT, a modified version of ASTM G34, did not predict the exfoliation behavior of AA2060 tempers at seacoast during the standard testing time. Exfoliation did form in the susceptible temper (AA2060-T3) with extended exposure time, but 7-d of ANCIT exposure and 4-w of ASTM G34 exposure were required. In contrast, corrosion was quite severe for the exfoliation resistant AA2060-T86 temper even after short exposure times. Dry bottom (DB) ASTM G85, an acidified cyclic salt spray test, successfully distinguished between the exfoliation susceptible and resistant tempers after a 4 week exposure, but the test severity depended greatly on the equipment brand used for exposure.

Several factors were found to be important during constant immersion tests (ASTM G34 and ANCIT). The low solution pH in fresh ASTM G34 solution provided very fast cathodic kinetics via proton reduction. However, the pH increased with exposure time and caused cathodic kinetics to slow. NO_3^- reduction seemed to be the dominant cathodic reaction in ANCIT, but these kinetics also slowed over time due to consumption of NO_3^-. The fast cathodic kinetics provided by H^+ at the start of ASTM G34 testing caused severe corrosion in the exfoliation resistant AA2060-T86 material. In fact, small blisters were observed on this sample after just 6-h of exposure to ASTM G34. The exfoliation susceptible -T3 temper, however, did not form exfoliation within the standard 4-d exposure period in spite of the very fast cathodic kinetics. While the fast cathodic kinetics in fresh ASTM G34 solution drove significant attack in AA2060-T86, the corrosion rate of AA2060-T3 seemed to be limited by anodic kinetics.

During ANCIT exposures, anodic kinetics were accelerated for AA2060-T3 due to the higher exposure temperature in ANCIT. Although exfoliation did not form during the standard exposure period (2-d), exfoliation blisters were observed in the susceptible temper after 7-d of testing, which was accelerated compared to the 4 week period required in ASTM G34. These results indicated that accelerating cathodic kinetics in a full immersion environment was not the key to accelerating exfoliation in Al-Cu-Li alloys. The fast cathodic kinetics in ASTM G34 and ANCIT only served to increase the corrosion rate of the exfoliation resistant temper. Instead, exfoliation should be accelerated by increasing anodic kinetics through elevated temperature, and a moderate level of cathodic kinetics should be used to support the anodic reactions. These results lead to the hypothesis that a moderate level of cathodic kinetics should be utilized during accelerated corrosion testing of Al-Cu-Li alloys such that excessive attack does not occur in the exfoliation resistant temper.

This hypothesis was supported by results from full immersion testing in solutions containing hydrogen peroxide (H_2O_2) and potassium persulfate ($K_2S_2O_8$), both of which are powerful oxidizing agents. A common method used to increase corrosion rate during accelerated corrosion testing is to add an oxidizing agent with reduction kinetics faster than oxygen reduction (ORR) and proton reduction. It was found that H_2O_2 produced faster cathodic kinetics than $K_2S_2O_8$ did, but the cathodic kinetics of $K_2S_2O_8$ could be manipulated by adjusting solution pH and adding aluminum chloride ($AlCl_3$). However, as in the case of ASTM G34, fast cathodic kinetics did not lead to the acceleration of exfoliation in the susceptible -T3 temper.

Cathodic kinetics were also important during salt spray testing, and relative humidity (RH) was found to play a key role in corrosion kinetics. During period of high humidity, the sample area covered by electrolyte was at a maximum, and the sample area available to support cathodic reactions was large. During drying, electrolyte droplets shrank, which most likely caused the total available cathodic current to decrease. As samples experienced wet/dry cycles, cathodic kinetics increased and decreased. RH may have also impacted anodic kinetics through the changes in equilibrium chloride (Cl^-) concentration during wetting and drying.

The RH played a significant role in the severity of attack during exposures because of its impact on cathodic and anodic kinetics. Dry bottom (DB) and wet bottom (WB) ASTM G85-A2 were performed in two different chamber brands, and exposure results were different for the different brands. Seemingly small differences in chamber operation caused RH to be significantly different during the dry air purge and dwell periods in the two chambers. In chamber Brand 2, the low RH during the dwell period (17% - 20.5%) caused corrosion kinetics to slow, and only mild exfoliation formed in the susceptible temper after 4 weeks of exposure. It was most likely slow cathodic kinetics leading to anode stifling that cased corrosion kinetics to be slow during the periods of low RH. It was shown that a more moderated RH (77% - 61%) during the dwell period was appropriate for accelerating exfoliation. Two modified cyclic salt spray tests were designed to have higher RH during the dwell period, and both tests produced higher corrosion kinetics and faster exfoliation formation compared to the standard test. The moderate RH during the dwell cycle of the modified tests provided sufficient cathodic kinetics to allow propagation of fissures in AA2060-T3, but cathodic kinetics were not so fast that an unrealistic degree of attack formed in the exfoliation resistant -T86 temper. Additional high-strength aluminum alloys (AA7075, AA2024) were exposed to the modified tests, and both tests could correctly distinguish between exfoliation-resistant and susceptible tempers.

7.2 Technological Impact

7.2.1 Accelerated Testing Under Full Immersion Conditions

Full immersion testing can play a role in studying alloys intended for use in atmospheric environments, but caution must be used when applying standard tests developed for legacy alloys to new generation alloys. Improvements to constant immersion tests have proceeded in the past mostly by trial and error, but the work presented in this dissertation provides a basis for test design by an understanding of the electrochemical role of each testing variable. Some methods of accelerating corrosion may have unintended impacts that must be considered.

7.2.2 Laboratory Atmospheric Corrosion Testing

The work presented in this dissertation is already being utilized to improve laboratory atmospheric corrosion testing for exfoliation corrosion of Al-Li alloys. Inconsistency in testing results has been an issue for ASTM G85-A2 for quite some time, and an ASTM task force has been designated to develop an improved standard for salt spray testing of Al-Li alloys. This work is being used to recommend stricter relative humidity requirements during the dry and dwell periods of testing in the new standard.

8. Recommended Future Work

The work presented in this dissertation outlined the roles of several key testing parameters in both constant immersion testing and in laboratory atmospheric corrosion testing. Opportunities for additional research topics are outlined below:

- **Impact of NO_3^- on exfoliation formation**

  Potassium nitrate (KNO_3) is included in the ANCIT solution to provide cathodic kinetics faster than oxygen reduction. However, it was found in this work that NO_3^- also caused a reduction in anodic kinetics, most likely by competing with Cl^- for sites within the oxide film on Al. It was noted that for all the oxidizing agents used in full immersion testing in this work (NO_3^-, H_2O_2, $S_2O_8^{2-}$), exfoliation was only ever observed after immersion in nitrate-containing solutions. For samples exposed to solutions containing other oxidizing agents (H_2O_2, $S_2O_8^{2-}$) the rate of general attack was too high to allow corrosion products to become trapped in grain boundaries, which is necessary for exfoliation formation. A hypothesis was developed that the reduction in anodic kinetics caused by NO_3^- would lead to a reduction in the passive current for surface grains that were not undergoing active dissolution. The impact of NO_3^- on exfoliation formation compared to other oxidizing agents would be an interesting topic for further study. This understanding could be important for future development of immersion tests for exfoliation corrosion.

- **Impact of aluminum chloride ($AlCl_3$) on cathodic kinetics**

  The observed behavior of aluminum chloride ($AlCl_3$) during accelerated corrosion testing could not be fully explained by the results presented in this work. When used in NO_3^- containing solutions, the slope of the NO_3^- cathodic line changed indicating a possible mechanism change. When used in $S_2O_8^{2-}$ solutions, the diffusion limiting current for $S_2O_8^{2-}$ increased dramatically. When used in solutions containing no added oxidizing agents, the diffusion limiting current for proton reduction increased significantly. The impact of $AlCl_3$ on cathodic kinetics is interesting for the purpose of accelerated corrosion testing, but the impact on proton reduction is especially important. During localized corrosion in aluminum alloys, Al^{3+} and Cl^- are expected to accumulate within fissures. If $AlCl_3$ has such a significant impact on H^+ reduction, the accumulation of Al^{3+} within fissures may create a source of cathodic current from within fissures.

- **Reducing severity of AA2060-T86 attack in full immersion testing**

  One topic which could not be explored in depth in this work was the unrealistic degree of attack that occurred for AA2060-T86 during ASTM G34 and ANCIT exposures. For any accelerated immersion test to be applied to alloys intended for use in atmospheric environments, the test must be able to distinguish type and extent of attack for a range of alloy tempers. It was hypothesized in this work that the fast cathodic kinetics present in the full immersion tests were unsuccessful at accelerating exfoliation in the susceptible -T3 temper and instead caused an unrealistic degree of attack in the resistant -T86 temper. Further investigation into the attack morphology and dissolution mechanisms for AA2060-T86 in ASTM G34 and ANCIT may shed some light on this topic.

- **Deconstructing mechanisms during wet-dry cycling**

  A method was devised to monitor potential and R_p during wetting and drying in cyclic salt spray testing. This method had its limitations, but new sensors for in-situ corrosion monitoring are becoming available. As new tools become available, the mechanisms proposed here can be further explored and tested.